Toward Development of Radical Materials for Charge Storage: Synthesis and Electrochemistry of Benzotriazinyl Radical Derivatives

by

Nicholas Alfred Oakley
B.Sc., McMaster University, 2007

A Thesis Submitted in Partial Fulfillment
of the Requirements for the Degree of

MASTER OF SCIENCE

in the Department of Chemistry

Supervisory Committee

Toward Development of Radical Materials for Charge Storage:
Synthesis and Electrochemistry of Benzotriazinyl Radical Derivatives

by

Nicholas Alfred Oakley
B.Sc., McMaster University, 2007

Supervisory Committee

Dr. Natia L. Frank, (Department of Chemistry)
Supervisor

Dr. David A. Harrington, (Department of Chemistry)
Departmental Member

Dr. Jeremy E. Wulff, (Department of Chemistry)
Departmental Member

Abstract

Supervisory Committee
Dr. Natia L. Frank, (Department of Chemistry)
Supervisor
Dr. David A. Harrington (Department of Chemistry)
Departmental Member
Dr. Jeremy E. Wulff (Department of Chemistry)
Departmental Member

The benzotriazinyl radical is a highly stable organic radical that is known to possess fast and reversible oxidation and reduction electrochemical processes. Such properties make it an ideal candidate for use as an anodic or cathodic charge storage material in a new class of high-power secondary batteries known as organic radical batteries. Towards this application, several new benzotriazinyl radical derivatives were synthesized and fully characterized using electronic absorption, EPR, and IR spectroscopy as well as elemental analysis and mass spectrometry. The electrochemical properties of the radicals were studied using cyclic voltammetry.

The introduction of electron donating groups onto the structure of the radical was found to result in cathodic shifts in both of the electrochemical processes, without loss of reversibility. It was also found that in some cases functional groups led to the destabilization of the radical to a known chemical oxidation pathway that resulted in the formation of closed-shell iminoquinone compounds. These materials demonstrated good multi-electron accepting properties, undergoing two reversible one-electron reduction processes.

Synthetic methodologies were developed for the preparation of two new classes of benzotriazinyl biradicals. One class used an expansion of a known benzotriazinyl radical synthesis to prepare a *m*-phenylene-bridged biradical, while the other class used microwave-assisted synthesis to prepare biradicals bridged by electron accepting aromatic diimides. Spectroscopic studies of both classes of biradical showed electronic isolation of the two radicals within each molecule, consistent with computational predictions. This resulted in minimal perturbation of the electrochemistry of these compounds from that of typical benzotriazinyl radicals.

The solid state properties of a selection of benzotriazinyl radical derivatives were studied. Structural information obtained through single crystal X-ray diffraction studies showed significant intermolecular π-π and hydrogen bonding interactions. These solid state interactions were found to provide pathways for magnetic exchange, as determined using SQUID magnetometry. Additionally, preliminary conductivity studies indicated semiconducting behaviour in the compounds that were studied, warranting further studies.

Anionic polymerization of a vinyl-functionalized benzotriazinyl radical was investigated as a method for the synthesis of a pendant benzotriazinyl polyradical with a saturated backbone. The electrochemistry of the putative polymer was identical to the monomer, maintaining reversibility of both the oxidation and reduction processes and verifying that the polymer could be used as an anodic or cathodic charge storage material. SQUID magnetometry was used to estimate a polymer spin content to be ~ 44 %.

Table of Contents

List of Figures

List of Schemes

List of Tables

List of Numbered Compounds

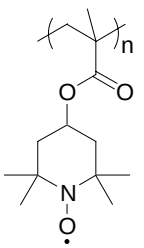

1.1

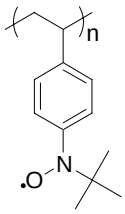

1.2

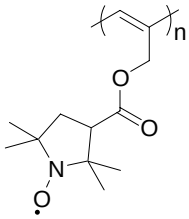

1.3

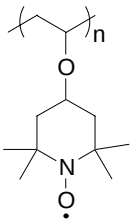

1.4

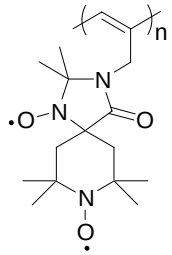

1.5

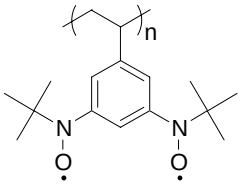

1.6

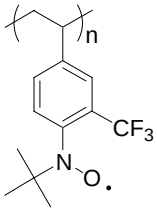

1.7

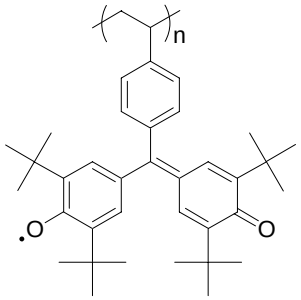

1.8

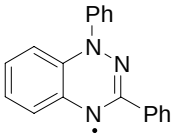

1.9

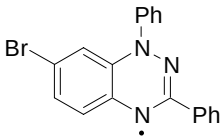

1.10

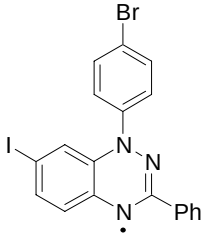

1.11

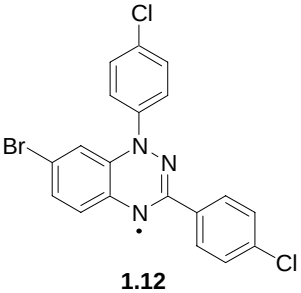

1.12

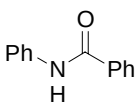

1.13

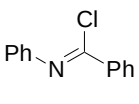

1.14

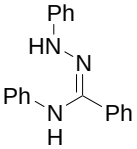

1.15

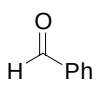

1.16

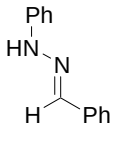

1.17

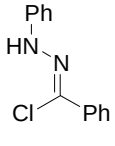

1.18

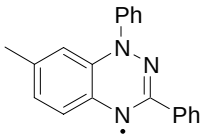

2.1

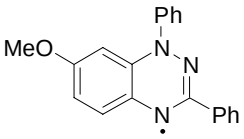

2.2

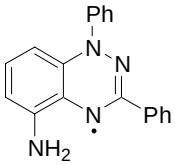

2.3

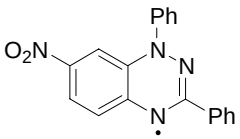

2.4

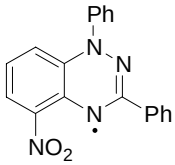

2.5

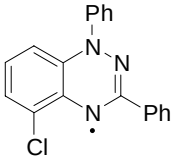

2.6

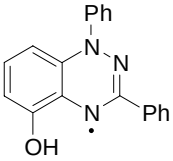

2.7

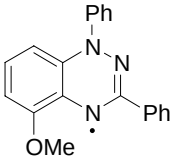

2.8

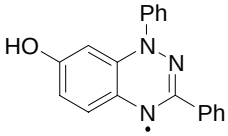

2.9

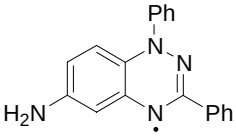

2.10

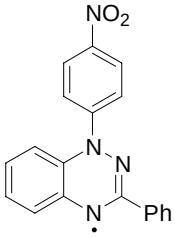

2.11

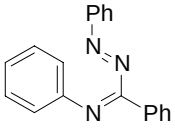

2.12

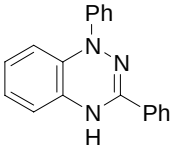

2.13

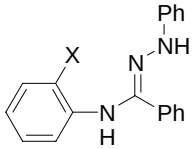

2.14

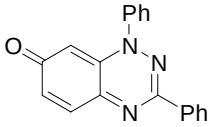

2.15

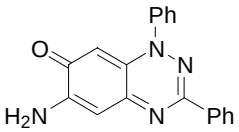

2.16

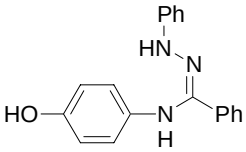

2.17

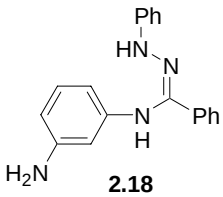

2.18

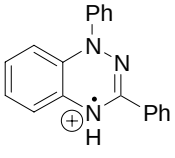

2.19

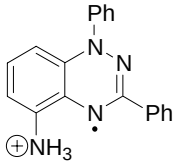

2.20

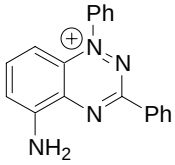

2.21

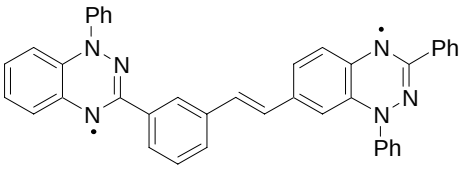

3.1

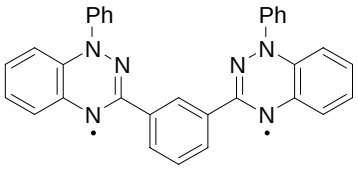

3.2

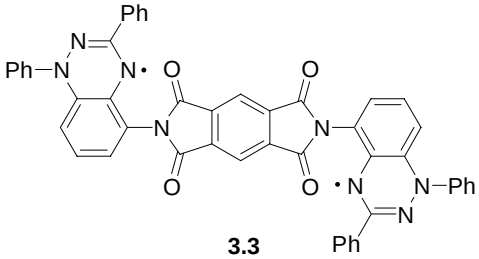

3.3

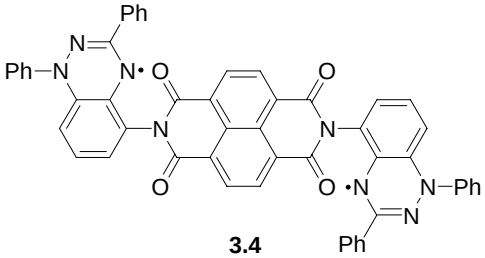

3.4

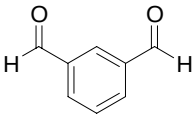

3.5

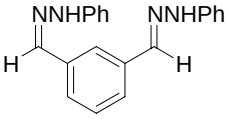

3.6

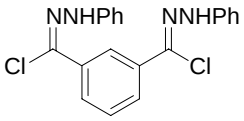

3.7

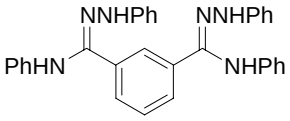

3.8

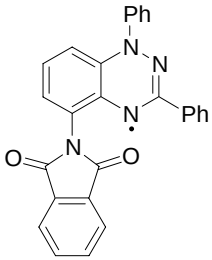

3.9

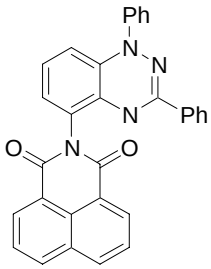

3.10

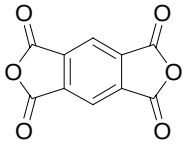

3.11

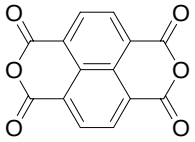

3.12

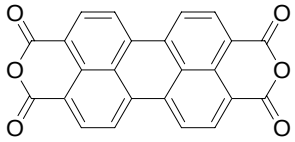

3.13

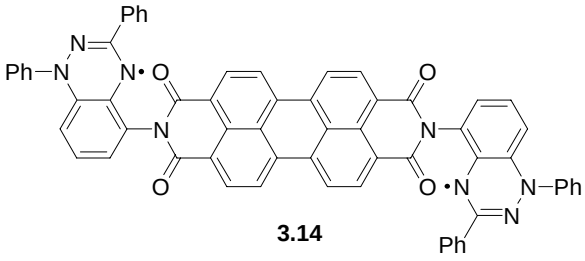

3.14

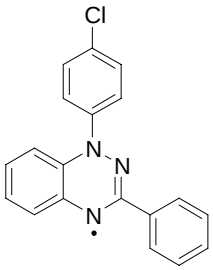

4.1

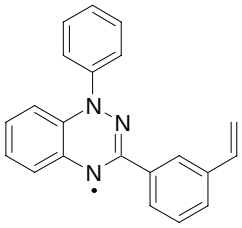

4.2

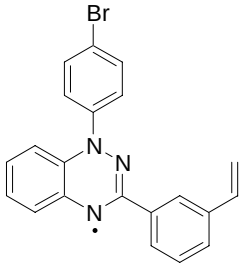

4.3

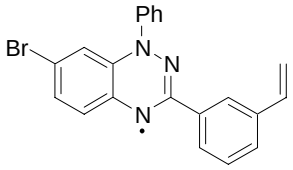

5.1

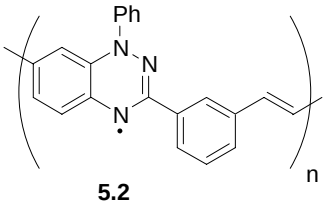

5.2

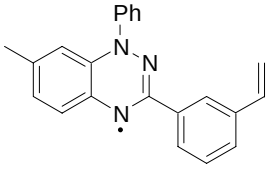

5.3

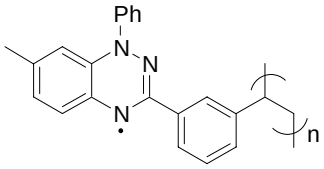

5.4

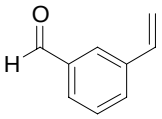

5.5

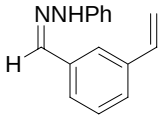

5.6

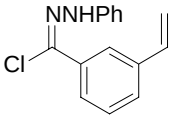

5.7

List of Abbreviations

6-31G(d,p)	a split valence plus polarization basis set
a	hyperfine coupling constant
AcOH	acetic acid
Å	Angstrom
$[Bu_4][PF_6]$	tetrabutylammonium hexafluorophosphate
n-BuLi	*n*-butyl lithium
C	Curie constant or Coulomb
°C	degrees Celsius
cm	centimeter
cm^{-1}	wavenumber
DBU	1,8-diazabicyclo[5.4.0]undec-7-ene
DFT	density functional theory
DMF	dimethylformamide
DMSO	dimethylsulfoxide
DPPH	2,2-diphenyl-1-picrylhydrazyl
emu	electromagnetic units
eV	electron volt
E_{cell}	electrochemical cell potential or disproportionation energy
$E_{1/2(ox)}$	oxidation half-wave potential
$E_{1/2(red)}$	reduction half-wave potential
ΔE_p	peak-to-peak separation between anodic and cathodic waves

E_{SOMO}	SOMO energy
EDG	electron donating group
ENDOR	electron-nuclear double resonance
EPR	electron paramagnetic resonance
ESI-MS	electrospray ionization mass spectrometry
EtOH	ethanol
EWG	electron withdrawing group
F	Faraday constant (96 485.34 $C \cdot mol^{-1}$)
Fc	ferrocene
Fc^+	ferrocenium
g	g-factor
G	Gauss
H	applied magnetic field
HOMO	highest occupied molecular orbital
Hz	Hertz
IR	infrared
J	magnetic exchange parameter
k	Boltzmann constant (0.69503877 cm^{-1} K^{-1})
K	Kelvin
LUMO	lowest unoccupied molecular orbital
m	meta
m_s	magnetic spin quantum number
M	molarity, or magnetization

$mAh \cdot g^{-1}$	milliampere hours per gram
mol	mole
mV	millivolt
MeCN	acetonitrile
MeOH	methanol
Me_2S	dimethyl sulfide
MHz	megahertz
MW	microwave or megawatt
N	Avogadro's number (6.0221367×10^{23} mol^{-1})
nm	nanometer
NCS	*N*-Chlorosuccinimide
NMR	nuclear magnetic resonance
Oe	Oersted
OMe	methoxy
ORB	organic radical battery
ppm	parts per million
PTMA	poly(4-methacryloyloxy-2,2,6,6-tetramethylpiperidin-*N*-oxyl)
Q	McConnell equation proportionality constant
S	spin multiplicity or siemens
SCE	saturated calomel electrode
SOMO	singly occupied molecular orbital
SQUID	superconducting quantum interference device
T	temperature

T_c	critical temperature
TCNQ	7,7,8,8-tetracyano-*p*-quinodimethane
TD-DFT	time-dependant density functional theory
TEA	triethylamine
TEMPO	2,2,6,6-tetramethyl-1-piperidinyloxy
THF	tetrahydrofuran
TLC	thin layer chromatography
TTF	1,1',3,3'-tetrathiafulvalene
UB3LYP	unrestricted Becke 3-parameter Lee-Yang-Parr
UV	ultraviolet
V	volt
XRD	X-ray diffraction
β	Bohr magneton (4.66864374×10^5 cm^{-1} G^{-1})
ε	extinction coefficient
θ	Weiss constant
λ	wavelength
ρ	spin density
χ	magnetic susceptibility
χT	magnetic moment

Acknowledgments

First and foremost I would like to thank my supervisor Dr. Natia Frank. Her encouragement and patience during my research terms as an undergraduate student gave me the confidence to pursue research at the graduate level, and her continual guidance and support throughout the course of my degree have greatly enhanced my development as a chemist.

Thanks also to all of the graduate students in the department who have made my time here enjoyable. Specifically to my fellow Frank Group members both past and present - Mark Zsombor, Brynn Dooley, Michelle Paquette, Jordan Cramen, Olga Sarycheva, and Bin Yan – thanks for all the helpful discussion and advice, and for making me a slave to three o'clock coffee time.

I also wish to thank the departmental office staff for their administrative help and the support and instrument staff for keeping operational all of the instruments and laboratory equipment that were vital for my work.

Lastly I want to thank my brother Simon for all of his pearls of brotherly wisdom, and of course my parents, for their unending support.

Chapter 1 Organic materials for charge storage

1.1 Electrochemical energy storage

Energy is an issue of great importance in modern society from many perspectives. In terms of energy production, the dwindling global supplies of fossil fuels and the environmental issues associated with their use have led to much interest in the use of renewable energy sources (*i.e.* solar or wind power) as a more sustainable and environmentally benign alternative. One major advantage of fossil fuels however, is that they are not only sources of energy, but also stores of energy that are easily transported. Many of the renewable energy sources on the other hand, cannot be stored or transported without being first converted into electricity.[1] As a result, new materials are required that are capable of the efficient and reliable storage and conversion of electrochemical energy.

Electrochemical energy storage is also an important issue in the development of technologies such as electric and hybrid electric vehicles and various portable electronic devices. These require systems of electrochemical energy storage which combine good performance in areas such as energy and power densities, cycle lives, and charge/discharge rates, with practical considerations such as safety, cost, size and weight, and environmental impact.[2]

Along with fuel cells and electrochemical capacitors, batteries represent commonly used devices for the storage and conversion of electrochemical energy which are expected to play an important role in meeting future energy needs.[3-6] It has been noted however, that improvements in battery performance have been slow in forthcoming and that new technological breakthroughs are needed in order to meet these needs.[7] Tied to

improvements in battery performance are advances in materials chemistry in the development of new charge storage materials. Towards this end, we set out to develop novel redox-active molecular systems which could be used as charge storage materials in a promising new generation of organic-based secondary batteries.

1.2 Battery technology

A battery is an energy storage device that consists of two electrodes, connected through an external circuit, which are immersed in an electronically insulating but ionically conducting electrolyte. These devices operate through electrochemical redox processes that occur at the active electrode materials which convert stored chemical energy into electrical energy. The anodic active material is oxidized during battery discharge while the cathodic active material is reduced, resulting in a flow of electrons through the external circuit with overall charge neutrality maintained through the movement of the counter-ions of the electrolyte (Figure 1.1). If the battery is rechargeable (secondary) then this entire process is reversible. The nature of the operation of a battery means that its performance characteristics, particularly in terms of energy and power capabilities, are directly tied to the electrode charge storage materials, and thus many different electrochemical systems have been investigated.[8-10]

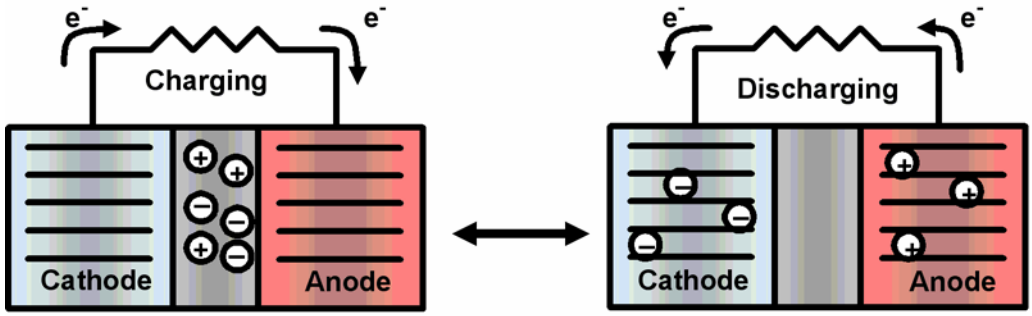

Figure 1.1 Secondary battery operation.

The major commercially available secondary batteries make use of inorganic electrode components for charge storage. The oldest of these devices, still widely used in the automotive industry among other areas, is the lead-acid battery, which uses metallic lead and lead dioxide as anodic and cathodic active components, respectively. Lead-acid batteries are low cost and reliable systems, but are hindered by low energy densities and the toxicity of their lead components.[6] Another early technology still in use is the Ni-Cd battery, which is able to provide exceptional power performance.[6] Other commonly used electrochemical systems are those based on lightweight active materials, such as Ni-MH, Na-$NiCl_2$, and Na-S batteries.[11-13]

The leading edge of secondary battery technology is represented by the lithium-ion battery. These devices were first commercialized on a large scale in the early 1990s, and have since become the major power supplies for portable electronics and are poised for application in zero-emission vehicles. Many different varieties of these batteries have been developed, but their general operation involves the intercalation of lithium ions into and out of graphite-based anodes and lithium metal oxide cathodes. They have been found to provide high power and energy capabilities compared to most other common secondary batteries.[14-17]

While the various forms of inorganic charge storage materials have in general been highly successful in battery applications, many of them have common disadvantages related to cost in materials and processing, availability and environmental impact of heavy metal components, and safety. To address some of these issues, a different approach to battery design recently investigated is the use of organic charge storage materials. This area of research was initiated by the discovery that polyacetylene can be

reversibly oxidized and reduced using *p*- and *n*-type doping, leading to increased conductivity of the polymer upon doping.[18,19] Since then the charge storage properties of many other organic conducting polymers capable of similar reversible doping processes, such as polyaniline, polythiophene, and polypyrrole, have been investigated for both battery and supercapacitor applications.[20,21] Organic materials are appealing for use in such devices not only because they are more environmentally friendly than metal-based electronics, but also because they allow for the design of very lightweight, thin, and flexible devices, with tuning of properties through structural modification.[22,23] These principles were recently demonstrated in the development of a paper battery, in which both electrodes were entirely composed of a cellulose/polypyrrole composite material, which showed very fast charging rates and good charge/discharge cycling durability.[24]

The disadvantages with the use of organic conducting polymers for charge storage are associated with the doping processes that are required for charge and discharge.[22] The levels of doping in the polymers are too low to provide effective energy densities and are not constant, which leads to fluctuating voltages. In addition there can be chemical stability problems associated with the doped polymers that can lead to the degradation of battery performance over time. As a result, organic batteries based on conjugated polymers have not been developed commercially.

1.3 Organic radical batteries

1.3.1 Concept and performance

The organic radical battery (ORB) is a very recent[25] development in secondary battery technology that confers the same benefits associated with the use of organic conducting polymers for charge storage, while effectively eliminating the

disadvantages.[26] ORBs use stable organic polyradicals rather than closed-shell organic polymers, and the charging and discharging processes are based on the rapid and quantitative oxidation and reduction of each radical unit, leading to much higher energy and power densities. The high stabilities of the different oxidation states of the radicals also means that the batteries can be cycled through thousands of charge/discharge cycles with no significant degradation in voltage or capacity. Prototype ORBs that combine composite polyradical/conducting carbon cathodes with graphite anodes (Figure 1.2) have been developed and tested, and have been found to have significantly better power densities than Li-ion batteries, charging times on the order of minutes, and very long cycle lives.[27,28] The design of thin film, flexible, and semi-transparent ORBs has also been demonstrated.[29] There is great potential for the further improvement is ORB performance through new developments in battery and polyradical design, and ORBs are expected to be highly viable as future energy storage devices.[30]

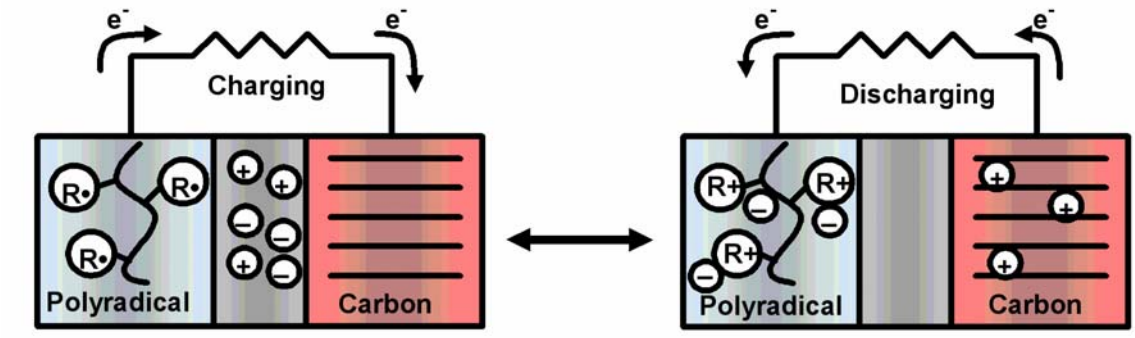

Figure 1.2 ORB charging and discharging using polyradical cathode and graphite anode.[30]

1.3.2 ORB polyradical cathodes

ORB research has to date focussed almost exclusively on the use of nitroxide radicals as the redox active charge storage unit. The two possible redox processes of

nitroxide radicals, oxidation to the oxoammonium cation (*p*-type doping) and reduction to the aminoxy anion (*n*-type doping), are shown in Figure 1.3. Of these two processes, only the oxidation to the cation is typically fast and reversible enough to be applicable to ORB charge storage.[31] As a result, the nitroxide radicals are used almost purely as cathode-active materials whereby the cation represents the charged state and discharge occurs through reduction back to the radical.

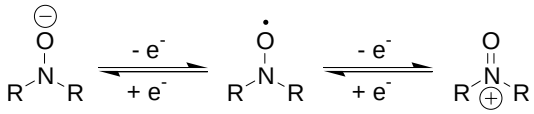

Figure 1.3 Nitroxide radical oxidation and reduction processes.[31]

The radicals used in ORB electrodes are typically appended to saturated polymer backbones as pendant groups. Polymerization is necessary in order obtain low solubility, thus providing good cycling stability by preventing the radicals from leaching into the electrolyte solution.[31] Additionally, it provides amorphous, swollen electrode structures, allowing high counterion mobility for rapid charge and discharge.[30] Due to the insulating nature of the polyradicals, they are generally mixed with conducting carbon to form composite electrodes, and several studies have been devoted to designing composite electrodes with maximized active polyradical content and optimal charge storage properties.[29,32-36] In addition to the polyradical systems, materials in which nitroxide radicals are appended to DNA-lipid complexes[37] or ionic liquids[38] have also been successfully demonstrated to be practical for charge storage in ORB cathodes.

The most commonly used nitroxide radical in ORB research to date has been the 2,2,6,6-tetramethyl-1-piperidinyloxy radical (TEMPO). The initial TEMPO-based polyradical that was investigated and which is commonly referred to for comparison with

other ORB polyradicals is poly(4-methacryloyloxy-2,2,6,6-tetramethylpiperidin-*N*-oxyl) (PTMA, **1.1**).[25,31,39,40] Other TEMPO-based systems that have been investigated include those which incorporate TEMPO into polyacetylene,[41] polynorbornene,[29,41] polyvinylether,[42] poly(7-oxanorbornene),[43] cellulose,[44] DNA,[37] and ionic liquid[38] backbones. Polyradicals containing nitroxide radicals other than TEMPO include poly(nitroxylstyrene)s (*i.e.* **1.2**)[45] and polymers of 2,2,5,5-tetramethyl-1-pyrrolidinyloxy radicals (*i.e.* **1.3**).[46] All of these various materials have been designed for use as cathode active materials, with the structural variations intended to improve factors such as the radical densities within the polymers, charging capacities, and electrode processing and performance.

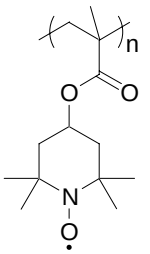

1.1

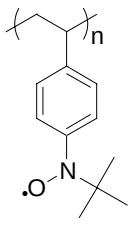

1.2

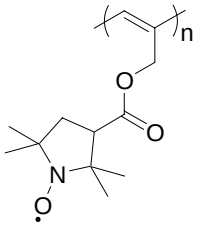

1.3

1.3.3 Challenges in ORB research

One of the main challenges in the further development of ORB technology is the need to improve in the charging capacities of the polyradical electrodes. The charging capacity of a material is a measure of the per mass amount of charge that it can store, and improvements in the charging capacity of an electrode charge storage material led to improvements in the overall energy density of a battery, which is one property that is lower in ORBs than in comparable Li-ion batteries.[30] The theoretical charging capacity of a polyradical can be calculated using Equation 1.1, where *n* is the number of electrons

transferred per monomer unit, F is the Faraday constant (96 485.34 C·mol^{-1}), M is the monomer molecular weight, and the term 1000 / 3600 converts the results to units of mAh·g^{-1}.

$$Capacity = \frac{1000 \times nF}{3600 \times M} \qquad (1.1)$$

The charging capacity can therefore be increased through the use of either lighter radical monomer units (smaller M), or monomers capable of multiple electron transfer processes (larger n). For example, the theoretical charging capacity of **1.1** is 111 mAh·g^{-1},[25] while the more compact polyvinylether **1.4** with a smaller M has the highest theoretical capacity of the TEMPO-based systems, 135 mAh·g^{-1}.[44] More dramatic increases in theoretical charging capacities can be obtained by increasing n, such as in the case of polyradicals **1.5** (174 mAh·g^{-1})[47] and **1.6** (194 mAh·g^{-1})[45] in which the monomer units are diradicals, though these two systems suffer from problems associated with electrochemical instability. In comparison with ORB electrodes, the theoretical capacities of metal-based electrodes are greater than ~140 mAh·g^{-1}.[47]

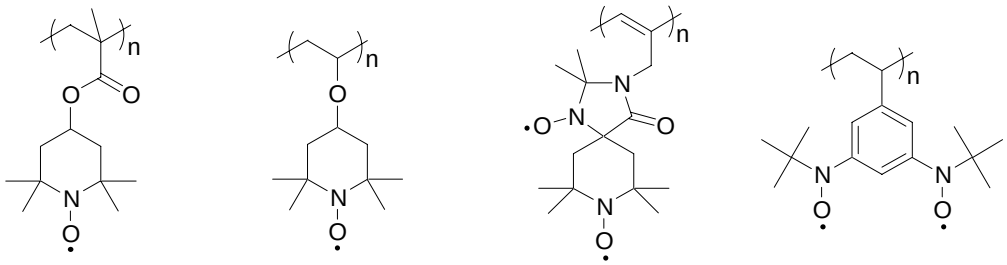

	1.1	**1.4**	**1.5**	**1.6**
***M* (g/mol)**	240.32	198.28	307.39	276.37
n	1	1	2	2
***Capacity* (mAh ·g^{-1})**	111	135	174	194

Figure 1.4 Effect of altering M and n on theoretical charging capacities of polyradicals.

A second major challenge in ORB research is associated with the electrochemical limitations of the nitroxide radical. While many different *p*-dopable nitroxide polyradicals have been highly successful in developing cathodic materials, the lack of a reversible reduction process in these systems prevents them from being used as *n*-dopable anodic materials. It is ultimately desirable to have both *p*- and *n*-type radical materials as this would allow for the development of fully organic radical batteries, in which the cathode is composed of a *p*-dopable organic radical and the anode is composed an *n*-dopable organic radical.

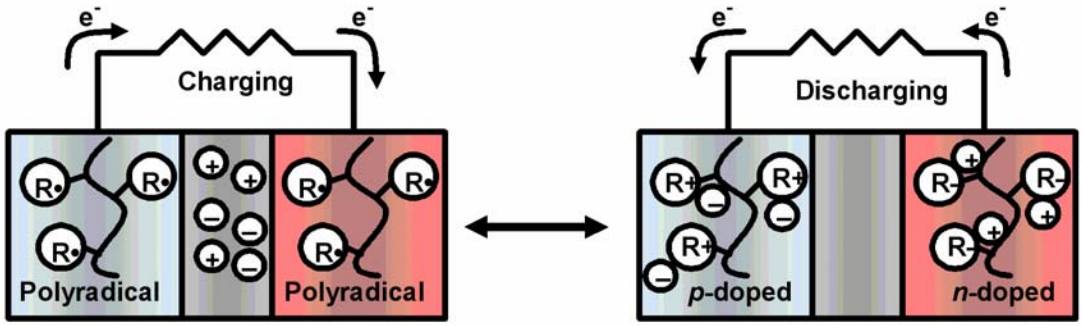

Figure 1.5 Charging and discharging of a fully organic radical battery.[30]

There have been reports on the successful design of entirely organic radical batteries which demonstrate proof of concept. The *n*-dopable anodic materials are composed of a structurally modified nitroxide radical **1.7**[45], with a stabilized and reversible reduction process, or an *n*-dopable galvinoxyl radical **1.8**[48] (Figure 1.6). It is therefore of interest to expand upon the range of available radical systems for ORB application, in order to provide new anodic and cathodic materials for the further development of entirely organic batteries.

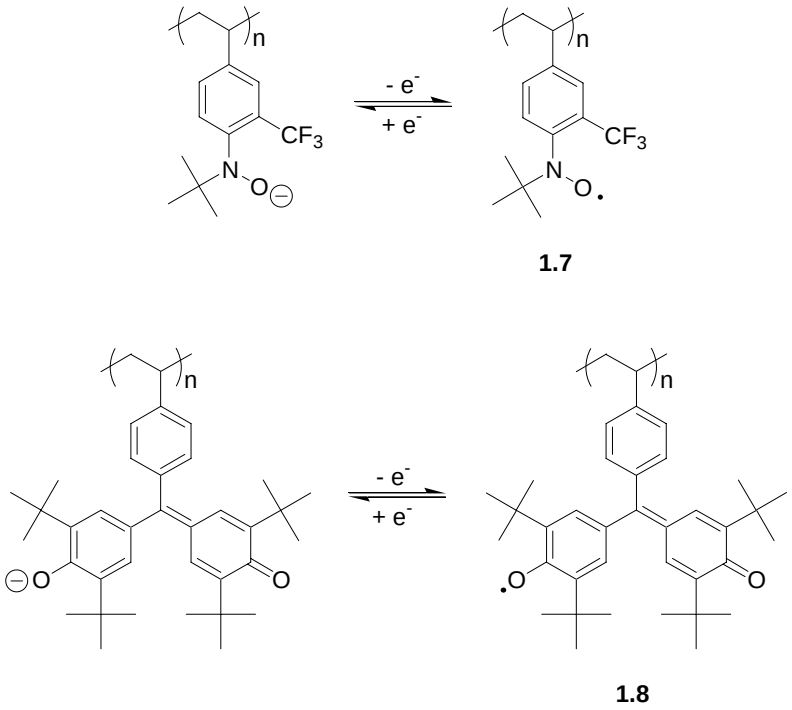

Figure 1.6 *n*-Doping of a modified nitroxide radical (top) and a galvinoxyl radical (bottom).

1.3.4 Thesis goal

To address the challenges facing ORB development, we have investigated a new class of redox-active stable organic radicals for ORB charge storage, the 1,3-diphenyl-1,2,4-benzotriazinyl radical. We were interested in using a radical that was highly electrochemically tunable and versatile, which could lead to potential improvements in electrode charging capacity and could be used as both anodic and cathodic materials.

1.4 The benzotriazinyl radical

1.4.1 Introduction and electrochemistry

Originally discovered in 1968,[49,50] benzotriazinyl radicals are a class of organic radicals that have not been intensively studied. The benzotriazinyl radical is characterized

by an exceptionally high stability which arises from a combination of steric protection and delocalization of the unpaired electron, setting it amongst a limited number of examples of stable organic radicals.[51] Its high stability enables it to be handled under ambient conditions in solution and the solid state using standard organic chemistry techniques, which is important for the design of materials to be used in a charge storage capacity.

The parent radical in the class, and the one that has been studied the most comprehensively, is 1,3-diphenyl-1,2,4-benzotriazinyl (**1.9**).[52-56] Like the nitroxide radical, benzotriazinyl radicals can undergo one-electron oxidation ($E_{1/2}$ = 0.103 V vs SCE) and reduction ($E_{1/2}$ = -0.960 V vs SCE) processes to form a cation and an anion, respectively.[56] Unlike the nitroxide radical however, both of these redox processes are fast and reversible.

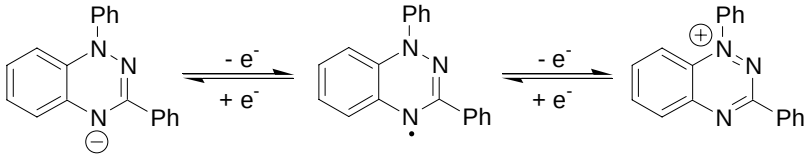

1.9

Figure 1.7 Reversible oxidation and reduction of benzotriazinyl radical **1.9**.

Another aspect of the benzotriazinyl radical that is highly appealing to charge storage applications is that its electrochemistry has been shown to be tunable. Previous work carried out within the Frank group on several halogen-functionalized benzotriazinyl radicals showed that predictable shifts in both the oxidation and reduction processes of the radicals could be obtained upon substitution (Figure 1.8).[57] The oxidation and reduction processes were shifted to more positive potentials relative to those of **1.9** due to

the overall electron withdrawing effects of the halogens, and in all cases both of the redox processes fully retained their reversibility.

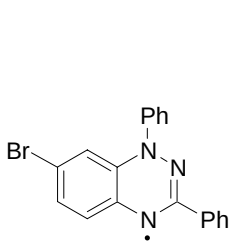

1.10

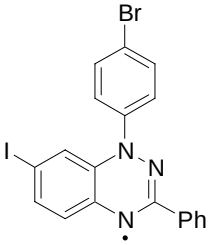

1.11

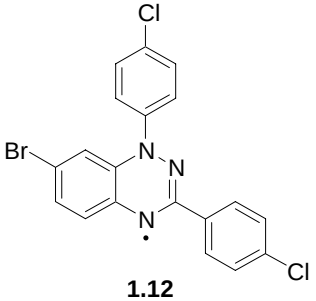

1.12

$E_{1/2(ox)}$ **(V vs SCE)**	0.280	0.329	0.400
$E_{1/2(red)}$ **(V vs SCE)**	-0.746	-0.675	-0.609

Figure 1.8 Functional group effects on the electrochemistry of benzotriazinyl radicals.

Electrochemical tunability is important in the design of electrode charge storage materials because increases in the electrochemical potential between the anode and the cathode of a battery (E_{cell}) lead to increases in the energy and power densities of the battery.[8] In order for a radical to be used as a cathodic material (*p*-doped) it is desirable to have a large positive oxidation potential, while for an anodic material (*n*-doped) it is best to have a large negative reduction potential, thus maximizing E_{cell}. Electrochemical tunability in ORB nitroxide radicals has been explored and is possible, but requires the synthesis of entirely new molecular structures[58] and is therefore not as convenient as simple functional group modification. In order for functional group modification to be considered convenient however, a robust and easily modifiable synthetic methodology for stable radicals is needed.

1.4.2 Synthesis of benzotriazinyl radicals

The traditional synthetic methodology for the parent benzotriazinyl radical **1.9** is through a procedure developed by Neugebauer (Scheme 1.1).[52]

Scheme 1.1 Neugebauer's synthesis of benzotriazinyl radical **1.9**.

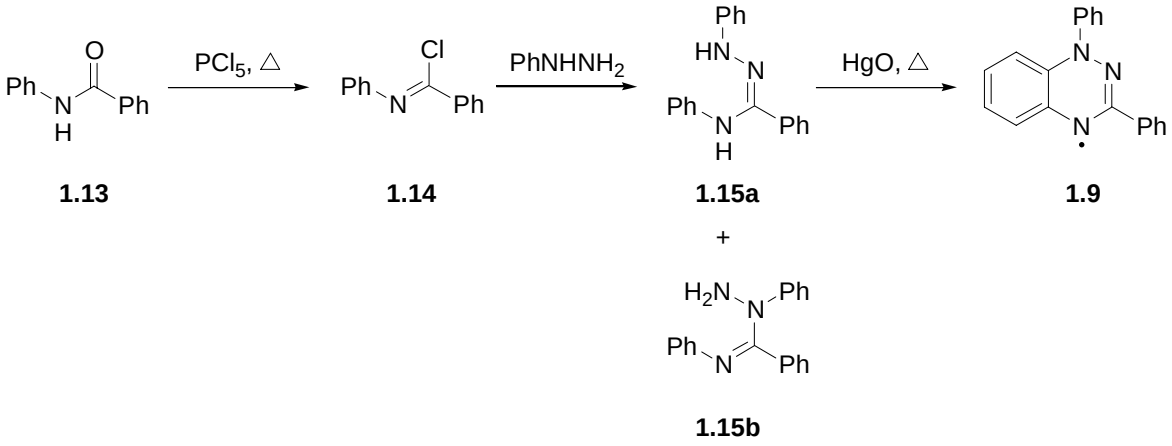

In this synthesis, benzanilide **1.13** is first converted to the benzimidoyl chloride **1.14** through the use of PCl_5.[59] The iminyl-chloride **1.14** is an unstable material and is converted *in situ* to the amidrazone **1.15** by condensation with phenylhydrazine, leading to two the isomers **1.15a** and **1.15b**. Finally, treatment of the amidrazone **1.15a** with oxidative conditions results in ring closure and oxidation to form the radical product, **1.9**, in a 51 % yield. The final ring closure and oxidation step has also been shown to be initiated through the use of acidic[49] or high temperature[61] conditions.

While Scheme 1.1 is successful in the synthesis of **1.9**, previous work in our group found that it was not practical towards the synthesis of functionalized radicals.[57] The instability of the benzimidoyl chloride **1.14** was found to be problematic, and the harsh conditions employed in its generation severely limited the range of accessible functional groups. The overall yield was in addition lowered by the formation of two

isomers of **1.15**, requiring separation or sacrificed yield at this step. Therefore a new synthetic methodology was developed, as shown in Scheme 1.2.

Scheme 1.2 Frank group synthesis of benzotriazinyl radical **1.9**.[57]

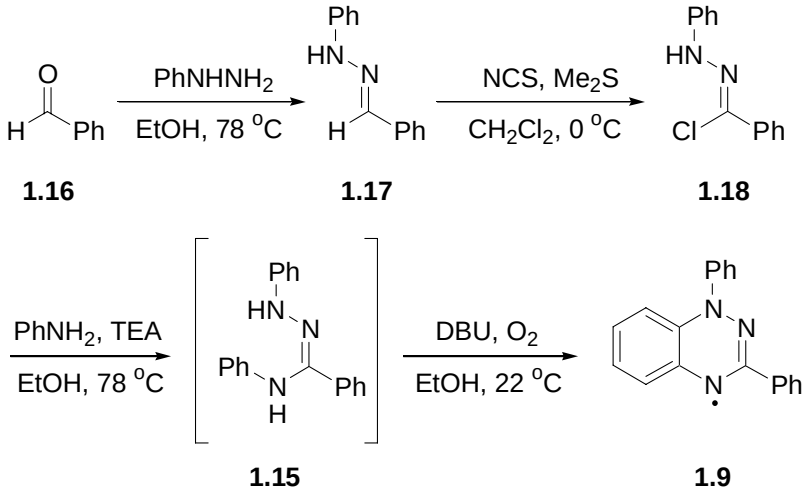

In this modified synthesis, benzaldehyde **1.16** is condensed with phenylhydrazine to yield the phenylhydrazone **1.17** in an 87 % yield. The phenylhydrazone is then chlorinated using a procedure developed by Patel[60] to form the chlorohydrazone **1.18** in a 78 % yield. The chlorohydrazone **1.18** can then be condensed with aniline to give the amidrazone **1.15** in high conversion. The generation of amidrazone **1.15** can be achieved under milder conditions than those employed in Scheme 1.1, and by incorporating stable intermediates that can be easily isolated and purified. *In situ* treatment of **1.15** with 1,8-diazabicyclo[5.4.0]undec-7-ene (DBU) under aerobic conditions then results in slow ring closure and oxidation to form **1.9** over ~24 - 48 hours. It has been demonstrated that this methodology allows for the introduction of a range of different functional groups without modification of the reaction conditions. The modular nature of the synthetic process means that functional groups can be installed at positions in all three of the aromatic rings of the radical through the use of appropriately functionalized starting materials.

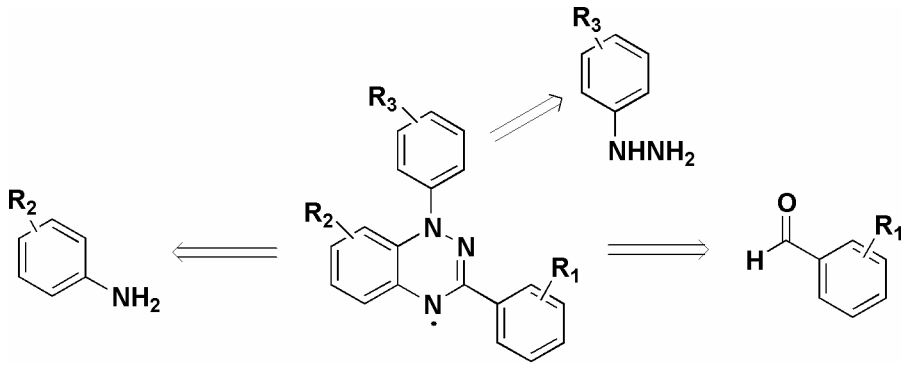

Figure 1.9 Modular construction of functionalized benzotriazinyl radicals.

1.6 Thesis scope and objectives

The electrochemical properties and ease of synthesis of the benzotriazinyl radical make it of great interest for study as an ORB charge storage material. Previous electrochemical studies on the parent radical **1.9** as well as the functionalized radicals **1.10** – **1.12** suggest that it could be used as either an anodic or a cathodic material over a range of tunable potentials.[57] We were therefore interested in the further study of the synthesis and properties of benzotriazinyl radical systems in order to expand upon what is known about this class of radicals. Examination of structure-property relationships, with regards to the effects of structure on the electrochemistry of the radical, would allow for the design of benzotriazinyl radical charge storage materials.

The second chapter of this thesis presents work carried out on the synthesis and solution based spectroscopic and electrochemical characterization of a series of new functionalized benzotriazinyl radicals. The aim of this portion of the thesis project was to examine the effects of electron donating and withdrawing functional groups on the redox potentials of benzotriazinyl radicals, in order to design radicals particularly suited to anodic or cathodic applications.

In the third chapter three new benzotriazinyl biradicals are examined. This area of research was carried out to investigate the potential use of low-solubility oligomeric materials for charge storage. In addition we were interested in designing compounds capable of multiple electron transfer processes, towards the development of high energy density materials. The synthesis and the solution based spectroscopy and electrochemistry of the biradicals are presented and discussed.

Beyond being used as charge storage materials, organic radicals are of interest for a variety of other organic-based electronic devices that take advantage of the solid state properties of the radicals. The investigation of intermolecular interactions between the benzotriazinyl radicals in the solid state is facilitated by analysis of X-ray diffraction data, magnetic behaviour which depends on non-covalent interactions and orbital overlap considerations, and solid-state reflectance data. It is therefore of interest to study these properties in the context of the molecular and crystal packing structures of the radicals in order to develop structure-property relationships. The fourth chapter consists of an examination of the solid state physical properties, both magnetic and conductive, of several of the benzotriazinyl radicals presented in the previous two chapters.

Finally, the fifth chapter presents preliminary studies carried out towards the synthesis of benzotriazinyl pendant polyradicals for direct comparison with the existing ORB nitroxide polyradicals. We were interested in determining whether the benzotriazinyl radical could be successfully incorporated into a saturated polymer backbone as a pendant group, and whether the intrinsic electrochemical properties of the radical were retained. The synthesis, spin content, and solution state spectroscopy and electrochemistry of a possible benzotriazinyl polyradical are discussed.

Chapter 2 Functionalized benzotriazinyl radicals

2.1 Introduction

As discussed in Chapter 1, battery energy and power densities can be increased by increasing the potential difference between the anode and the cathode, and it is therefore useful to be able to design electrode charge storage materials with tunable redox potentials. While it has been shown for benzotriazinyl radicals that halide functional groups can be used to achieve positive shifts in redox potentials,[57] a more comprehensive study of the electrochemistry of functionalized benzotriazinyl radicals has not been carried out. In fact, there are only a handful of literature examples of the synthesis of functionalized benzotriazinyl radicals, and the electrochemical properties of these compounds have not been reported.[52,54,61] We therefore set out to synthesize a new series of functionalized benzotriazinyl radicals bearing both strong electron donating (EDG) and withdrawing (EWG) groups, in order to investigate the effects of the functional groups on the reversibility and the redox potentials of the radical electrochemistry. Additionally, we were interested in studying the effects of functionalization on the spectroscopic properties and the stabilities of benzotriazinyl radicals.

2.1.1 Synthetic design

Unlike closed shell molecules in which oxidation and reduction involve the HOMO and LUMO, respectively, the oxidation and reduction of organic radicals both involve the SOMO of the radical.[62] A shift in the energy of the SOMO can therefore lead to a shift in the electrochemical potentials. Raising or lowering of the SOMO energy can

be accomplished by the functionalization at a position of high electron density in the SOMO.

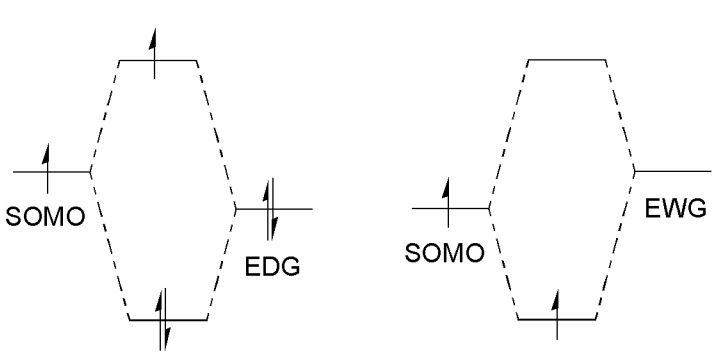

Figure 2.1 The effects of electron donating groups (EDGs) and electron withdrawing groups (EWGs) on the energy of the SOMO.

DFT geometry optimization and electronic structure calculations carried out on **1.9** at the UB3LYP/6-31G(d,p) level can be used to predict the topology and the energy of the SOMO of the radical (Figure 2.2). The SOMO is delocalized over the central benzotriazinyl core and the N1-linked phenyl ring with nodes between positions C5-C6 and C7-C8 of the annelated ring. Functionalization at positions on both the annelated ring and the N1-phenyl ring are therefore predicted to lead to significant electronic effects.

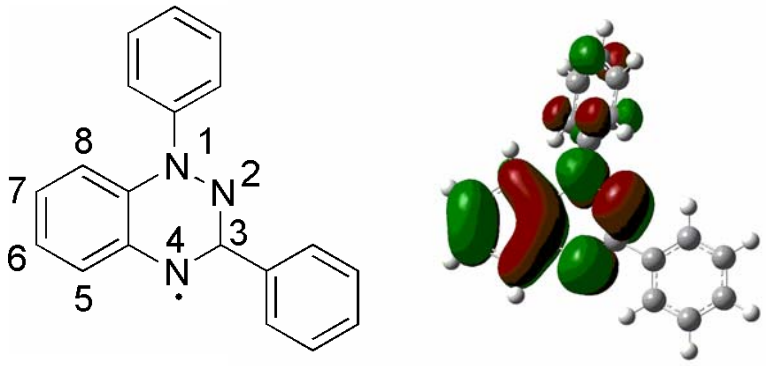

Figure 2.2 SOMO of **1.9** calculated at UB3LYP/6-31G(d,p), generated with isovalue = 0.0004 in GaussView 3.09.

2.1.2 Target compounds

Based on the model of the SOMO of **1.9**, we attempted to synthesize the series of benzotriazinyl radicals **2.1**-**2.10**, where the functional groups were located at positions on the annelated benzene ring and were of both electron withdrawing and donating nature. Of these target radicals, only **2.1**-**2.3** were successfully isolated, and the syntheses and characterization of these compounds will be discussed in Section 2.2 along with the challenges associated with the preparation of radicals **2.4**-**2.8**. The attempted syntheses of radicals **2.9** and **2.10** were found to lead to a new class of closed-shell compounds, which will be discussed separately in Section 2.3.

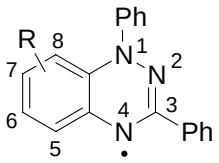

1.9	R = H	**2.6**	R = 5-Cl
2.1	R = 7-Me	**2.7**	R = 5-OH
2.2	R = 7-OMe	**2.8**	R = 5-OMe
2.3	R = 5-NH_2	**2.9**	R = 7-OH
2.4	R = 7-NO_2	**2.10**	R = 6-NH_2
2.5	R = 5-NO_2		

Figure 2.3 Target functionalized benzotriazinyl radicals.

Results and discussion

2.2 Synthesis and properties of functionalized benzotriazinyl radicals

2.2.1 Synthesis

The synthesis of the benzotriazinyl radicals studied in the course of this project followed the general methodology outlined in Scheme 1.2. The first step of the synthesis required the preparation of chlorohydrazone **1.18**.

Scheme 2.1 Synthesis of chlorohydrazone **1.18**.[a]

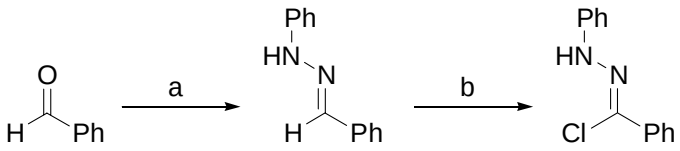

1.16 **1.17** **1.18**

[a]*Reagents and conditions*: a) $PhNHNH_2$, EtOH, 78 °C, 40 minutes, 87 %. b) NCS, Me_2S, CH_2Cl_2, 0 °C, 30 minutes, 78 %.

The condensation of benzaldehyde with phenylhydrazine in refluxing ethanol resulted in the isolation of phenylhydrazone **1.17** as a crystalline solid in 87 % yield. The phenylhydrazone was then chlorinated using the NCS-Me_2S Corey-Kim reagent[63] to form **1.18**, which could be purified and isolated in high yield (78 %) using silica gel flash chromatography. The conditions used for this reaction were slightly modified from those of the literature, which required the addition of **1.17** to a solution of the Corey-Kim reagent at -40 °C and subsequent stirring and slow warming of the reaction to 0 °C over several hours.[60] It was found that by instead carrying out the entire process at 0 °C a much shorter reaction time was achievable, with no reduction in yield. Once **1.18** was prepared the second step of the synthesis could be carried out, which involved the condensation of **1.18** with an aniline derivative to form the desired functionalized radical. Scheme 2.2 describes the general methodology that was applied to the target compounds listed in Figure 2.3.

Scheme 2.2 General synthesis of functionalized benzotriazinyl radicals.[a]

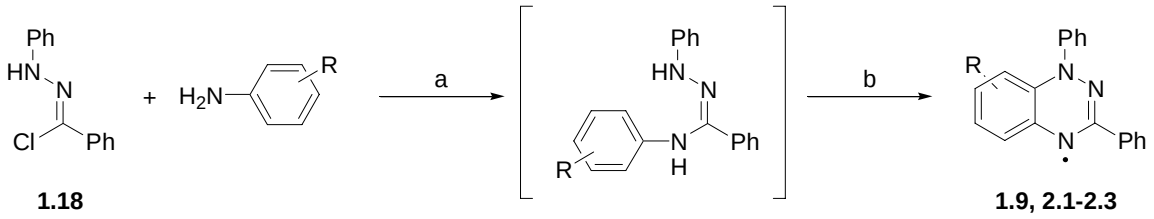

[a]*Reagents and conditions*: a) TEA, EtOH, 78 °C, 5-10 minutes b) DBU, EtOH, 22 °C, 18-48 hours. Final yields of radical based on amount of **1.18** used: 44 % (**1.9**), 45 % (**2.1**), 13 % (**2.2**) 53 % (**2.3**).

The condensation of **1.18** with the aniline derivative resulted in the generation of an amidrazone intermediate. This condensation was carried out by dropwise addition of an ethanolic solution of the chlorohydrazone to a refluxing solution of the aniline and TEA. By using approximately a two-fold excess of aniline and high temperatures, the immediate reaction of the chlorohydrazone with aniline was achieved upon mixing, allowing for reaction completion in 5 – 10 minutes. While it is possible to isolate the amidrazone intermediate, this was not typically done in the course of this work, due primarily to instability of the amidrazones towards silica gel chromatography, leading to decreased yields. Instead the reaction of **1.18** with the aniline was monitored by TLC, until the clean transformation to the amidrazone could be observed. Upon complete conversion of **1.18**, DBU was added to the crude reaction solution which was then stirred under aerobic conditions at room temperature (~ 300 K) for approximately 1-2 days. This resulted in the generation of the radical product, which could be purified using column chromatography in satisfactory yields. Using this methodology, the functionalized radicals **2.1**-**2.3** as well as the parent radical **1.9** were synthesized and isolated. These four radicals were found to be very stable in solution and the solid state, and were

characterized by electronic absorption, EPR, and IR spectroscopy, as well as ESI-MS and elemental analysis.

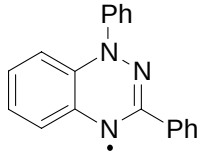

1.9

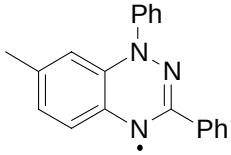

2.1

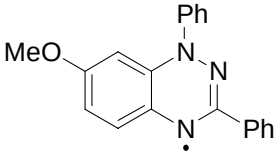

2.2

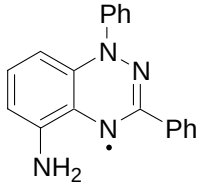

2.3

The methodology of Scheme 2.2 was not found to be successful in the synthesis of the two nitro-functionalized radicals **2.4** and **2.5**. In these cases, clean formation of the amidrazone could be observed by TLC analysis, but treatment with DBU did not result in radical formation to any appreciable amount. Instead of generation of intensely coloured solutions, indicative of radical formation, the reaction solutions remained pale yellow/orange in colour even after several days. Isolation of the major products using column chromatography yielded small amounts of pale yellow oils which, although EPR spectroscopy did show them to contain some paramagnetic material, were predominantly impure mixtures of diamagnetic compounds. It is possible that strong electron withdrawing groups such as the nitro group impede either the ring closure reaction of the amidrazone or final oxidation to form the radical. The only previous benzotriazinyl radical which has been synthesized bearing a nitro group, **2.11**, required refluxing of the precursor compound in EtOH for 5-6 days with no oxidants or for 1-2 days in the presence of the strong oxidizing agents AgO or HgO to achieved radical formation, suggesting that the conditions employed in Scheme 2.2 may have been too mild.[61]

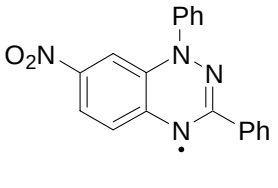

2.4

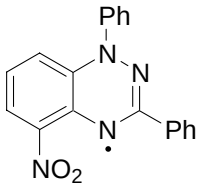

2.5

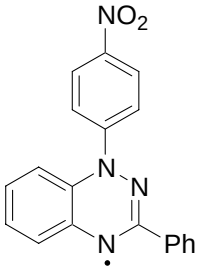

2.11

Challenges arose in the preparation of functionalized radicals **2.6**-**2.8** due to loss of functionality during the ring closure and oxidation step. Unlike for **2.4** and **2.5**, the attempted syntheses of the three *ortho* functionalized radicals **2.6**-**2.8** following Scheme 2.2 did produce dark brown paramagnetic products. Characterization of the products using IR spectroscopy however, yielded spectra that exactly matched that of the parent radical **1.9**. In addition, analysis of the products using ESI-MS revealed loss of functionalization, confirming that the products were in fact simply the parent radical **1.9**. In these cases, it appeared that the functional groups may have acted as leaving groups during the ring closure of their respective amidrazone intermediates, suggesting alternative mechanistic routes for ring closure.

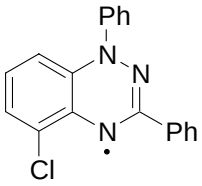

2.6

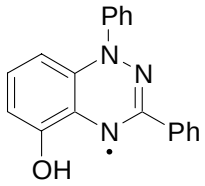

2.7

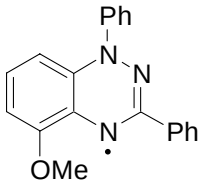

2.8

The active involvement of the functional groups in the ring closure was supported by the observation that upon treatment of the amidrazones with DBU, radical formation occurred significantly faster than normal. For example, in the case of the attempted synthesis of **2.8**, it was possible to isolate the product **1.9** after only 1 hour, compared

with 48 the hours required in the conventional synthesis described above, and in a comparable yield (Scheme 2.3). The only radical that was successfully synthesized with an *ortho* functional group was the amino radical **2.3**, which may have been due to the poor leaving group ability of the NH_2^- anion compared with Cl^-, OH^-, and MeO^-.

Scheme 2.3 Conventional and functional group assisted synthesis of **1.9**.[a]

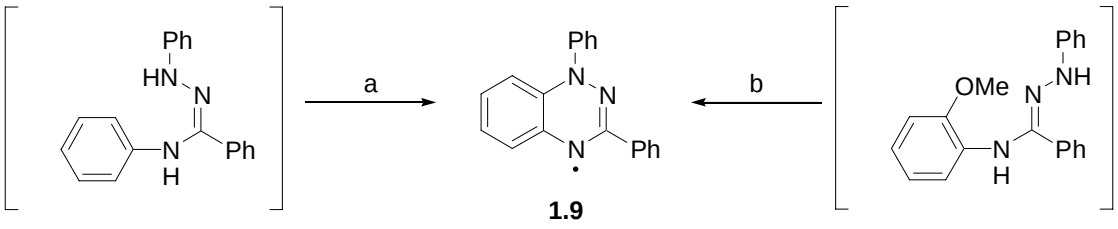

1.9

[a]*Reagents and conditions*: a) DBU, EtOH, 22 °C, 48 hours, 44 % b) DBU, EtOH, 22 °C, 1 hour, 47 %.

Formation of benzotriazinyl radical **1.9** from the amidrazone **1.15** is believed to occur, under oxidative conditions, by the mechanism shown in Figure 2.4. Initial oxidation of the amidrazone is known to lead to formation of the imidrazone **2.12**.[52] Electrocyclic ring closure of the imidrazone, followed by oxidation by atmospheric O_2, is believed to lead to final generation of the radical.

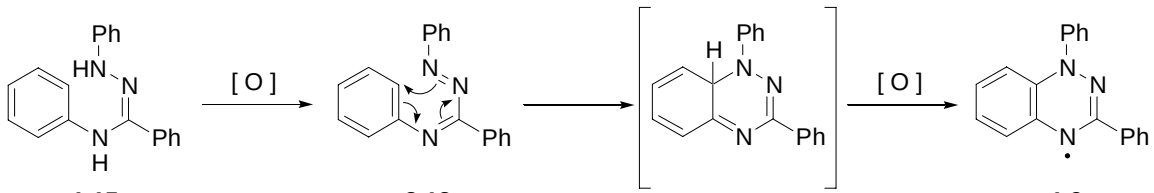

1.15 **2.12** **1.9**

Figure 2.4 Possible mechanism for benzotriazinyl radical formation under oxidative conditions.

The synthetic methodology developed in the Frank group for improved ring closure involves the use of base catalysis with DBU. While the mechanism for this

process is not known, the results for the attempted preparation of radicals **2.6**-**2.8** give significant mechanistic insight. As shown in Figure 2.5, initial deprotonation of **1.15** followed by nucleophilic attack by an $S_{RN}1$ mechanism and subsequent oxidation *via* loss of a hydride would be required for generation of the benzotriazine **2.13**. Alternately, the use of amidrazone **2.14** bearing a leaving group would facilitate the rapid generation of **2.13**. In both cases, oxidation of **2.13** would then occur upon exposure to atmospheric O_2, as has been previously reported,[49] leading to **1.9**. The rapid generation of **2.13** through the use of a leaving group would effectively speed up the rate limiting step, consistent with the observed results.

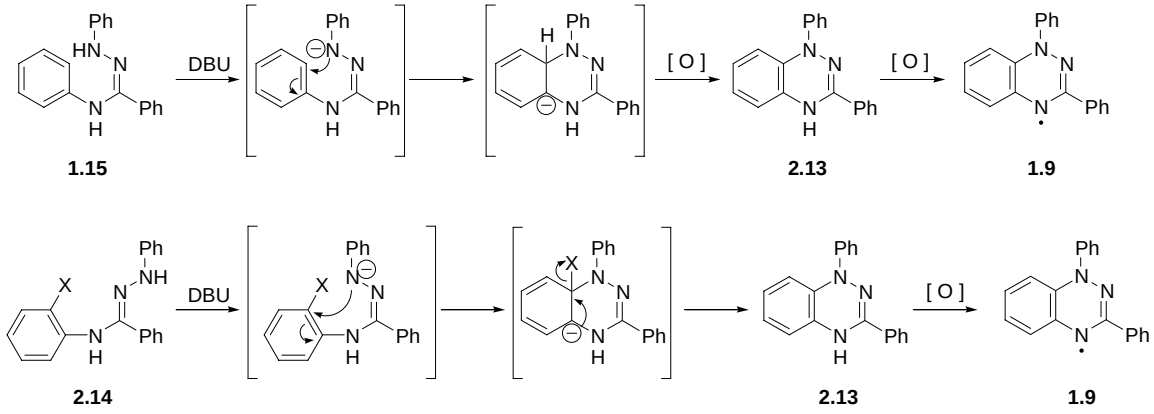

Figure 2.5 Possible mechanisms for base-catalyzed benzotriazinyl radical formation, with a leaving group (bottom) and without a leaving group (top).

2.2.2 Electronic absorption spectroscopy

Electronic absorption spectroscopy of **1.9** and the functionalized radicals **2.1**-**2.3** was carried out in order to investigate the effect of the functional groups on the electronic structure of the benzotriazinyl radicals. The spectra of **1.9**, **2.1**, and **2.2** are compared in Figure 2.6.

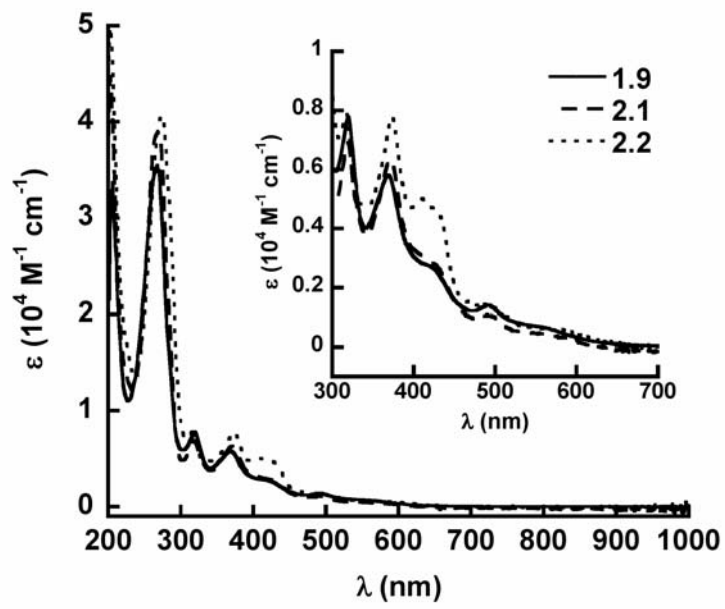

Figure 2.6 Electronic absorption spectra of **1.9**, **2.1**, and **2.2** in MeOH at 298 K.

Table 2.1 Absorption data for radicals **1.9** and **2.1** - **2.3**.

	λ_{max} (ε)[a]					
1.9	206 (3.4)	269 (3.5)	319 (0.8)	369 (0.6)	420 (0.3)	491 (0.1)
2.1	203 (4.5)	269 (3.9)	319 (0.7)	372 (0.6)	430 (0.3)	495 (0.1)
2.2	204 (5.0)	273 (4.1)	317 (0.8)	373 (0.5)	428 (0.5)	498 (0.1)
2.3	205 (4.3)	239 (2.6)	298 (2.2)	320 (1.4)	586 (0.1)	676 (0.1)

[a] λ_{max} in nm, $\varepsilon \times 10^4$ M^{-1} cm^{-1}.

The electronic absorption spectrum of the parent radical was found to be consistent with the literature.[52] The spectrum consists of π-π* transitions in the UV region (λ_{max} = 268 nm, 320 nm, 369 nm), as well as several low intensity transitions throughout visible region due to HOMO-SOMO and SOMO-LUMO transitions (λ_{max} = 420 nm, 491 nm, 550 nm), with tailing absorbance out to approximately 650 nm. The multiple transitions in the visible region lead to the dark brown/black colour in the solid

state, and an orange/brown colour in solution. As shown in Table 2.1, the methyl- and methoxy-functionalized radicals **2.1** and **2.2** have almost identical spectra as the parent radical with only minor bathochromic shifts in λ_{max}, indicating only minor perturbations of the electronic structures due to these functional groups.

In constrast with **2.1** and **2.2**, the amino-functionalized radical **2.3** has a significantly different electronic absorption spectrum than that of **1.9**, indicating a large changes in the electronic structure of the radical (Figure 2.7). The dominant feature of the spectrum is a very broad, low intensity transition from approximately 500-800 nm, consistent with the very deep blue colour of the radical in solution and the solid state. TD-DFT (UB3LYP/6-31G(d,p)) calculations suggest that the transitions in this region are dominanted by HOMO-SOMO and SOMO-LUMO.

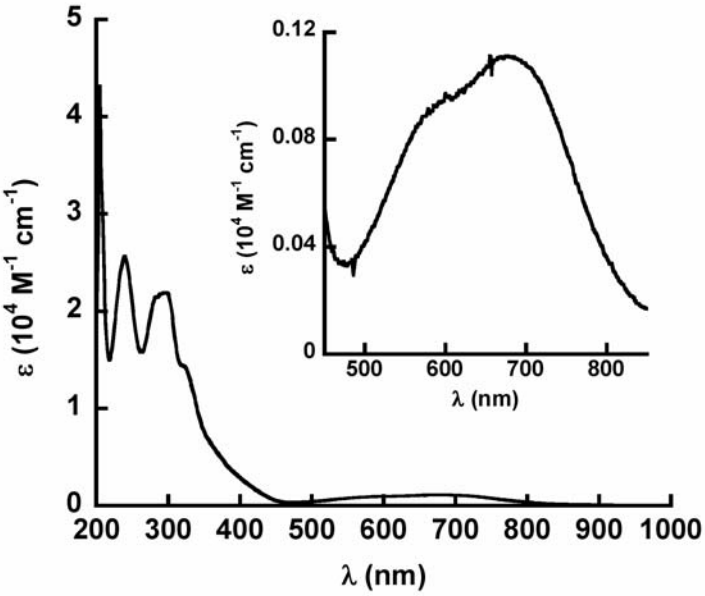

Figure 2.7 Electronic absorption spectrum of **2.3** in MeOH at 298 K.

2.2.3 EPR spectroscopy

This section presents the EPR spectra of radicals **1.9** and **2.1**-**2.3**, as well as the corresponding hyperfine coupling constants and spin densities. EPR spectroscopy was used to determine the impact of the functional groups on the distributions of the unpaired electron across the radical structures. The experimental coupling constants to the nitrogen and hydrogen atoms were determined through simulation of the EPR spectra, though couplings to the hydrogen atoms of the two phenyl rings of the radicals were not included in the simulation parameters as they had been previously determined to be minor relative to the couplings within the central benzotriazinyl ring system.[52] The experimental spin densities were calculated using the McConnell equation[64] (Equation 2.1) where a is the measured hyperfine coupling constant, Q is a semiempirical proportionality constant (28.6 G for the N atoms, and -27 G for the H atoms),[52,65] and ρ is the spin density.

$$a = Q\rho \qquad (2.1)$$

The EPR spectrum of **1.9** shows a seven line splitting pattern (2nI + 1) consistent with hyperfine coupling of the unpaired electron with all three (n = 3) of the nitrogen atoms (I = 1) in the molecule, with weaker superhyperfine coupling to the hydrogen atoms of the benzene ring of less than 1 G leading to broadening of the resonance (Figure 2.9). Previous reports in the literature have used isotopic substitution,[52,53] as well as ENDOR experiments,[61] to measure and assign the hyperfine coupling constants of the unpaired electron to all of the nitrogen and hydrogen atoms in **1.9**. The assignments of the hyperfine coupling constants of **1.9** measured in this study were therefore made by comparison with the literature, and were found to be in good agreement as shown in Table 2.2. Table 2.2 also lists for comparison the spin densities that were calculated using

DFT from a geometry optimization at the UB3LYP/6-31G(d,p) level, and it can be seen that there are significant discrepancies between the calculated and experimental spin densities. The DFT calculations place the spin densities on the protons of the benzene ring an order of magnitude lower than their experimental values, and the spin densities of N2 and N4 at almost twice their experimental values. In effect, the DFT calculations predict a preference for resonance structures **1.9a** and **1.9b** over **1.9c**, while the unambiguous experimental assignments of the hyperfine coupling constants in the literature suggest a greater contribution from **1.9c**.

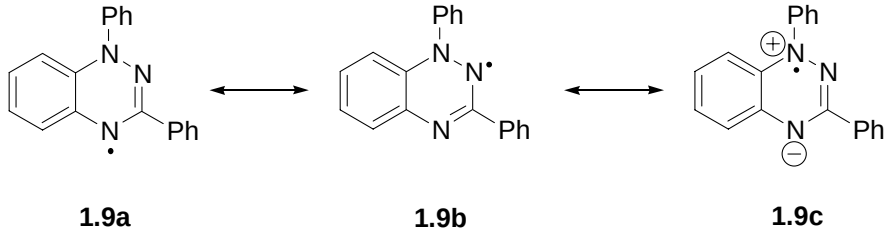

1.9a **1.9b** **1.9c**

Figure 2.8 Resonance structures of **1.9**.

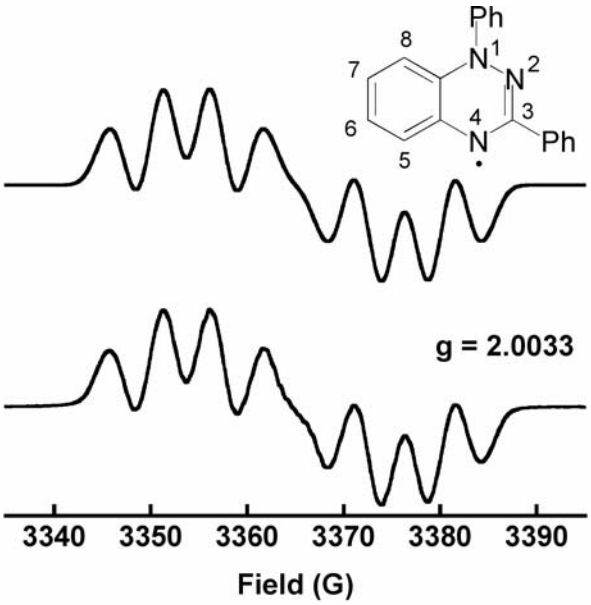

Figure 2.9 EPR spectrum of **1.9** in degassed toluene at 298 K (bottom), and simulated spectrum (top).

Table 2.2 Hyperfine coupling constants (a) and spin densities (ρ) of **1.9**.

Atom	a_{exp} (G) [a]	a_{lit} (G) [b]	$\lvert\rho_{exp}\rvert$ [c]	$\lvert\rho_{lit}\rvert$ [b]	$\lvert\rho_{comp}\rvert$ [d]
N1	7.5	7.5	0.26	0.26	0.262
N2	5.0	5.1	0.17	0.18	0.300
N4	4.9	5.1	0.17	0.18	0.320
H5	1.4	1.4	0.05	0.05	0.003
H6	1.3	1.1	0.05	0.04	0.001
H7	1.6	1.9	0.06	0.07	0.004
H8	0.7	0.8	0.03	0.03	0.001

[a]Experimentally determined coupling constants. [b]Literature values.[52] [c]Experimental spin densities calculated using Equation 2.1. [d]Spin densities calculated using DFT at UB3LYP/6-31G(d,p).

The following three pages present the experimental and simulated EPR spectra of the functionalized radicals **2.1**-**2.3**, as well as the corresponding coupling constants and spin densities. The assignments of the experimentally determined coupling constants and spin densities for each of the atoms were made through comparison with the assignment for **1.9**. The computationally determined spin densities have also been included for comparison, although they show the same discrepancies with the experimental results as for the parent radical **1.9**, suggesting the poor predictability of DFT for these delocalized radicals.

From the coupling constants obtained for all three functionalized radicals, it is evident that the unpaired electron is delocalized onto the functional groups. In the case of **2.1** and **2.3**, the spin density distribution onto the methyl and methoxy groups, respectively, does not significantly reduce the spin density present on the nitrogen atoms or protons of the benzene ring, relative to **1.9**. In the case of **2.3** on the other hand, there is a distinct reduction of the spin density in the annelated ring due to spin delocalization onto the amino group, with little perturbation of the spin densities of N1, N2, and N4 of the central triazinyl ring.

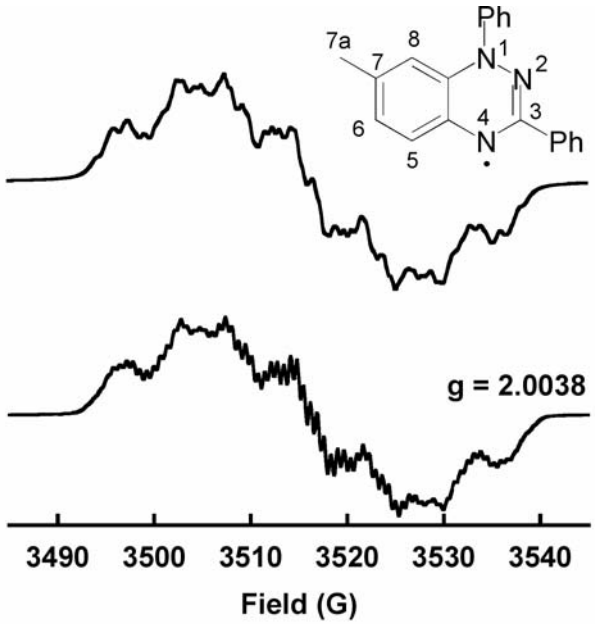

Figure 2.10 EPR spectrum of **2.1** in degassed toluene at 298 K (bottom), and simulated spectrum (top).

Table 2.3 Hyperfine coupling constants (a) and spin densities (ρ) of **2.1**.

Atom	a_{exp} (G) [a]	$\lvert\rho_{exp}\rvert$ [b]	$\lvert\rho_{comp}\rvert$ [c]
N1	7.4	0.26	0.257
N2	4.9	0.17	0.300
N4	4.9	0.17	0.321
H5	1.4	0.05	0.003
H6	1.4	0.05	0.002
H7a	1.7	0.06	0.002
H8	0.8	0.03	0.001

[a]Experimentally determined coupling constants. [b]Experimental spin densities calculated using Equation 2.1. [c]Spin densities calculated using DFT at UB3LYP/6-31G(d,p).

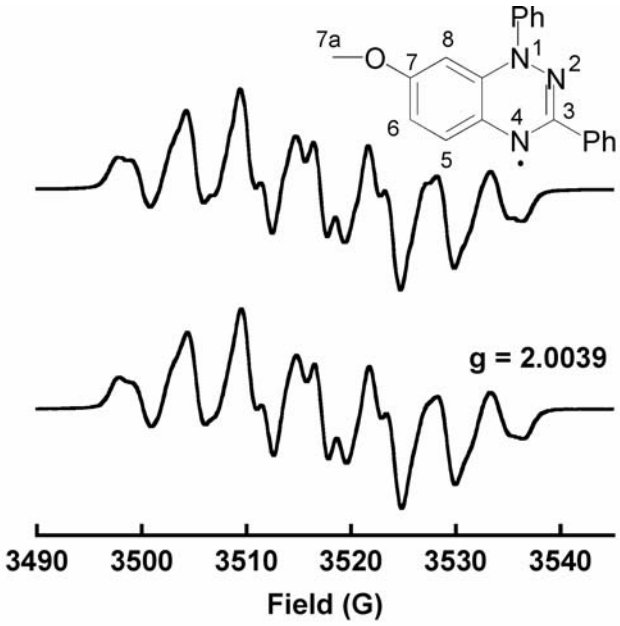

Figure 2.11 EPR spectrum of **2.2** in degassed toluene at 298 K (bottom), and simulated spectrum (top).

Table 2.4 Hyperfine coupling constants (a) and spin densities (ρ) of **2.2**.

Atom	a_{exp} (G) [a]	$\lvert\rho_{exp}\rvert$ [b]	$\lvert\rho_{comp}\rvert$ [c]
N1	6.9	0.24	0.239
N2	5.1	0.18	0.312
N4	5.1	0.18	0.325
H5	1.7	0.06	0.004
H6	1.6	0.06	0.003
H7a	0.6	0.02	0.001
H8	0.6	0.02	0.000

[a]Experimentally determined coupling constants. [b]Experimental spin densities calculated using Equation 2.1. [c]Spin densities calculated using DFT at UB3LYP/6-31G(d,p).

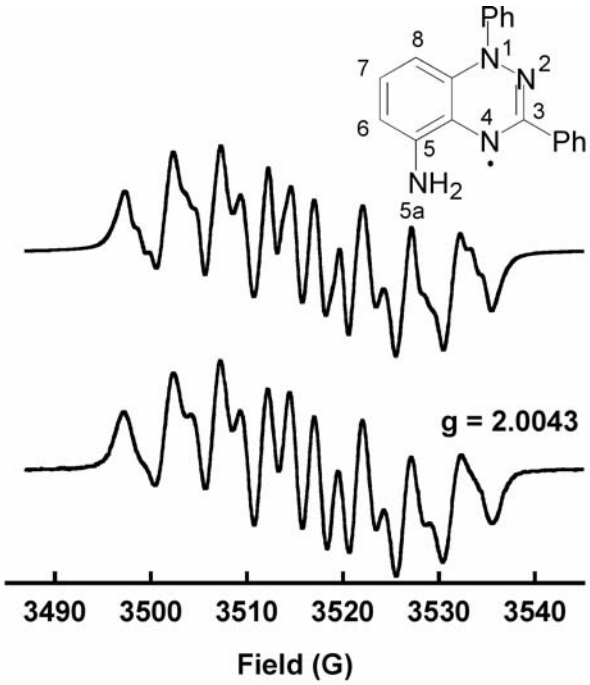

Figure 2.12 EPR spectrum of **2.3** in degassed toluene at 298 K (bottom), and simulated spectrum (top).

Table 2.5 Hyperfine coupling constants (a) and spin densities (ρ) of **2.3**.

Atom	a_{exp} (G) [a]	$\lvert\rho_{exp}\rvert$ [b]	$\lvert\rho_{comp}\rvert$ [c]
N1	7.4	0.26	0.256
N2	5.1	0.18	0.293
N4	4.7	0.16	0.327
N5a	1.3	0.05	0.025
H5a	0.3	0.01	0.001
H6	0.7	0.02	0.001
H7	0.8	0.03	0.004
H8	0.6	0.02	0.001

[a]Experimentally determined coupling constants. [b]Experimental spin densities calculated using Equation 2.1. [c]Spin densities calculated using DFT at UB3LYP/6-31G(d,p).

2.2.4 Electrochemistry

Cyclic voltammetry carried out on the parent radical **1.9** shows the oxidation of the radical occurring at 0.20 V vs SCE and the reduction occurring at -0.83 V vs SCE (Figure 2.13). While these values are both approximately 0.1 V more positive than the literature oxidation and reduction potentials (Section 1.4.1), they are consistent with previous measurements of **1.9** carried out using the same voltammetric analyzer.[57] All of the electrochemical potentials of the functionalized benzotriazinyl radicals that will be discussed in this section will therefore be compared with the potentials of **1.9** that were measured in this work instead of with the literature values, in order to maintain internal consistency.

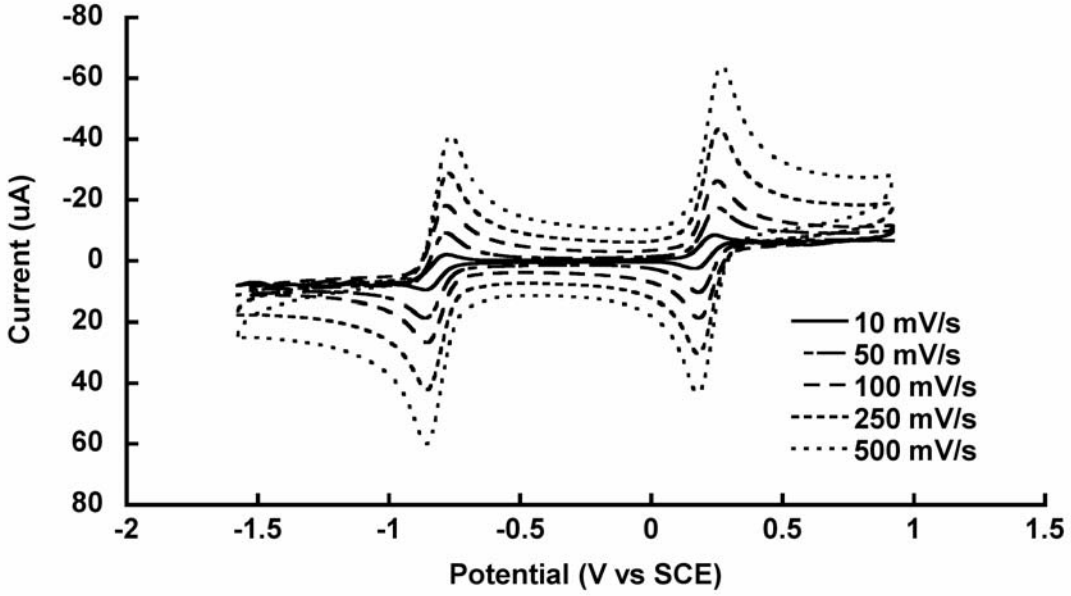

Figure 2.13 Cyclic voltammograms of **1.9** in MeCN with 0.1 M $[Bu_4N][PF_6]$ supporting electrolyte, glassy carbon working electrode, silver reference electrode, platinum counter electrode, 10 – 500 mV/s scan rates.

The peak-to-peak separations (ΔE_p) of the anodic and cathodic waves of both of the electrochemical processes of **1.9** are ~70 mV at a scan rate of 100 mV/s, which is

very close to the ΔE_p value of 59 mV characteristic of fully reversible Nernstian electrochemistry. In addition, the ΔE_p values do not increase with increasing scan rates, consistent with fast and reversible electron transfer processes.[66]

The cyclic voltammograms of radicals **2.1**-**2.3** are displayed in Figure 2.14. As with radical **1.9**, all three of the functionalized radicals show the expected reversible one-electron oxidation and one-electron reduction processes characteristic of benzotriazinyl radicals. In all three cases both the oxidation and reduction potentials exhibit cathodic shifts relative to those of **1.9**, with the shifts being larger for **2.2** and **2.3** than for **2.1** (Table 2.6). The electrochemical E_{cell} values, or disproportionation energies, for the radicals **1.9** and **2.1**-**2.3** are all roughly the same, with the values for the functionalized radicals slightly lower than that of the parent radical. This is consistent with a small amount of extra delocalization of the unpaired electron onto the functional groups.

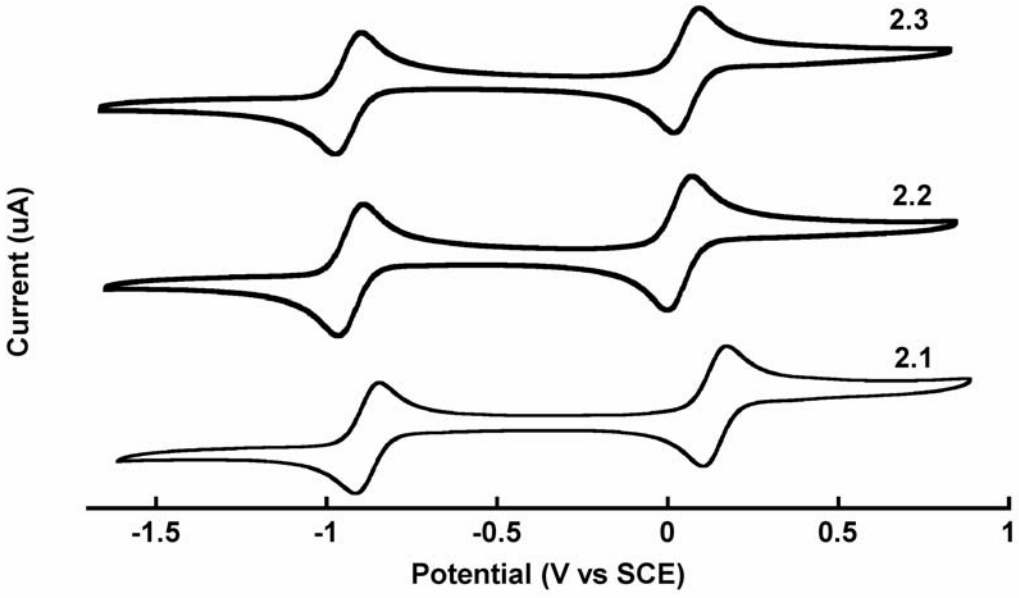

Figure 2.14 Cyclic voltammograms of radicals **2.1**-**2.3** in MeCN with 0.1 M $[Bu_4N][PF_6]$ supporting electrolyte, glassy carbon working electrode, silver reference electrode, platinum counter electrode, 100 mV/s scan rate.

Table 2.6 Electrochemical data of **1.9** and **2.1**-**2.3**. $E_{1/2}$ in V vs SCE and E_{cell} in V.

	$E_{1/2(ox)}$[a]	$E_{1/2\ (red)}$[a]	E_{cell}[b]
1.9	0.20	-0.83	1.03
2.1	0.14	-0.88	1.01
2.2	0.05	-0.91	0.96
2.3	0.07	-0.92	0.99

[a]$E_{1/2}$ calculated as the average of the peak potentials of the anodic and cathodic waves of the electrochemical process. [b]$E_{cell} = |E_{1/2(ox)} - E_{1/2(red)}|$.

The cathodic shifts in the redox potentials of **2.1**-**2.3** relative to those of **1.9** indicate that the functionalized radicals are easier to oxidize and harder to reduce than the parent radical, more so for **2.2** and **2.3** than for **2.1**. This trend can be correlated to the trend in the energies of the SOMOs of the radicals as calculated by DFT (Table 2.7). The SOMO energy of **2.1** is slightly higher than that of **1.9** while the energies of **2.2** and **2.3** are raised to a greater extent, consistent with the electrochemical data and with the relative electron donating abilities of the three functional groups. In this respect the methyl group can be considered weakly inductively donating while the methoxy and amino groups can be considered to be strong resonance donors. Therefore, it can be seen that the trends in the redox potentials of the radicals can be attributed to predictable functional group effects, based on well-understood inductive and resonance effects.

Table 2.7 Trends in SOMO energies of **1.9** and **2.1**-**2.3**.[a]

	1.9	**2.1**	**2.2**	**2.3**
E_{SOMO} (eV)	-4.46	-4.35	-4.30	-4.30

[a]Calculated by DFT at UB3LYP/6-31G(d,p) level.

These results provide the first demonstrations of the ability to cause a negative shift in the redox potentials of benzotriazinyl radicals using electron donating groups, making the radicals easier to oxidize and harder to reduce. As for radical **1.9**, the ΔE_p values of all of the electrochemical processes of the three functionalized radicals are ~70 mV and are independent of scan rate, confirming that the electron transfer processes of these radicals are also fast and highly reversible. When these results are combined with the previously measured redox potentials of halide functionalized benzotriazinyl radicals (Section 1.4.1), the electrochemical versatility of the benzotriazinyl radical be seen. The oxidation potentials have now been measured to range from 0.05 (**2.2**) to 0.40 (**1.12**) V vs SCE, a range of 0.35 V, while the reduction potentials can range from -0.92 (**2.3**) to -0.61 (**1.12**) V vs SCE, a range of 0.31 V, all the while maintaining reversibility at both extremes. These ranges in the electrochemical potentials are larger than those found in related series of functionalized nitroxide radicals[67] and π-delocalized heterocyclic verdazyl[68] and thiazyl radicals,[69] which reflects the particularly strong interaction of the functional groups with the SOMO of the benzotriazinyl radical.

2.3 Synthesis and properties of benzotriazine iminoquinones

An additional consideration to the effects of functional groups on the electrochemistry of benzotriazinyl radicals is the effect of substitution on the stability of the radicals. While the parent benzotriazinyl radical is a very stable compound, it was previously reported that when left exposed to oxygen for long periods of time an oxidative side product can form, which was isolated and identified by ^{1}H-NMR spectroscopy as the closed shell iminoquinone **2.15** (Scheme 2.4).[52] This oxidative degradation pathway of **1.9** was found to be very minor however (5 % yield isolated after

stirring a solution of **1.9** under air for one week), and it typically does not pose a significant problem in handling the radical, or with solid-state stabilities.

Scheme 2.4 Oxidation of **1.9** in air.

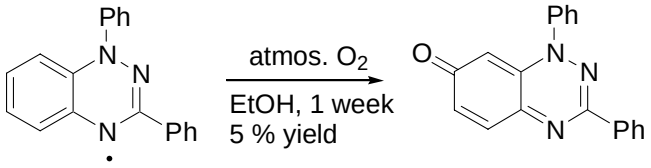

1.9 **2.15**

On the other hand, we found that the use of certain functional groups can destabilize the radical towards formation of the closed shell iminoquinone. In attempting to synthesize radicals **2.9** and **2.10**, the benzotriazine iminoquinones **2.15** and **2.16** were isolated exclusively.

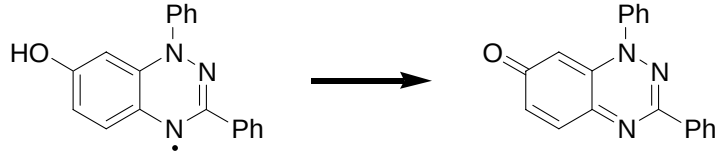

2.9 **2.15**

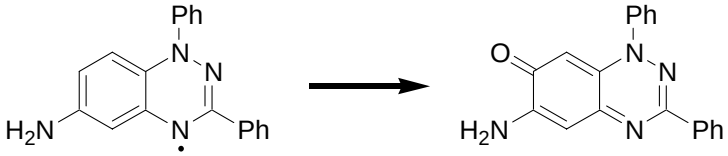

2.10 **2.16**

Figure 2.15 Functional group-assisted formation of benzotriazine iminoquinones.

2.3.1 Synthesis

Attempts to synthesize **2.9** and **2.10** using the standard DBU-mediated ring closure of Scheme 2.2 resulted in a broad product distribution without significant isolation of radicals **2.9** or **2.10**. By changing to oxidative ring-closure conditions however (AgO or atmospheric oxygen), much cleaner reactions resulted and it was possible to isolate the

major products of the the reaction mixtures as **2.15** and **2.16**, without obvious formation of the corresponding radicals (Scheme 2.5).

Scheme 2.5 Synthesis of benzotriazine iminoquinones **2.15** and **2.16**.[a]

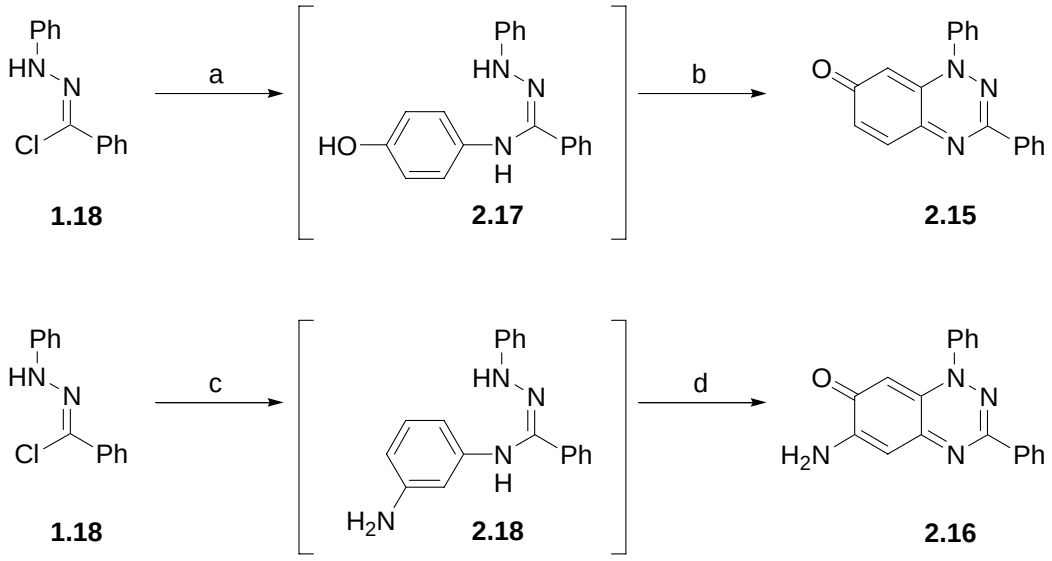

[a] *Reagents and conditions*: a) 4-aminophenol, TEA, EtOH 78 °C, 5 minutes b) AgO, EtOH 22 °C, 48 hours, 40 % yield from **1.18**. c) 1,3-diaminobenzene, TEA, EtOH, 78 °C, 5 minutes d) 22 °C, EtOH, 48 hours, 29 % yield from **1.18**.

In the syntheses of **2.15** and **2.16**, a solution of chlorohydrazone **1.18** in ethanol was added to a refluxing solution of TEA and either 4-aminophenol or 1,3-diaminobenzene in ethanol to quickly form the respective amidrazone intermediates **2.17** and **2.18**, as determined by TLC analysis. AgO was then added to the solution of crude **2.17**, which went on to form the dark purple iminoquinone **2.15** after stirring at room temperature for two days. The crude solution of **2.18** on the other hand could be simply stirred in the presence of atmospheric oxygen for two days at room temperature to form the bright orange iminoquinone **2.16**. The ability to form **2.16** under milder oxidizing conditions than those used to form **2.15** is most likely a result of the strong electron donating effect of the amino group *ortho* to the site of oxidation in **2.16**.

2.3.2 Spectroscopic characterization

The closed shell nature of **2.15** and **2.16** was confirmed by the clean and non-broadened NMR spectra acquired for both compounds. The loss of aromaticity in the annelated rings of these compounds can be seen in their ^{1}H-NMR spectra through the appearance of alkene protons, while the presence of a ketone in both compounds is confirmed through observation of resonances at 182.10 and 172.62 ppm in the ^{13}C-NMR spectra of **2.15** and **2.16**, respectively, typical for α-β unsaturated ketones. Infrared spectroscopy was also used to confirm the presence of the conjugated ketones in both compounds, with C=O stretching bands appearing at 1621 cm^{-1} for **2.15** and 1634 cm^{-1} for **2.16**.

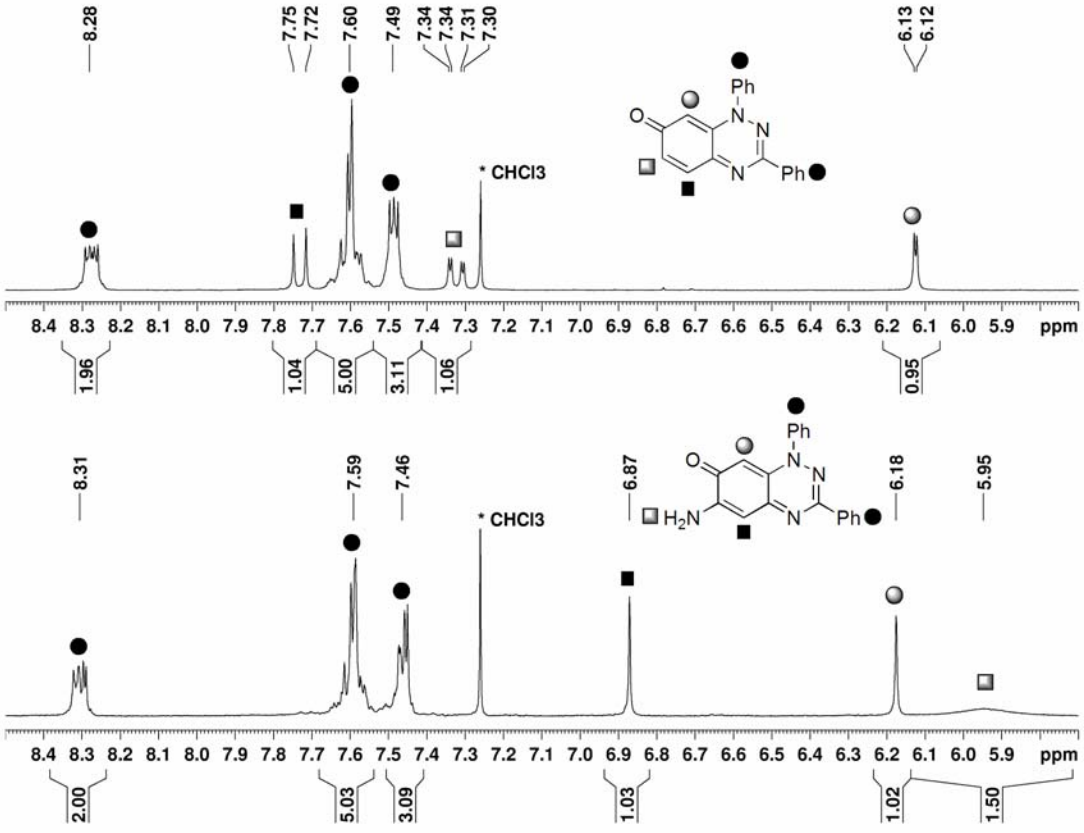

Figure 2.16 ^{1}H-NMR spectra of **2.15** (top) and **2.16** (bottom) in $CDCl_3$.

The electronic absorption spectra of **2.15** and **2.16** are quite different than those of benzotriazinyl radicals. Compound **2.15** has three strong absorbances in the ultraviolet region (λ_{max} = 202 nm, 298 nm, and 330), and one broad, lower intensity absorbance in the visible region (λ_{max} = 542 nm) resulting in a very deep purple colour in both solution and the solid state. Compound **2.16** has ultraviolet absorptions similar to **2.15** (λ_{max} = 202 nm and 284 nm), and an intense transition in the visible region (λ_{max} = 425 nm), with a lower intensity shoulder at approximately 560 nm, resulting in an intense orange colour in both solution and the solid state.

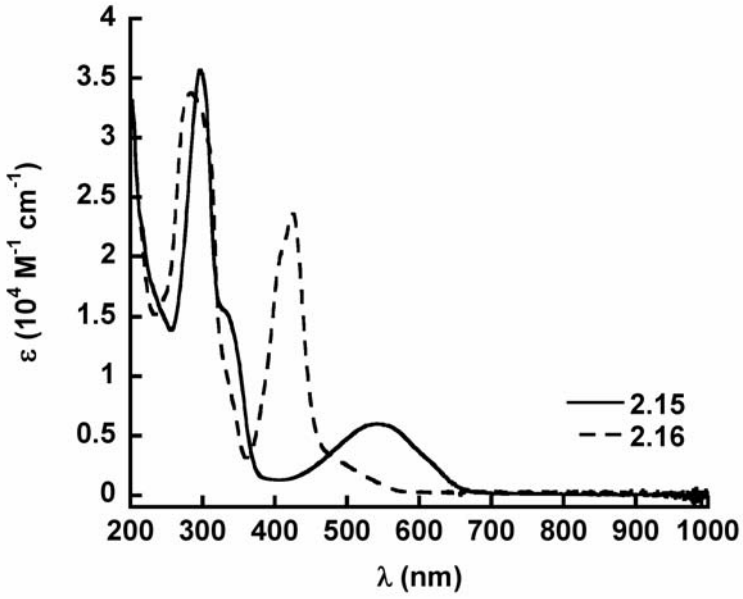

Figure 2.17 Electronic absorption spectra of compounds **2.15** and **2.16** in MeOH at 298 K.

2.3.3 Electrochemistry

The cyclic voltammograms of **2.15** and **2.16** are shown in Figure 2.18. Unlike benzotriazinyl radicals, the benzotriazine iminoquinones were found to have irreversible oxidation processes and two successive reversible one-electron reduction processes (Table 2.8). As with the benzotriazinyl radicals, a functional group effect can be seen in

comparing the reduction potentials of the two iminoquinones, with a cathodic shift in the potentials of **2.16** relative to those of **2.15** due to the presence of the amino group of **2.16** making the compound more electron-rich and therefore harder to reduce.

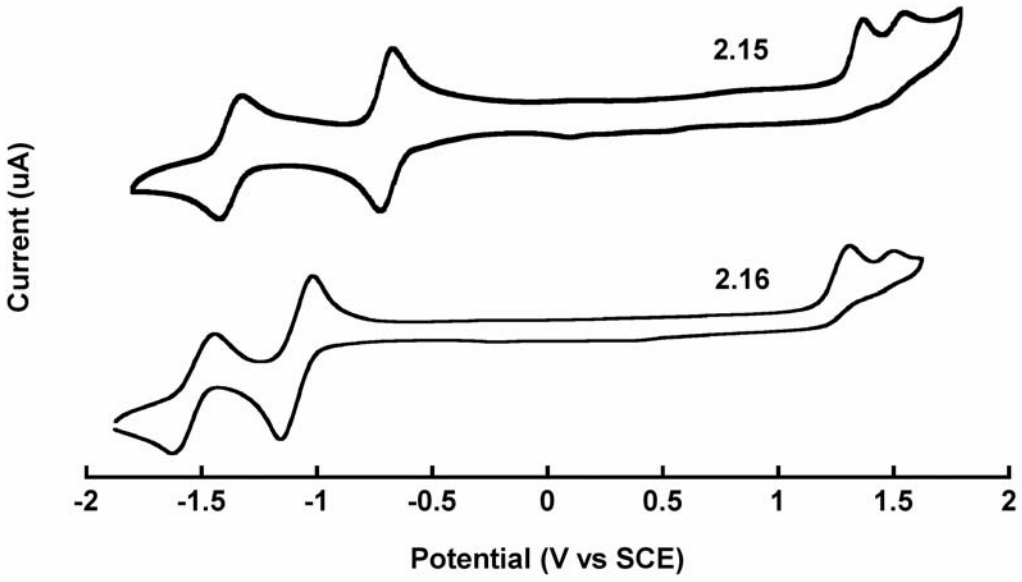

Figure 2.18 Cyclic voltammograms of **2.15** in MeCN and **2.16** in CH_2Cl_2 with 0.1 M $[Bu_4N][PF_6]$ supporting electrolyte, glassy carbon working electrode, silver reference electrode, platinum counter electrode, 100 mV/s scan rate.

Table 2.8 Electrochemical data of **2.15** and **2.16**. $E_{1/2}$ in V vs SCE, ΔE_p in mV, and E_{cell} in V.

	$E_{1/2(red1)}$ [a]	ΔE_p [b]	$E_{1/2(red2)}$ [a]	ΔE_p [b]	E_{cell} [c]	$E_{an(ox1)}$ [d]	$E_{an(ox2)}$ [d]
2.15	-0.72	60	-1.37	100	0.65	1.38	1.56
2.16	-1.09	140	-1.54	185	0.45	1.32	1.50

[a] $E_{1/2}$ calculated as the average of the peak potentials of the anodic and cathodic waves. [b] ΔE_p calculated as the difference in peak potentials of the anodic and cathodic waves. [c] $E_{cell} = |E_{1/2(red2)} - E_{1/2(red1)}|$. [d] Peak potential of the anodic wave of the irreversible oxidation process.

It is clear that **2.15** and **2.16** undergo electrochemical reductions in the same way as the related compound 1,4-benzoquinone, being first reduced to a radical anion, and then to a dianion. In this way they could potentially be used as two-electron acceptors in the design of cathodic charge storage materials.

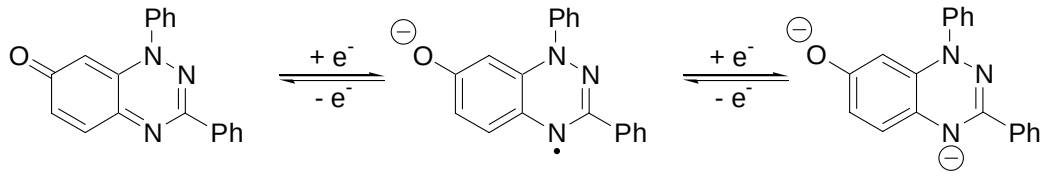

Figure 2.19 Electrochemical processes of **2.15**.

2.4 Isolation of a benzotriazinyl radical cation

Treatment of radical **1.9** with acid has been shown to result in the formation of the radical cation **2.19**, which has been characterized by EPR spectroscopy.[53] This section presents the synthesis and solution state characterization of a related radical cation **2.20**, which was initially isolated while attempting to react the amino-functionalized radical **2.3** with Co(II) to investigate possible coordination chemistry modes.

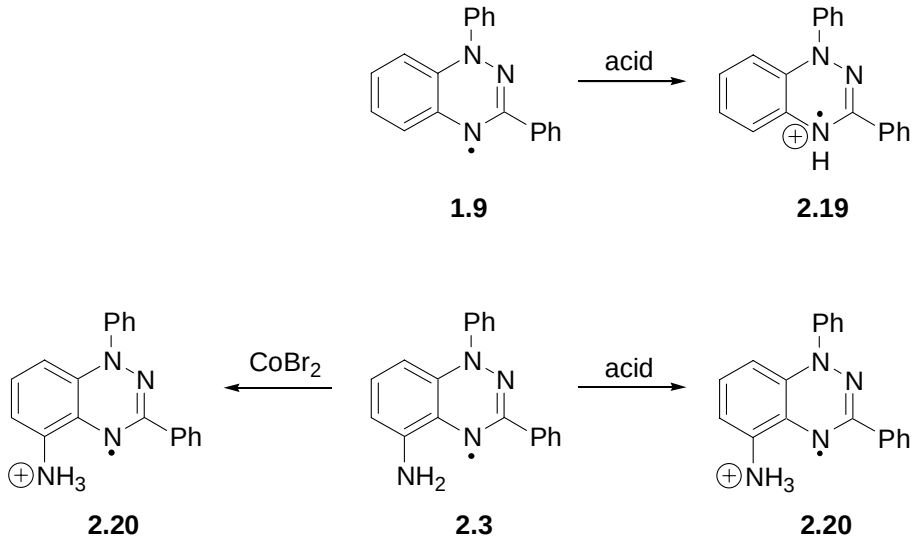

Figure 2.20 Benzotriazinyl radical cation formation.

2.4.1 Synthesis and solution state characterization

Scheme 2.6 $CoBr_2$ synthesis of radical cation **2.20**.[a]

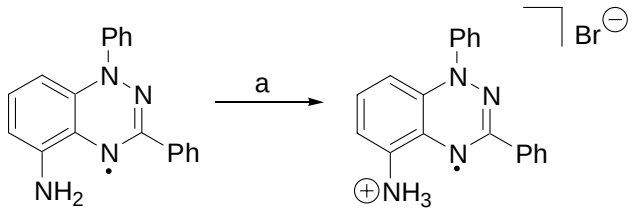

2.3 **2.20**

[a]*Reagents and conditions*: a) $CoBr_2$, MeOH, 55 °C, 40 min, 96 %.

In the initial preparation of **2.20**, a solution of $CoBr_2$ in methanol was added to a stirred solution of **2.3** in methanol at 55 °C. Upon addition of $CoBr_2$, the solution changed colour from a dark blue to a vibrant blue/green. When the reaction solution was cooled and left to stand, dark blue crystals were formed. X-ray diffraction analysis of single crystals of **2.20** revealed that the isolated material was not a cobalt complex, but rather a bromide salt with the molecular structure shown in Figure 2.21. A full analysis of this crystal structure will be given in Chapter 4.

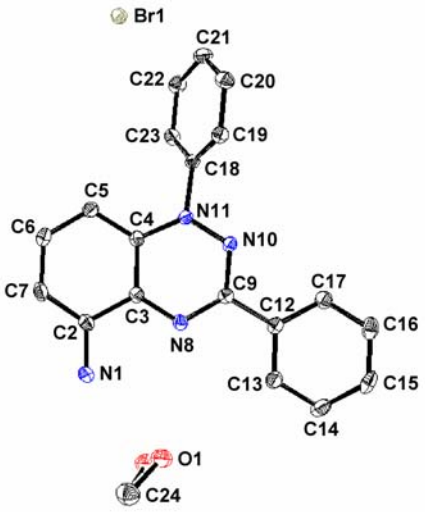

Figure 2.21 Molecular structure of the bromide salt of radical cation **2.20**. Thermal ellipsoids drawn at the 50 % probability level.

The isolated bromide salt was found to be silent by ^{1}H-NMR, consistent with it being a paramagnetic product and indicating that the cationic material may be a protonated benzotriazinyl radical cation such as **2.20** and not a closed-shell cation such as structure **2.21**. Additionally, heating radical **2.3** in the absence of $CoBr_2$ led to no reaction, suggesting that $CoBr_2$ or a Lewis acid was critical for generation of the radical cation, and that simple thermal decomposition was not responsible for the formation of **2.20**.

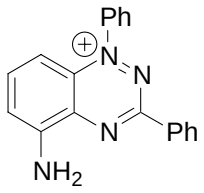

2.21

EPR spectroscopy (Figure 2.22) also confirmed the solution state paramagnetic nature of the bromide salt, and was consistent with the assignment of the cation as being the radical cation **2.20** with a g-value of 2.0041. The spectrum of the salt is the same as that of the amino radical **2.3**, with only minor changes in the hyperfine coupling constants to the nitrogen atoms and superhyperfine couplings to the hydrogen atoms (Table 2.9). This supports protonation occurring at the nitrogen of the primary amine, rather than at one of the nitrogens within the triazinyl ring, as protonation at a ring nitrogen would drastically change the observed hyperfine coupling constants of all three ring nitrogens, as observed by Neugebauer in the case of radical cation **2.19**.[53] Alternately, the proton may simply be highly transient over all four nitrogen atoms of the molecule in the solution state, thus resulting in no observable coupling to any of them.

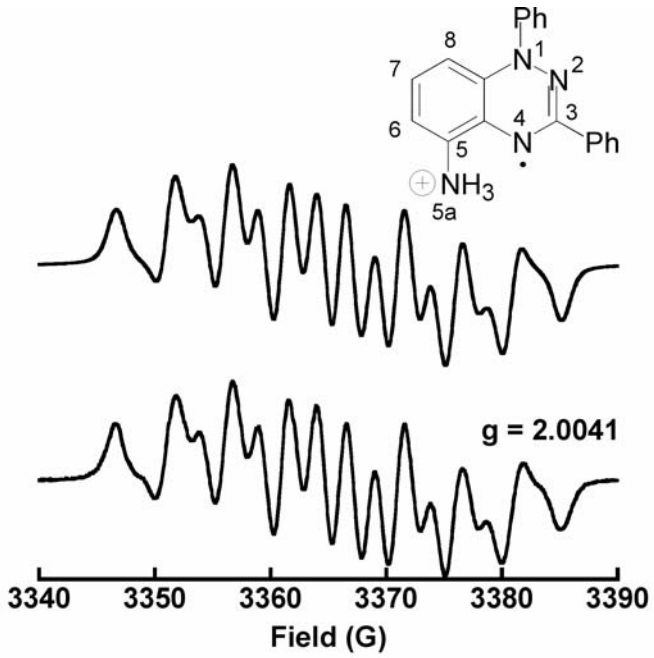

Figure 2.22 EPR spectrum of **2.20** in degassed CH_2Cl_2 at 298 K (bottom), and simulated spectrum (top).

Table 2.9 Hyperfine coupling constants (a) and spin densities (ρ) of **2.20**.

Atom	a_{exp} (G) [a]	$\lvert\rho_{exp}\rvert$ [b]	$\lvert\rho_{comp}\rvert$ [c]
N1	7.4	0.26	0.295
N2	5.1	0.18	0.272
N4	4.7	0.16	0.264
N5a	1.3	0.05	0.003
H5a	0.3	0.01	0.002
H6	0.6	0.02	0.005
H7	0.6	0.02	0.001
H8	0.4	0.01	0.004

[a]Experimentally determined coupling constants. [b]Experimental spin densities calculated using Equation 2.1. [c]Spin densities calculated using DFT at UB3LYP/6-31G(d,p).

Finally, the electronic absorption spectrum of the bromide salt is also indicative of the formation of the charged species **2.20**. The spectrum is characterized by a very broad, low intensity absorbance band stretching from approximately 500 – 1000 nm, which shows significant solvatochromic behaviour, undergoing a bathochromic shift of ~ 100 nm with decreasing solvent polarity (Table 2.10). This trend is consistent with a polar ground state, which would be preferentially stabilized in more polar solvents.

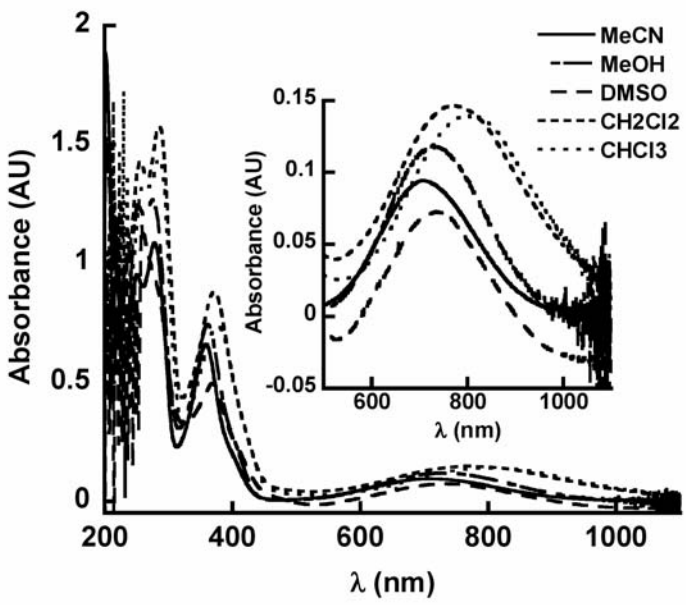

Figure 2.23 Electronic absorption spectra of **2.20** at 298 K.

Table 2.10 Solvatochromic behaviour of **2.20**.

λ_{max} (nm)				
MeCN	MeOH	DMSO	CH_2Cl_2	$CHCl_3$
709	732	735	771	810

For additional support for the characterization of **2.20** as a radical cation, an independent synthesis of **2.20** was carried out. As Neugebauer's previous work had shown that the protonated radical cation **2.19** could be synthesized by treatment of **1.9** with acid,[53] the amino radical **2.3** was also treated with acid to determine whether the same product as isolated by Scheme 2.6 could be generated.

Scheme 2.7 Acidic synthesis of radical cation **2.20**.[a]

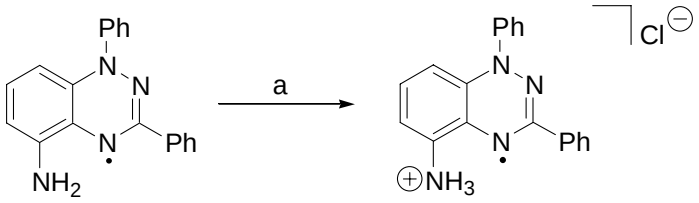

2.3 **2.20**

[a]*Reagents and conditions*: a) $HCl_{(g)}$, diethyl ether, 22 °C, 5 min., 23 %.

Using the methodology shown in Scheme 2.7, freshly produced HCl gas was bubbled through a solution of **2.3** in dry diethyl ether, immediately resulting in the precipitation of a dark blue/green chloride salt which was filtered and purified using silica gel flash chromatography. Solution state characterization of the chloride salt carried out using ^{1}H-NMR, EPR, and electronic absorption spectroscopy revealed identical properties to those of the bromide salt, confirming that treatment of **2.3** with acid also produced the radical cation **2.20**, which is consistent with Neugebauer's findings.

2.5 Conclusions

We have successfully synthesized and fully characterized three new functionalized benzotriazinyl radicals bearing EDGs. Most importantly, we have shown that EDGs can be used to cause shifts in the radical redox potentials which are consistent

with the donor abilities of the functional groups, and that these shifts can be understood and predicted through examination of the SOMO energy levels of the radicals. In combination with the previously observed effects of EWGs on the radical redox potentials, we can now look to design benzotriazinyl radical systems with either very high or very low redox potentials using appropriate functional groups. From the perspective of ORB applications, this allows us to combine electrodes composed of different radicals to achieved desired cell potentials. For example, the combination of a material containing **1.12** in a cathodic charge storage capacity (E_{ox} = 0.40 V vs SCE) and a material containing **2.1** in an anodic charge storage capacity (E_{red} = -0.94 V vs SCE) could lead to an entirely organic, benzotriazinyl radical-based battery with a theoretical E_{cell} of 1.34 V.

Additionally, we have determined that considerations must be made in selecting functional groups with respect to both radical formation and stability. Significantly, we can use functional groups to selectively form closed-shell benzotriazine iminoquinones, which possess two reversible one-electron reduction processes and are thus potential candidates to act as multi-electron anodic charge storage materials towards the design of high energy density batteries.

2.6 Experimental

2.6.1 General procedures and characterization

All reagents were purchased from commercial suppliers (Aldrich, Acros, Strem) and used without further purification. NMR spectra were collected on a 300 MHz Bruker spectrometer (Appendix D). Infrared spectra were collected using KBr pressed pellets on a Perkin Elmer Spectrum One spectrometer. Electronic absorption spectra were recorded

using an Agilent 8453 UV-Vis spectrometer (10^{-5} M of analyte). Mass spectra were obtained using a Q-TOF II instrument with an electrospray ionization source operating in positive mode. Elemental analysis was carried out by Dr. Yun Ling at the Department of Chemistry, University of British Columbia, Vancouver, B.C. DFT geometry optimization and electronic structure calculations were carried out using Gaussian 03W[70] with the 6-31G(d,p) basis set at the UB3LYP level of theory (Appendix C).

EPR spectra were collected on a Bruker EMX spectrometer. Solutions of 10^{-4} M concentration of analyte in toluene were degassed using freeze-pump-thaw cycles or nitrogen bubbling. Solid DPPH was used as a reference compound for calculating experimental g-values. Simulated spectra were obtained using Winsim2002 software.

Cyclic voltammetry experiments were carried out using a Bioanalytical Systems CV50 voltammetric analyzer using a glassy carbon working electrode (3.0 mm diameter), a platinum counter electrode, and a silver wire pseudo-reference electrode. All experiments were carried out at room temperature (~298 K). Electrochemical solutions were prepared in HPLC grade acetonitrile or dichloromethane using 1 mM of analyte and 0.1 M of tetrabutylammonium hexafluorophosphate electrolyte, and were purged of oxygen using argon bubbling. After the analyte data were collected, 1 mM of ferrocene internal standard was added to the solution and a final data set was obtained. The analyte peak potentials were then referenced to the Fc/Fc^+ redox couple at 0.40 V vs SCE in MeCN and 0.46 V vs SCE in CH_2Cl_2.[71]

2.6.2 Syntheses

The synthesis and full characterization of compounds **1.9**, **1.17** and **1.18** using the methods discussed below have been previously reported.[57]

1,3-diphenyl-1,2,4-benzotriazinyl (1.9):[57] A solution of aniline (0.14 mL, 1.5 mmol) and triethylamine (0.20 mL, 1.5 mmol) in 12 mL anhydrous ethanol was heated to reflux. A second solution of **1.18** (0.17 g, 0.73 mmol) in 15 mL anhydrous ethanol was added dropwise to the refluxing solution over about 5 minutes. The reaction was stirred at reflux for 30 minuites, then removed from the heat and treated with DBU (0.20 mL, 1.5 mmol), and finally stirred for 48 hours at room temperature. The solvent was then removed and the crude material was purified using silica gel flash chromatography (95:5 hexanes:ethyl acetate) to isolate **1.9** as a dark brown powder (91 mg, 0.32 mmol, 44 %). FT-IR (KBr): 3060 (w), 1586 (m), 1482 (s), 1450 (s), 1395 (s), 753 (m), 681 (s) cm^{-1}. UV-Vis (MeOH): λ_{max}/nm ($\varepsilon \times 10^4$ mol^{-1} cm^{-1}): 206 (3.4), 268 (3.5), 319 (0.8), 369 (0.6), 420 sh (0.3), 491 (0.1). MS (ESI): *m/z* 284 (M^+).

Benzaldehyde phenylhydrazone (1.17):[57] Phenylhydrazine (6.2 mL, 62 mmol) was added to a solution of benzaldehyde (6.0 mL, 60 mmol) in anhydrous ethanol (70 mL). The reaction solution was stirred at reflux under air for 40 minutes. It was then allowed to cool to room temperature, resulting in the formation of long white needle crystals. These were filtered, washed with hexanes, and dried under vacuum to yield purified **1.17** (10.3 g, 52 mmol, 87 %). ^{1}H-NMR (300 MHz, CD_2Cl_2) δ 7.70 (br s, 1H), 7.68 (s, 1H), 7.65 (d, 2H, J = 7 Hz), 7.41-7.21 (m, 5H), (7.10 (d, 2H, J = 8 Hz), 6.85 (t, 1H, 7 Hz); ^{13}C-NMR (300 MHz, CD_2Cl_2) δ 144.81, 137.48, 135.43, 129.33, 128.62, 128.44, 126.21, 120.15, 112.76. FT-IR (KBr): 3312 (m), 3027 (w), 1602 (s), 1592 (s), 1566 (s), 1522 (s), 1494 (s), 1261 (s), 1066 (s), 929 (m), 750 (s), 691 (s), 504 (s) cm^{-1}.

Phenylhydrazone benzoyl chloride (1.18):[57] A solution of *N*-chlorosuccinimide (9.0 g, 67 mmol) in dichloromethane (200 mL) was cooled to 0 °C in an ice bath. To this solution was added dimethyl sulfide (4.9 mL, 67 mmol), and the mixture was stirred for 10 minutes. A solution of **1.17** (10.3 g, 52 mmol) in 150 mL dichloromethane was then added dropwise over 10 minutes, and the reaction was stirred at 0 °C for a further 20 minutes. It was then warmed to room temperature and concentrated. The crude material was purified using silica gel flash chromatography (9:1 hexanes:dichloromethane) to yield **1.18** as a white crystalline solid (9.35 g, 78 %). ^{1}H-NMR (300 MHz, CD_2Cl_2) δ 8.09 (br s, 1H), 7.93 (dd, 2H, J = 9, 3 Hz), 7.43-7.28 (m, 5H), 7.18 (d, 2H, 9 Hz), 6.93 (t, 1H, 6 Hz); ^{13}C-NMR (300 MHz, CD_2Cl_2) δ 143.33, 134.45, 129.41, 129.22, 128.42, 126.40, 124.69, 121.18, 113.43. FT-IR (KBr): 3306 (m), 3060 (w), 1601 (m), 1582 (m), 1505 (m), 1268 (m), 1137 (m), 942 (m), 755 (m), 684 (m), 510 (m) cm^{-1}.

7-methyl-1,3-diphenyl-1,2,4-benzotriazinyl (2.1): A solution of 4-methylaniline (0.19 g, 1.8 mmol) and triethylamine (0.14 mL, 1.0 mmol) in 5 mL anhydrous ethanol was heated to reflux. A second solution of **1.18** (0.20 g, 0.87 mmol) in 6 mL anhydrous ethanol was added dropwise to the refluxing solution over about 5 minutes. The reaction was then removed from the heat, treated with DBU (0.25 mL, 1.7 mmol), and then stirred for 18 hours at room temperature. The resulting black precipitate of **2.1** which formed was filtered and washed with methanol, then dried to a black powder. This was recrystallized by slow evaporation of a 2:1 MeOH:CH_2Cl_2 solution as small black crystals (0.12 g, 0.40 mmol, 45 %). FT-IR (KBr): 3060 (w), 3025 (w), 2918 (w), 1591 (m), 1502 (s), 1490 (s), 1392 (s), 1326 (m), 1169 (m), 1023 (w), 803 (m), 758 (m), 695

(s) cm^{-1}. UV-Vis (MeOH): λ_{max}/nm ($\varepsilon \times 10^4$ mol^{-1} cm^{-1}): 203 (4.5), 269 (3.9), 319 (0.7), 372 (0.6), 430 sh (0.3), 495 (0.1). MS (ESI): *m/z* 298 (M^+). Anal Calcd for $C_{20}H_{16}N_3$: C, 80.51; H, 5.41; N, 14.08. Found C, 80.18; H, 5.49; N, 13.89.

7-methoxy-1,3-diphenyl-1,2,4-benzotriazinyl (2.2): A solution of 4-methoxyaniline (0.22 g, 1.8 mmol) and triethylamine (0.14 mL, 1.0 mmol) in 5 mL anhydrous ethanol was heated to reflux. A second solution of **1.18** (0.20 g, 0.87 mmol) in 7 mL anhydrous ethanol was added dropwise to the refluxing solution over about 5 minutes. The reaction was then removed from the heat, treated with DBU (0.25 mL, 1.7 mmol), and then stirred for 22 hours at room temperature. The solvent was then removed and the crude material was purified by silica gel flash chromatography (9:1 hexanes:EtOAc) to isolate **2.2** as a dark green powder. This was recrystallized by slow evaporation of a 2:1 MeOH:CH_2Cl_2 solution as small dark green needles (35.8 mg, 0.11 mmol, 13 %). FT-IR (KBr): 3060 (w), 3008 (w), 2939 (w), 2840 (w), 1606 (m), 1589 (m), 1553 (w), 1501 (s), 1488 (s), 1394 (s), 1214 (s), 1032 (s), 849 (m), 795 (m), 772 (m), 690 (m) cm^{-1}. UV-Vis (MeOH): λ_{max}/nm ($\varepsilon \times 10^4$ mol^{-1} cm^{-1}): 204 (5.0), 273 (4.1), 317 (0.8), 373 (0.8), 411 (0.5), 428 (0.5), 498 (0.1).). MS (ESI): *m/z* 314 (M^+). Anal Calcd for $C_{20}H_{16}N_3O$: C, 76.41; H, 5.13; N, 13.37. Found C, 75.90; H, 5.19; N, 13.19.

5-amino-1,3-diphenyl-1,2,4-benzotriazinyl (2.3): A solution of 1,2-diaminobenzene (0.95 g, 8.8 mmol) and triethylamine (0.7 mL, 5 mmol) in 20 mL anhydrous ethanol was heated to reflux. A second solution of **1.18** (0.50 g, 2.2 mmol) in 40 mL anhydrous ethanol was added dropwise to the refluxing solution over about 5 minutes. The reaction

was then removed from the heat, stirred for a further 2 minutes, treated with DBU (0.7 mL, 5 mmol), and then stirred for 18 hours at room temperature. The solvent was then removed and the crude material was purified using silica gel flash chromatography (85:15 hexanes:ethyl acetate) to isolate **2.3** as a dark blue crystalline solid (0.35 g, 1.2 mmol, 53 %). X-ray quality single crystals were grown from hot heptane. FT-IR (KBr): 3390 (m), 3293 (m), 3060 (w), 1604 (s), 1569 (s), 1482 (s), 1468 (s), 1392 (s), 1282 (s), 782 (m), 771 (m), 739 (m), 693 (s) cm^{-1}. UV-Vis (MeOH): λ_{max}/nm ($\varepsilon \times 10^4$ mol^{-1} cm^{-1}): 205 (4.3), 239 (2.6), 298 (2.2), 320 sh (1.4), 586 (0.1), 676 (0.1). MS (ESI): *m/z* 299 (M^+). Anal. Calcd. for $C_{19}H_{10}N_4$: C, 76.23; H, 5.05; N, 18.72. Found C, 76.21; H, 4.97; N, 18.51.

1,3-diphenyl-1,2,4-benzotriazine-7-one (2.15): 4-aminophenol (50 mg, 0.44 mmol) and triethylamine (0.06 mL, 0.4 mmol) were dissolved in 5 mL anhydrous ethanol, and the solution was heated to reflux. A second solution of **1.18** (50 mg, 0.22 mmol) in 10 mL anhydrous ethanol was then added dropwise to the refluxing solution over about 5 minutes. The reaction was then removed from the heat and AgO (30 mg, 0.24 mmol) was added. The solution was stirred under air at room temperature for 48 hours. The solvent was then removed and the crude material was purified using silica gel flash chromatography (1:1 hexanes:EtOAc, then 4 % MeOH in CH_2Cl_2) to isolate **2.15** as a dark purple powder, which was recrystallized by slow evaporation of a 2:1 MeOH:CH_2Cl_2 solution as purple needles (26 mg, 0.09 mmol, 40 %). ^{1}H-NMR (300 MHz, $CDCl_3$) δ 8.28 (dd, 2H, J = 7, 3 Hz), 7.73 (d, 1H, J = 10 Hz), 7.60 (m, 5H), 7.49 (m, 3H), 7.32 (dd, 1H, J = 10, 2 Hz), 6.12 (d, 1H, J = 2 Hz). ^{13}C-NMR (300 MHz, $CDCl_3$) δ 182.10, 154.90, 150.79, 142.43, 141.00, 136.52, 133.76, 132.16, 130.62, 130.21,

130.06, 128.82, 126.68, 125.58, 97.74. FT-IR (KBr): 3056 (w), 1621 (m), 1612 (m), 1590 (s), 1539 (s), 1519 (s), 1492 (s), 1445 (m), 1386 (m), 1330 (m), 1308 (m), 1234 (m), 1100 (m), 852 (m), 691 (m). UV-Vis (MeOH): λ_{max}/nm ($\varepsilon \times 10^4$ mol^{-1} cm^{-1}): 202 (3.3), 298 (3.6), 330 (1.6), 542 (0.6). MS (ESI): *m/z* 300 ($[M+H]^+$). Anal. Calcd. for $C_{19}H_{13}N_3O$: C, 76.24; H, 4.38; N, 14.04. Found C, 75.15; H, 4.34; N, 13.44.

6-amino-1,3-diphenyl-1,2,4-benzotriazine-7-one (2.16): 1,3-diaminobenzene (95 mg, 0.88 mmol) and triethylamine (0.06 mL, 0.4 mmol) were dissolved in 5 mL anhydrous ethanol, and the solution was heated to reflux. A second solution of **1.18** (50 mg, 0.22 mmol) in 10 mL anhydrous ethanol was then added dropwise to the refluxing solution over about 5 minutes. The reaction was then removed from the heat and stirred under air for 48 hours. The solvent was removed and the crude material purified using two silica gel flash columns (first column 6 % MeOH in CH_2Cl_2, second column 40 % EtOAc in CH_2Cl_2) to isolate **2.16** as a bright orange powder (20 mg, 0.06 mmol, 29 %). ^{1}H-NMR (300 MHz, $CDCl_3$) δ 8.30 (dd, 2H, J = 8, 2 Hz), 7.59 (m, 5H), 7.46 (m, 3H), 6.87 (s, 1H), 6.18 (s, 1H), 5.95 (br s, 2H). ^{13}C-NMR (300 MHz, d^6-DMSO) δ 172.62, 154.69, 151.89, 150.64, 141.68, 135.52, 135.26, 129.97, 129.93, 128.68, 126.44, 126.27, 97.87, 97.83, 93.59. FT-IR (KBr): 3413 (m), 3292 (m), 3059 (m), 2924 (m), 1634 (m), 1574 (s), 1547 (s), 1490 (s), 1448 (m), 1390 (m), 1359 (m), 1311 (m), 1292 (m), 1275 (m), 840 (m), 769 (m), 685 (m) cm^{-1}. UV-Vis (MeOH): λ_{max}/nm ($\varepsilon \times 10^4$ mol^{-1} cm^{-1}): 202 (3.3), 284 (3.4), 425 (2.4), 500 sh (0.3). MS (ESI): *m/z* 315 ($[M+H]^+$). Anal. Calcd. for $C_{19}H_{14}N_4O$: C, 72.60; H, 4.49; N, 17.82. Found C, 71.34; H, 4.55; N, 17.29.

5-ammonium-1,3-diphenyl-1,2,4-benzotriazinyl (2.20): *Bromide salt:* The precursor radical **2.3** (116 mg, 0.388 mmol) was dissolved in 6 mL of MeOH at 55 °C. A solution of $CoBr_2$ (85 mg, 0.39 mmol) in 2 mL MeOH was then added, and the reaction was stirred for 40 minutes. The reaction solution was then cooled to room temperature and left to sit overnight, forming small dark blue needle crystals of the bromide salt of **2.20**. These were filtered, washed with CH_2Cl_2 and MeOH, and dried under vacuum (142 mg, 0.372 mmol, 96 %). X-ray quality single crystals were grown by slow evaporation of a saturated methanol solution. FT-IR (KBr): 3368 (m), 3292 (m), 3150 (m), 1637 (m), 1508 (m), 1480 (m), 1370 (m), 1173 (m). UV-Vis (MeOH): λ_{max}/nm (AU): 203 (2.2), 252 (1.5), 275 (1.5), 361 (0.9), 732 (0.1). MS (ESI): *m/z* 300 ($[M+H]^+$). Anal Calcd for $C_{19}H_{16}BrN_4 \cdot CH_3OH$: C, 58.26; H, 4.89; N, 13.59. Found C, 57.49; H, 4.51; N, 13.61.

Chloride salt: **2.3** (60 mg, 0.20 mmol) was dissolved in 10 mL of freshly distilled diethyl ether. HCl gas, generated by the dropwise addition of $HCl_{(aq)}$ into $H_2SO_{4(aq)}$,was bubbled through the solution of **2.3** for approximately 5 minutes, immediately forming a blue/green precipitate. The precipitate was then filtered, was washed from the frit using methanol and then purified by silica gel flash chromatography (8 % MeOH in CH_2Cl_2) to isolate the chloride salt of **2.20** as dark blue crystals (16 mg, 0.05 mmol, 25 %). Solution state electronic absorption and EPR spectroscopic data is identical to that of the bromide salt.

Chapter 3 Benzotriazinyl biradicals

3.1 Introduction

The synthesis of materials capable of undergoing multiple electron transfer processes is of much interest in the design of high energy density batteries.[7] This concept has been investigated in ORB research through the synthesis of polyradicals **1.5**[47] and **1.6**[45], in which the monomer units are diradicals and thus capable of two separate one-electron oxidation processes, leading to high theoretical charging capacities as discussed in Chapter 1. It was found however that degradation of the polymer backbone of **1.5** occurred before both radical sites were oxidized, while the oxidations of the radicals of **1.6** were in fact both irreversible due to a lack of stabilizing substituents *para* to the radical sites.

On the other hand, previous work in the Frank group has shown that benzotriazinyl biradicals such as **3.1** can be synthesized for which both of the radicals sites are capable of undergoing reversible oxidation and reduction processes.[57] We were therefore interested in designing new benzotriazinyl biradicals and studying their electrochemical properties as model systems for multi-electron charge storage materials.

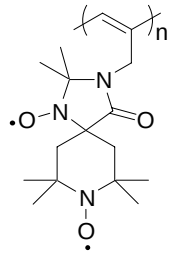

1.5

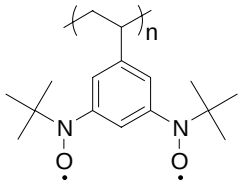

1.6

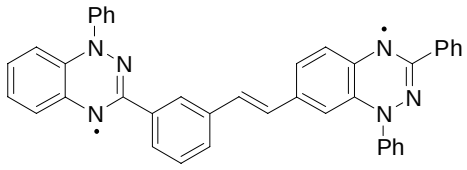

3.1

This chapter presents the synthesis and the solution state spectroscopy and electrochemistry of the three new benzotriazinyl biradicals **3.2**-**3.4**. Biradical **3.2** is the

first benzotriazinyl example of the known class of *m*-phenylene-bridged biradicals, while biradicals **3.3** and **3.4** are the first examples of biradicals with aromatic diimide bridges. In the study of biradicals it is of particular interest to investigate how the intramolecular interactions of the two unpaired electrons are governed by molecular structure, and how these interactions affect the electronic coupling between radical moieties. It was of interest to determine the effect of the bridge on the electronic coupling and electrochemical properties of benzotriazinyl biradicals

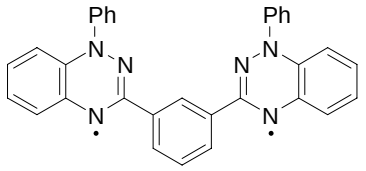

3.2

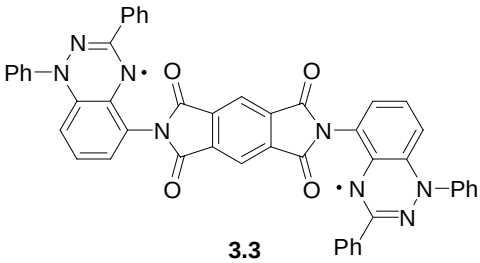

3.3

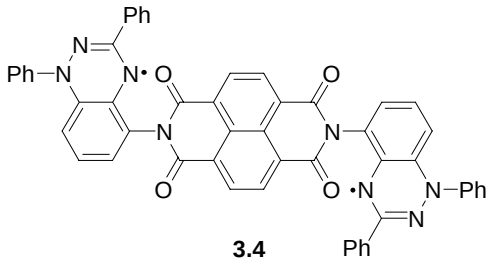

3.4

Results and discussion

3.2 *m*-Phenylene-bridged biradicals

The *m*-phenylene bridge has been well studied as a linker in organic biradicals and typically mediates intramolecular ferromagnetic exchange between the two radical moieties *via* a spin polarization mechanism.[72] For the work presented in this chapter, we were interested in examining the intramolecular electronic interactions of the two radical moieties with regards to how communication between the radicals would affect the redox potentials and the reversibility of the electrochemistry of the system. For systems with strong intramolecular coupling, unique redox processes are observed for each of the two

radicals, while for systems with weak or with no electronic interactions the two radicals undergo essentially identical redox processes to those of the monomeric unit.[73-75]

DFT geometry optimization and electronic structure calculations carried out on biradical **3.2** (UB3LYP/6-31G(d,p)) predict a triplet ground state with a singlet-triplet gap of 14 cm^{-1}. In both the singlet and the triplet state the two radical moieties are electronically isolated from each other (Figure 3.1). Consistent with the SOMO of **1.9** (Figure 2.2), the SOMOs of **3.2** are distributed predominantly over the central benzotriazinyl ring systems. The nodal positions at the carbons linking the triazinyl rings to the bridging phenylene unit prevent electronic coupling between the two unpaired electrons through the bridge, and thus it can be predicted that there will be minimal perturbation of the electrochemistry of **3.2** relative to that of the parent radical **1.9**.

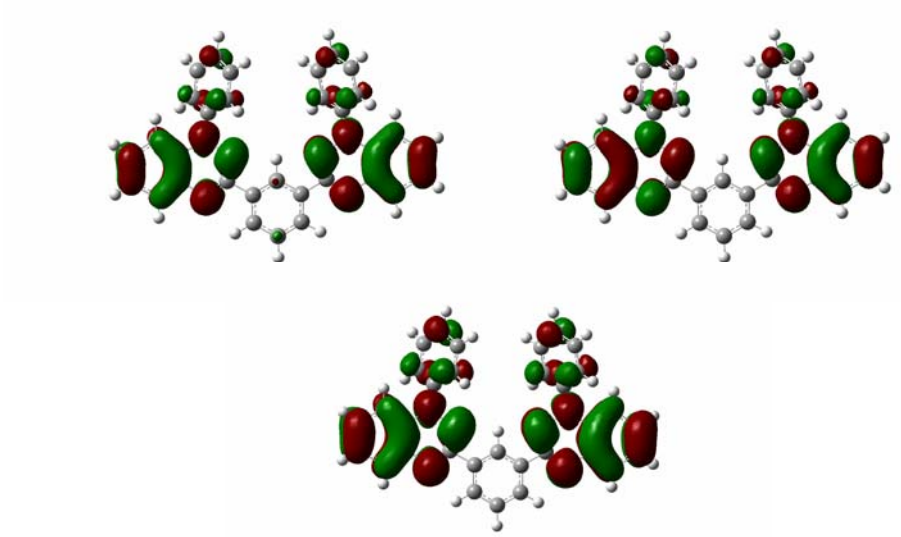

Figure 3.1 SOMO of biradical **3.2** (triplet state top, singlet state bottom) calculated at UB3LYP/6-31G(d,p), generated with isovalue = 0.0004 in GaussView 3.09.

3.3 Synthesis and properties of *m*-phenylene-bridged biradical

3.3.1 Synthesis

The synthesis of biradical **3.2** was carried out using a modification of the methodology that was used to prepare the radicals discussed in Chapter 2.

Scheme 3.1 Synthesis of benzotriazinyl biradical **3.2**.[a]

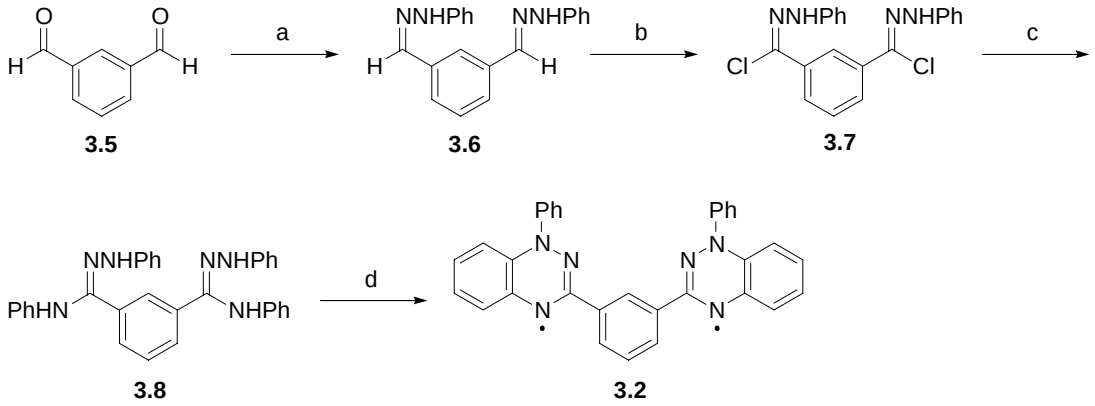

[a] *Reagents and conditions*: a) H_2NNHPh, EtOH, 78 °C, 3 hours, 91 % b) NCS, Me_2S, CH_2Cl_2, 0-22 °C, 1 hour, 74 % c) H_2NPh, TEA, 78 °C, 10 min., 76 % d) DBU, CH_2Cl_2, 22 °C, 22 hours, 46 %.

Phenylhydrazine was condensed with isophthalaldehyde in refluxing ethanol to form dihydrazone **3.6** in 91 % yield, which was then chlorinated using the Corey-Kim reagent to produce dichlorohydrazone **3.7** in 74 % yield. Reaction of **3.7** with aniline in refluxing ethanol in the presence of TEA resulted in the formation of diamidrazone **3.8**. Rather than performing the final ring closure and radical formation *in situ* using the crude solution of **3.8**, the diamidrazone was isolated and purified. Fortunately the diamidrazone was found to be quite stable and could be easily purified using silica gel flash chromatography, and was isolated in 76 % yield. A solution of purified **3.8** in CH_2Cl_2 could then be treated with DBU and stirred overnight to form biradical **3.2** in 46 % yield following purification by alumina gel flash chromatography. The lack of any N-H

stretches in the IR spectrum of the product suggested double ring closure and complete oxidation to the biradical.

3.3.2 Spectroscopic Characterization

The electronic absorption spectrum of **3.2** was found to be quite similar to that of the parent radical **1.9**. The lack of any new absorption bands or any major shifts in the absorption bands of **3.2** relative to **1.9** is consistent with the two radical moieties of **3.2** being electronically isolated from one another, as predicted computationally.

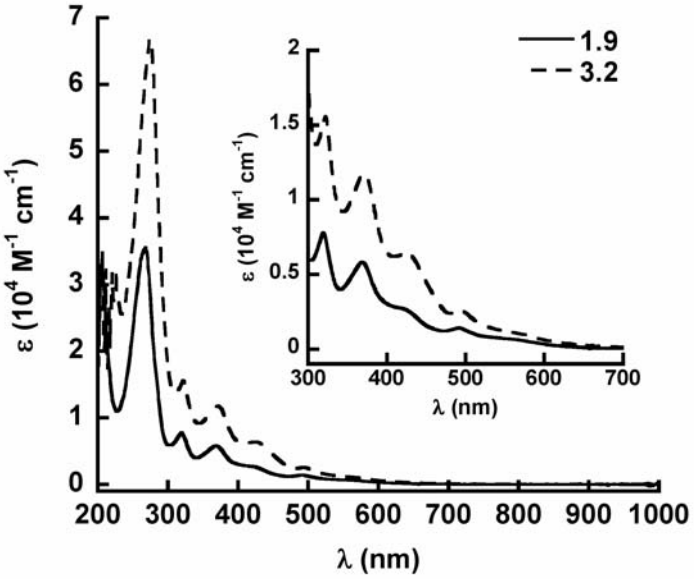

Figure 3.2 Electronic absorption spectra of parent benzotriazinyl radical **1.9** in MeOH and of biradical **3.2** in CH_2Cl_2 at 298 K.

Table 3.1 Comparison of absorption data of **1.9** and **3.2**.

	λ_{max} (ε)[a]				
1.9	269 (3.5)	319 (0.8)	369 (0.6)	420 (0.3)	491 (0.1)
3.2	274 (6.7)	322 (1.6)	372 (1.2)	425 (0.6)	494 (0.3)

[a] λ_{max} in nm, $\varepsilon \times 10^4$ M^{-1} cm^{-1}.

The room temperature EPR spectrum of biradical **3.2** consists of a single resonance, due to magnetic dipole-dipole interactions between the two unpaired electrons which lead to a broadening of the signal and elimination of any observable hyperfine coupling. Zero-field splitting can be observed upon lowering of the temperature, which is consistent with population of a triplet state (Figure 3.3). By measuring the peak-to-peak separations between the appropriate resonances in the spectrum,[76] the zero-field splitting parameters were calculated to be $|D/hc| = 0.00478$ cm^{-1} and $|E/hc| = 0.000179$ cm^{-1}. The axial parameter D is associated with the strength of the magnetic dipole-dipole interaction and becomes larger as the average distance between the radical moieties decreases. The measured value of D for **3.2** is consistent with those of related *m*-phenylene-bridged biradicals.[73,75] Additional support for the existence of a populated triplet state at low temperature is the observation of a low intensity half-field signal ($\Delta m_s = 2$ transition), due to the forbidden transition of the biradical between an $m_s = +1$ and $m_s = -1$ state.

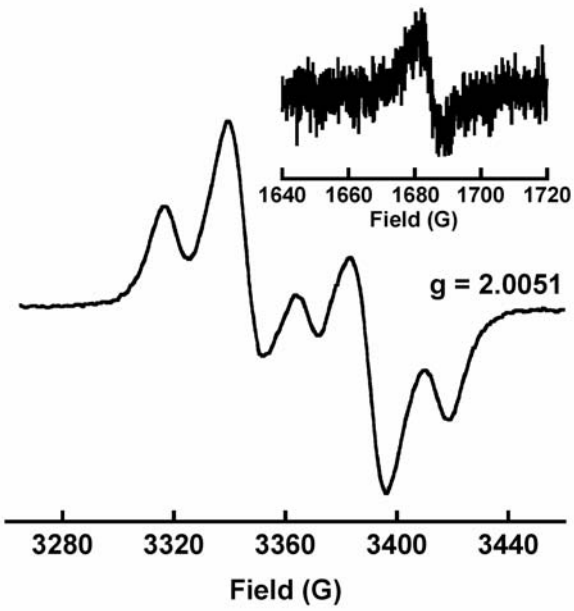

Figure 3.3 EPR spectrum of biradical **3.2** in degassed toluene at 165 K showing zero-field splitting. Inset: Half-field transition at 120 K.

3.3.3 Electrochemistry

Biradical **3.2** was found to have two reversible redox couples. The integrated current of each process was roughly double that of the one-electron process of an equimolar amount of ferrocene, suggesting that the two processes are two-electron transfers. The process at 0.23 V vs SCE, can be assigned to the oxidation of both radical moieties to form a dication, while the process at -0.84 V vs SCE can be assigned to reduction of both radicals to form a dianion. These redox potentials are very similar to those of the parent radical **1.9**, suggesting that there is no significant electronic coupling between the radicals.

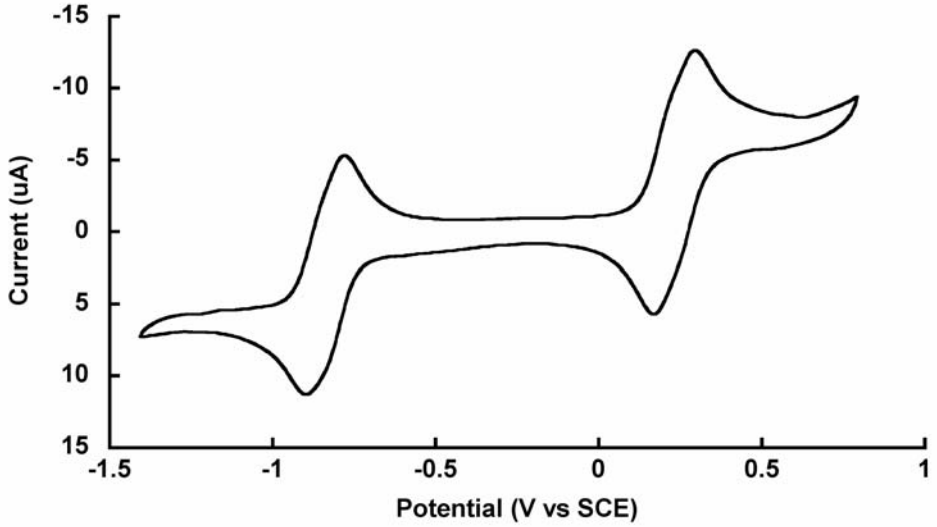

Figure 3.4 Cyclic voltammogram of **3.2 i**n MeCN, 0.1 M $[Bu_4N][PF_6]$ electrolyte, glassy carbon working electrode, silver reference electrode, platinum counter electrode, 50 mV/s scan rate.

Table 3.2 Electrochemical data of biradical **3.2**. $E_{1/2}$ in V vs SCE, ΔE_p in mV, E_{cell} in V.

$\mathbf{E_{1/2(ox)}}^{a}$	$\mathbf{\Delta E_p}^{b}$	$\mathbf{E_{1/2(red)}}^{a}$	$\mathbf{\Delta E_p}^{b}$	$\mathbf{E_{cell}}^{c}$
0.23	126	-0.85	118	1.08

[a]$E_{1/2}$ calculated as the average of the peak potentials of the anodic and cathodic waves. [b]ΔE_p calculated as the difference in peak potentials of the anodic and cathodic waves. [c]$E_{cell} = |E_{1/2(ox)} - E_{1/2(red)}|$.

In an attempt to confirm that both of the biradical electrochemical processes were two-electron transfers, an analysis of scan rate dependencies was carried out. Equation 3.1 relates the dependency of peak current on scan rate,[66] where i_p is the peak current (in amperes), n is the number of electrons transferred, A is the surface area of the working electrode (0.07 cm^2, from a diameter of 0.30 cm), D is the diffusion coefficient (in cm^2/s), υ is the scan rate (in V/s), and C is the concentration of analyte (10^{-6} mol/cm^3). The diffusion coefficient was estimated from the molecular volume of the biradical using a spherical model represented by Equation 3.2.[77] In this equation the product of the Boltzmann constant and the temperature, kT, has a value of 4.12×10^{-21} J at 298 K, V is the volume (6.29×10^{-22} cm^3 as determined by single point DFT calculation at UB3LYP/6-31G(d,p)), and η is the viscosity of the acetonitrile solvent (3.41×10^{-3} g/(cm·s) at 298 K)[77]. Using Equation 3.2 the diffusion coefficient of **3.2** was estimated to be 1.2×10^{-5} cm^2/s.

$$i_p = (2.69 \times 10^5) n^{\frac{3}{2}} A D^{\frac{1}{2}} \nu^{\frac{1}{2}} C \qquad (3.1)$$

$$D = \frac{kT}{6\pi(\frac{3V}{4\pi})^{\frac{1}{3}}\eta} \qquad (3.2)$$

The scan rate analysis was carried out using the anodic peak current of the of the oxidation process (E_p = 0.29 V vs SCE). The peak current was corrected for the capacitance current by subtracting the value of the current in the plateau region at ~ 0 V vs SCE. A plot of the peak current against the square root of the scan rate (Figure 3.5) at

rates of 50, 100, 150, 250, 500, and 600 mV/s resulted in a linear relationship with a slope equal to the absolute value of $i_p/\upsilon^{1/2}$ (5.23×10^{-5} A/(V/s)$^{1/2}$). This value was then used in Equation 3.1 along with the known values of A, D, and C to solve for the number of electrons transferred, resulting in a value of n = 0.86. This is in contrast to the initial experimental results mentioned above which used an equimolar amount of ferrocene to estimate the biradical electron transfers to be two-electron processes, or n = 2. One possible explanation for this discrepancy is that the spherical model used to estimate the diffusion coefficient was inappropriate for biradical **3.2**, resulting in an error in the value of D. It has also been stated that the effective area of the working electrode may be different from its actual area, which would affect the value of A.[77] However, if the calculated value of n is taken to be accurate, then it suggests that the observed electrochemical processes of **3.2** are one-electron transfer processes rather than two.

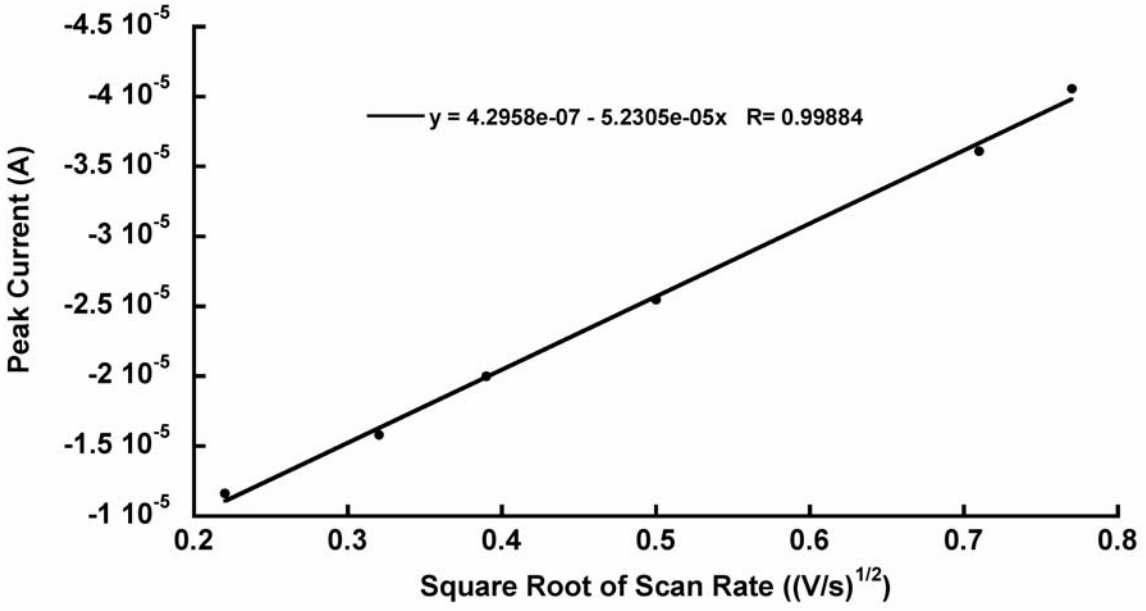

Figure 3.5 Plot of peak current (E_p = 0.29 V vs SCE) against the square root of the scan rate for scan rates of 0.05, 0.10, 0.15, 0.25, 0.50, and 0.60 V/s.

The nature of the electron transfer processes in related biradicals has been discussed previously.[73-75] The electron transfer process can be described either as two consecutive one-electron processes or a single simultaneous two-electron process. In the first case, a single one-electron oxidation or reduction would lead to the formation of a radical cation or anion, respectively. A second oxidation or reduction would then lead to a dication or dianion. In the second case, the biradical would be directly oxidized or reduced to a dication or dianion with no intermediate radical ions formed. For **3.2** it is not immediately clear if the redox couples are due to single two-electron process or two slightly overlapping one-electron processes. An analysis of the ΔE_p values of both processes (~ 120 mV) suggests the latter case, as a single fully reversible two-electron process is predicted to have a ΔE_p value of 29 mV.[66] Furthermore, for two radicals that are non-interacting, as suggested by the electronic absorbance spectroscopy of **3.2**, the potential difference between two sequential one-electron processes would be only 35 mV and they would therefore appear to overlap.[66]

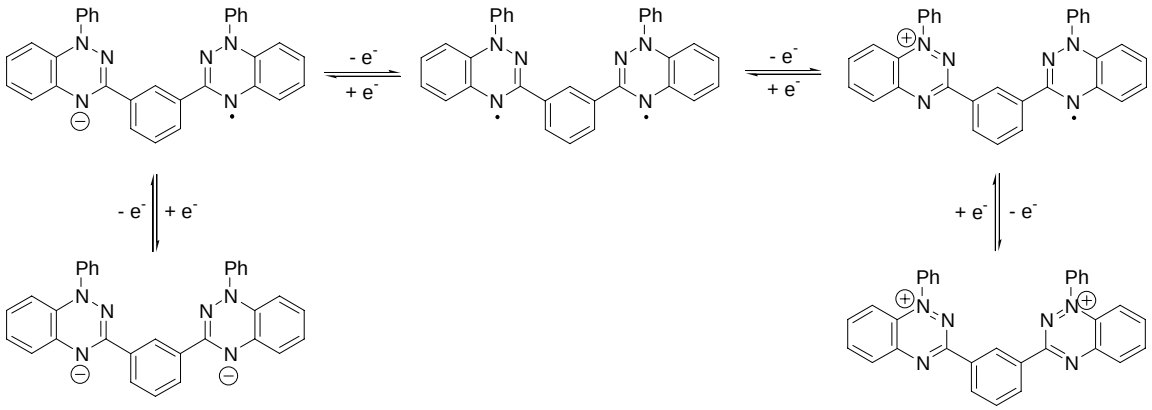

Figure 3.6 Possible electrochemical processes of biradical **3.2**.

3.4 Aromatic diimide-bridged biradicals

The second class of benzotriazinyl biradical studied utilizes aromatic diimide bridges between the radical moieties. Aromatic diimides are known to be good electron acceptors that can undergo two consecutive reversible one-electron reduction processes, forming a radical anion and a dianion (*i.e.* Figure 3.7).[78] It has been established that the electron accepting ability increases with the size of the central aromatic system, as observed by positive shifts in both reduction potentials,[78] and that the combination of aromatic diimides with good electron donors can lead to donor-acceptor charge transfer interactions[79] and solid state ordering.[80,81] These properties have led to interest in the development of aromatic diimide materials for organic electronic applications such as photovoltaic cells,[82] molecular switches,[83] and electrochromic devices.[84]

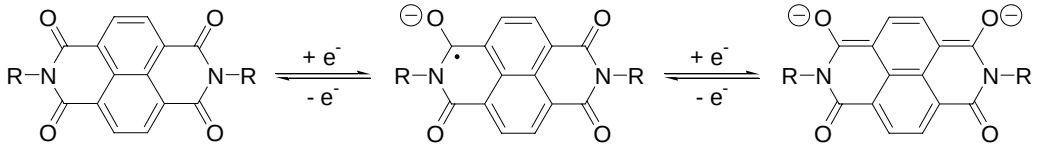

Figure 3.7 Electrochemistry of a naphthalene diimide.

Biradicals **3.3** and **3.4** were of interest to us for two reasons. First, they combined good electron donors (the benzotriazinyl radicals) with good electron acceptors (the aromatic bridges), allowing for examinations of potential intra- and intermolecular charge transfer processes, which could lead to interesting magnetic or charge transport properties. This aspect will be discussed further in Chapter 4. Secondly, they combined multiple redox-active sites within a single molecular system which was of interest

towards the examination of the electrochemistry of the biradicals for potential effectiveness as multi-electron charge storage materials.

To computationally predict the electronic structure of biradicals **3.3** and **3.4**, DFT geometry optimization and electronic structure calculations were performed on the model compounds **3.9** and **3.10** (UB3LYP/6-31G(d,p)). The calculated SOMOs and LUMOs of both of the model compounds are shown in Figure 3.8. In both compounds the SOMO is localized entirely on the radical, while the LUMO is localized entirely on the aromatic imide moiety, and so charge-transfer in the biradicals could involve a SOMO-LUMO transition between the radical and the diimide. Computation suggests a significant torsion angle between the radical and the imide of ~ 65° for **3.9** and ~ 90° for **3.10,** as well as a nodal position at the linking nitrogen atom of both models. The large torsion angle and nodal position at the point of attachment suggests that intramolecular electronic interactions in the actual biradicals may be minimal.

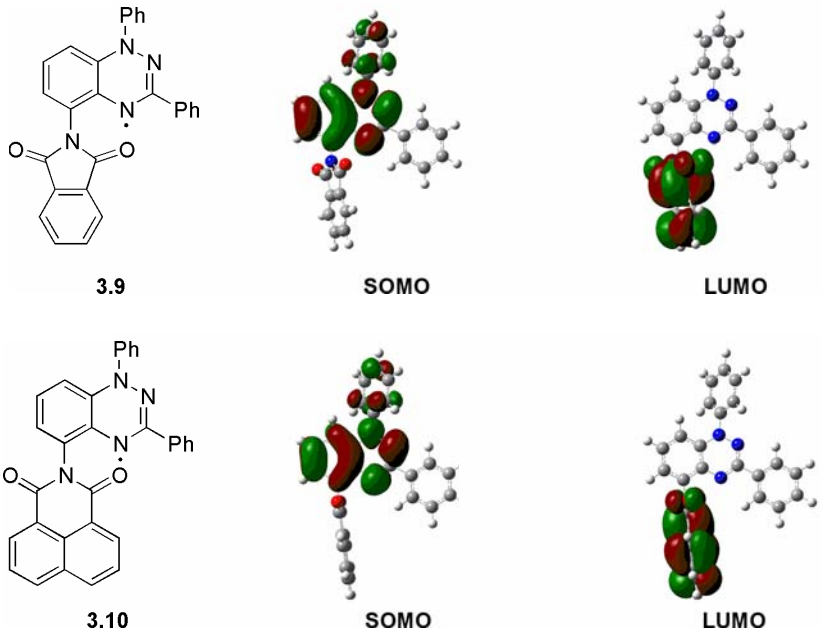

Figure 3.8 Electronic structures of **3.9** and **3.10** calculated at UB3LYP/6-31G(d,p), generated with isovalue = 0.0004 in GaussView 3.09.

3.3 Synthesis and properties of aromatic diimide bridged biradicals

3.3.1 Synthesis

The synthetic methodology for the generation of biradicals **3.3** and **3.4** involves the condensation of the amino-functionalized radical **2.3** with the corresponding aromatic dianhydrides **3.11** and **3.12**.

Scheme 3.2 Syntheses of benzotriazinyl biradicals **3.3** and **3.4**.[a]

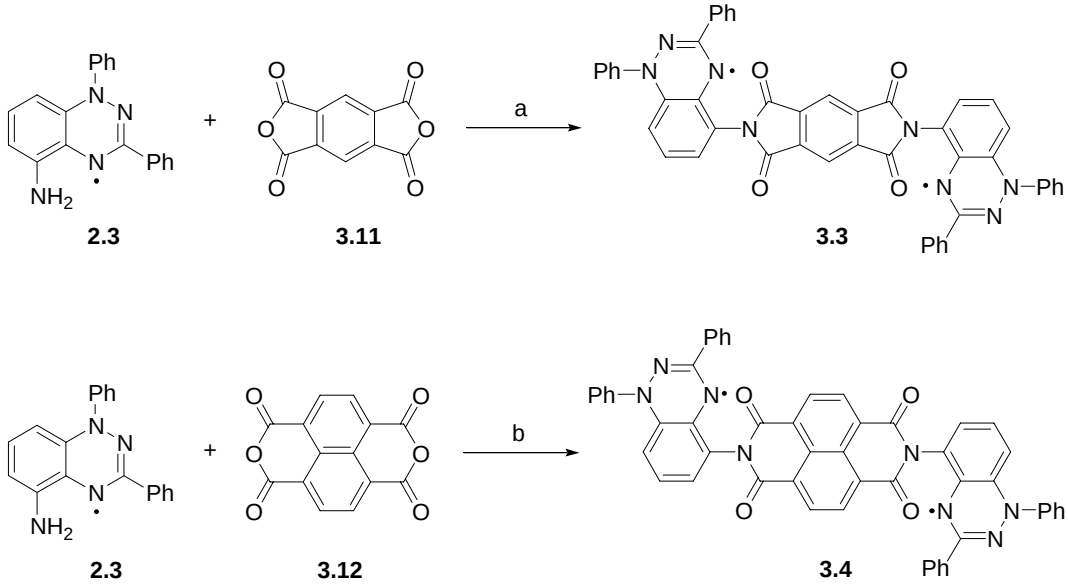

[a] *Reagents and conditions*: a) AcOH, MW 120 °C, 20 minutes, 81 % b) AcOH, MW 120 °C, 20 minutes, 75 %.

Initially, biradicals **3.3** and **3.4** were synthesized using conventional heating methods that have been used previously for the preparation of aromatic diimides.[85] While this procedure was successful in the preparation of the desired biradicals, the reactions did not proceed cleanly, resulting in difficult work-ups of and yields that were lower than desired (~ 30 %). An alternate method for the synthesis of aromatic diimides utilizes microwave chemistry which has been found to lead to high conversions, fast reaction times, and few side products.[86] Scheme 3.2 outlines the syntheses of **3.3** and **3.4** that were

successfully carried out using microwave methodology. The amino-functionalized radical **2.3** and the required aromatic dianhydride (**3.11** or **3.12**) were dissolved in a small amount of glacial acetic acid in a microwave reaction vessel, and the reaction was then heated to an internal temperature of 120 °C for 20 minutes. The resulting solution was then poured into an excess of water, causing the product to precipitate. Filtration and washing of the precipitate with water and MeOH, followed by recrystallization from hot DMF, resulted in analytically pure products in high yields (81 % for **3.3** and 75 % for **3.4**). IR spectroscopy confirmed the formation of both **3.3** and **3.4** by the complete absence of any N-H stretches or anhydride C=O stretches associated with either the starting radical **2.3** or the starting aromatic dianhydrides. In addition two new diimide C=O stretches, one symmetric and one asymmetric, associated with the aromatic diimide biradical products were clearly observed.

Several attempts were also made to synthesize the next larger biradical in the series, **3.14**, incorporating the perylene bridging unit. As with the two smaller biradicals, the synthesis of this compound was tried by both conventional and microwave heating methodologies. The major problem encountered in the preparation of **3.14** was the insolubility of dianhydride **3.13** in the solvent systems that were used. In all reactions attempted, unreacted starting materials were fully recovered, with no conversion evident.

Scheme 3.3 Unsuccessful synthesis of biradical **3.12**.[a]

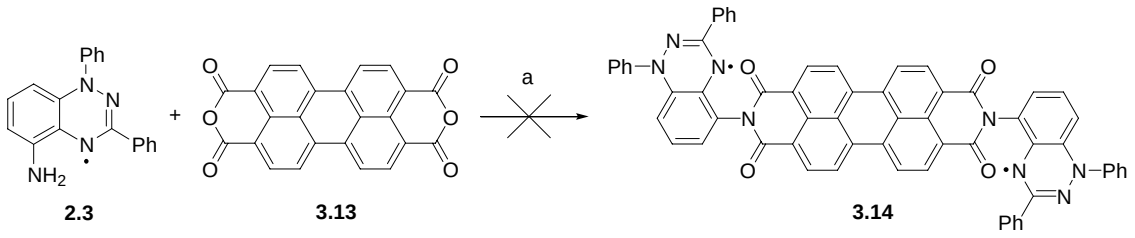

[a]*Reagents and conditions:* a) Method I: DMF, 153 °C, 9 hours; Method II: quinoline, 210 °C, 6 hours; Method III: AcOH, MW 120 °C, 20 minutes.

3.3.3 Spectroscopic characterization

The solution state electronic absorption spectra of both **3.3** and **3.4** are very similar to that of the parent radical **1.9** (Figure 3.9). In both of the biradicals, the characteristic benzotriazinyl absorption bands are present with slight bathochromic shifts evident relative to the parent radical **1.9**, suggesting little conjugation between the benzotriazinyl radical moieties (Table 3.3). This can be attributed to the large predicted torsion angles between the radicals and the diimide bridges, which arise due to steric interactions. Biradical **3.4** also exhibits two very strong absorbances at 359 nm and 379 nm that are consistent with those observed in other naphthalene diimides.[87] Absorbances of **3.3** that could be attributed to the benzene bridge may be obscured by the benzotriazinyl radical π-π* transitions, based on comparison to previous studies of the spectroscopy of benzene diimides.[88]

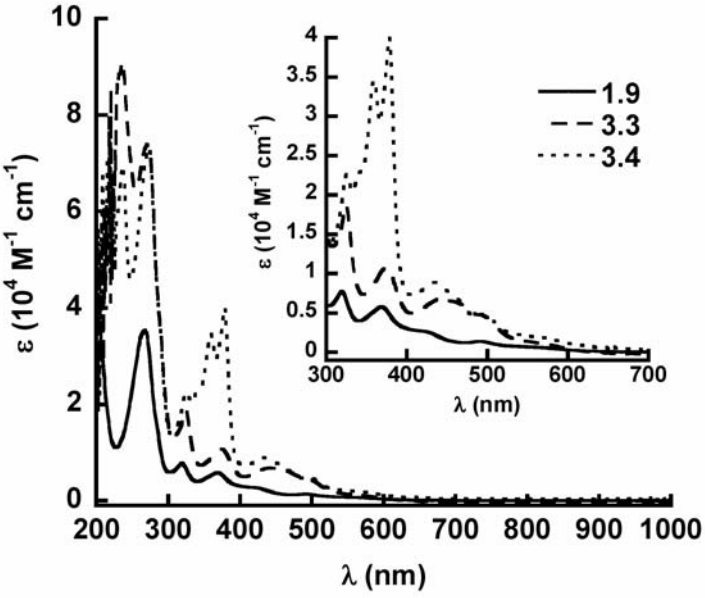

Figure 3.9 Electronic absorption spectra of parent benzotriazinyl radical **1.9** in MeOH, and of biradicals **3.3** and **3.4** in CH_2Cl_2 at 298 K.

Table 3.3 Comparison of absorption data of **1.9**, **3.3**, and **3.4**.

	λ_{max} (ε)[a]					
1.9	269 (3.5)	319 (0.8)	-	369 (0.6)	420 (0.3)	491 (0.1)
3.3	270 (7.4)	325 (1.9)	-	374 (1.1)	440 (0.7)	492 (0.5)
3.4	273 (7.3)	325 (2.3)	359 (3.5)	379 (4.0)	437 (0.9)	496 (0.5)

[a] λ_{max} in nm, $\varepsilon \times 10^4$ M^{-1} cm^{-1}.

The EPR spectra of both **3.3** and **3.4** in toluene at room temperature consist of a single broad resonance due to dipole-dipole relaxation as is observed for the *meta*-linked biradical **3.2**. Unlike the spectrum of **3.2** discussed above, the spectra of **3.3** and **3.4** did not change as the temperature was lowered to 120 K. Zero-field splitting was not observed, nor was a half-field transition. These observations are consistent with the absence of a population of the triplet state in the temperature range examined, suggesting degenerate singlet-triplet states with a gap of ~ 0 kcal.

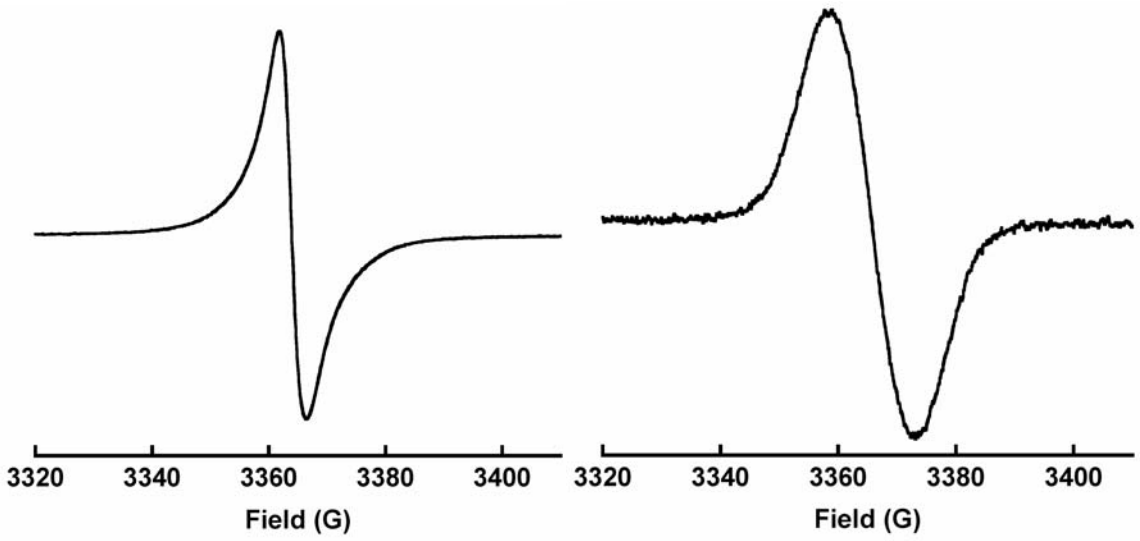

Figure 3.10 EPR spectra of **3.3** (left) and **3.4** (right) in degassed toluene at 298 K.

3.3.4 Electrochemistry

The electrochemistry of biradicals **3.3** and **3.4** was examined using cyclic voltammetry. The cyclic voltammogram of the benzene-bridged biradical **3.3** (Figure 3.11), has a reversible process at 0.43 V vs SCE and an irreversible process with a cathodic peak potential of -0.78 V vs SCE. The process at 0.43 V can likely be attributed to the oxidation of the two benzotriazinyl radicals to form a dication. This potential is higher than the oxidation potential of **1.9**, consistent with the electron withdrawing effect of the diimide bridge. For the same reasons as discussed for biradical **3.2**, the observed oxidation process is either two overlapping one-electron processes or a single two-electron process based with a ΔE_p value of 100 mV.

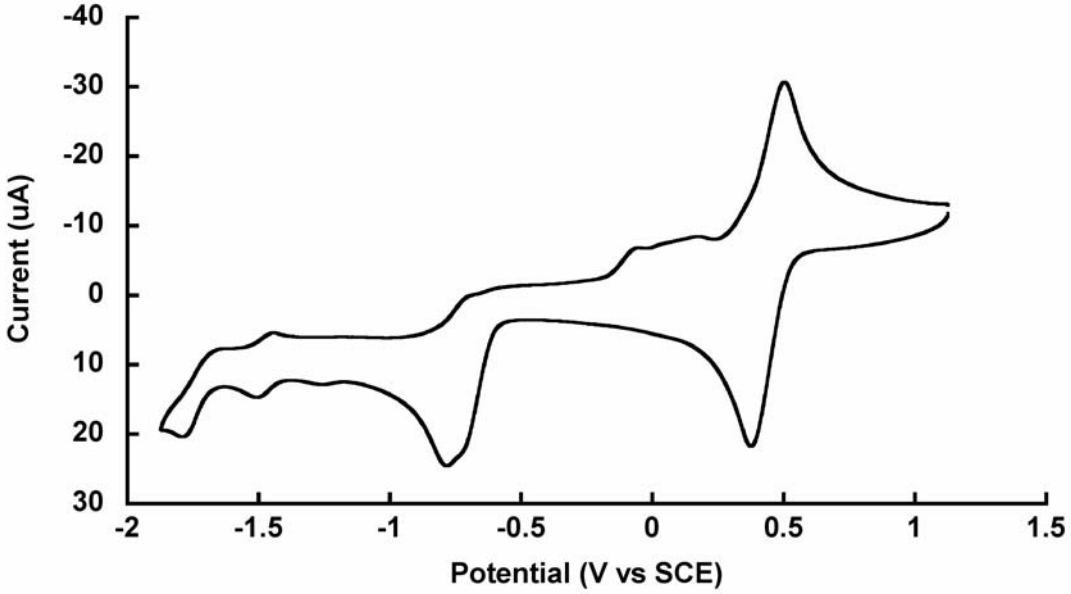

Figure 3.11 Cyclic voltammogram of biradical **3.3** in CH_2Cl_2, 0.1 M $[Bu_4N][PF_6]$ electrolyte, glassy carbon working electrode, silver reference electrode, platinum counter electrode, 100 mV/s scan rate.

It is not immediately obvious whether the irreversible process at -0.78 V is due to the reduction of the radical or of the benzene diimide bridge. However, the total area of

the reduction process is approximately the same as that of the cathodic wave of the oxidation process, and so it is likely that the reduction is that of the two radicals. If it were a reduction of the bridge, then the peak area would be roughly half that of the oxidation wave corresponding to a one-electron process. An investigation of the scan rate dependence of the reduction wave showed that the process at -0.78 V vs SCE became quasi-reversible at higher scan rates (Figure 3.11). This suggests that the reduction process is electrochemically reversible, but chemically irreversible, with the charged species that is formed undergoing either a chemical reaction or decomposition.[66]

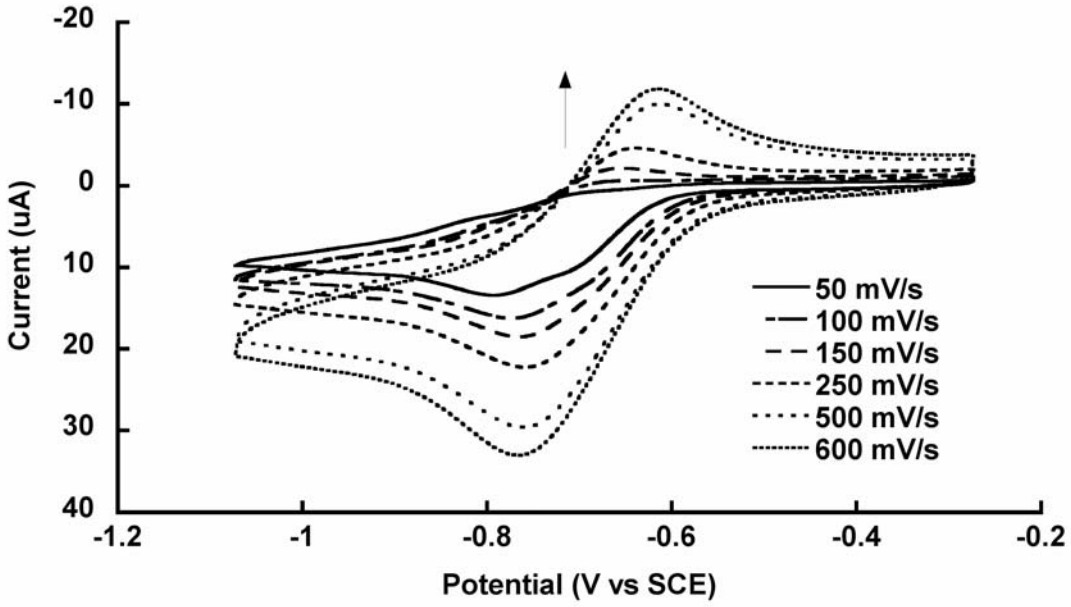

Figure 3.12 Scan rate dependency of the reduction process at -0.78 V vs SCE of biradical **3.3** in CH_2Cl_2, 0.1 M $[Bu_4N][PF_6]$ electrolyte, glassy carbon working electrode, silver reference electrode, platinum counter electrode, 50 - 600 mV/s scan rate.

The electrochemistry of biradical **3.4** is quite different from that of **3.3** in that four distinct and reversible redox processes are apparent in the cyclic voltammogram (Figure 3.12). The two processes at 0.44 V vs SCE and -0.82 V vs SCE each have approximately twice the total area of each the remaining two processes at -0.59 V vs SCE and -1.27 V vs

SCE. The two larger redox couples are therefore assigned to the electrochemistry of the two radicals, while the two smaller redox couples are assigned to the two individual one-electron reductions of the bridge.

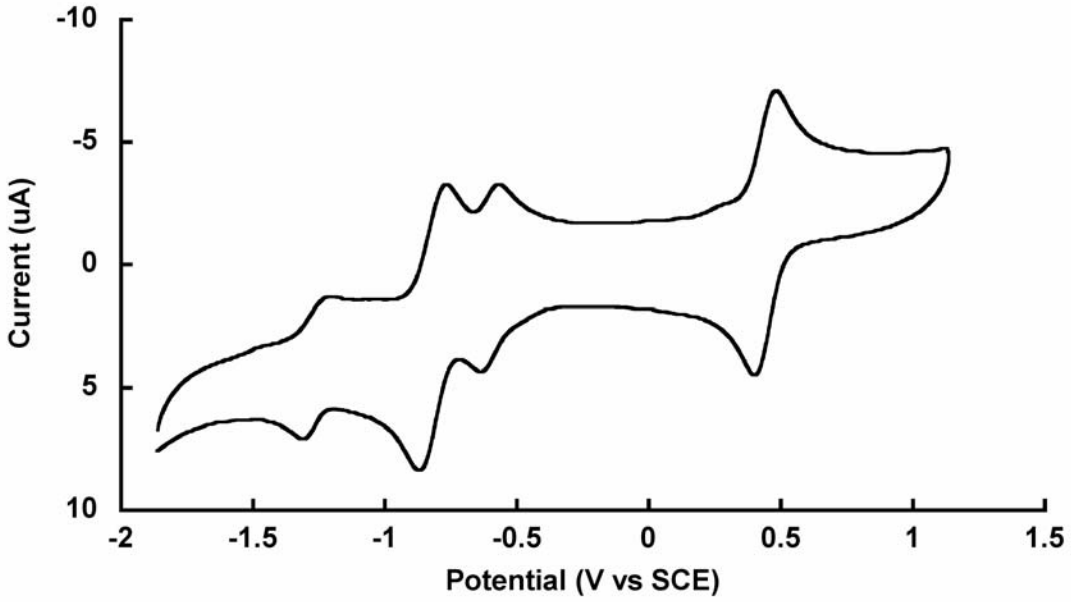

Figure 3.13 Cyclic voltammogram of biradical **3.4** in CH_2Cl_2, 0.1 M $[Bu_4N][PF_6]$ electrolyte, glassy carbon working electrode, silver reference electrode, platinum counter electrode, 100 mV/s scan rate.

The electrochemical process at 0.44 V is assigned to the oxidation of the two radicals of **3.4** to form a dication. As with **3.3**, this oxidation process is at a higher potential than the parent radical **1.9** radical due to the electron withdrawing effect of the naphthalene diimide. Unlike **3.3**, the reduction of the radicals of **3.4** to form a dianion is reversible, occurring at -0.82 V vs SCE. The first reduction of the bridge occurs just before the first reduction of the two radicals at -0.59 V, while the second bridge reduction occurs at the lowest potential of all the processes, -1.27 V. These two reduction processes occur in the normal range for naphthalene diimides.[78] Overall, the reduction potential of the radicals is not shifted relative to the reduction of the parent radical **1.9** due to the

relative potentials of the radical and the bridge. The diimide bridge is reduced to a radical anion at a more positive potential than the benzotriazinyl radicals, and thus the bridge is not as strong an electron acceptor relative to its neutral state. As a result, the E_{cell} value for the radical electrochemistry is 1.26 V, about 0.26 V larger than that of the parent benzotriazinyl radical.

In comparing the electrochemistry of **3.3** and **3.4** it can be seen that while both biradicals are stable to oxidation, **3.3** is not stable to reduction whereas **3.4** is. This can possibly be attributed to the better electron accepting ability of the naphthalene bridge of **3.4** relative to the smaller benzene bridge of **3.3**. The larger bridge may be better suited to stabilize the build-up of negative charge that occurs upon reduction of both the bridge and the two radical moieties. While other benzene-bridged diimides related to **3.3** have displayed two reversible reduction processes,[78] the electron-rich character of the benzotriazinyl radicals is likely what shuts these processes down in the case of **3.3**. Therefore it can be determined that the structure of **3.4** lends itself to charge storage application better than that of **3.3**, as **3.4** could act as a two electron donor and a four electron acceptor, whereas **3.3** could only act as a two electron donor.

Table 3.4 Electrochemical data of biradicals **3.3** and **3.4**. $E_{1/2}$ in V vs SCE and ΔE_p in mV.

	$\mathbf{E_{1/2(ox)}}^a$	$\mathbf{\Delta E_p}^b$	$\mathbf{E_{1/2(red1)}}^a$	$\mathbf{\Delta E_p}^b$	$\mathbf{E_{1/2(red2)}}^a$	$\mathbf{\Delta E_p}^b$	$\mathbf{E_{1/2(red3)}}^a$	$\mathbf{\Delta E_p}^b$
3.3	0.44	130	-0.79[c]	-	-	-	-	-
3.4	0.44	98	-0.59	79	-0.82	108	-1.27	91

[a]$E_{1/2}$ calculated as the average of the peak potentials of the anodic and cathodic waves. [b]ΔE_p calculated as the difference in peak potentials of the anodic and cathodic waves. [c]Peak potential of the cathodic wave.

3.4 Conclusions

Three new benzotriazinyl biradicals were synthesized and characterized as model compounds for multi-electron charge storage materials. The *m*-phenylene-bridged biradical **3.2** was found to exhibit the reversible redox chemistry expected for benzotriazinyl radicals, with no apparent interaction between the two radical sites, and could thus act as a two electron acceptor or donor material. The aromatic diimide-bridged biradicals **3.3** and **3.4** were found to have electrochemical properties that were dependent on the nature of the aromatic bridge. The small benzene bridge of **3.3** was not a good enough electron acceptor to stabilize the negative charge generated by the reduction of the benzotriazinyl radicals. The larger naphthalene bridge however, was stable to the reductions of both of the radicals as well as to its own two reduction processes. For charge storage materials based on benzotriazinyl radicals bridged with aromatic diimide therefore, the use of the larger naphthalene bridged would provide greater electrochemical stability and versatility.

3.5 Experimental

The general procedures and experimental techniques that were used are the same as those that were discussed in Section 2.6.1. The determination of two-electron processes in the cyclic voltammetry of **3.2** was carried out by comparing the integrated currents of the biradical electrochemical processes with the integrated current of the one-electron electrochemical process of an equimolar amount of ferrocene internal standard. The low solubilities of biradicals **3.3** and **3.4** prevented such quantitative comparisons and so the assignments of two-electron and one-electron processes in these two biradicals are tentative.

3.5.1 Syntheses

1,3-bis-(1-phenyl-1,2,4-benzotriazinyl)-benzene (3.2): 3.10 (0.40 g, 0.81 mmol) was dissolved in 20 mL CH_2Cl_2 along with DBU (0.6 mL, 4 mmol). The reaction was stirred at 22 °C for 48 hours. The solvent was then removed and the crude dark brown material was purified using neutral alumina flash chromatography (8:2 hexanes:EtOAc) to isolate **3.2** as very small dark brown microcrystalline needles (0.18 g, 0.37 mmol, 46 %). X-ray quality single crystals were grown by slow evaporation of a saturated EtOAc solution of the biradical. FT-IR (KBr): 3061 (w), 2924 (w), 1592 (m), 1484 (s), 1381 (s), 1204 (m), 754 (s), 696 (s), 617 (m) cm^{-1}. UV-Vis (CH_2Cl_2): λ_{max}/nm ($\varepsilon \times 10^4$ mol^{-1} cm^{-1}): 274 (6.7), 322 (1.6), 372 (1.2), 425 (0.6), 494 (0.3), 550 sh (0.1). MS (ESI): *m/z* 490 (M^+). Anal Calcd for $C_{32}H_{22}N_6$: C, 78.35; H, 4.52; N, 17.13. Found C, 77.96; H, 4.55; N, 16.86.

N,N'-bis-(1,3-diphenyl-1,2,4-benzotriazinyl)-1,2,4,5-benzenetetracarboxylic diimide (3.3): A solution of **2.3** (0.20 g, 0.69 mmol) and 1,2,4,5-benzenetetracarboxylic dianhydride (70 mg, 0.32 mmol) in 3.0 mL of glacial acetic acid was prepared in a 5 mL microwave reaction vial. The reaction was heated in a microwave reactor to an internal temperature of 120 °C for 20 minutes. The reaction solution was then poured into 60 mL distilled water, and the resulting precipitate of **3.3** was filtered and washed with excess water and MeOH. The product was then dried under vacuum to a dark brown powder which was recrystallized from hot DMF to form small black crystals (0.20 g, 0.26 mmol, 81 %). FT-IR (KBr): 3060 (w), 1778 (m), 1731 (s), 1594 (m), 1477 (s), 1451 (s), 1373 (s), 1108 (s), 767 (m), 720 (m), 692 (s) cm^{-1}. UV-Vis (CH_2Cl2): λ_{max}/nm ($\varepsilon \times 10^4$ mol^{-1} cm^{-1}): 270 (7.4), 325 (1.9), 374 (1.1), 440 (0.7), 460 sh (0.6), 492 sh (0.5), 550 sh (0.1).

MS (ESI): *m/z* 780 (M^+). Anal Calcd for $C_{48}H_{28}N_8O_4$: C, 73.84; H, 3.61; N, 14.35. Found C, 73.26; H, 3.73; N, 14.39.

N,N'-bis-(1,3-diphenyl-1,2,4-benzotriazinyl)-1,4,5,8-naphthalenetetracarboxylic diimide (3.4): A solution of **2.3** (0.20 g, 0.69 mmol) and 1,4,5,8-naphthalenetetracarboxylic dianhydride (86 mg, 0.32 mmol) in 3 mL of glacial acetic acid was prepared in a 5 mL microwave reaction vial. The reaction was heated in a microwave reactor to an internal temperature of 120 °C for 20 minutes. The reaction solution was then poured into 60 mL distilled water, and the resulting precipitate of **3.4** was filtered and washed with excess water and MeOH. The product was then dried under vacuum to a dark brown powder which was recrystallized from hot DMF as small black crystals (0.20 g, 0.24 mmol, 75 %). FT-IR (KBr): 3060 (w), 1715 (s), 1678 (s), 1581 (s), 1477 (s), 1448 (s), 1394 (s), 1349 (s), 1249 (s), 766 (s), 750 (s), 694 (s), 625 (m) cm^{-1}. UV-Vis (CH_2Cl_2): λ_{max}/nm ($\varepsilon \times 10^4$ mol^{-1} cm^{-1}): 273 (7.3), 325 (2.3), 340 (2.3), 359 (3.5), 379 (4.0), 437 (0.9), 450 sh (0.8), 496 (0.5), 550 sh (0.2). MS (ESI): *m/z* 830 (M^+). Anal Calcd for $C_{52}H_{30}N_8O_4$: C, 75.17; H, 3.64; N, 13.49. Found C, 74.23; H, 3.68; N, 13.45.

Isophthalaldehyde diphenylhydrazone (3.6): Isophthalaldehyde (2.0 g, 15 mmol) was dissolved in 150 mL anhydrous EtOH at reflux. To this solution was added phenylhydrazine (3.2 mL, 32 mmol). The reaction was stirred at reflux for 3 hours, forming a large amount of yellow precipitate. The precipitate was filtered and washed with hexanes to yield **3.6** as a fine yellow powder (4.30 g, 13.7 mmol, 91 %). ^{1}H-NMR (300 MHz, d^6-DMSO) δ 10.50 (s, 2H), 8.01 (s, 2H), 7.95 (s, 1H), 7.38 (dd, 2H, J = 8, 2

Hz), 7.50 (t, 1H, J = 8 Hz), 7.34 (t, 4H, J = 9 Hz), 7.20 (dd, 4H, J = 9, 1 Hz), 6.87 (tt, 2H, J = 7, 1 Hz); ^{13}C-NMR (300 MHz, d^6-DMSO) δ 146.60, 137.61, 137.55, 130.56, 130.36, 126.32, 124.42, 120.23, 113.42. FT-IR (KBr): 3315 (m), 3053 (w), 1602 (s), 1578 (s), 1511 (s), 1486 (s), 1254 (s), 1136 (s), 750 (s), 694 (s), 508 (s) cm^{-1}.

Diphenylhydrazone isophthaloyl dichloride (3.7): *N*-Chlorosuccinimide (4.0 g, 30 mmol) was dissolved in 100 mL dichloromethane, and the solution was cooled to 0 °C in an ice bath. Dimethyl sulfide (2.2 mL, 30 mmol) was then added to this solution, and the mixture was stirred for 10 minutes. A suspension of **3.6** (4.12 g, 13.1 mmol) in 50 mL dichloromethane was then added to the cold reaction solution over about 10 minutes. The reaction was then stirred and allowed to warm to room temperature over 1 hour. The solvent was then removed and the crude material was purified using silica gel flash chromatography (8:2 hexanes:dichloromethane) to isolate **3.7** as a fluffy white solid (3.70 g, 9.65 mmol, 74 %). ^{1}H-NMR (300 MHz, CD_2Cl_2) δ 8.40 (t, 1H, J = 2 Hz), 8.08 (s, 2H), 7.87 (dd, 2H, J = 9, 3 Hz), 7.40 (t, 1H, J = 9 Hz), 7.26 (t, 4H, J = 9 Hz), 7.15 (d, 4H, J = 9 Hz), 6.89 (tt, 2H, J = 9, 2 Hz); ^{13}C-NMR (300 MHz, CD_2Cl_2) δ 143.19, 134.80, 129.44, 128.52, 126.88, 124.33, 123.96, 121.36, 113.50. FT-IR (KBr): 3314 (m), 3055 (w), 1604 (s), 1575 (s), 1505 (s), 1264 (s), 1147(s), 939 (s), 741 (s), 686 (s), 504 (s) cm^{-1}.

Diamidrazone (3.8): Aniline (0.5 mL, 5 mmol) and TEA (0.7 mL, 5 mmol) were dissolved in 2 mL anhydrous EtOH, and the solution was heated to 70 °C. A suspension of **3.7** (0.50 g, 1.3 mmol) in 20 mL anhydrous EtOH was added dropwise to the hot reaction solution over 5 minutes. The reaction was then stirred for a further 5 minutes before being cooled to room temperature. The solvent was removed and the crude orange

oil was purified using silica gel flash chromatography (9:1 CH_2Cl_2:EtOAc) to isolate **3.8** as a yellow oily material which was then precipitated from CH_2Cl_2/pentane as an off-white powder (0.49 g, 0.99 mmol, 76 %). ^{1}H-NMR (300 MHz, CD_2Cl_2) δ 8.03 (t, 1H, J = 2 Hz), 7.71 (br s, 2H), 7.68 (dd, 2H, J = 8, 2 Hz), 7.33 (t, 1H, J = 8 Hz), 7.23 (m, 8H), 7.06 (d, 4H, J = 8 Hz), 6.92 (tt, 2H, J = 8, 1 Hz), 6.86 (tt, 2H, J = 8, 1 Hz), 6.70 (d, 4H, J = 8 Hz), 5.75 (br s, 2H); ^{13}C-NMR (300 MHz, CD_2Cl_2) δ 145.45, 142.21, 137.52, 135.43, 129.72, 129.57, 128.89, 127.00, 125.14, 121.13, 120.48, 116.56, 113.59. FT-IR (KBr): 3376 (m), 3350 (m), 3297 (m), 3049 (w), 1598 (s), 1496 (s), 1430 (m), 1299 (m), 1242 (s), 1167 (m), 748 (s), 692 (s), 503 (m) cm^{-1}. MS (ESI): *m/z* 497 ($[M+H]^+$).

Chapter 4 Solid state properties of benzotriazinyl radicals

4.1 Introduction

The previous two chapters were devoted primarily to studies of the solution state electrochemistry of benzotriazinyl radicals for use in charge storage applications. Solid state properties have also been shown to be important considerations in the design of charge storage materials with respects to the transport of electrons and counter-ions through the electrode.[7,26] Insight into the magnitude and nature of intermolecular interactions in the solid state for organic radicals systems can be gained from analysis of magnetic properties and charge transport, both of which depend critically on through space orbital overlap. Structural analysis carried out by single crystal X-ray diffraction (XRD) can provide information on the potential pathways for such intermolecular interactions.

4.1.1 Magnetic properties of organic radicals

Organic radicals are one category of materials that are being studied as potential molecular magnets, which are of interest as alternatives to conventional atom-based metallic magnets due to the tunability, potential for multifunctionality, and ease of fabrication that is associated with molecular systems.[89] The magnetic behaviour of an organic radical will vary depending on the nature and strength of magnetic exchange interactions. In systems that lack exchange interactions the spins will be disordered in the presence of an applied magnetic field, and the material will act as a paramagnet, while in cases where ferromagnetic or antiferromagnetic exchange occur the spins will align in a

parallel or antiparallel manner, respectively, in the presence of an applied field (Figure 4.1).

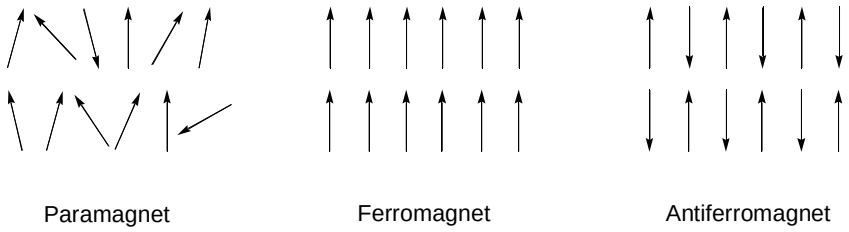

Figure 4.1 Classes of spin alignment.

The magnetic exchange interaction can be defined by an exchange integral, J, where J is positive for ferromagnetic exchange and negative for antiferromagnetic exchange for the Heisenburg Hamiltonian described as $H = -JS_1 \cdot S_2$, where S_1 and S_2 are isotropic spins. In the superexchange model, which involves orbital overlap as a pathway to exchange, J can be defined using Equation 4.1, where k, β, and l are electron exchange integrals and U is the energy difference between ground and excited singlet states.[90] Generally speaking, the ferromagnetic component to J, $J_F = 2k$, is much smaller than the antiferromagnetic exchange component, $J_{AF} = -4(\beta+l)^2/U$, and as a result antiferromangetic exchange is most often observed. In situations where direct orbital overlap occurs orthogonally the antiferromagnetic exchange term goes to zero, and ferromagnetic behaviour is observed.[90]

$$J = J_F + J_{AF} = 2k - \frac{4(\beta + l)^2}{U} \qquad (4.1)$$

The nature of the magnetic exchange will affect the observed magnetic properties of a material. The net induced magnetization within the solid in the presence of the

applied magnetic field can be expressed using Equation 4.2, where M is the magnetization, H is the applied field, and the proportionality constant χ is the magnetic susceptibility of the compound.

$$M = \chi H \tag{4.2}$$

In paramagnetic systems with non-interacting spins, the magnetic susceptibility χ can be expressed using the Curie law (Equation 4.3). This describes the dependence of χ on the temperature, T, related through the Curie constant, C, which is defined using Equation 4.4 where S is the spin quantum number, N is Avogadro's number (6.0221367×10^{23} mol^{-1}), g is the g-factor of the unpaired electron, β is the Bohr magneton ($4.66864374 \times 10^{-5}$ cm^{-1} G^{-1}), and k is the Boltzmann constant (0.69503877 cm^{-1} K^{-1}).

$$\chi = \frac{C}{T} \tag{4.3}$$

$$C = \frac{Ng^2\beta^2S(S+1)}{3k} \tag{4.4}$$

The Curie-Weiss law (Equation 4.5) is an extension of the Curie law that takes into account deviations from Curie behaviour caused by an internal field due to weak magnetic exchange interactions between spins. The Weiss constant θ is indicative of the magnitude and nature of the exchange. Values of θ greater than zero indicate ferromagnetic exchange, with an observed increase in χ compared with a non-exchanging

system, while values less than zero indicate antiferromagnetic exchange, with an observed decrease in χ.

$$\chi = \frac{C}{(T - \theta)} \qquad (4.5)$$

When the energy of the exchange interaction is weaker than the available thermal energy (kT), the spins will have multiple orientations with respect to the external field and the material will exhibit paramagnetic behaviour. In the case of particularly strong exchange interactions the material will display significant deviations from Curie-Weiss behaviour. This occurs below a critical temperature, T_c, at which point the energy of the exchange interaction is strong enough that that long range ordering of the spins will occur.

4.1.2 Charge transport in radicals

The idea of using neutral radicals as conducting materials was first proposed by Haddon in 1975.[91] It is based on the principle that overlap between the SOMOs of ordered π-delocalized radical molecules will give rise to a half-filled band structure which could lead to conduction through the promotion of electrons into vacant orbitals of the unfilled band. This concept has been extensively investigated using phenalenyl,[92] thiazyl,[93] and thiaselenazolyl[94] radical systems.

As with the magnetic properties of radicals, the conductivity of neutral radicals is largely dependent on solid state interactions.[95] Peierls distortions[96], which result in alternating long and short distances between molecules in a π-stack, open up a gap

between the empty and filled electronic bands, leading to insulating behaviour. This distortion can be inhibited through multi-dimensional inter-stack interactions,[97] which can also themselves influence the band gap.[98] Another consideration which is important to conduction is the ease at which the electrons are transferred between radical sites, described as the on site Coulomb energy. This is related to the ionization potential and electron affinity of the radicals, and thus minimizing the gap between the oxidation and reduction potentials of the radicals becomes an important issue.[93]

4.1.3 Solid state properties of benzotriazinyl radicals

In the solid state, the molecules of the parent benzotriazinyl radical **1.9** form one-dimensional chains of slipped π-stacks (Figure 4.2).[55] The relatively minimal overlap of the regions of high spin densities between neighbouring radicals results in weak antiferromagnetic exchange with $\theta = -2.2 \pm 0.2$ K.[54]

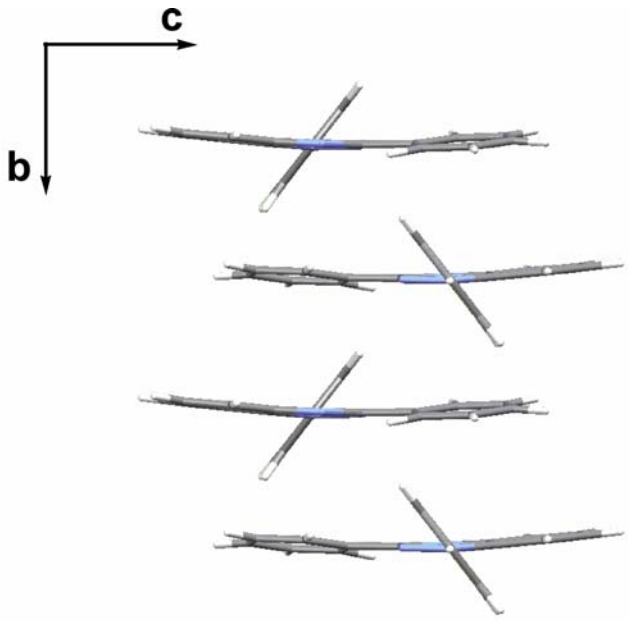

Figure 4.2 π-Stacking in the parent radical **1.9**.[55]

While other benzotriazinyl radicals that have been characterized show the formation of linear π-stacks, changes in intermolecular interactions lead to a wide range of magnetic behaviours. For example, the chloro-functionalized radical **4.1** displays exceptionally strong antiferromagnetic exchange, due to particularly large intermolecular overlap of the high spin density benzotriazinyl rings,[54] while ferromagnetic exchange has been observed in radicals such as **4.2** and **4.3**,[57] attributed to overlap between regions of positive and negative spin density on neighbouring radicals as per the McConnell I mechanism.[99]

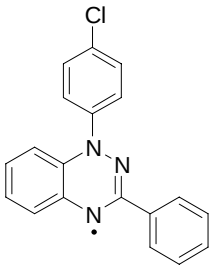

4.1

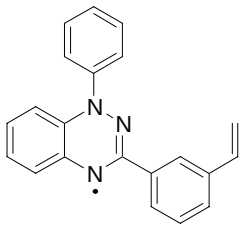

4.2

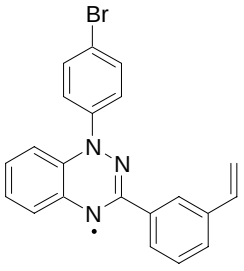

4.3

The conductivities of several benzotriazinyl radical systems have also been investigated. It has been found that conjugated benzotriazinyl polyradicals can be *p*-doped with I_2 resulting in room temperature conductivities on the order of 10^{-2} $S \cdot cm^{-1}$.[57] Additionally, a donor-acceptor salt has been prepared through the combination of **1.9** as the electron donor with TCNQ as the electron acceptor.[56] This salt displayed semiconducting behaviour with a conductivity of 10^{-4} $S \cdot cm^{-1}$, a value which was found to increase by over three orders of magnitude upon the application of pressure due to structural rearrangements that removed Peierls distortions and improved orbital overlap.

The intrinsic conductivity of neutral **1.9** itself however, has been found to be poor, on the order of 10^{-9} S·cm^{-1}.[57]

This chapter will present solid state studies that were carried out on the amino-functionalized benzotriazinyl radical **2.3**, its corresponding radical cation **2.20**, the *m*-phenylene bridged biradical **3.2**, and the two aromatic diimide-bridged biradicals **3.3** and **3.4**. Crystal structures of **2.3**, **2.20**, and **3.2** were obtained, which allowed for analyses of the magnetic properties of these compounds with respects to their solid-state interactions. While structures were not obtained for **3.3** and **3.4**, solid-state diffuse reflectance spectroscopy was used to investigate the presence of intermolecular interactions in these donor-acceptor compounds. Finally, the results of preliminary conductivity measurements on all five compounds will be briefly discussed.

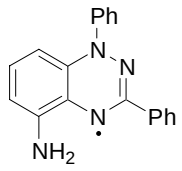

2.3

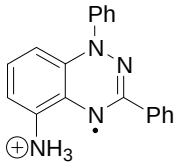

2.20

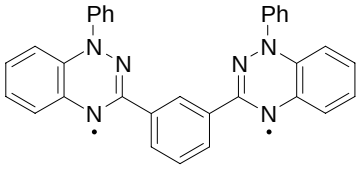

3.2

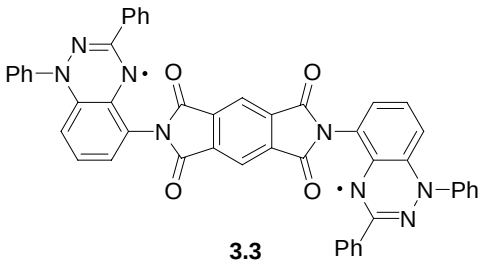

3.3

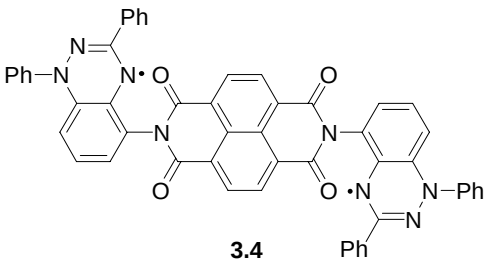

3.4

Results and discussion

4.2 5-Amino-1,3-diphenyl-1,2,4-benzotriazinyl radical (2.3)

4.2.1 Molecular structure

X-ray quality crystals of **2.3** were grown from hot heptane. The molecule crystallizes in the monoclinic crystal system with the C2/c space group with eight molecules in the unit cell.[100] Twinning of the crystals resulted in disorder in the N-linked phenyl ring of the molecule as described below.

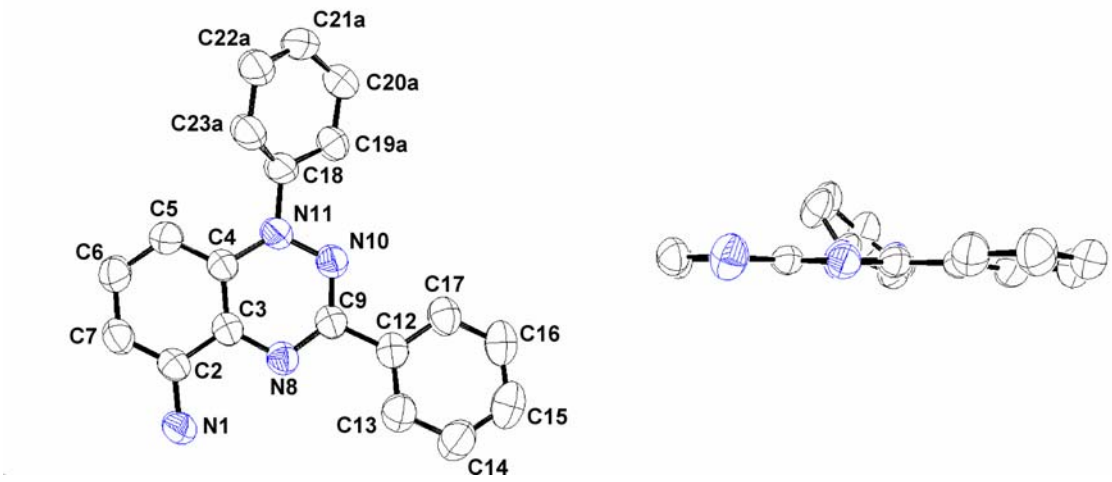

Figure 4.3 Molecular structure of **2.3**, face view (left) and side view (right). Rotational disorder of the N-linked phenyl ring is not shown. Thermal ellipsoids are drawn at the 50 % probability level.

The molecular structure of the amino-functionalized radical **2.3** is consistent with that of the parent radical **1.9**. The fused benzotriazinyl ring system is highly planar, with the two phenyl rings twisted out of the plane. In one occupancy, the plane of the disordered N-linked phenyl ring makes an angle of 41.1° with the plane of the benzotriazinyl ring, while in the other occupancy the angle is 50.5° in the opposite

direction. The angle between the plane of the benzotriazinyl ring and the plane of the C-linked phenyl ring is lower, at 7.7°. These angles are very similar to those found in **1.9**, of 55.9° for the N-linked ring and 10.5° for the C-linked ring. There are no significant deviations in the bond lengths of the benzotriazinyl ring of **2.3** from those of **1.9**, suggesting a similar degree of delocalization. In particular, the bond lengths of N8-C9 (1.334(2) Å), C9-N10 (1.335(2) Å), and N10-N11 (1.3689(19) Å) fall between the values for typical C-N and N-N single and double bonds, while the bond length of N1-C2 (1.379(2) Å) is consistent with the expected value of a C*ar*-NH_2 bond (1.375 Å).[101]

4.2.2 Crystal packing

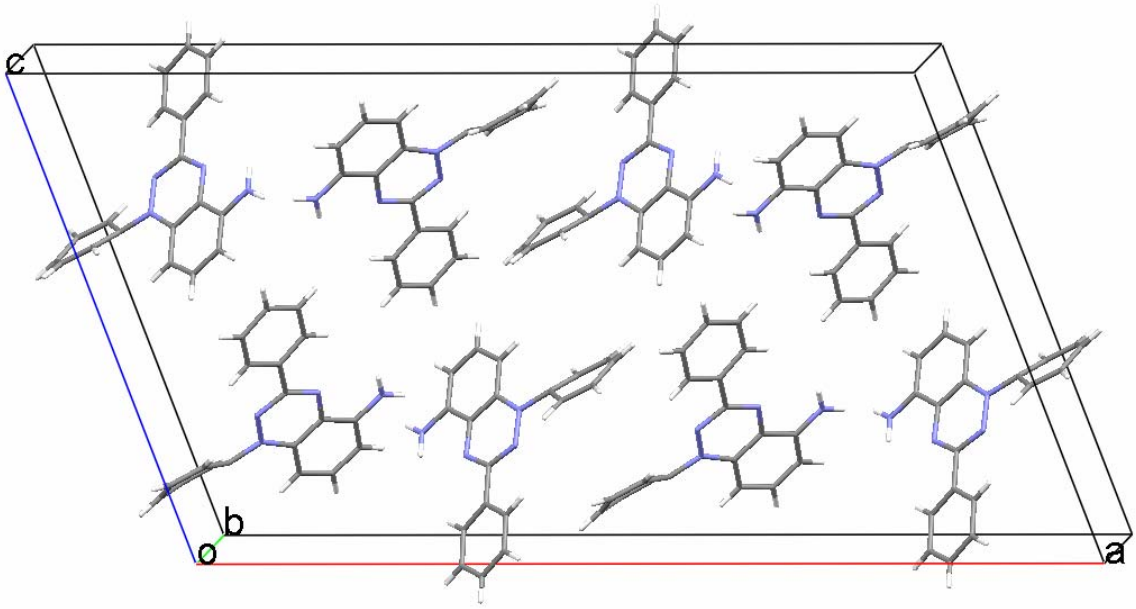

Figure 4.4 Unit cell of **2.3**. Disorder of the N-linked phenyl ring is not shown.

Two main forms of intermolecular interactions can be observed in the crystal packing of **2.3**. First, when viewed down the *b*-axis the radicals form head-to-head slipped π-stacks with an interplanar distance of 3.54 Å and a slippage angle of 45°,

whereby the triazinyl ring of one molecule partially overlaps with the benzene ring of its neighbour in the stack (Figure 4.5). These π-π interactions are possible due to the highly planar nature of the radicals, and the resulting π-stacks have been found in the all other benzotriazinyl radicals for which structural information has been obtained.

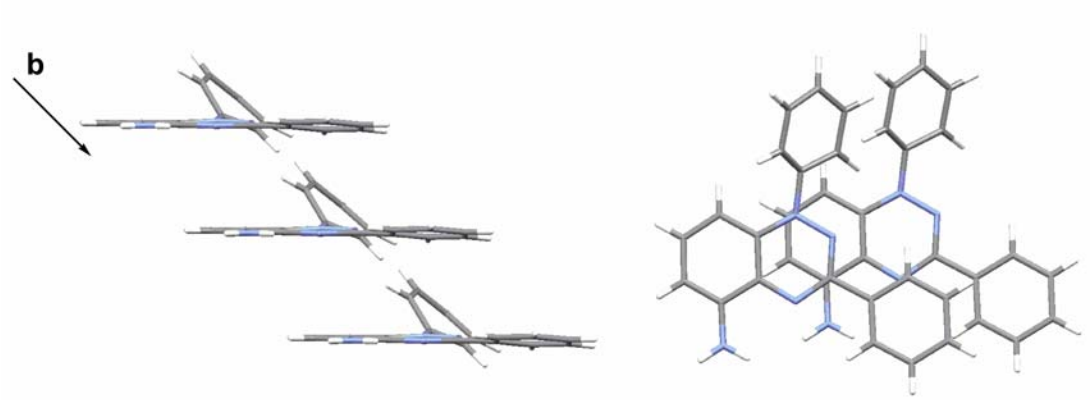

Figure 4.5 Slipped π-stacks down the *b*-axis in the crystal packing of **2.3**. Side view (left) and top view (right).

The second form of intermolecular interaction is unique to **2.3**. Along with the π-stacks, there also exists down the *b*-axis a chain of hydrogen bonding interactions between the amino groups of adjacent π-stacks (Figure 4.6). The N-N distance is 3.284(2) Å, which is approaching the sum of the van der Waals radii of the nitrogen atoms (~3.10 Å).[102]

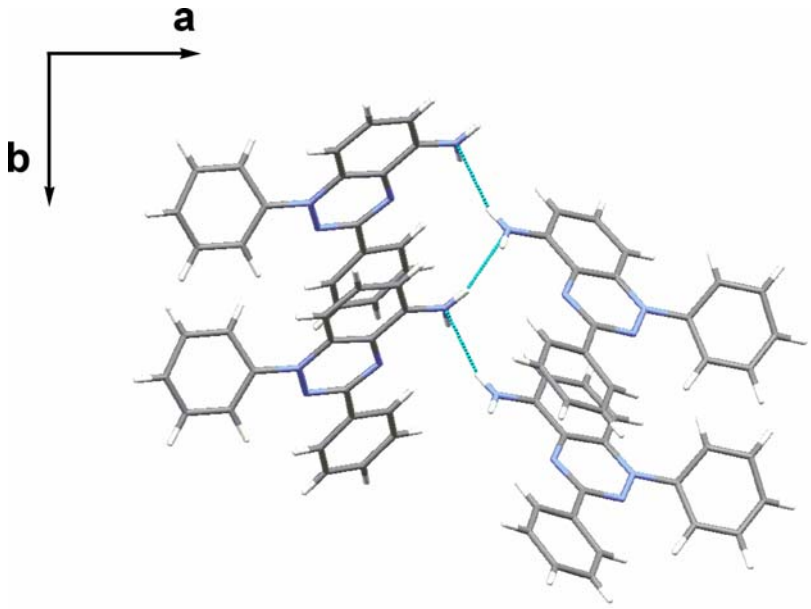

Figure 4.6 Inter-chain hydrogen bonding in **2.3** along the *b*-axis, viewed down the *c*-axis.

Therefore it can be seen that **2.3** displays two-dimensional solid state ordering, compared with the one-dimensional ordering found in **1.9**. Whereas **1.9** forms isolated linear π-stacks, **2.3** forms linear π-stacks which form interchain interactions *via* hydrogen bonding. There are also additional interactions between the N-linked phenyl rings both within and between the π-stacks, but due to the disorder of these rings the nature of the interactions is somewhat disrupted.

4.2.3 Magnetic behaviour

Both EPR spectroscopy and DFT calculations (Section 2.2.3) show a significant amount of spin density distributed over the benzotriazinyl ring of **2.3**, as well as on to the nitrogen atom of the amino group. The intermolecular interactions discussed above can be expected to lead to effective magnetic exchange pathways, as they bring the regions of high spin density of neighbouring molecules into close proximity.

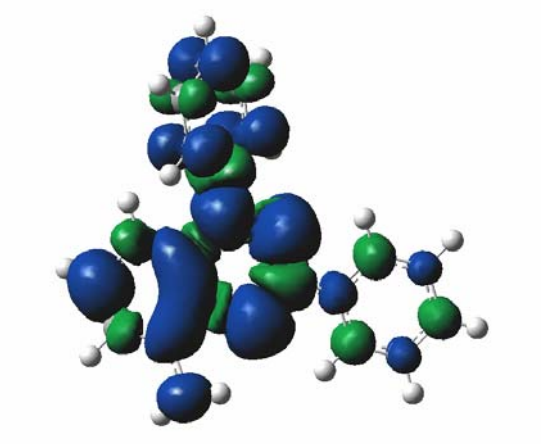

Figure 4.7 SCF spin density of **2.3** calculated at UB3LYP/6-31G(d,p), generated with isovalue = 0.0004 in GaussView 3.09.

The magnetization of a polycrystalline sample of **2.3** was measured as a function of temperature over the temperature range of 4–300 K at a constant applied field of 10000 Oe using a Quantum Design Magnetic Property Measurement System (MPMS). The magnetic susceptibility (χ) was corrected for diamagnetic contributions using Pascal's constants.

The magnetic susceptibility of **2.3** increases gradually as the temperature decreases to a maximum value of 0.0025 emu·mol^{-1} at 64.2 K, at which point it decreases rapidly, indicative of strong antiferromagnetic exchange (Figure 4.8, left). At very low temperature the susceptibility sharply increases once again due to residual unpaired spins, forming a Curie tail. A plot of the magnetic moment (χT) versus temperature also reveals strong antiferromagnetic exchange (Figure 4.8, right). The moment at 300 K is 0.275 emu·K·mol^{-1}, which is lower than the expected moment of 0.375 emu·K·mol^{-1} for a non-exchanging purely paramagnetic S = ½ radical. As the temperature decreases, the moment decreases to a minimum value of 0.010 emu·K·mol^{-1} at 4.36 K.

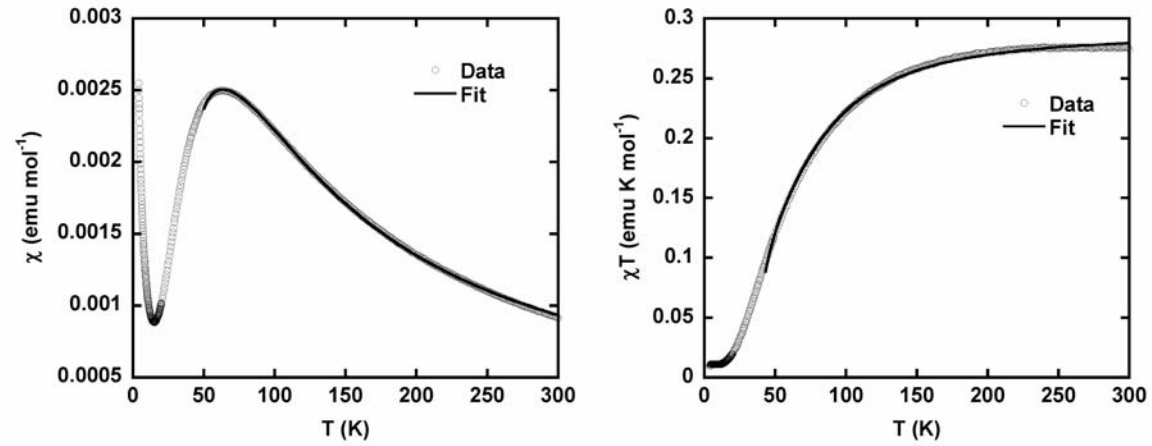

Figure 4.8 Temperature dependence of the magnetic susceptibility (left) and magnetic moment (right) of **2.3** measured at 10000 Oe from 4 – 300 K. Data was fit using the Padé model with a mean field approximation (Equation 4.7).

Full numerical analysis of magnetic exchange requires the use of analytical models which are based on the nature of the exchange pathways. Unfortunately, the only analytical models that have been developed are for cases of one-dimensional exchange, while **2.3** is a two-dimensional system. Therefore in order to attempt to model the magnetic behaviour of **2.3** it was assumed that the major pathway for exchange is *via* the π-stacks, and that the inter-chain exchange would be minor in comparison and could be accounted for by a generalized mean field approximation. The model that was used was the Padé model (Equation 4.6), which is appropriate for fitting both ferromagnetic and antiferromagnetic exchange through linear chains.[90] In this expression, f is a purity factor that represents the proportion of the spins in the sample which follow the model being used, N is Avogadro's number (6.0221367×10^{23} mol^{-1}), g is the g factor of the unpaired electron (2.0043 for **2.3**), β is the Bohr magneton ($4.66864374 \times 10^{-5}$ cm^{-1} G^{-1}), k is the Boltzmann constant (0.69503877 cm^{-1} K^{-1}) T is the temperature, and J is the magnetic exchange parameter.

$$\chi = f\,\frac{Ng^2\beta^2}{4kT}\left[\frac{C}{D}\right]^{2/3} \qquad (4.6)$$

$$C = 1.0 + 5.7979916y + 16.902653y^2 + 29.376885y^3 + 29.832959y^4 + 14.036918y^6$$

$$D = 1.0 + 2.7979916y + 7.0086780y^2 + 8.6538644y^3 + 4.5743114y^4$$

$$y = J/2kT$$

The expression for χ is incorporated into Equation 4.7 to give an expression for χ', which includes the mean field approximation. In this equation 2zJ' is the mean field exchange parameter, where z represents the number of nearest neighbours for magnetic exchange, and J' is the exchange term.

$$\chi' = \frac{\chi}{1 - (2zJ'/Ng^2\beta^2)\chi} \qquad (4.7)$$

Using Equation 4.7, both χ and χT were fit versus temperature to extract values for f, J, and 2zJ'. The results are shown in Table 4.1. The values acquired from both fits are in excellent agreement with one another. The negative values of J are consistent with antiferromagnetic exchange, and their magnitudes indicate that the exchange is strong for an organic system. The mean field magnetic exchange parameter however, is positive (ferromagnetic) and approximately equal to J, assuming a value of z = 3. The fact that the mean field expression used to fit minor exchange interactions results in an exchange parameter that is not insignificant reflects the limitations of using a one-dimensional model to fit a two-dimensional system. These results do suggest however, that in **2.3** both

the through π-stack exchange and the inter-stack exchange through hydrogen bonding contribute significantly to the overall magnetic behaviour of the radical.

Table 4.1 Magnetic exchange parameters of **2.3** acquired using Equation 4.7.

	J (cm^{-1})	**2zJ' (cm^{-1})**	**f**	**R^2**
χ vs T	-33.20 ± 0.05	175.14 ± 1.75	0.76	0.9996
χT vs T	-32.70 ± 0.09	172.91 ± 2.54	0.76	0.998

The contributions of hydrogen bonding to magnetic exchange pathways has been investigated largely with nitronyl nitroxide radicals, through the use of a several different structural components capable of such interactions (Figure 4.9).[103-108] In some of these systems the major effect of the hydrogen bonding is simply to provide a mechanism for intermolecular contact to bring together the high spin sites of the radicals or provide high dimensionality, while in other cases the exchange is thought to be actively mediated, typically in a ferromagnetic fashion, by the hydrogen bonds. In the case of **2.3** it is clear that hydrogen bonding plays both roles and can be seen to provide a mechanism for strong and multidimensional intermolecular interaction in benzotriazinyl radicals.

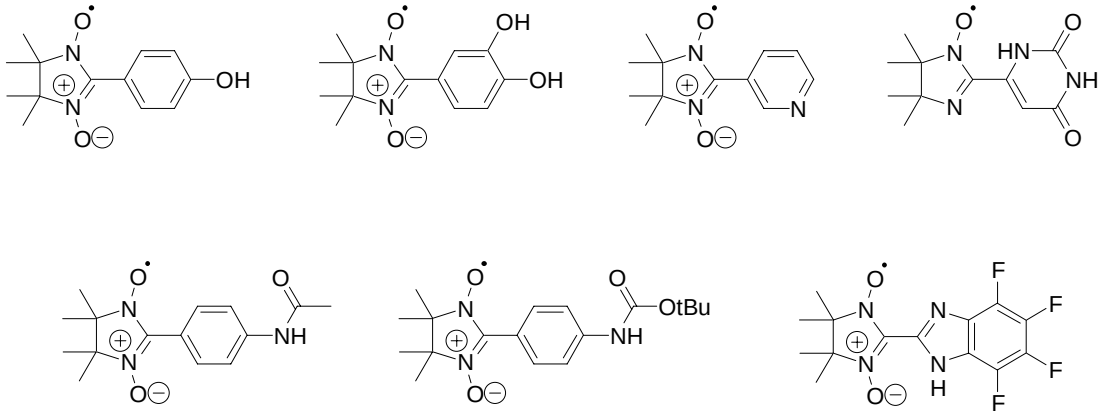

Figure 4.9 Radicals capable of solid-state hydrogen bonding interactions.

4.3 5-Ammonium-1,3-diphenyl-1,2,4-benzotriazinyl bromide (2.20)

4.3.1 Molecular structure

Single crystals of **2.20** suitable for XRD study were grown from MeOH. The molecule crystallizes in the monoclinic crystal system with the $P2_1/n$ (#14) space group with four molecules in the unit cell.[100]

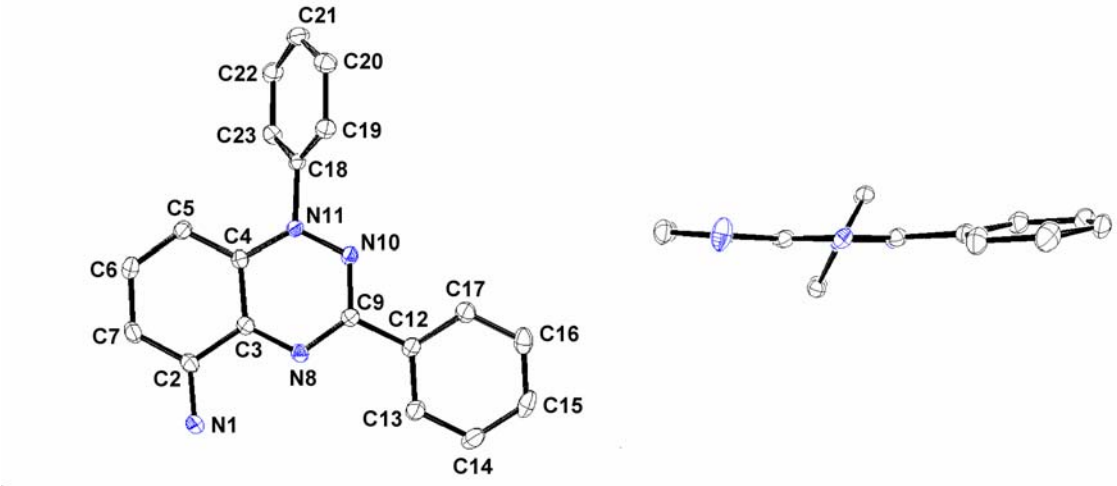

Figure 4.10 Molecular structure of **2.20**, face view (left) and side view (right). Thermal ellipsoids are shown at the 50 % probability level. Bromide anion and MeOH solvent molecule are not shown.

The main structural features of **2.20** are similar to those of **1.9** and **2.3**. The molecule has a nearly planar benzotriazinyl ring system, with the plane of the C-phenyl ring twisted by 10.5° and the plane of the N-phenyl ring twisted by 64.1°. Examination of the bond lengths of the benzotriazinyl ring system of **2.3** however, reveal some significant differences from the equivalent bond lengths in **1.9** and **2.3** (Table 4.2), indicating an overall change in the electronic structure of the system. Specifically, C3-N8, C4-N11, and N10-N11 seem to possess significantly more double bond character (shorter bond lengths) in **2.20** than in **1.9** and **2.3**, while with the exception of the C9-N10

bond length which is not significantly changed, the remaining bond lengths of **2.20** are longer than in **1.9** and **2.3**, consistent with more single bond character.

Table 4.2 Comparison of bond lengths in **1.9**, **2.3**, and **2.20**.

Bond	Bond length (Å)		
	1.9	**2.3**	**2.20**
N1-C2	n/a	1.379(2)	1.327(4)
C2-C3	1.393(2)	1.413(2)	1.459(3)
C2-C7	1.372(3)	1.376(3)	1.393(4)
C3-C4	1.408(3)	1.406(2)	1.441(4)
C3-N8	1.375(2)	1.370(2)	1.318(3)
C4-C5	1.390(3)	1.388(3)	1.391(4)
C4-N11	1.401(2)	1.392(2)	1.367(3)
C5-C6	1.375(2)	1.379(3)	1.386(3)
C6-C7	1.389(3)	1.379(2)	1.392(4)
N8-C9	1.324(2)	1.334(2)	1.347(3)
C9-N10	1.337(2)	1.335(2)	1.336(3)
N10-N11	1.361(2)	1.369(2)	1.322(3)

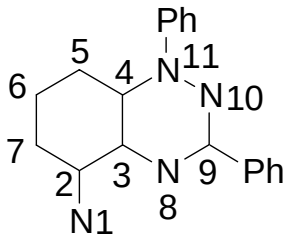

Figure 4.11 Atomic numbering scheme for Table 4.2.

In comparing the N1-C2 bond in **2.20** and in **2.3** it can be seen that the bond length is shortened in **2.20** relative to **2.3**. The shortening of the N1-C2 bond is inconsistent with the existence of an $-NH_3^+$ group as this is expected to lead to an increase of the N1-C2 bond length relative to the neutral amine.[101] As the molecule must be protonated, this observation implies protonation of one of the ring nitrogens instead of the amino nitrogen. This is contrary to the solution state EPR observations (Section 2.4.1), and suggests a difference between the solution and solid state structures of the molecule. Figure 4.12 shows some possible tautomeric and resonance structures that could contribute to an overall solid state structure which would be consistent with the observed shortened N1-C2 bond length.

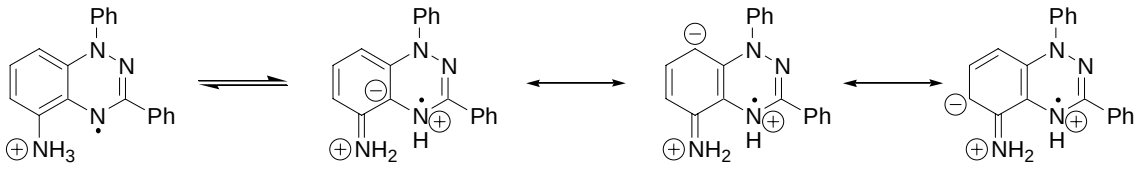

Figure 4.12 Possible tautomeric and resonance contributors to the molecular structure of **2.20**.

4.3.2 Crystal packing

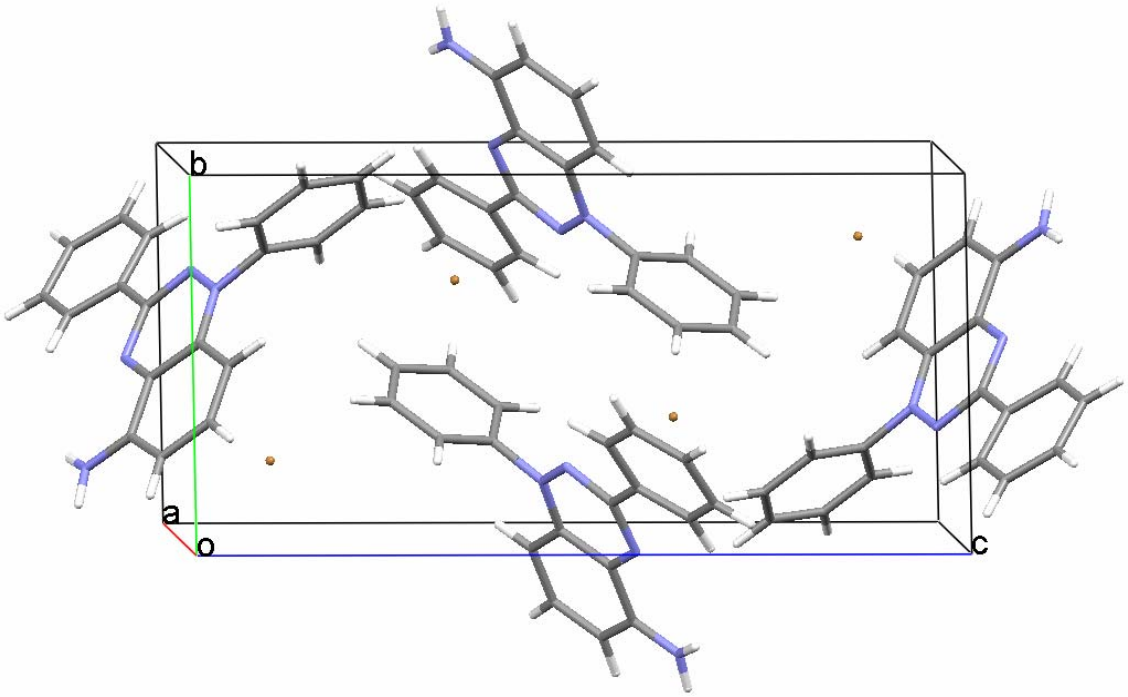

Figure 4.13 Unit cell of **2.20**. MeOH solvent molecules removed for clarity.

The intermolecular interactions of the radical cation are different from those of the neutral radical **2.3**. The molecules of **2.20** form chains of head-to-tail dimers along the *a*-axis, with close contacts both within (Figure 4.14) and between (Figure 4.15) the dimers. The head-to-tail orientation results in the direct overlap of the C-linked phenyl ring of one molecule with the triazinyl ring of the other.

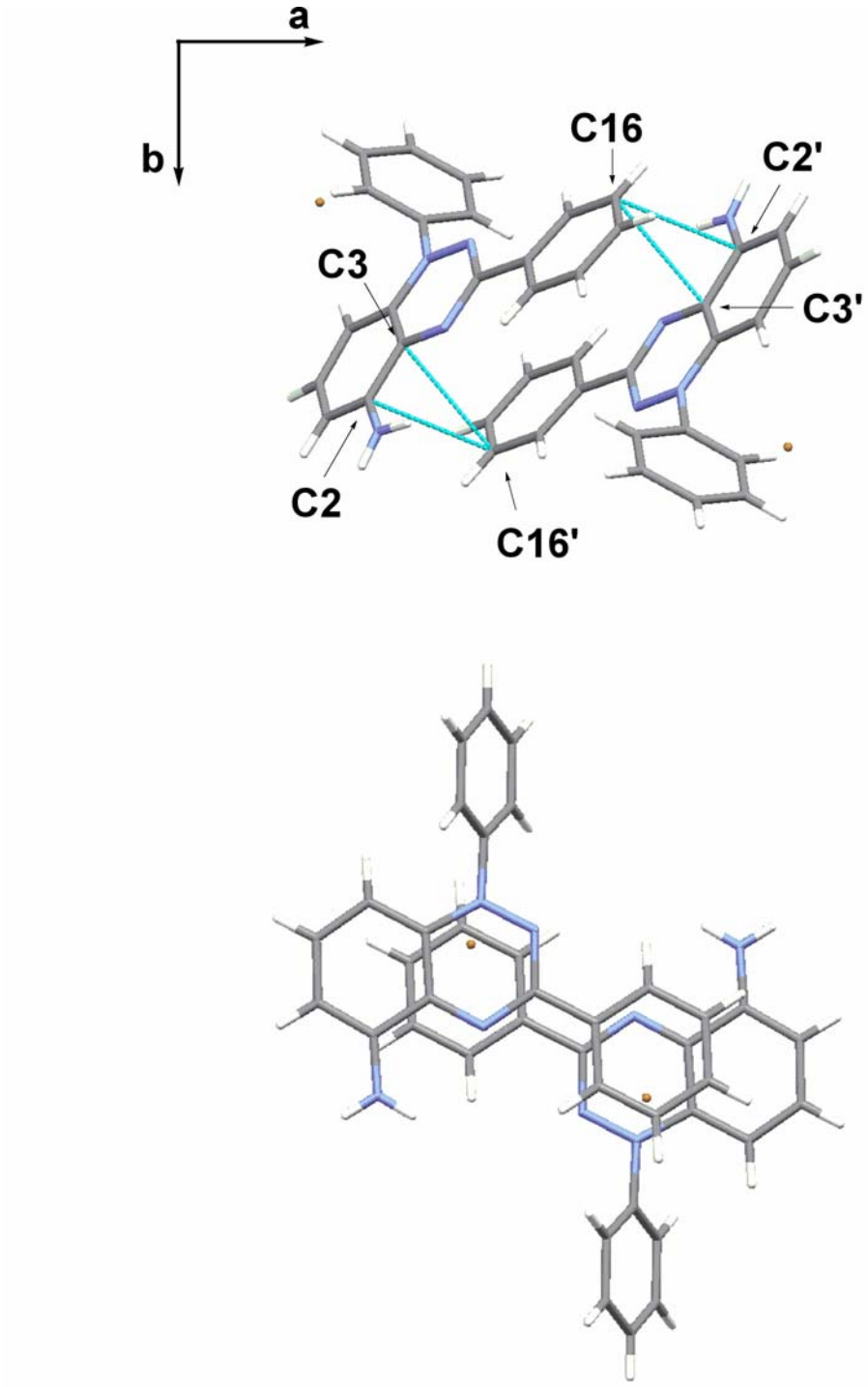

Figure 4.14 Dimer of **2.20** viewed down the *c*-axis showing intra-dimer close contacts (top), and dimer viewed from the top showing overlap (bottom).

The shortest intermolecular distances within the dimers are C2···C16' (3.26 Å) and C3···C16' (3.28 Å) (Figure 4.14, top), while between dimers the closest contacts are C5···C6" (3.36 Å) (Figure 4.15). These distances are all within the sum of the van der Waal's radii of two carbon atoms (~3.40 Å),[102] consistent with weak bonding interactions that are stronger than the intermolecular interactions typically found between benzotriazinyl radicals. Strong intermolecular interactions leading to π-dimers have been observed in other radical cation species, despite the requirement of bringing together positively charged systems.[109]

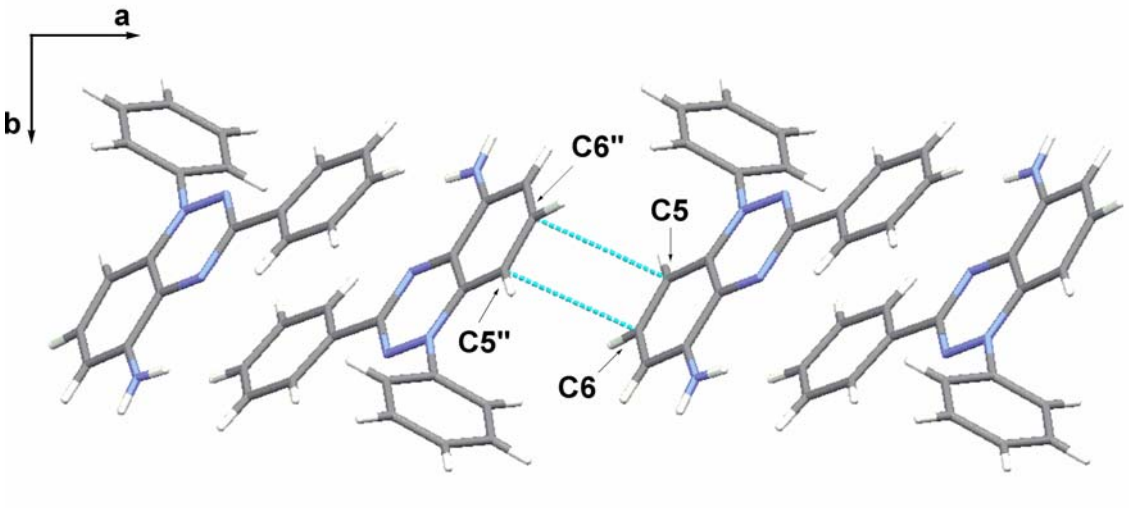

Figure 4.15 Inter-dimer close contacts of **2.20** viewed down the *c*-axis.

4.3.3 Magnetic behaviour

Magnetic measurements on a polycrystalline sample of **2.20** was carried out over the temperature range of 4–300 K at 10000 Oe using a Quantum Design MPMS. These measurements revealed that in the solid state the bulk material is diamagnetic over the

entire temperature range. This is in direct opposition to the solution state paramagnetism of **2.20** that was observed through EPR and NMR spectroscopy, and can be attributed to the weak bonding within and between the dimers of **2.20** resulting in strong antiferromagnetic exchange of the radicals in the solid state. In particular, the C5···C6" inter-dimer interactions bring the high-spin density of the benzene rings of neighbouring molecules into close proximity, making this a likely pathway for magnetic exchange. As the exchange interactions are akin to weak bonding interactions, dissolution of the material breaks the radical cations into isolated paramagnetic molecules.

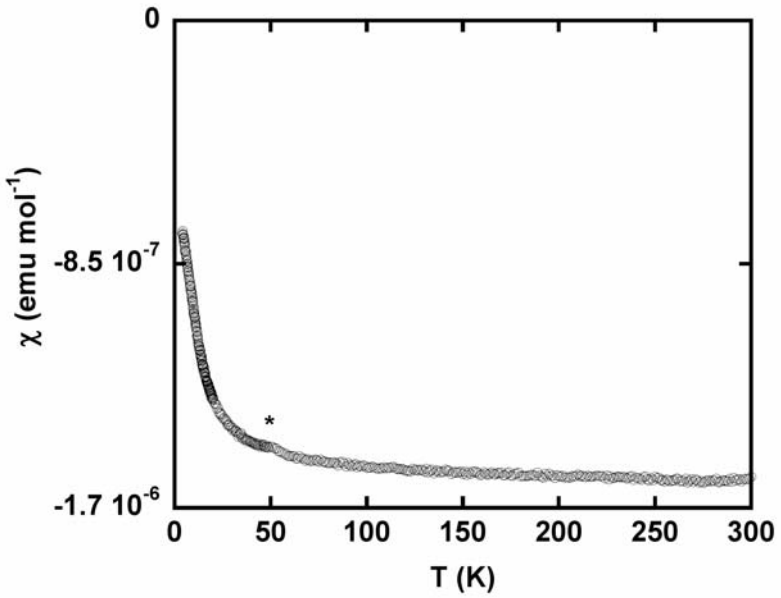

Figure 4.16 Temperature dependence of the magnetic susceptibility χ of radical cation **2.20** measured at 10000 Oe from 4 – 300 K (* oxygen).

4.4 1,3-bis-(1-phenyl-1,2,4-benzotriazinyl)-benzene (3.2)

4.4.1 Molecular structure

X-ray quality single crystals of **3.2** were grown from EtOAc. The molecule crystallizes in the monoclinic crystal system with the $P2_1/n$ (#14) space group with four molecules in the unit cell.[100]

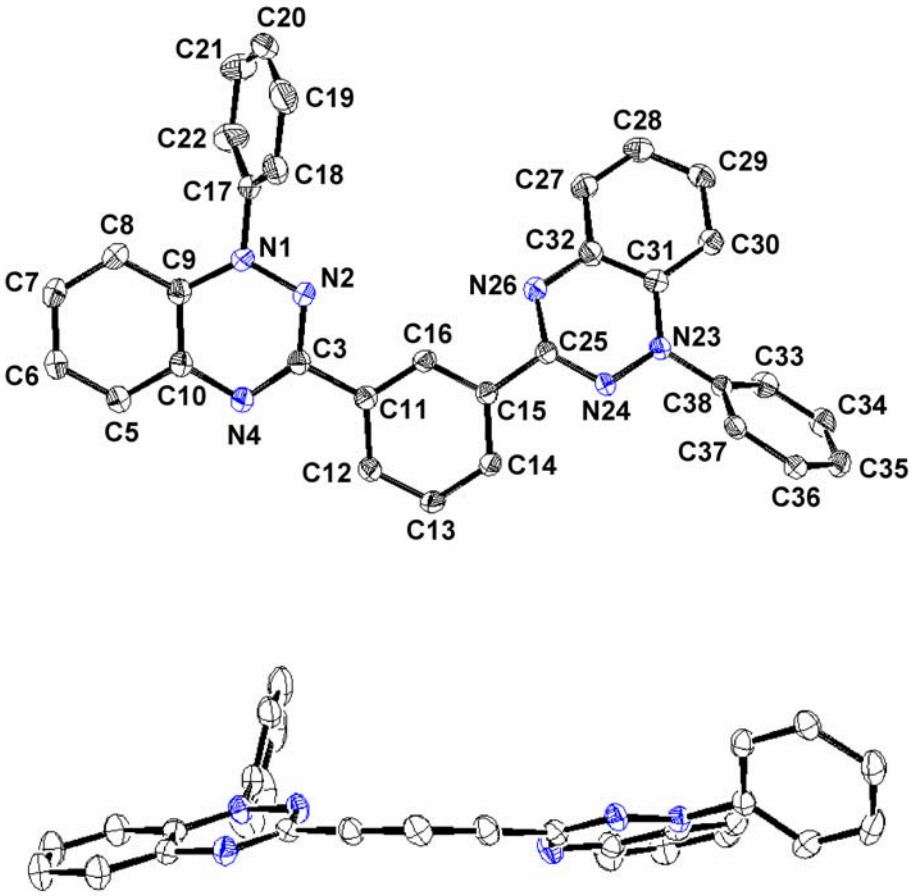

Figure 4.17 Molecular structure of **3.2**, face view (top) and side view (bottom). Thermal ellipsoids are shown at the 50 % probability level.

The benzotriazinyl ring system comprised of atoms N1 through C10 is highly planar, while the ring system comprised of atoms N23 through C32 is distorted, with the entirety of the benzene ring C27→C32 bent out of the plane formed by N23-N24-C25-N26 (Figure 4.14). The displacements out of the plane range from 0.09 Å for C32 to 0.41 Å for C29. The distortion does not affect the bond lengths however, which are nearly identical between each benzotriazinyl ring and in comparison with **1.9**. The slight distortions are therefore most likely due to packing interactions and not differences in electronic structure.

Figure 4.18 Comparison of the planarity of the two benzotriazinyl rings of **3.2**.

The torsion angle of the phenyl ring at N1 is 66.5°, compared with 43.7° for the phenyl ring at N23, while the bridging phenylene ring is twisted out of the plane of the benzotriazinyl at C3 by 19.2°, compared with 13.8° with respect to the benzotriazinyl at C25. Both of these final two rotational angles are larger than the equivalent angle found in **1.9** (10.5°), resulting in significant distortion in the planarity of the entire biradical (Figure 4.16, bottom).

4.4.2 Crystal packing

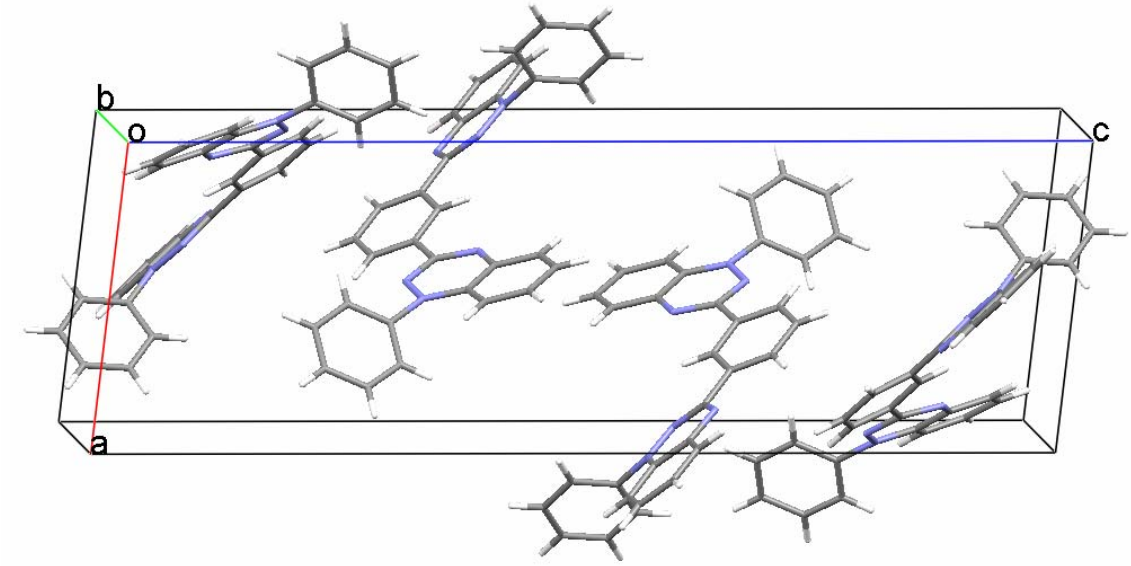

Figure 4.19 Unit cell of biradical **3.2**.

The main form of ordering in **3.2** is in the form of linear chains down the *b*-axis, similar to typical benzotriazinyl radicals (Figure 4.20, top). Unlike these radicals however, the biradical does not form well ordered π-stacks, likely due to the torsions of the phenyl rings preventing parallel and direct π-π interactions between the aromatic rings of adjacent molecules. The closest interaction is between the N1→N4 triazinyl ring of one molecule and the C27'→C32' benzene ring of its neighbour, with an angle of 23° between the planes of these two rings. Table 4.3 lists selected intermolecular close contact distances along the overlap between the biradicals (Figure 4.20, bottom). These distances are either within the sums of the van der Waals radii of the atoms or slightly larger (C···C 3.40 Å, C···N 3.25 Å).[102]

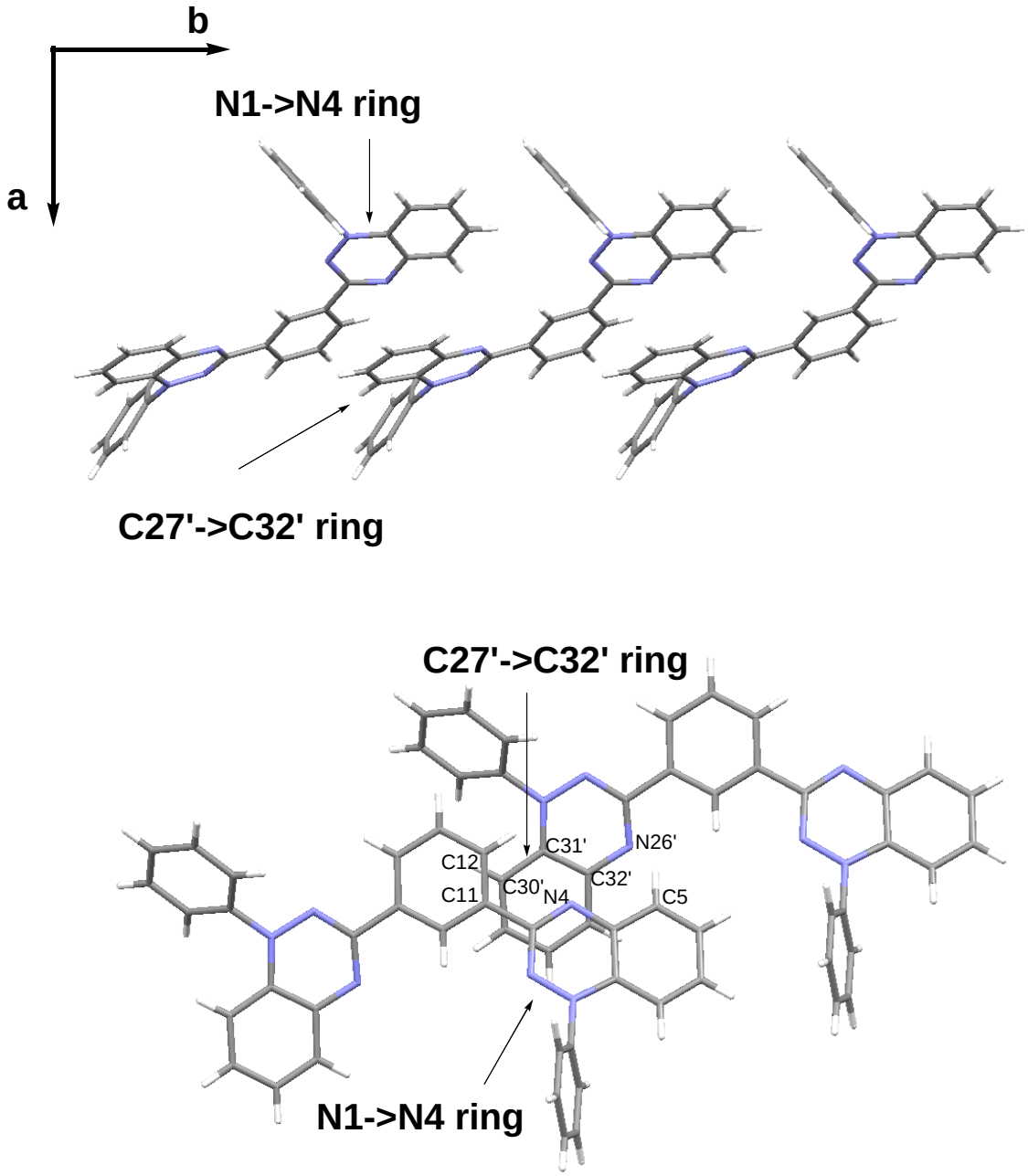

Figure 4.20 Linear chains along the *b*-axis in the crystal packing of **3.2**, viewed down the *c*-axis (top). Intermolecular overlap viewed from the top (bottom).

Table 4.3 Selected intermolecular contact distances.

Atoms	Distance (Å)
N4···C31’	3.372
N4···C32’	3.392
C5···N26’	3.413
C11···C30’	3.299
C12···C30’	3.315

In addition to the linear chains, there also exists a more complicated three dimensional array of intra- and interchain tilted-T interactions between the two N-linked phenyl rings and the other aromatic rings of the biradicals, resulting in overall three-dimensional ordering (Figure 4.21). The N1 phenyl rings provide interactions along the linear chains and between neighbouring chains along the *a*-axis, while the N23 phenyl rings provide interchain interactions along the *a*-axis and *c*-axis. The torsion angles of each of the two phenyl rings appear to be optimized to maximize the edge to face interactions with all of their neighbouring aromatic rings.

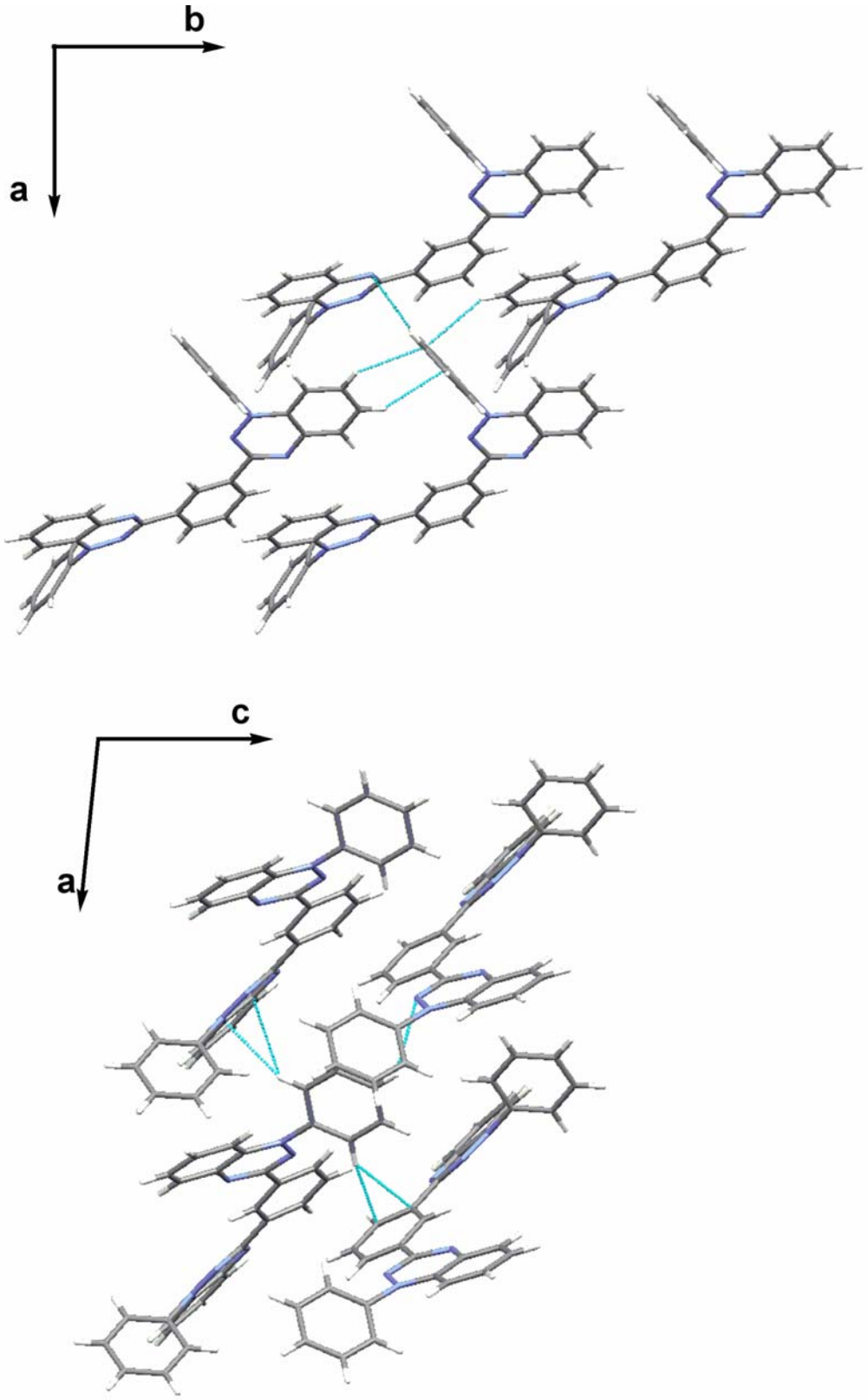

Figure 4.21 Intermolecular close contacts of N1 phenyl ring (top) and N23 phenyl ring (bottom).

4.4.3 Magnetic behaviour

As was mentioned in Section 3.2, the *m*-phenylene bridge is known to generally lead to intramolecular ferromagnetic exchange in biradicals, through a pathway of spin polarization in which atoms in a π-conjugated system have alternating positive and negative spin densities (Figure 4.22).[72] The magnitude of the exchange is generally weak, and is a function of the spin densities at the *m*-phenylene positions, the presence and nature of substituent groups on the bridge,[110] as well as the torsion angles between the radicals and the bridge.[111] As **3.2** was the first example of a *m*-phenylene-bridged benzotriazinyl biradical, it was of interest to investigate the nature of the magnetic exchange through the bridge in this particular class of biradical.

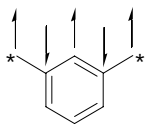

Figure 4.22 Ferromagnetic exchange through spin polarization in *m*-phenylene bridges.

In the solution state, EPR spectroscopy of **3.2** confirmed the population of a triplet ground state at low temperatures (Section 3.3.2). Additionally, DFT calculations carried out on the singlet and triplet states of **3.2** revealed a triplet ground state with a singlet-triplet gap of J = 14 cm^{-1}, suggesting weak ferromagnetic exchange of a magnitude similar to that observed in related verdazyl[75] and nitronyl nitroxide *m*-phenylene biradicals.[112]

Magnetic measurements on a polycrystalline sample of **2.3** was carried out over the temperature range of 4–300 K at 10000 Oe using a Quantum Design MPMS. The magnetic susceptibility (χ) was corrected for diamagnetic contributions by correcting for

the non-zero slope of the paramagnetic regime of a plot of magnetic moment versus temperature from the measured susceptibility data.

The measurements showed weak ferromagnetic exchange in the biradical, consistent with the solution state and computational observations. Between approximately 150 and 300 K the magnetic moment (χT) is equal to approximately 0.71 emu K mol^{-1}, just below the value for two non-interacting unpaired electrons (0.750 emu K mol^{-1}). Once the temperature drops below ~150 K the magnetic moment increases, first gradually and then sharply, to a maximum value of 1.40 emu K mol^{-1} at 4.74 K. This maximum is higher than the χT value for an isolated S = 1 biradical (1.00 emu K mol^{-1}), indicating that there is a combination of intramolecular and intermolecular ferromagnetic exchange contributions to the magnetic moment.

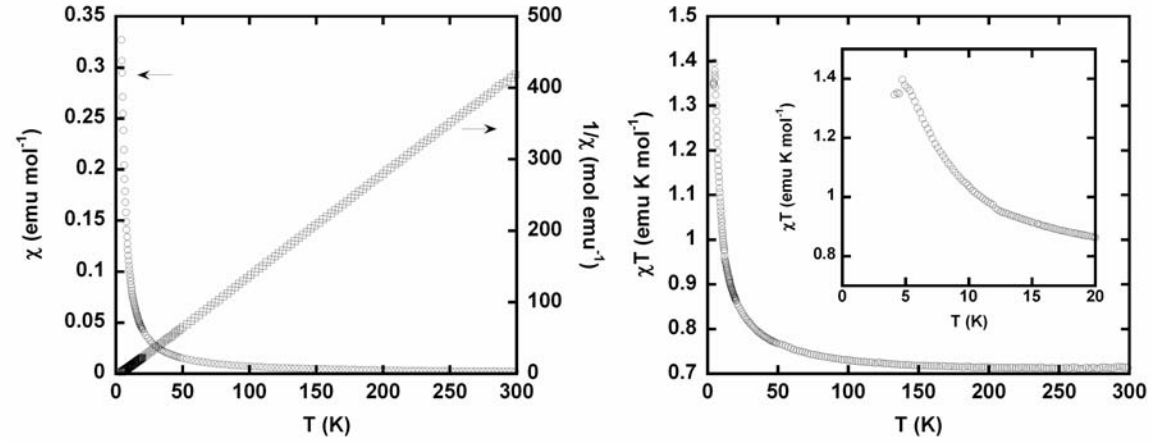

Figure 4.23 Temperature dependence of the magnetic susceptibility χ (red) and $1/\chi$ (blue) of **3.2** (left plot) and temperature dependence of the magnetic moment χT of **3.2** (right plot). Data obtained from 4 – 300 K using a magnetic field of 10000 Oe.

A quantification of the bulk magnetic properties of **3.2** (intra- and intermolecular) using a Curie-Weiss fit (Equation 4.4) of the inverse magnetic susceptibility resulted in a Curie constant of C = 0.70 emu·K·mol^{-1} and a Weiss constant of θ = 3.4 K. The Curie

constant is consistent with the expected value for two non-interacting unpaired electrons of 0.750 emu·K·mol^{-1}, while the small and positive Weiss constant is indicative of weak ferromagnetic exchange. Further measurements on a magnetically dilute sample of the biradical within a polymer matrix are needed to isolate the specific intermolecular exchange parameters from the intramolecular exchange parameters.

4.5 Diffuse reflectance spectroscopy

Diffuse reflectance spectroscopy was used to investigate solid state intermolecular interactions in the parent radical **1.9**, the amino-functionalized radical **2.3**, the radical cation **2.20**, and biradicals **3.2**-**3.4**. The following three pages present comparisons of the solid and solution state absorbance data of these compounds. For all six compounds there are no new transitions that appear in the solid state, but there are distinct bathochromic shifts in the onsets of absorbance in the solid state relative to the solution state of ~ 100 – 300 nm, implying the existence of lower energy transitions in the solid state. Such transitions would arise from significant intermolecular interactions. In the cases of **1.9**, **2.3**, **2.20**, and **3.2** it is known from the crystal structures that these interactions are largely π-π in nature, with additional hydrogen bonding in **2.3**. While the structures of **3.3** and **3.4** have not been determined, the intermolecular interactions could potentially be donor-acceptor interactions between donor benzotriazinyl radicals and acceptor aromatic bridges.

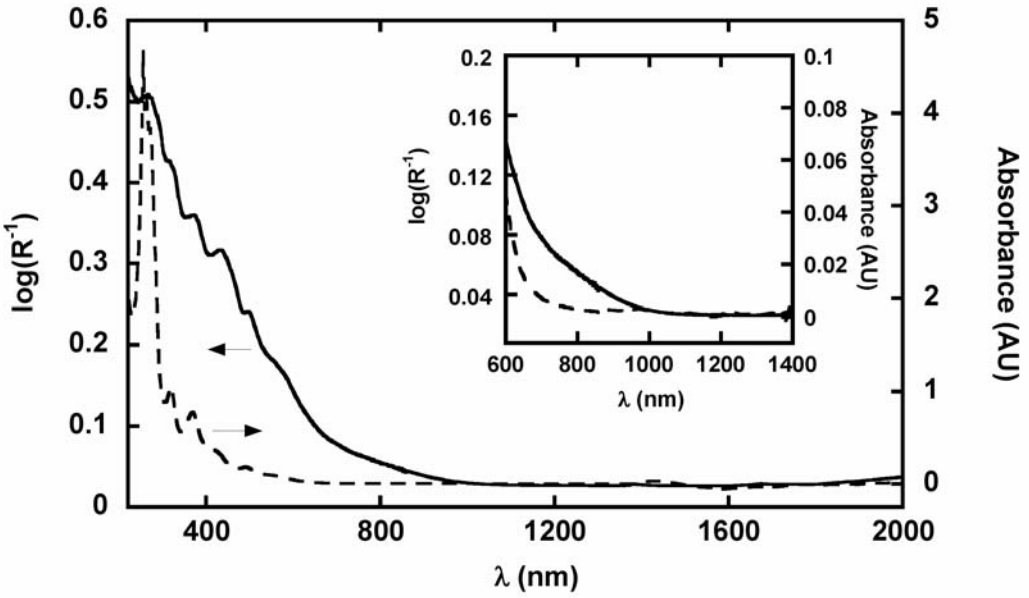

Figure 4.24 Solid state diffuse reflectance spectrum (solid line) and solution state absorption spectrum (dashed line) spectroscopy of parent benzotriazinyl radical **1.9**.

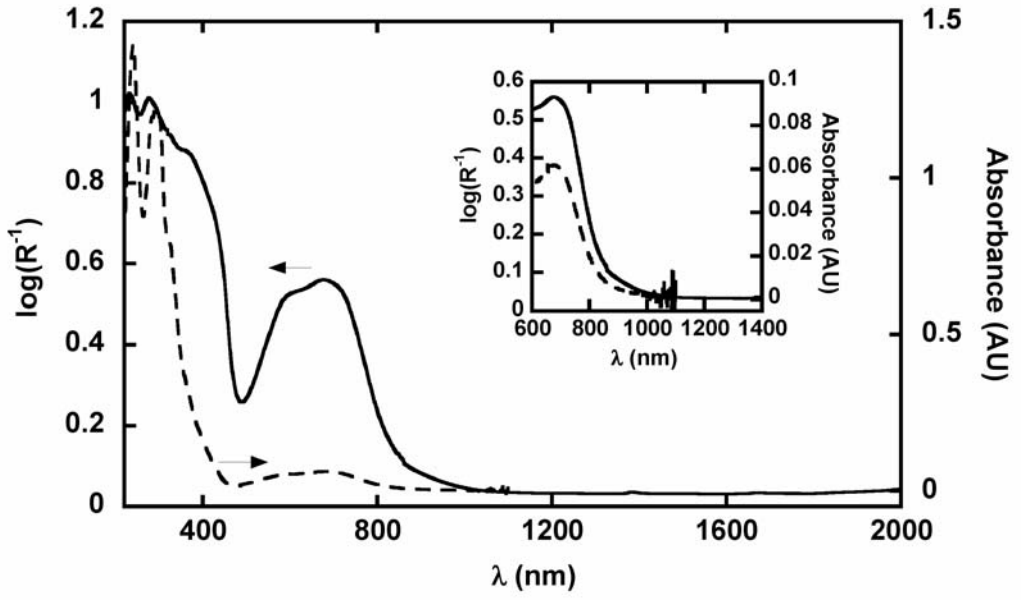

Figure 4.25 Solid state diffuse reflectance spectrum (solid line) and solution state absorption spectrum (dashed line) spectroscopy of amino-functionalized benzotriazinyl radical **2.3**.

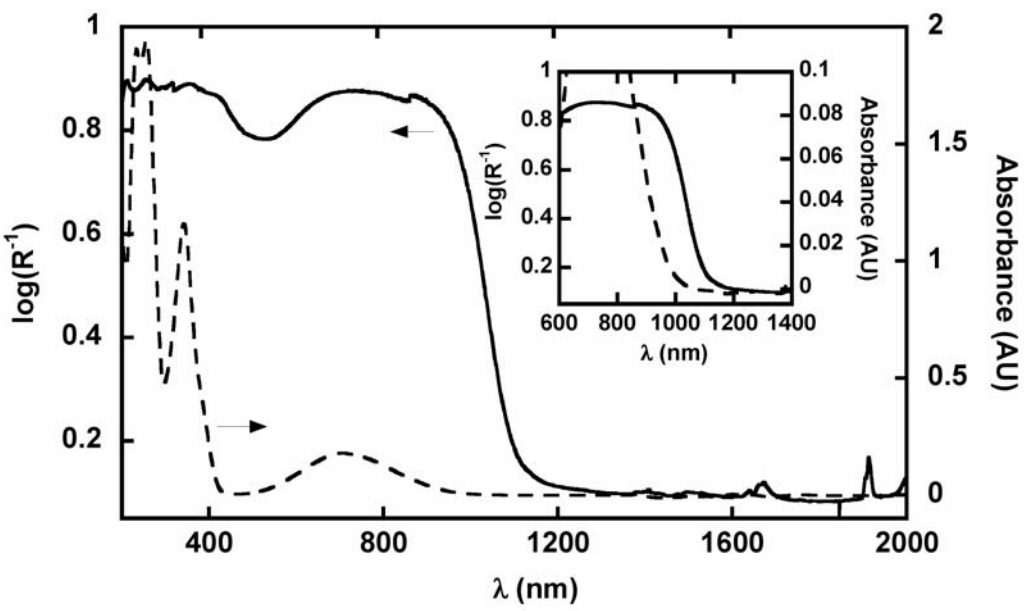

Figure 4.26 Solid state diffuse reflectance spectrum (solid line) and solution state absorption spectrum (dashed line) spectroscopy of radical cation **2.20**.

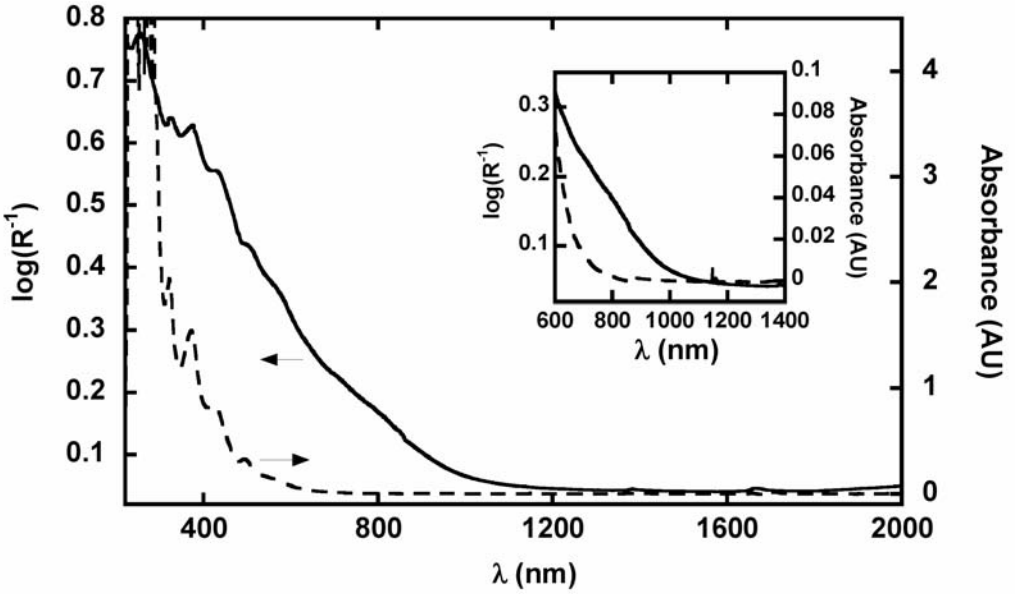

Figure 4.27 Solid state diffuse reflectance spectrum (solid line) and solution state absorption spectrum (dashed line) spectroscopy of biradical **3.2**.

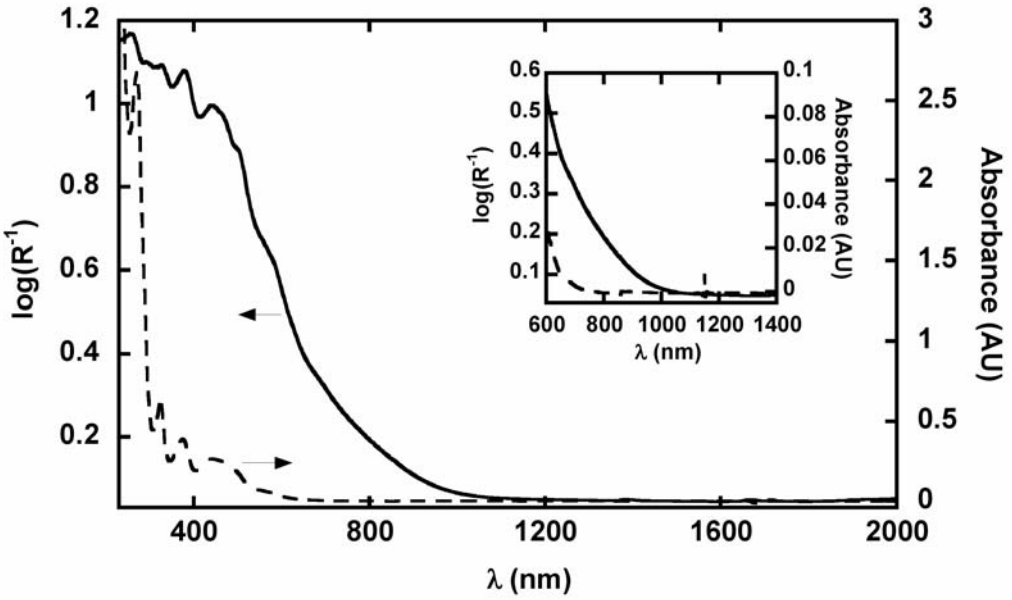

Figure 4.28 Solid state diffuse reflectance spectrum (solid line) and solution state absorption spectrum (dashed line) spectroscopy of biradical **3.3**.

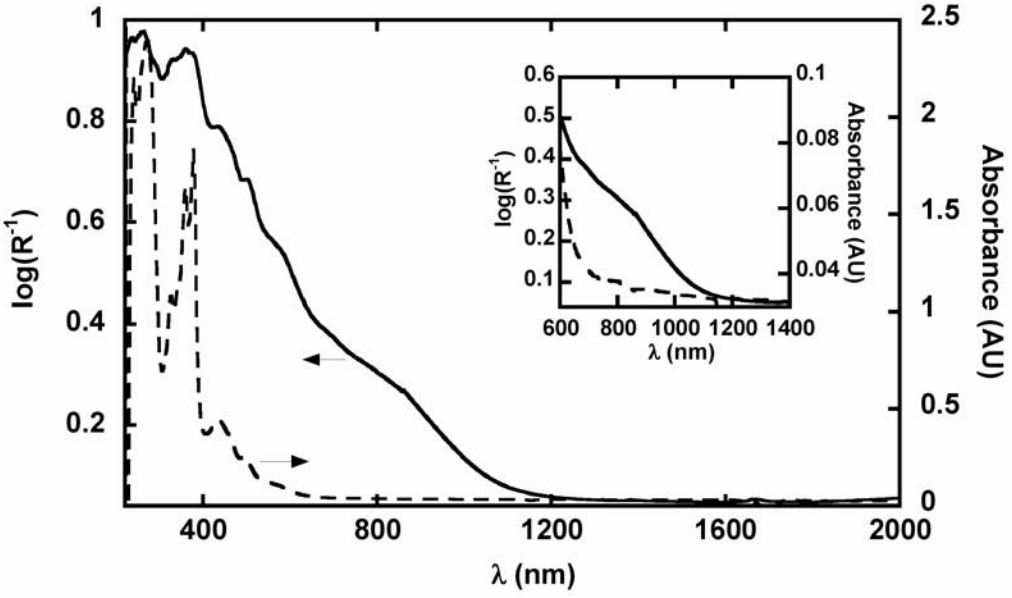

Figure 4.29 Solid state diffuse reflectance spectrum (solid line) and solution state absorption spectrum (dashed line) spectroscopy of biradical **3.4**.

4.6 Conductivity measurements

Preliminary conductivity measurements were carried out on radicals **2.3**, **2.20**, and **3.2-3.4** using a two-probe pressed pellet apparatus.[113] The apparatus was calibrated using the TTF-TCNQ charge transfer salt, which has a known conductivity of ~ 1 - 10 $S \cdot cm^{-1}$ using this form of pressed pellet measurement.[113] The average conductivity of TTF-TCNQ was measured to be on the order of 10^{-1} $S \cdot cm^{-1}$, roughly one to two orders of magnitude lower the accepted literature value. Therefore the average measured conductivities of **2.3** and **3.2-3.4** as listed in Table 4.4 were corrected for this discrepancy using Equation 4.8, where σ_{exp} is the average measured conductivity of the sample, σ_{TTF} is the measured conductivity of TTF-TCNQ of 10^{-1} $S \cdot cm^{-1}$, σ_{lit} is the literature conductivity of TTF-TCNQ taken to be 10 $S \cdot cm^{-1}$, and σ_{corr} is the corrected sample conductivity. The conductivity of **2.20** was found to be too low to be measurable, and so is listed as < 10^{-9} $S \cdot cm^{-1}$. The full and uncorrected data sets for all of the compounds are listed in the experimental section of this chapter. Given the reproducibility level of the data, the conductivities are considered to be accurate to within roughly one order of magnitude.

$$\frac{\sigma_{exp}}{\sigma_{TTF}} = \frac{\sigma_{corr}}{\sigma_{lit}} \qquad (4.8)$$

Table 4.4 Average conductivity values.

σ_{corr} ($S \cdot cm^{-1}$)[a]				
2.3	**2.20**	**3.2**	**3.3**	**3.4**
10^{-5}	< 10^{-9}	10^{-4}	10^{-5}	10^{-5}

[a]Calculated using equation 4.8.

The conductivity of **1.9** of 10^{-9} S·cm^{-1},[57] measured using the same pressed pellet apparatus used for the measurements taken in this thesis, can be seen to be approximately four to five orders of magnitude lower than the conductivities of **2.3** and **3.2**-**3.4**, which are all in the semiconducting regime. As stated in Section 4.1.2, the conductivities of neutral radicals depend upon both structural ordering and the binding energy of the unpaired electrons to the radical sites, represented by the value of E_{cell}. As there is essentially no change in the E_{cell} value of **1.9** compared with **2.3** and **3.2**, the improvements in conductivity in these two compounds is likely due to intermolecular interactions. However, complete analysis of the charge transport properties of these two radicals will require accurate four-probe conductivity measurements on single crystals, as well as band structure calculations. Similarly, for biradicals **3.3** and **3.4** it will be necessary to obtain crystal structures in order to fully analyze their charge transport behaviour. The improved conductivity in these two compounds could be due to a combination of structural effects or electronic effects, as their solid state diffuse reflectance spectra revealed the possibility of intermolecular charge transfer interactions.

4.7 Conclusions

The effects of molecular structure on the solid state ordering and magnetic behaviour of radicals **2.3**, **2.20** and **3.2** was examined. The amino-group of **2.3** was found to result in the formation of hydrogen-bonding between linear π-stacks of the radical molecules, giving rise to two-dimensional ordering. The strong antiferromagnetic exchange observed for this compound appeared to have contributions from both forms of intermolecular interactions. Conversely, the amino-functionalized radical cation **2.20** was found to order in one dimension, forming linear chains of dimers which resulted in strong

antiferromagnetic exchange and diamagnetic behaviour. Finally, the *m*-phenylene bridge of biradical **3.2** was found to lead to weak intramolecular ferromagnetic exchange, with the possibility of additional intermolecular ferromagnetic exchange interactions. While the contorted molecular structure of this compound resulted in poorer π-overlap than typically observed in benzotriazinyl radicals, there exists a network of three-dimensional interactions between the phenyl rings and other aromatic components of the biradicals. While no structural information was obtained for the biradicals **3.3** and **3.4**, solid state diffuse reflectance spectroscopy indicated the presence of significant intermolecular interactions.

The preliminary conductivity measurements that were carried out suggest that benzotriazinyl radicals are of interest to investigate as possible neutral radical conductors. Radicals **2.3** and **3.2**-**3.4** all displayed improved conductivities relative to the parent benzotriazinyl radical **1.9**, and merit further and more extensive studies in order to determine the structural or electronic factors leading to increased conductivities.

4.8 Experimental

4.8.1 X-ray crystallography

X-ray diffraction data on **2.3** were collected by Dr. Abdeljalil Assoud at the University of Waterloo using a Bruker APEX I CCD detector on a D8 3-circle goniometer with Mo-Kα radiation (λ = 0.71073 Å). The structure was solved by direct methods using SHELXS-90[114] and refined by least-squares methods on F^2 using SHELXL-97[115] incorporated in the SHELXTL[116] suite of programs. X-ray diffraction data on **2.20** and **3.2** were collected by Dr. Brian Patrick at the University of British Columbia using a Bruker APEX II diffractometer with graphite monochromated Mo-Kα

radiation (λ = 0.71073 Å). Structures were solved by direct methods using SIR97[117] and refined by least-squares methods on F^2 using SHELXL-97[115] via the WinGX[118] interface. Complete tables of crystallographic parameters and of bond lengths and angles can be found in Appendices A and B.

4.8.2 Magnetic measurements

Magnetic data was collected using a Quantum Design Quantum Design Magnetic Property Measurement System (MPMS-XL5) operating at a field strength of 10000 Oe, over temperature ranges of 4–300 K. 15-20 mg of sample was accurately weighed and loaded into a gelule which was sealed with Kapton tape. The gelule was inserted into a plastic straw tube for loading into the instrument. The diamagnetic moment of **2.3** was accounted for using Pascal's constants to get correction value of -1.819×10^{-4} emu K mol^{-1}, while the diamagnetic moment of **3.2** was accounted for using the slope of the high-temperature paramagnetic regime of the plot of magnetic moment versus temperature to get a correction value of -6.74×10^{-4} emu K mol^{-1}. The diamagnetic contribution of the gelule and straw sample holder of -2.4×10^{-7} emu K mol^{-1} had a negligible effect on the data.

4.8.3 Spectroscopy

Diffuse reflectance and electronic absorbance spectra were obtained using a Perkin Elmer Lambda 1050 spectrometer. Diffuse reflectance spectroscopy was carried out using thin films of sample layered onto quartz slides from solutions of CH_2Cl_2. Solution spectroscopy was carried out using MeOH sample solutions.

4.8.4 Conductivity measurements

The pressed pellet measurements were carried out as described in the literature.[113] Roughly 1-2 mg of sample was loaded into a hollow glass cylindrical sample holder and then compressed between two probes using an adjustable goniometer head to form a pellet of measurable width. The resistance across the pellet was measured using a Fluke 1587 Insulation Multimeter. The measured resistance was converted to conductivity using Equation 4.9, where σ is the conductivity in $S \cdot cm^{-1}$, Δl is the width of the pellet in cm, R is the measured resistance in Ω, and A is the surface area of the probe tips (0.02043 cm^2). In cases when the resistance of the sample was too high to be measured using the multimeter, a resistor with a known resistance of 1.019 MΩ was set up in parallel with the sample allowing for the measurement of a total resistance R_T. The resistance of the sample could then be calculated using Equation 4.10, where R_P is the resistance of the parallel resistor and R_S is the sample resistance.

$$\sigma = \frac{\Delta l}{R \times A} \tag{4.9}$$

$$R_S = \frac{R_P \times R_T}{R_P - R_T} \tag{4.10}$$

Table 4.5 lists the uncorrected conductivity data calculated using Equation 4.9. The resistance of the radical cation **2.20** was too high to be measured even with the use of the parallel resistor, and so no data was obtained for this compound.

Table 4.5 Pressed pellet conductivity data (uncorrected).

Trial	Conductivity ($S \cdot cm^{-1}$)				
	TTF-TCNQ	**2.3**	**3.2**	**3.3**	**3.4**
1	9×10^{-1}	2×10^{-6}	2×10^{-6}	9×10^{-9}	1×10^{-6}
2	2×10^{-1}	2×10^{-7}	2×10^{-6}	2×10^{-6}	1×10^{-8}
3	1×10^{-1}	5×10^{-7}	1×10^{-6}	6×10^{-7}	1×10^{-6}
4	7×10^{-1}	6×10^{-7}	2×10^{-6}	6×10^{-7}	2×10^{-6}
5	7×10^{-1}	5×10^{-7}	9×10^{-7}	2×10^{-8}	1×10^{-8}
6	-	9×10^{-7}	8×10^{-7}	5×10^{-7}	2×10^{-7}
Avg.	5×10^{-1}	8×10^{-7}	1×10^{-6}	6×10^{-7}	7×10^{-7}

Chapter 5 Towards benzotriazinyl polyradicals

5.1 Introduction

To date, investigations into the use of organic polyradicals for charge storage in ORBs have focussed mainly on the use of the nitroxide radical as the charge storage unit. One of the main advantages of the nitroxide radical is that it has a low molecular weight (*i.e.* 156.26 g·mol^{-1} for the TEMPO radical, Figure 5.1), allowing for high theoretical charging capacities (Equation 1.1). The benzotriazinyl radical on the other hand has a higher molecular weight (*i.e.* 284.33 g·mol^{-1} for **1.9**), which lowers the theoretical capacity. The large advantage of the benzotriazinyl radical over the nitroxide radical however, lies in its versatile electrochemistry. As was discussed in Chapter 2, benzotriazinyl radicals can be easily structurally modified which leads to shifts in the redox potentials through predictable functional group effects. The careful tuning of redox processes in turn allows for the design of anode-specific or cathode-specific radicals. In Chapter 3 model multi-electron transfer benzotriazinyl biradicals were discussed that could lead to the design of high energy density charge storage materials. For these reasons, the benzotriazinyl radical is a good candidate for charge storage application in ORBs. We therefore wanted to investigate the synthesis and electrochemical properties of benzotriazinyl polyradicals, analogous to existing ORB nitroxide polyradicals, towards the development of cathodic and anodic charge storage materials.

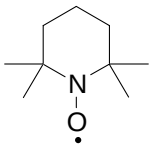

Figure 5.1 The TEMPO radical.

5.1.1 Benzotriazinyl polyradical design

The spin content of a polyradical is an important factor in evaluating its use as a charge storage material. Ideally, the spin content should be 100 %, meaning that every monomer unit within the polymer has an unpaired electron and is capable of acting as a charge source. Because the radicals represent the redox active sites of the polymer, a low spin content would effectively lower the charging capacity of the material on a per weight basis.

Previous work carried out within the Frank group towards the synthesis of benzotriazinyl polyradicals made use of metal-catalyzed coupling methodologies such as that shown in Scheme 5.1.[57] These procedures involve the coupling of appropriately functionalized benzotriazinyl radical monomers to form polyradicals. In these polymers, the benzotriazinyl radicals are embedded directly into the backbone of a conjugated polymer to form alternating copolymers. Depending on the experimental conditions used for coupling, the spin contents of the polyradicals as determined by SQUID magnetometry were found to range from ~ 20-65 %. The low spin densities were due to site defects that arose from direct coupling of the radical nitrogen in the catalytic cycle. We therefore set out to investigate alternate methods of polymerization that involved development of polyradicals in which the radical was a pendant group.

Scheme 5.1 Metal catalyzed polymerization of a benzotriazinyl radical.[57]

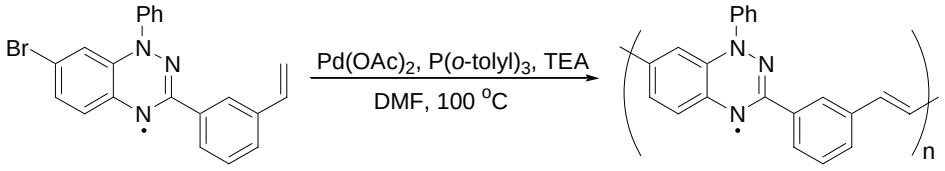

5.1 **5.2**

This chapter will present efforts towards the polymerization of the vinyl-functionalized monomer **5.3** using anionic polymerization to isolate a material that is tentatively assigned as polyradical **5.4**. The vinyl group was chosen as the polymerizable functional group due to its low molecular weight which would help to maximize the theoretical charging capacity. In addition, to maximize spin content of the polymer, a methyl substituent was placed at the 7-position of the benzotriazinyl to prevent long-term oxidation of the radical sites in the polyradical to closed shell iminoquinones related to **2.15**. Using Equation 1.1, the theoretical charging capacity of **5.4** can be calculated to be 83 $mAh \cdot g^{-1}$.

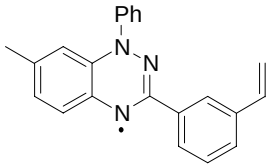

5.3

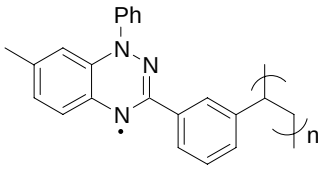

5.4

We were interested in investigating both the spin content and the electrochemical behaviour of compound **5.4**. In particular, we wanted to evaluate whether anionic polymerization would be a practical methodology towards the synthesis of high charging capacity benzotriazinyl polyradicals, and whether the polyradicals would retain the reversible oxidation and reduction processes characteristic of benzotriazinyl radicals. This would be necessary if they were to be used for both anodic and cathodic application.

Results and discussion

5.2 Synthesis and properties of benzotriazinyl monomer and polymer

5.2.1 Synthesis

Scheme 5.2 Synthesis of monomer **5.3**.[a]

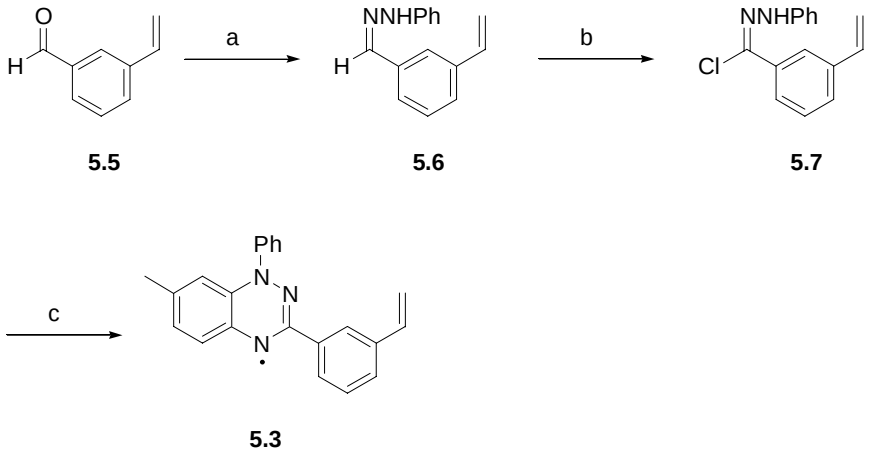

[a] *Reagents and Conditions:* a) $PhNHNH_2$, EtOH, 22 °C, 20 hours, 93 % b) NCS, Me_2S, CH_2Cl_2, 0 °C, 0.5 hours, 81 % c) i) 4-methylaniline, TEA, EtOH, 78 °C, 0.5 hours ii) DBU, EtOH, 22 °C, 20 hours, 39 % from **5.7**.

The synthesis of monomer **5.3** was carried out using the general Frank group synthesis as discussed in detail in Section 2.2.1. The commercially available starting material 3-vinylbenzaldehyde was condensed with phenylhydrazine to form hydrazone **5.6** in 93 % yield. Subsequent chlorination of **5.6** using the Corey-Kim reagent resulted in the formation of chlorohydrazone **5.7** in 81 % yield. Condensation of **5.7** with 4-methylaniline and treatment with DBU led to the isolation of benzotriazinyl radical **5.3** as a dark brown powder in 39 % yield following purification by silica gel flash chromatography.

Scheme 5.3 Anionic polymerization of **5.3**.[a]

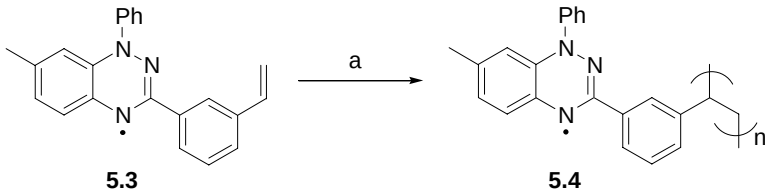

5.3 **5.4**

[a]*Reagents and conditions*: a) *n*-BuLi, THF, N_2 atmosphere, 22 °C, 18 hours, 70 % by mass.

Anionic polymerization of **5.3** was performed using *n*-BuLi as the polymerization initiator. A concentrated solution of the monomer in distilled THF was treated with *n*-BuLi solution under a nitrogen atmosphere. Initial attempts to accomplish the polymerization used catalytic (~ 10 %) amounts of *n*-BuLi, with monitoring of the reaction by TLC showing essentially no conversion of the monomer after extended time. Samples of the reaction solution were removed and added to excess MeOH without production of polymer precipitate, consistent with a lack of polymerization. It was found that by adding close to one equivalent (0.6 - 0.8 eq.) of *n*-BuLi a significant conversion of the monomer to polymer could be obtained. Possible reasons for the low yield during anionic polymerization may be due to early evidence suggesting that the benzotriazinyl radical can function as a polymerization inhibitor.[50] After allowing the reaction to stir overnight at room temperature, it was poured into an excess of MeOH, which resulted in the precipitation of compound **5.4** as a brown powder. This was filtered and washed with excess MeOH to get rid of any unreacted monomer.

5.2.2 Spectroscopic characterization

Although the exact structural properties of **5.4** could not be determined, some insight into its composition can be obtained using infrared, UV-Vis, and EPR spectroscopy. The infrared spectrum of **5.4** was consistent with its largely benzotriazinyl

radical nature, as it was not significantly different than the spectrum of monomer **5.3** and contained a strong peak at 1590 cm^{-1} which is characteristic of the C=N stretch in benzotriazinyl radicals. Additionally, peaks at 917 and 991 cm^{-1} attributable to C-H bends of the vinyl group in the spectrum of monomer **5.3** were significantly diminished in intensity in the spectrum of compound **5.4**, consistent with polymerization occurring through the vinyl group.

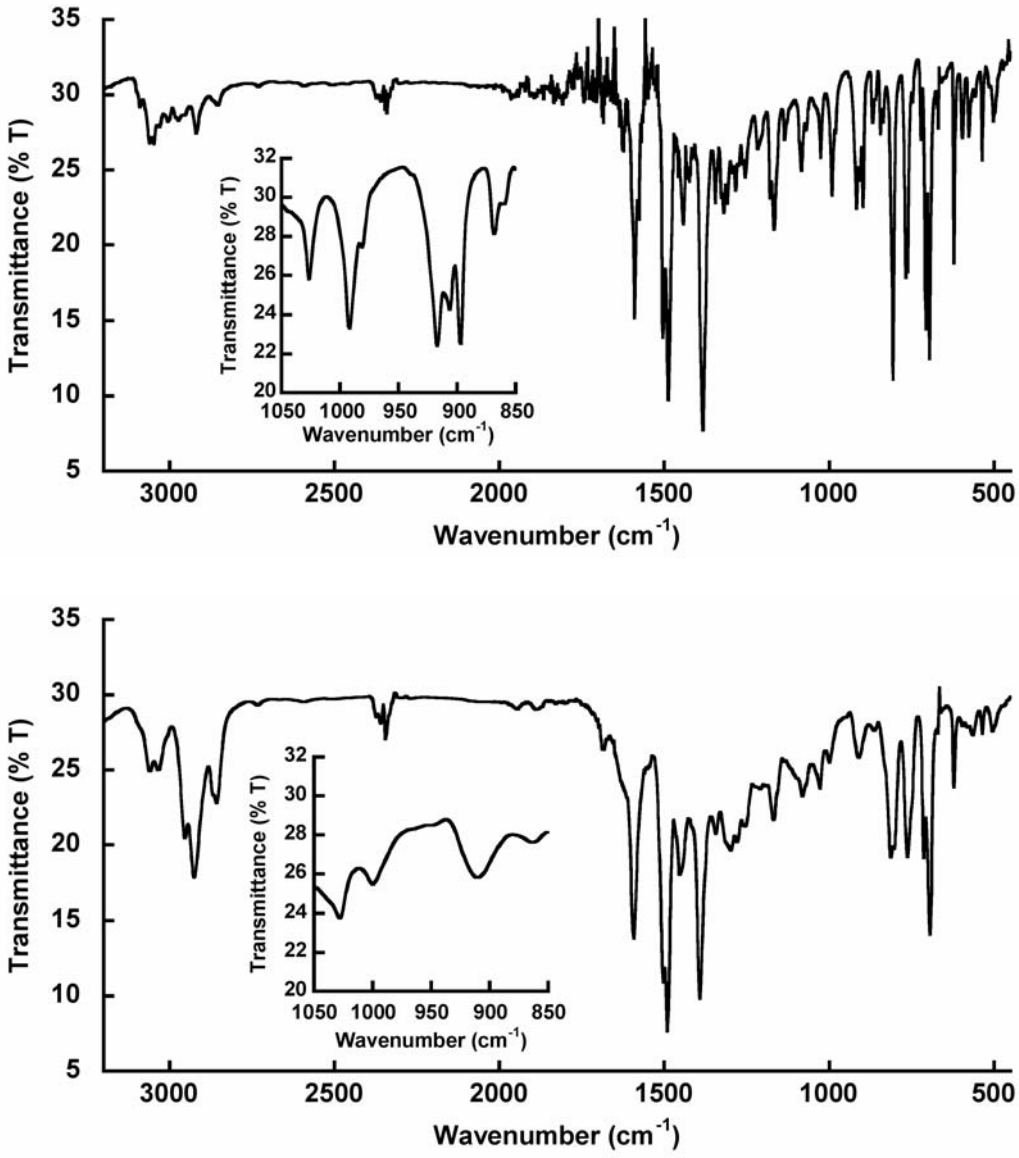

Figure 5.2 FT-IR spectra of monomer **5.3** (top) and polymer **5.4** (bottom).

The solution state electronic absorption spectra of **5.3** and **5.4** are compared in Figure 5.3. The characteristic benzotriazinyl radical absorption maxima present in the polymer are consistent with the presence of a significant proportion of radical sites within the polymer. There is effectively no bathochromic shift of the spectrum of the polymer relative to that of the monomer (Table 5.1), which is consistent with the non-conjugated polymer that would result from anionic polymerization through a vinyl group.

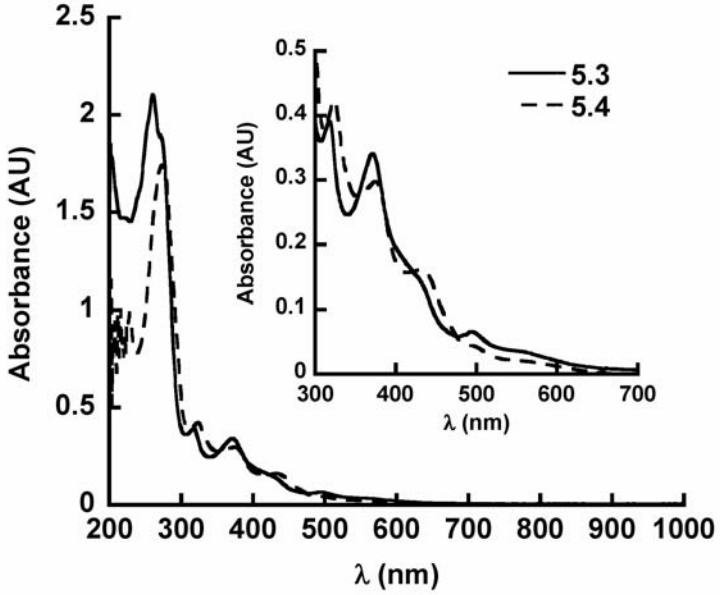

Figure 5.3 Absorption spectra of monomer **5.3** in MeOH and compound **5.4** in CH_2Cl_2 at 298 K.

Table 5.1 Absorption data for monomer **5.3** and compound **5.4**.

	λ_{max} (nm)				
5.3	271	318	371	431	493
5.4	275	324	375	432	495

The EPR spectrum of **5.3** displays a seven-line pattern which is slightly broadened due to superhyperfine coupling of less than 1 Gauss to the methyl group, analogous to compound **2.1**. The spectrum of compound **5.4**, on the other hand, exhibits a

single broad singlet with a width of ~ 50 Gauss. This is consistent with magnetic dipole-dipole interactions between the unpaired electrons of neighbouring radical sites within a polymer led to effective broadening of the resonance.

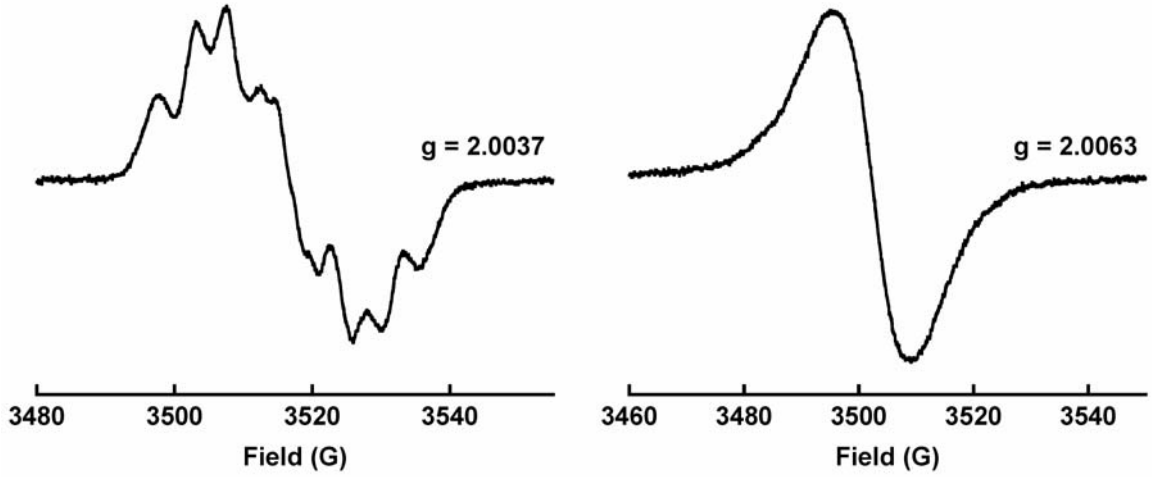

Figure 5.4 EPR spectra of **5.3** in toluene (left) and **5.4** in CH_2Cl_2 (right) at 298 K.

5.2.3 Polymer spin content determination

The temperature dependences of the magnetizations of powder samples of the radical compounds **5.3** and **5.4** were measured using a Quantum Design MPMS over the 4 – 300 K temperature range at an applied field of 10000 Oe. The magnetization was converted to magnetic susceptibility and corrected for diamagnetic contributions by subtracting the non-zero slope of χT vs T in the paramagnetic regime.

The approximate spin content of a polyradical can be determined through magnetic measurements. An isotropic S = ½ radical system with g = 2.00, if magnetically pure and in the paramagnetic temperature regime with no exchange interactions, will exhibit a molar magnetic moment (per mole of monomer unit for a polyradical) of 0.375 $emu \cdot K \cdot mol^{-1}$ in accord with the spin-only Curie law. Therefore the Curie constant, C =

$Ng^2\beta^2S(S+1)/3k_B$ as defined in Section 4.1.1, can be used to estimate the spin content in the system. For example, Figure 5.5 shows the temperature dependence of the molar magnetic moment (χT) and the inverse magnetic susceptibility ($1/\chi$) of monomer **5.3**. The room temperature magnetic moment is approximately 0.356 emu·K·mol^{-1} before decreasing at low temperatures due to weak antiferromagnetic exchange. A fit of the high temperature regime to the Curie-Weiss law (Equation 4.5), gives a Curie constant of C = 0.369 emu·K·mol^{-1} and a Weiss constant of θ = -6.5 K leading to a spin content of ~ 98%.

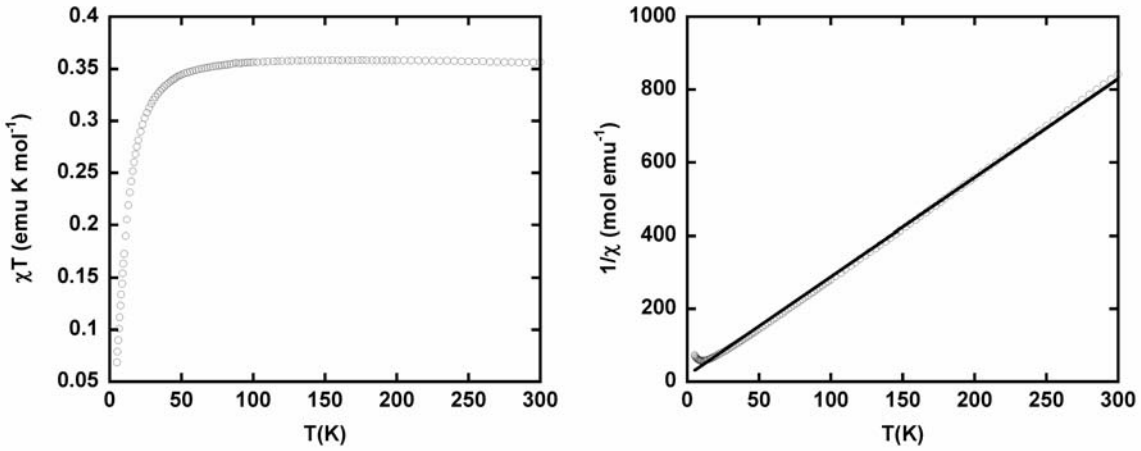

Figure 5.5 Temperature dependence of molar magnetic moment χT (left) and inverse susceptibility $1/\chi$ (right) of **5.3** measured at 10000 Oe. Curie-Weiss fit (R^2 = 0.998) of the inverse susceptibility shown with black line.

The magnetic data of compound **5.4** is shown in Figure 5.6. The theoretical number of benzotriazinyl radical units in the sample was calculated by dividing the mass of the polymer by the formula weight of monomer **5.3**. This number was then used to convert the measured magnetic susceptibility into a molar magnetic susceptibility and a molar magnetic moment per mole of monomer, negating the necessity of accurately determining the molecular weight of the polymer, which can be problematic for paramagnetic polymers with high optical densities. The magnetic moment (χT) of **5.4** at

room temperature is ~0.15 emu·K·mol^{-1}. As the temperature decreases, the moment decreases to ~0.12 emu·K·mol^{-1} at 4 K, consistent with extremely weak antiferromagnetic exchange. A Curie-Weiss analysis of the inverse susceptibility yields a Curie constant C of C = 0.163 emu·K·mol^{-1} and a Weiss constant θ = -2.9 K, also consistent with weak antiferromagnetic exchange.

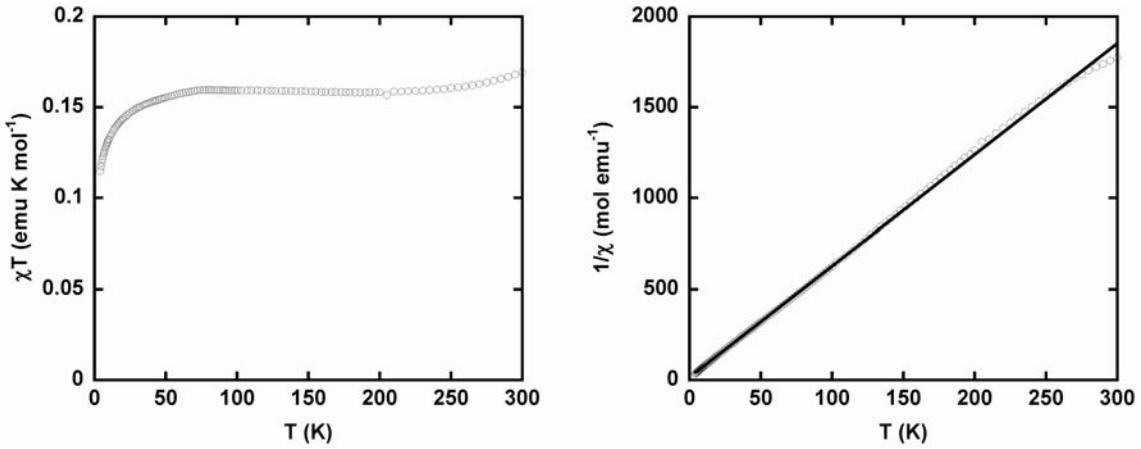

Figure 5.6 Temperature dependence of molar magnetic moment (left) and inverse susceptibility (right) of **5.4** measured at 10000 Oe. Curie-Weiss fit (R^2 = 0.999) of the inverse susceptibility shown with black line.

Based on the theoretical value of C = 0.375 emu·K·mol^{-1} for a spin content of 100 %, the experimental Curie constant results in a calculated spin content of roughly 44 % in compound **5.4**. This is comparable to the spin contents of the previous benzotriazinyl polyradicals that were synthesized using metal-catalyzed coupling techniques, and indicates the existence of a relatively large number of diamagnetic site defects within the polymer. The nature of the site defects have not been explored through model reactions, as was done with the metal-catalyzed coupling methodologies. However, reduction of the radical followed by reaction with the vinyl group leading to N-C bond formation is likely.

5.2.4 Electrochemistry

The electrochemical properties of compounds 5.3 and 5.4 as measured by cyclic voltammetry are compared in Figure 5.7 and
Table **5.2**.

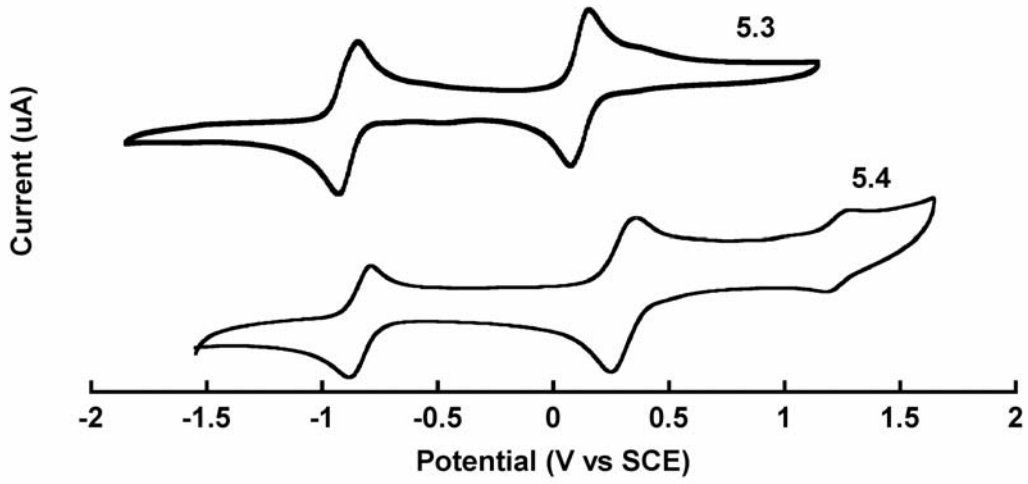

Figure 5.7 Cyclic voltammograms of **5.3** in MeCN and **5.4** in CH_2Cl_2 with 0.1 M $[Bu_4N][PF_6]$ supporting electrolyte, glassy carbon working electrode, silver reference electrode, platinum counter electrode, 100 mV/s scan rate.

Table 5.2 Electrochemical data of **5.3** and **5.4**. $E_{1/2}$ in V vs SCE, ΔE_p in mV, E_{cell} in V.

	$\mathbf{E_{1/2(ox)}}^a$	$\mathbf{\Delta E_p}^b$	$\mathbf{E_{1/2(red)}}^a$	$\mathbf{\Delta E_p}^b$	$\mathbf{E_{cell}}^c$
5.3	0.14	70	-0.87	75	1.01
5.4	0.22	108	-0.93	90	1.15

$^a E_{1/2}$ calculated as the average of the peak potentials of the anodic and cathodic waves. $^b \Delta E_p$ calculated as the difference in peak potentials of the anodic and cathodic waves. $^c E_{cell} = |E_{1/2(ox)} - E_{1/2(red)}|$.

It can be seen that both the monomer and potential polyradical have similar electrochemical properties. Importantly, the polyradical retains the reversible reduction

and oxidation processes that would be required for it to be used in both anodic and cathodic charge storage applications. The reduction process of **5.4** does have a smaller integration than that of the oxidation process however, which may be due to a lower degree of reversibility for reduction. There is also an additional minor reversible oxidation process that occurs at 1.16 V vs SCE which may be due to the site defects within the polyradical. All of the electrochemical features of **5.4** were found to be reproducible over three independently synthesized batches of the compound, suggesting that the synthetic methodology leads to reproducible batches of polymer.

5.3 Conclusion

The results presented in this chapter provide proof of principle for the preparation of a material that is tentatively assigned as a benzotriazinyl polyradical through the use of anionic polymerization. The 44 % spin content of the polyradical as determined by SQUID magnetometry is likely too low to consider anionic polymerization to be a viable synthesis of benzotriazinyl polyradicals for charge storage. The electrochemical properties of the polyradical suggest that a saturated polymer with pendant benzotriazinyl radical groups could theoretically be used in an anodic or cathodic capacity. Therefore it would be of interest to investigate alternate polymerization techniques in order to increase the spin content of the benzotriazinyl polyradicals.

5.4 Experimental

The general procedures and experimental techniques that were used are the same as those that were discussed in Section 2.6.1.

The magnetic measurements were carried out using the same procedure as outlined in Section 4.8.2. The diamagnetic moments of **5.3** and **5.4** were accounted for using the slopes of the high-temperature paramagnetic regimes of the plots of magnetic moment versus temperature to get a correction value of -3.27×10^{-4} emu K mol^{-1} for **5.3** and -2.52×10^{-4} emu K mol^{-1} for **5.4**. The diamagnetic contribution of the gelule and straw sample holder of -2.4×10^{-7} emu K mol^{-1} had a negligible effect on the data.

5.4.1 Syntheses

The synthesis and full characterization of compounds **5.6** and **5.7** using the methods discussed below have been previously reported.[57]

7-methyl-1-phenyl-3-(3"-vinylphenyl)-1,2,4-benzotriazinyl (5.3): A solution of 4-methylaniline (0.54 g, 5.0 mmol) and triethylamine (0.70 mL, 5.0 mmol) in anhydrous ethanol (30 mL) was heated to reflux. A second solution of **5.7** (0.61 g, 2.4 mmol) in 60 mL anhydrous ethanol was then added dropwise to the refluxing solution over approximately 10 minutes. The reaction was stirred at reflux for a further 20 minutes. The solution was cooled to room temperature and DBU (1.0 mL, 7 mmol) was added, followed by stirring at room temperature for approximately 20 hours. The solvent was removed and the crude material was purified using silica gel flash chromatography (95:5 hexanes:ethyl acetate) to isolate the **5.3** as an oily brown material. Sonication of the oil in pentane led to a precipitate of dark brown powder (0.30 g, 39 %). FT-IR (KBr): 3054 (w), 2962 (w), 1590 (m), 1503 (m), 1488 (s), 1383 (s), 1261 (m), 1085 (m), 1025 (m), 991 (m), 917 (m), 806 (s), 706 (s), 695 (s), 621 (m) cm^{-1}. UV-Vis (MeOH): λ_{max}/nm ($\varepsilon \times 10^4$ mol^{-1} cm^{-1}): 260 (3.81), 271 sh (3.42), 318 (0.71), 371 (0.62), 431 sh (0.26), 493 (0.12),

563 sh (0.06). MS (ESI): *m/z* 324 (M^+). Anal Calcd for $C_{22}H_{18}N_3$: C, 81.45; H, 5.59; N, 12.95. Found C, 81.59; H, 5.70; N, 12.87.

Poly(7-methyl-1-phenyl-3-(3"-vinylphenyl)-1,2,4-benzotriazinyl) (5.4): Monomer **5.3** (0.10 g, 0.31 mmol) was dissolved in 15 mL distilled THF under a nitrogen atmosphere. To this solution was added 2.5 M *n*-BuLi in hexanes (0.1 mL, 0.25 mmol). The reaction was stirred under nitrogen at room temperature for 18 hours, and poured into 20 mL methanol, resulting in the formation of a brown precipitate. The precipitate was filtered washed with methanol, and dried under vacuum to yield **5.4** as a brown powder (0.070 g, 70 % by mass). FT-IR (KBr): 3043 (w), 2926 (m), 2857 (m), 1593 (m), 1490, (s), 1443 (s), 1392 (s), 1166 (w), 869 (w), 814 (m), 694 (m) cm-1. UV-Vis (CH_2Cl_2): λ_{max}/nm (AU): 275 (1.74), 324 (0.42), 375 (0.30), 432 (0.16), 495 (0.04). It should be noted that no direct experimental evidence was obtained that points to **5.4** being a polymeric material. As a result all references to **5.4** being a polymer throughout this chapter represent a tentative assignment. Previous attempts to use GPC to obtain information on the mass of benzotriazinyl polyradicals did not lead to accurate results due to the existence of electronic absorptions of the polymers throughout the visible spectrum, leading to low signal to noise ratios.[57] Additionally, the paramagnetic nature of these materials prevents characterization through the use of NMR spectroscopy.

3-vinylphenylhydrazone (5.6):[57] Phenylhydrazine (2.0 mL, 20 mmol) was added to a solution of 3-vinylbenzaldehyde (2.0 mL, 16 mmol) in anhydrous ethanol (30 mL). The reaction solution was then stirred at room temperature for 20 hours. At this time, the pale

yellow precipitate that had formed was filtered, washed with hexanes, and dried under vacuum to yield **5.6** as a pale yellow powder (3.32 g, 15 mmol, 93 %). ^{1}H-NMR (300 MHz, CD_2Cl_2) δ 7.72 (br s, 1H), 7.69 (s, 1H), 7.54 (dt, 1H, J = 7, 2 Hz), 7.35-7.23 (m, 4H), 7.10 (d, 2H, J = 9 Hz), 6.85 (tt, 1H, J = 7, 2 Hz), 6.75 (dd, 1H, J = 18, 11 Hz), 5.81 (d, 1H, J = 18 Hz), 5.28 (d, 1H, J = 11 Hz). ^{13}C-NMR (300 MHz, $CDCl_3$) δ 144.58, 137.92, 137.12, 136.59, 135.55, 129.33, 128.80, 126.18, 125.68, 124.04, 120.19, 114.38, 112.81. FT-IR (KBr): 3318 (s), 3051 (w), 1595 (s), 1568 (s), 1483 (s), 1259 (s), 1138 (s), 998 (m), 917 (s), 753 (s) cm^{-1}.

3-vinylphenylchlorohydrazone (5.7):[57] *N*-Chlorosuccinimide (2.4 g, 18 mmol) was dissolved in dichloromethane (60 mL), and the solution was cooled to 0 °C in an ice bath. Dimethyl sulphide (1.3 mL, 18 mmol) was added to this solution, and the mixture was stirred for 10 minutes. A solution of **5.6** (3.3 g, 15 mmol) in 80 mL dichloromethane was added dropwise to the reaction solution over 20 minutes, and the reaction was stirred at 0 °C for a further 10 minutes. The reaction mixture was warmed to room temperature and concentrated. The crude material was purified by silica gel flash chromatography (9:1 hexanes:dichloromethane) to isolate **5.7** as a pale pink crystalline solid (3.11 g, 12 mmol, 81 %). ^{1}H-NMR (300 MHz, $CDCl_3$) δ 8.06 (br s, 1H), 7.94 (t, 1H, J = 2 Hz), 7.83 (dt, 1H, J = 8, 2 Hz), 7.45-7.30 (m, 4H), 7.19 (d, 2H, J = 8 Hz), 6.96 (tt, 1H, J = 8, 2 Hz), 6.78 (dd, 1H, J = 18, 12 Hz), 5.84 (d, 1H, J = 18 Hz), 5.33 (d, 1H, J = 12 Hz); ^{13}C-NMR (300 MHz, $CDCl_3$) δ 143.30, 137.82, 136.36, 134.75, 129.42, 128.57, 126.81, 125.80, 124.23, 114.80, 113.49. FT-IR (KBr): 3309 (s), 3051 (w), 1600 (s), 1579 (s), 1503 (s), 1435 (s), 1246 (s), 1137 (s), 987 (s), 900 (s), 750 (s), 692 (s) cm^{-1}.

Chapter 6 Conclusions and future work

Organic radical batteries show great potential as next generation energy storage devices, particularly for portable electronics and high power applications. The two major challenges facing ORB research are the lack of electrochemically versatile organic radical systems for the development of a range of anodic and cathodic materials, and the need for high energy density radical charge storage systems. The work carried out over the course of this thesis strongly suggests that the benzotriazinyl radical is a promising system to meet these challenges.

It has now been shown in this work and the previous work carried out in the Frank group that a variety of different functionalized benzotriazinyl radicals can be synthesized using an easily modifiable synthetic methodology. The functionalized radicals show electrochemical behaviour that can be predicted and explained based on electron donating and withdrawing functional group effects. Electron withdrawing groups have been shown to lead to positive shifts in the redox voltages of benzotriazinyl radicals, and now we have determined that the opposite effect can be obtained using electron donating groups. In all cases electrochemical reversibility is maintained, and therefore functionalized benzotriazinyl radicals can be prepared with both cathode- and anode-specific applications in mind. Further systematic studies of functionalized benzotriazinyl radicals bearing novel or multiple functional groups may lead to an expansion in the range of accessible electrochemical potentials at which reduction and oxidation of the radicals occurs.

Towards high energy density charge storage materials, we were successful in the synthesis and characterization of three model benzotriazinyl biradicals which show potential to act as multi-electron storage materials. All three of these compounds displayed reversible electrochemical behaviour that was explainable based on the electronic structure and intramolecular electronic communication between the different components of the biradical molecules. There are two possible directions in which this research could go in respects to charge storage materials. First, the model biradicals could be incorporated into polymer systems. For example, Scheme 6.1 shows one such potential polymer that could be synthesized by combining the methodologies used to prepare both the *m*-phenylene- and aromatic diimide-bridged biradicals. It would then be necessary to study and evaluate the electrochemistry of such polymers to determine if they could be used to store or release multiple electrons per monomer unit.

Scheme 6.1 Synthesis of a multi-electron transfer polyradical.

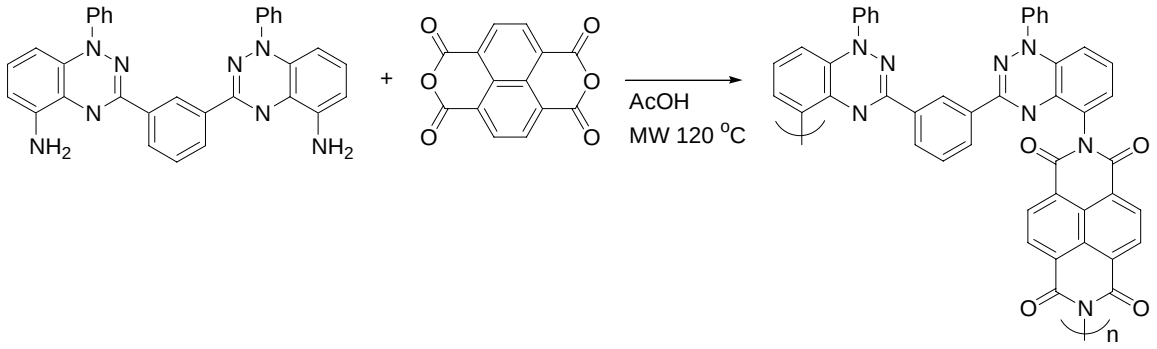

A second direction would be to directly test the charge storage properties of the biradicals themselves. One of the main reasons for using polymeric materials in the design of electrode materials is the need for insolubility. As it turns out, all three of the biradicals which were studied displayed lower solubility than typical benzotriazinyl radicals,

particularly in the cases of the two aromatic diimide-bridged biradicals **3.3** and **3.4**. It would therefore be interesting to study the charge storage properties of composite electrodes containing these biradicals as the active materials, in order to see if they would be stable towards dissolution into the electrolyte. The ability to use discrete oligomeric compounds such as biradicals could be advantageous over the use of polyradicals for charge storage, as they could be completely characterized and purified to maximize spin content.

Using anionic polymerization techniques, we were able to synthesize and electrochemically characterize a polymer bearing benzotriazinyl radicals as pendant side groups. It was found that the reversible electrochemistry of the monomer was maintained in the polymer structure, and that the electrochemical profile could be reliably reproduced over different synthetic batches of polymer. While the spin content of the polyradical was determined to be only ~ 44 %, it will still be of benefit to evaluate the charge storage properties of this polyradical in a composite electrode. Even if the charging capacity is low due to the low spin content, it is important to determine whether the benzotriazinyl radical can be reversibly charged and discharged in both cathodic and anodic capacities as an electroactive electrode material. Further studies towards the synthesis of benzotriazinyl polyradicals can then be looked into in an effort to increase the spin content.

So far, direct polymerization of benzotriazinyl radical monomers using either anionic or metal-catalyzed coupling resulted in the loss of a significant proportion of the radical sites. A possible alternate approach would be to append the radicals to a pre-formed polymer backbone, thus avoiding the radical polymerization step entirely. One

way in which this could be done is shown in Scheme 6.2, involving chemical procedures established over the course of this thesis that were successful in the synthesis of biradicals **3.3** and **3.4**. The simple condensation of the amino-functionalized radical **2.3** which a polymer backbone such as commercially available poly(ethylene-*alt*-maleic anhydride) may result in polyradicals with much higher spin densities than those obtained through the polymerization of benzotriazinyl radical monomers. This procedure would also provide a convenient method to monitor the completeness of the reaction through the use of IR spectroscopy to observe the conversion of anhydride C=O bands to diimide C=O bands.

Scheme 6.2 Polyradical synthesis using established condensation chemistry.

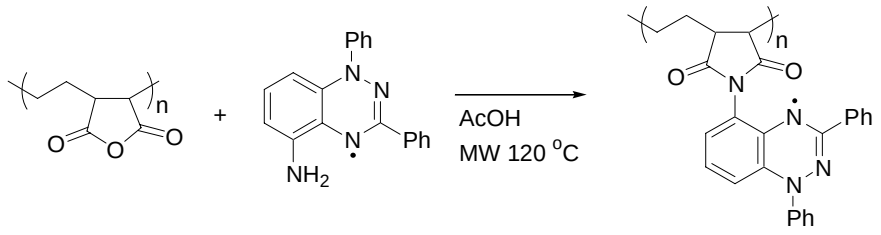

References

1. Dell, R.M.; Rand, D.A.J. *J. Power Sources* **2001**, *100*, 2-17.

2. Goodenough, J.B.; Kim, Y. *Chem. Mater.* **2010**, *22*, 587-603.

3. Liu, C.; Li, F.; Ma, L.-P.; Cheng, H.-P. *Adv. Mater.* **2010**, *22*, E28-E62.

4. Serrano, E.; Rus, G.; García-Martínez, J. *Renewable Sustainable Energy Rev.* **2009**, *13*, 2373-2384.

5. Baker, J. *Energy Policy* **2008**, *36*, 4368-4373.

6. Winter, M.; Brodd, R.J.; *Chem. Rev.* **2004**, *104*, 4245-4269.

7. Gao, X.-P.; Yang, H.-X. *Energy Environ. Sci.* **2010**, *3*, 174-189.

8. Barak, M. *Electrochemical Power Sources: Primary and Secondary Batteries*. Institution of Electrical Engineers: London and New York, 1980.

9. Linden, D. *Handbook of Batteries and Fuel Cells*. McGraw-Hill, Inc.: New York, 1984.

10. Palacín, M.R. *Chem. Soc. Rev.* **2009**, *38*, 2565-2575.

11. Lu, X.; Xia, G.; Lemmon, J.P.; Yang, Z. *J. Power Sources* **2010**, *195*, 2431-2442.

12. Zhao, X.; Ma, L. *Int. J. Hydrogen Energy* **2009**, *34*, 4788-4796.

13. Dustmann, C.-H. *J. Power Sources* **2004**, *127*, 85-92.

14. Whittingham, M.S. *Chem. Rev.* **2004**, *104*, 4271-4301.

15. Patil, A.; Patil, V.; Shin, D.W.; Choi, J-W.; Paik, D-S.; Yoon, S-J. *Mater. Res. Bull.* **2008**, *43*, 1913-1942.

16. Scrosati, B. Garche, J. *J. Power Sources* **2010**, *195*, 2419-2430.

17. Shukla, A.K.; Kumar, T.P. *Curr. Sci.* **2008**, *94*, 314-331.

18. Shirakawa, H.; Louis, E.J.; MacDiarmid, A.G.; Chiang, C.K.; Heeger, A.J. *J. Chem. Soc., Chem. Commun.* **1977**, 578-580.

19. MacInnes, D.; Druy, M.A.; Nigrey, P.J.; Nairns, D.P.; MacDiarmid, A.G.; Heeger, A.J. *J. Chem. Soc., Chem. Commun.* **1981**, 317-319.

20. Novak, P.; Muller, K.; Santhanam, K.S.V.; Haas, O. *Chem. Rev.* **1997**, *97*, 207-282.

21. Mastragostino, M.; Arbizzani, C.; Soavi, F. *J. Power Sources* **2001**, *97-98*, 812-815.

22. Nishide, H.; Oyaizu, K. *Science* **2008**, *319*, 737-738.

23. Schultze, J.W.; Karabulut, H. *Electrochim. Acta* **2005**, *50*, 1739-1745.

24. Nyström, G.; Razaq, A.; Strømme, M.; Nyholm, L.; Mihranyan, A. *Nano Lett.* **2009**, *9*, 3635-3639.

25. Nakahara, K.; Iwasa, S.; Satoh, M.; Morioka, Y.; Iriyama, J.; Suguro, M. *Chem. Phys. Lett.* **2002**, *359*, 351-354.

26. Oyaizu, K.; Nishide, H. *Adv. Mater.* **2009**, *21*, 2339-2344.

27. Nakahara, K.; Iriyama, J.; Iwasa, S.; Suguro, M.; Satoh, M.; Cairns, E.J. *J. Power Sources* **2007**, *163*, 1110-1113.

28. Satoh, M. *NEC J. of Adv. Tech.*, **2005**, *2*, 262-263.

29. Suga, T.; Konishi, H.; Nishide, H. *Chem. Commun.* **2007**, *17*, 1730-1732.

30. Nishide, H.; Suga, T. *Electrochem. Soc. Interface* **2005**, *14*, 32-36.

31. Bugnon, L.; Morton, C.J.H.; Novak, P.; Vetter, J.; Nesvadba, P. *Chem. Mater.* **2007**, *19*, 2910-2914.

32. Kim, J.-K.; Cheruvally, G.; Choi, J.-W.; Ahn, J.-H.; Choi, D.S.; Song, C.E. *J. Electrochem. Soc.* **2007**, *154*, A839-A843.

33. Nakahara, K.; Iriyama, J.; Iwasa, S.; Suguro, M.; Satoh, M.; Cairns, E.J. *J. Power Sources* **2007**, *165*, 398-402.

34. Nakahara, K.; Iriyama, J.; Iwasa, S.; Suguro, M.; Satoh, M.; Cairns, E.J. *J. Power Sources* **2007**, *165*, 870-873.

35. Kim, J.-K.; Cheruvally, G.; Ahn, J.-H.; Seo, Y.-G.; Choi, D.S.; Lee, S.-H.; Song, C.E. *J. Ind. Eng. Chem*. **2008**, *14*, 371-376.

36. Suguro, M.; Iwasa, S.; Nakahara, K. *Macromol. Rapid Commun*. **2008**, *29*, 1635-1639.

37. Qu, J.; Morita, R.; Satoh, M.; Wada, J.; Terakura, F.; Mizoguchi, K.; Ogata, N.; Masuda, T. *Chem.-Eur. J.* **2008**, *14*, 3250-3259.

38. Lee, S.H.; Kim, J.-K.; Cheruvally, G.; Choi, J.-W.; Ahn, J.-H.; Chauhan, G.S.; Song, C.E. *J. Power Sources* **2008**, *184*, 503-507.

39. Deng, L.; Li, X.; Xiao, L.; Zhang, Y. *J. Cent. South Univ. Technol.* **2003**, *10*, 190-194.

40. Nishide, H.; Iwasa, S.; Pu, Y.-J.; Suga, T.; Nakahara, K.; Satoh, M. *Electrochim. Acta* **2004**, *50*, 827-831.

41. Katsumata, T.; Satoh, M.; Wada, J.; Shiotsuki, M.; Sanda, F.; Masuda, T. *Macromol. Rapid Commun.* **2006**, *27*, 1206-1211.

42. Suguro, M.; Iwasa, S.; Kusachi, Y.; Morioka, Y.; Nakahara, K. *Macromol. Rapid Commun*. **2007**, *28*, 1929-1933.

43. Qu, J.; Katsumata, T.; Satoh, M.; Wada, J.; Masuda, T. *Polymer* **2009**, *50*, 391-396.

44. Qu, J.; Khan, F.Z.; Satoh, M; Wada, J.; Hayashi, H.; Mizoguchi, K.; Masuda, T. *Polymer* **2008**, *49*, 1490-1496.

45. Suga, T.; Pu, Y.-J.; Kasatori, S.; Nishide, H. *Macromolecules* **2007**, *40*, 3167-3173.

46. Qu, J.; Katsumata, T.; Satoh, M.; Wada, J.; Masuda, T. *Macromolecules* **2007**, *40*, 3136-3144.

47. Nesvadba, P.; Bugnon, L.; Maire, P.; Novák, P. *Chem. Mater.* **2010**, *22*, 783-788.

48. Suga, T.; Ohshiro, H.; Sugita, S.; Oyaizu, K.; Nishide, H. *Adv. Mater.* **2009**, *21*, 1627-1630.

49. Blatter, H.M.; Lukaszewski, H. *Tetrahedron Lett.* **1968**, 2701-2705.

50. Blatter, H.M. 1,4-Dihydro-1,2,4-benzotriazinyl radicals. US 65-505981 3423409, 19651101, 1969.

51. Hicks, R.G. *Org. Biomol. Chem.* **2007**, *5*, 1321-1338.

52. Neugebauer, F.A.; Umminger, I. *Chem. Ber.* **1980**, *113*, 1205-1225.

53. Neugebauer, F.A.; Umminger, I. *Chem. Ber.* **1981**, *114*, 2423-2430.

54. Mukai, K.; Inoue, K.; Achiwa, N.; Jamali, J.B.; Krieger, C.; Neugebauer, F.A. *Chem. Phys. Lett.* **1994**, *224*, 569-575.

55. Krieger, C.; Neugebauer, F.A. *Acta Crystallogr., Sect. C* **1996**, *C52*, 3124-3126.

56. Hutchison, K.A; Srdanov, G.; Menon, R.; Gabriel, J.-C.P.; Knight, B.; Wudl, F. *J. Am. Chem. Soc.* **1996**, *118*, 13081-13082.

57. Yan, B. Ph.D. Dissertation. *Towards the Development of Organic Magnetoconducting Materials: Structural, Magnetic, and Conducting Properties of Diaryl-1,2,4-Benzotriazinyl Radicals and Polyradicals*. University of Victoria, 2009.

58. Nakahara, K.; Iwasa, S.; Iriyama, J.; Morioka, Y.; Suguro, M.; Satoh, M.; Cairns, E.J. *Electrochim. Acta* **2006**, *52*, 921-927.

59. Wallach, O. *Justus Liebig's Annalen der Chemie* **1877**, *184*, 79.

60. Patel, H.V.; Kavita, V.A.; Pandey, S.P.; Fernandes, P.S. *Tetrahedron* **1996**, *52*, 661-668.

61. Kadirov, M.K.; Buzykin, B.I.; Gazetdinova, N.G. *Russ. Chem. Bull., Int. Ed.* **2002**, *51*, 1796-1799.

62. Koopmans, T. *Physica* **1934**, *1*, 104-113.

63. Corey, E.J.; Kim, C.U. *J. Am. Chem. Soc.* **1972**, *94*, 7586-7587.

64. McConnell, H.M.; *J. Chem. Phys.* **1956**, *24*, 632.

65. Stone, E.W.; Maki, A.H. *J. Chem. Phys.* **1963**, *39*, 1635-1642.

66. Bard, A.J.; Faulkner, L.R. *Electrochemical Methods*. John Wiley & Sons,Inc.: New York, 1980, p 213 - 248.

67. Manda, S.; Nakanishi, I.; Ohkubo, K.; Yakumaru, H.; Matsumoto, K.; Ozawa, T.; Ikota, N.; Fukuzumi, S.; Anazi, K. *Org. Biomol. Chem.* **2007**, *5*, 3951-3955.

68. Gilroy, J.B.; McKinnon, S.D.J.; Koivisto, B.D.; Hicks, R.G. *Org. Lett.* **2007**, *9*, 4837-4840.

69. Boeré, R.T.; Roemmele, T.L. *Coord. Chem. Rev.* **2000**, *210*, 369-445.

70. Frisch, M.J.; Trucks, G.W.; Schlegel, H.B.; Scuseria, G.E.; Robb, M.A.; Cheeseman, J.R.; Montgomery, J.A.; Vreven, J.T.; Kudin, K.N.; Burant, J.C.; Millam, J.M.; Iyengar, S.S.; Tomasi, J.; Barone, V.; Mennucci, B.; Cossi, M.; Scalmani, G.; Rega, N.; Petersson, G.A.; Nakatsuji, H.; Hada, M.; Ehara, M.; Toyota, K.; Fukuda, R.; Hasegawa, J.; Ishide, M.; Nakajima, H.; Honda, Y.; Kitao, O.; Nakai, H.; Klene, M.; Li, X.; Knox, J.E.; Hratchian, H.P.; Cross, J.B.; Adamo, C.; Jaramillo, J.; Gomperts, R.; Stratmann, R.E.; Yazyez, O.Y.; Austin, A.J.; Cammi, R.; Pomelli, C.; Ochterski, J.W.; Ayala, P.Y.; Morokuma, K.; Voth, G.A.; Salvador, P.; Dannenberg, J.J.; Zakrzewski, V.G.; Dapprich, S.; Daniels, A.D.; Strain, M.C.; Farkas, O.; Malick, D.K.; Rabuck, A.D.; Raghavachari, K.; Foresman, J.B.; Ortiz, J.V.; Cui, Q.; Baboul, A.G.; Clifford, S.; Cioslowski, J.; Stevanov, B.B.; Liu, G.; Liashenko, A.; Piskorz, P.; Komaromi, I.; Martin, R.L.; Fox, D.J.; Keith, T.; Al-Laham, M.A.; Peng, C.Y.; Nanayakkara, A.; Challacombe, M.; Gill, P.M.W.; Johnson, B.; Chen, W.; Wong, M.W.; Gonzalez, C.; Pople, J.A. *Gaussian 03*, Revision C.02; Gaussian, Inc.; Wallingford, CT, 2004.

71. Connelly, N.G.; Geiger, W.E. *Chem. Rev.* **1996**, *96*, 877-910.

72. Rajca, A. *Chem. Rev.* **1994**, *94*, 871-893.

73. Rajca, A.; Utamapanya, S.; Xu, J. *J. Am. Chem. Soc.* **1991**, *113*, 9235-9241.

74. Beekman, R.A.; Boeré, R.T.; Moock, K.H.; Parvez, M. *Can. J. Chem.* **1998**, *76*, 85-93.

75. Gilroy, J.B.; McKinnon, S.D.J.; Kennepohl, P.; Zsombor, M.S.; Ferguson, M.J.; Thompson, L.K.; Hicks, R.G. *J. Org. Chem.* **2007**, *72*, 8062-8069.

76. Weil, J.A.; Bolton, J.R.; Wertz, J.E. *Electron Paramagnetic Resonance. Elemental Theory and Practical Applications*. John Wiley & Sons, Inc.: New York. 1994.

77. Tsierkezos, N.G. *J. Solution Chem.* **2007**, *36*, 289-302.

78. Viehbeck, A.; Goldberg, M.J.; Kovac, C.A. *J. Electrochem. Soc.* **1990**, *137*, 1460-1466.

79. Langford, S.J.; Latter, M.J.; Woodward, C.P. *Photochem. Photobiol.* **2006**, *82*, 1530-1540.

80. Koshkakaryan, G.; Klivansky, L.M.; Cao, D.; Snauko, M.; Teat, S.J.; Struppe, J.O.; Liu, Y. *J. Am. Chem. Soc.* **2009**, *131*, 2078-2079.

81. Kato, S.; Nonaka, Y.; Shimasaki, T.; Goto, K.; Shinmyozu, T. *J. Org. Chem*. **2008**, *73*, 4063-4075.

82. Angadi, M.A.; Gosztola, D.; Wasielewski, M.R. *J. Appl. Phys.* **1998**, *83*, 6187-6189.

83. Debreczeny, M.P.; Svec, W.A.; Marsh, E.M.; Wasielewski, M.R. *J. Am. Chem. Soc.* **1996**, *118*, 8174-8175.

84. Lee, S.K.; Zu, Y.; Herrmann, A.; Geerts, Y.; Mllen, K.; Bard, A.J. *J. Am. Chem. Soc.* **1999**, *121*, 3513-3520.

85. Gosztola, D.; Niemczyk, M.P.; Svec, W.; Lukas, A.S.; Wasielewski, M.R. *J. Phys. Chem. A* **2000**, *104*, 6545-6551.

86. Guzmán-Lucero, D.; Likhanova, N.V.; Höpfl, H.; Guzmán, J.; Likhatchev, D.; Martínez-Palou, R. *ARKIVOC*, **2006**, 7-20.

87. Andric, G.; Boas, J.F.; Bond, A.M.; Fallon, G.D.; Ghiggino, K.P.; Hogan, C.F.; Hutchison, J.A.; Lee, M.A.-P.; Langford, S.J.; Pilbrow, J.R.; Troup, G.J.; Woodward, C.P. *Aust. J. Chem.* **2004**, *57*, 1011-1019.

88. LaFemina, J.P.; Arjavalingam, G.; Hougham, G. *J. Chem. Phys.* **1989**, *90*, 5154-5160.

89. Miller, J.S.; Epstein, A.J. *Angew. Chem., Int. Ed.* **1994**, *33*, 385-415.

90. Kahn, O. *Molecular Magnetism*. Wiley-VCH Inc.: New York. 1993.

91. Haddon, R.C. *Nature*, **1975**, *256*, 394-396.

92. Bag, P.; Itkis, M.E.; Pal, S.K.; Donnadieu, B.; Tham, F.S.; Park, H.; Schlueter, J.A.; Siegrist, T.; Haddon, R.C. *J. Am. Chem. Soc.* **2010**, *132*, 2684-2694.

93. Rawson, J.M.; Alberola, A.; Whalley, A. *J. Mater. Chem.* **2006**, *16*, 2560-2575.

94. Tse, J.S.; Leitch, A.A.; Yu, X.; Bao, X.; Zhang, S.; Liu, Q.; Jin, C.; Secco, R.A.; Desgreniers, S.; Ohishi, Y.; Oakley, R.T. *J. Am. Chem. Soc.* **2010**, *132*, 4876-4886.

95. Haddon, R.C. *Aust. J. Chem.* **1975**, *28*, 2343-2351.

96. Peierls, R.C. *Quantum Theory of Solids*. Oxford University Press: London. 1953.

97. Miller, J.S.; Epstein, A.J. *Prog. Inorg. Chem.* **1976**, *20*, 1-151.

98. Davis, W.M.; Hicks, R.G.; Oakley, R.T.; Zhao, B.; Taylor, N.J. *Can. J. Chem.* **1993**, *71*, 180-185.

99. McConnell, H.M. *J. Chem. Phys.* **1963**, *39*, 1910.

100. **2.3:** Formula: $C_{19}H_{14}N_4$; FW: 299.35; Crystal system: monoclinic; Space group: *C*2/*c*; a: 33.557(4) Å; b: 4.9877(5) Å; c: 19.167(2) Å; β: 108.904(2) °; V: 3035.1(5) Å^3; Z: 8; ρ_{calc}: 1.310 g·cm^{-3}; μ: 0.081 mm^{-1}; T: 296 K; λ: 0.71073 Å; R_1: 0.0999; wR_2: 0.1005. $R_1 = \Sigma(|F_0|-|F_c|)/\Sigma|F_0|$; $wR_2 = [\Sigma(w(F_0^2-F_c^2)^2)/\Sigma w(F_0^2)^2]^{1/2}$. **2.20:** Formula: $C_{20}H_{19}N_4OBr$; FW: 411.30; Crystal system: monoclinic; Space group: $P2_1/n$ (#14); a: 13.5654(5) Å; b: 8.1787(3) Å; c: 17.6303(7) Å; β: 110.828(2) °; V: 1828.1(1) Å^3; Z: 4; ρ_{calc}: 1.494 g·cm^{-3}; μ: 2.265 mm^{-1}; T: 103 K; λ: 0.71073 Å; R_1: 0.046; wR_2: 0.078. $R_1 = \Sigma(|F_0|-|F_c|)/\Sigma|F_0|$; $wR_2 = [\Sigma(w(F_0^2-F_c^2)^2)/\Sigma w(F_0^2)^2]^{1/2}$. **3.2:** Formula: $C_{32}H_{22}N_6$; FW: 490.56; Crystal system: monoclinic; Space group: $P2_1/n$ (#14); a: 9.283(1) Å; b: 9.106(1) Å; c: 28.552(4) Å; β: 96.318(2) °; V: 2398.8(6) Å^3; Z: 4; ρ_{calc}: 1.358 g·cm^{-3}; μ: 0.083 mm^{-1}; T: 103 K; λ: 0.71073 Å; R_1: 0.080; wR_2: 0.116. $R_1 = \Sigma(|F_0|-|F_c|)/\Sigma|F_0|$; $wR_2 = [\Sigma(w(F_0^2-F_c^2)^2)/\Sigma w(F_0^2)^2]^{1/2}$.

101. Allen, F.H.; Kennard, O.; Watson, D.G.; Brammer, L.; Orpen, A.G.; Taylor, R. *J. Chem. Soc. Perkin Trans. 2* **1987**, S1-S19.

102. Rowland, R.S.; Taylor, R. *J. Phys. Chem.* **1996**, *100*, 7384-7391.

103. Hernàndez, E.; Mas, M.; Molins, E.; Rovira, C.; Veciana, J. *Angew. Chem., Int. Ed.* **1993**, *32*, 882-884.

104. Cirujeda, J.; Ochando, L.E.; Amigó, J.M.; Rovira, C.; Rius, J.; Veciana, J. *Angew. Chem., Int. Ed.* **1995**, *34*, 55-57.

105. Okuno, T.; Otsuka, T.; Awaga, K. *J. Chem. Soc., Chem. Commun.* **1995**, 827-828.

106. Taylor, P.; Serwinski, P.R.; Lahti, P.M. *Chem. Commun.* **2003**, 1400-1401.

107. Aboaku, S.; Lahti, P.M. *Polyhedron* **2007**, *26*, 1959-1964.

108. Murata, H.; Miyazaki, Y.; Inaba, A.; Paduan-Filho, A.; Bindilatti, V.; Oliveira, N.F.; Delen, Z.; Lahti, P.M.. *J. Am. Chem. Soc.* **2008**, *130*, 186-194.

109. Anderson, H.L. *Nature Chemistry* **2010**, *2*, 12-13.

110. Shultz, D.A.; Bodnar, S.H.; Lee, H.; Kampf, J.W.; Incarvito, C.D.; Rheingold, A.L. *J. Am. Chem. Soc.* **2002**, *124*, 10054-10061.

111. Fang, S.; Lee, M.-S.; Hrovat, D.A.; Border, W.T. *J. Am. Chem. Soc.* **1995**, *117*, 6727-6731.

112. Hayakawa, K.; Shiomi, D.; Ise, T.; Sato, K.; Takui, T. *J. Mater. Chem.* **2006**, *16*, 4146-4154.

113. Wudl, F.; Bryce, M.R. *J. Chem. Educ.* **1990**, *67*, 717-718.

114. Sheldrick, G.M. SHELXS-90. *Acta Crystallogr., Sect. A* **1990**, *46*, 467-473.

115. Sheldrick, G.M. SHELXL-97. Program for the Refinement of Crystal Structures, University of Gottingen, Gottingen, Germany, 1997.

116. SHELXTL, Version 6.12 Program Library for Structure Solution and Molecular Graphics, Bruker Advanced X-ray Solutions, Inc., Madison, WI, 2001.

117. Altomare, A.; Burla, M.C.; Camalli, M.; Cascarano, G.L.; Giacovazzo, C.; Guagliardi, A.; Moliterni, A.G.G.; Polidori, G.; Spagna, R. *J. Appl. Crystallogr.* **1999**, *32*, 115-119.

118. Farrugia, L.J. *J. Appl. Crystallogr.* **1999**, *32*, 837-838.

Appendix A Crystallographic parameters

Table A.1 Crystallographic parameters

	2.3	**2.20**	**3.2**
Formula	$C_{19}H_{14}N_4$	$C_{20}H_{19}N_4OBr$	$C_{32}H_{22}N_6$
FW	299.35	411.30	490.56
Dimensions (mm)	0.40 × 0.20 × 0.01	0.07 × 0.23 × 0.50	0.07 × 0.18 × 0.60
a (Å)	33.557(4)	13.5654(5)	9.283(1)
b (Å)	4.9877(5)	8.1787(3)	9.106(1)
c (Å)	19.167(2)	17.6303(7)	28.552(4)
α (deg)	90.0	90.0	90
β (deg)	108.904(2)	110.828(2)	96.318(2)
γ (deg)	90.0	90.0	90
Volume ($Å^3$)	3035.1(5)	1828.1(1)	2398.8(6)
ρ_{calc} ($g \cdot cm^{-3}$)	1.310	1.494	1.358
System	monoclinic	monoclinic	monoclinic
Space group	*C*2/*c*	$P2_1/n$ (#14)	$P2_1/n$ (#14)
Z	8	4	4
μ (mm^{-1})	0.081	2.265	0.083
T (K)	296	103	103
$2\theta_{max}$ (deg)	56.0	56.1	56.1
Unique reflections	3661 (R_{int} = 0.0343)	4422 (R_{int} = 0.060)	5751 (R_{int} = 0.047)
R_1[a]	0.0999	0.046	0.080
wR_2[b]	0.1005	0.078	0.116

[a] $R_1 = \Sigma(|F_0|-|F_c|)/\Sigma|F_0|$, [b] $wR_2 = [\Sigma(w(F_0^2-F_c^2)^2)/\Sigma w(F_0^2)^2]^{1/2}$

Appendix B Complete listings of bond lengths and angles

Table B.1 Bond lengths (Å) and angles (deg) for **2.3**.

N(1)-C(2)	1.379(2)
C(2)-C(7)	1.376(2)
C(2)-C(3)	1.413(2)
C(3)-N(8)	1.370(2)
C(3)-C(4)	1.406(2)
C(4)-C(5)	1.388(2)
C(4)-N(11)	1.392(2)
C(5)-C(6)	1.379(2)
C(6)-C(7)	1.379(2)
N(8)-C(9)	1.334(2)
C(9)-N(10)	1.335(2)
C(9)-C(12)	1.483(2)
N(10)-N(11)	1.3689(19)
N(11)-C(18)	1.435(2)
C(12)-C(13)	1.377(2)
C(12)-C(17)	1.389(2)
C(13)-C(14)	1.387(3)
C(14)-C(15)	1.369(3)
C(15)-C(16)	1.371(3)
C(16)-C(17)	1.381(3)
C(18)-C(19B)	1.210(4)
C(18)-C(19A)	1.385(4)
C(18)-C(23A)	1.414(5)
C(18)-C(23B)	1.567(4)
C(19A)-C(19B)	1.329(5)
C(19A)-C(20A)	1.384(5)
C(19A)-C(20B)	1.935(7)
C(19B)-C(20B)	1.384(6)
C(19B)-C(23A)	1.429(6)
C(19B)-C(20A)	1.842(6)
C(19B)-C(22A)	1.924(6)
C(20A)-C(20B)	1.248(7)
C(20A)-C(21A)	1.356(8)
C(20A)-C(21B)	1.57(2)
C(20B)-C(21A)	0.91(3)
C(20B)-C(22A)	1.383(7)
C(20B)-C(21B)	1.51(3)
C(20B)-C(23A)	2.019(7)
C(21A)-C(21B)	0.700(12)
C(21A)-C(22A)	1.390(10)
C(21A)-C(22B)	1.85(3)
C(21B)-C(22B)	1.26(2)
C(21B)-C(22A)	1.64(2)
C(22A)-C(23A)	1.386(5)
C(22B)-C(23B)	1.384(5)
C(7)-C(2)-N(1)	122.20(16)

C(7)-C(2)-C(3)	119.20(16)
N(1)-C(2)-C(3)	118.58(17)
N(8)-C(3)-C(4)	122.82(15)
N(8)-C(3)-C(2)	118.18(15)
C(4)-C(3)-C(2)	118.99(16)
C(5)-C(4)-N(11)	123.17(16)
C(5)-C(4)-C(3)	120.97(16)
N(11)-C(4)-C(3)	115.85(16)
C(6)-C(5)-C(4)	118.38(17)
C(7)-C(6)-C(5)	121.81(19)
C(2)-C(7)-C(6)	120.59(17)
C(9)-N(8)-C(3)	115.36(14)
N(8)-C(9)-N(10)	127.39(17)
N(8)-C(9)-C(12)	118.31(16)
N(10)-C(9)-C(12)	114.26(16)
C(9)-N(10)-N(11)	116.35(14)
N(10)-N(11)-C(4)	122.19(14)
N(10)-N(11)-C(18)	113.02(14)
C(4)-N(11)-C(18)	124.66(16)
C(13)-C(12)-C(17)	118.25(18)
C(13)-C(12)-C(9)	120.29(17)
C(17)-C(12)-C(9)	121.44(17)
C(12)-C(13)-C(14)	120.8(2)
C(15)-C(14)-C(13)	120.5(2)
C(14)-C(15)-C(16)	119.2(2)
C(15)-C(16)-C(17)	120.8(2)
C(16)-C(17)-C(12)	120.5(2)
C(19B)-C(18)-C(19A)	61.2(3)
C(19B)-C(18)-C(23A)	65.5(3)
C(19A)-C(18)-C(23A)	117.3(3)
C(19B)-C(18)-N(11)	126.2(3)
C(19A)-C(18)-N(11)	117.8(2)
C(23A)-C(18)-N(11)	119.2(2)
C(19B)-C(18)-C(23B)	118.2(3)
C(19A)-C(18)-C(23B)	87.3(2)
C(23A)-C(18)-C(23B)	90.6(3)
N(11)-C(18)-C(23B)	115.3(2)
C(19B)-C(19A)-C(20A)	85.5(4)
C(19B)-C(19A)-C(18)	52.9(2)
C(20A)-C(19A)-C(18)	119.6(4)
C(19B)-C(19A)-C(20B)	45.7(3)
C(20A)-C(19A)-C(20B)	40.0(3)
C(18)-C(19A)-C(20B)	86.1(3)
C(18)-C(19B)-C(19A)	66.0(3)
C(18)-C(19B)-C(20B)	125.1(4)
C(19A)-C(19B)-C(20B)	91.0(4)
C(18)-C(19B)-C(23A)	64.2(3)
C(19A)-C(19B)-C(23A)	120.2(4)
C(20B)-C(19B)-C(23A)	91.7(4)
C(18)-C(19B)-C(20A)	101.3(3)
C(19A)-C(19B)-C(20A)	48.5(3)
C(20B)-C(19B)-C(20A)	42.6(3)
C(23A)-C(19B)-C(20A)	114.3(3)
C(18)-C(19B)-C(22A)	98.0(3)
C(19A)-C(19B)-C(22A)	114.8(3)
C(20B)-C(19B)-C(22A)	45.9(3)
C(23A)-C(19B)-C(22A)	46.0(2)

C(20A)-C(19B)-C(22A)	78.3(3)
C(20B)-C(20A)-C(21A)	40.6(13)
C(20B)-C(20A)-C(19A)	94.5(4)
C(21A)-C(20A)-C(19A)	119.9(5)
C(20B)-C(20A)-C(21B)	63.7(9)
C(21A)-C(20A)-C(21B)	26.4(9)
C(19A)-C(20A)-C(21B)	115.4(7)
C(20B)-C(20A)-C(19B)	48.7(3)
C(21A)-C(20A)-C(19B)	81.9(8)
C(19A)-C(20A)-C(19B)	46.0(2)
C(21B)-C(20A)-C(19B)	93.1(7)
C(21A)-C(20B)-C(20A)	76.1(10)
C(21A)-C(20B)-C(22A)	71.3(6)
C(20A)-C(20B)-C(22A)	129.4(5)
C(21A)-C(20B)-C(19B)	135.1(14)
C(20A)-C(20B)-C(19B)	88.7(4)
C(22A)-C(20B)-C(19B)	88.1(4)
C(21A)-C(20B)-C(21B)	17.3(13)
C(20A)-C(20B)-C(21B)	68.6(7)
C(22A)-C(20B)-C(21B)	68.8(7)
C(19B)-C(20B)-C(21B)	118.0(7)
C(21A)-C(20B)-C(19A)	107.4(14)
C(20A)-C(20B)-C(19A)	45.5(3)
C(22A)-C(20B)-C(19A)	111.5(4)
C(19B)-C(20B)-C(19A)	43.4(3)
C(21B)-C(20B)-C(19A)	92.2(6)
C(21A)-C(20B)-C(23A)	103.0(10)
C(20A)-C(20B)-C(23A)	113.0(4)
C(22A)-C(20B)-C(23A)	43.3(3)
C(19B)-C(20B)-C(23A)	45.0(3)
C(21B)-C(20B)-C(23A)	91.3(7)
C(19A)-C(20B)-C(23A)	74.4(2)
C(21B)-C(21A)-C(20B)	140(3)
C(21B)-C(21A)-C(20A)	94(3)
C(20B)-C(21A)-C(20A)	63.3(8)
C(21B)-C(21A)-C(22A)	98(2)
C(20B)-C(21A)-C(22A)	70.4(11)
C(20A)-C(21A)-C(22A)	120.1(8)
C(21B)-C(21A)-C(22B)	25.7(16)
C(20B)-C(21A)-C(22B)	114.5(11)
C(20A)-C(21A)-C(22B)	82.1(13)
C(22A)-C(21A)-C(22B)	84.6(11)
C(21A)-C(21B)-C(22B)	140(2)
C(21A)-C(21B)-C(20B)	22.7(13)
C(22B)-C(21B)-C(20B)	117.8(12)
C(21A)-C(21B)-C(20A)	59(2)
C(22B)-C(21B)-C(20A)	97.6(10)
C(20B)-C(21B)-C(20A)	47.7(9)
C(21A)-C(21B)-C(22A)	57.1(15)
C(22B)-C(21B)-C(22A)	98.4(10)
C(20B)-C(21B)-C(22A)	51.8(8)
C(20A)-C(21B)-C(22A)	95.5(14)
C(20B)-C(22A)-C(23A)	93.6(4)
C(20B)-C(22A)-C(21A)	38.3(11)
C(23A)-C(22A)-C(21A)	119.1(5)
C(20B)-C(22A)-C(21B)	59.4(9)
C(23A)-C(22A)-C(21B)	114.7(6)

C(21A)-C(22A)-C(21B)	25.0(7)
C(20B)-C(22A)-C(19B)	46.0(3)
C(23A)-C(22A)-C(19B)	47.8(3)
C(21A)-C(22A)-C(19B)	78.0(6)
C(21B)-C(22A)-C(19B)	88.1(7)
C(21B)-C(22B)-C(23B)	124.7(11)
C(21B)-C(22B)-C(21A)	14.0(8)
C(23B)-C(22B)-C(21A)	110.7(6)
C(22A)-C(23A)-C(18)	118.8(4)
C(22A)-C(23A)-C(19B)	86.2(3)
C(18)-C(23A)-C(19B)	50.3(2)
C(22A)-C(23A)-C(20B)	43.1(3)
C(18)-C(23A)-C(20B)	82.2(3)
C(19B)-C(23A)-C(20B)	43.2(2)
C(22B)-C(23B)-C(18)	116.0(3)

Table B.2 Bond lengths (Å) and angles (deg) for **2.17**.

C(2)-N(1)	1.327(3)
C(2)-C(7)	1.393(3)
C(2)-C(3)	1.459(3)
C(3)-N(8)	1.318(3)
C(3)-C(4)	1.441(3)
C(4)-N(11)	1.367(3)
C(4)-C(5)	1.391(3)
C(5)-C(6)	1.386(3)
C(5)-H(5)	0.9500
C(6)-C(7)	1.392(3)
C(6)-H(6)	0.9500
C(7)-H(7)	0.9500
C(9)-N(10)	1.336(3)
C(9)-N(8)	1.347(3)
C(9)-C(12)	1.473(3)
C(12)-C(13)	1.395(3)
C(12)-C(17)	1.399(3)
C(13)-C(14)	1.391(3)
C(13)-H(13)	0.9500
C(14)-C(15)	1.385(4)
C(14)-H(14)	0.9500
C(15)-C(16)	1.383(4)
C(15)-H(15)	0.9500
C(16)-C(17)	1.387(3)
C(16)-H(16)	0.9500
C(17)-H(17)	0.9500
C(18)-C(19)	1.379(3)
C(18)-C(23)	1.388(3)
C(18)-N(11)	1.448(3)
C(19)-C(20)	1.389(3)
C(19)-H(19)	0.9500
C(20)-C(21)	1.388(3)
C(20)-H(20)	0.9500

C(21)-C(22)	1.387(3)
C(21)-H(21)	0.9500
C(22)-C(23)	1.386(3)
C(22)-H(22)	0.9500
C(23)-H(23)	0.9500
C(24)-O(1)	1.400(4)
C(24)-H(24A)	0.9800
C(24)-H(24B)	0.9800
C(24)-H(24C)	0.9800
N(1)-H(1A)	0.87(3)
N(1)-H(1B)	0.84(4)
N(10)-N(11)	1.322(3)
O(1)-H(1O)	0.76(4)
O(1B)-H(1O)	0.83(4)

N(1)-C(2)-C(7)	123.8(2)
N(1)-C(2)-C(3)	119.1(2)
C(7)-C(2)-C(3)	117.1(2)
N(8)-C(3)-C(4)	122.0(2)
N(8)-C(3)-C(2)	118.8(2)
C(4)-C(3)-C(2)	119.1(2)
N(11)-C(4)-C(5)	124.2(2)
N(11)-C(4)-C(3)	114.20(19)
C(5)-C(4)-C(3)	121.6(2)
C(6)-C(5)-C(4)	117.4(2)
C(6)-C(5)-H(5)	121.3
C(4)-C(5)-H(5)	121.3
C(5)-C(6)-C(7)	123.5(2)
C(5)-C(6)-H(6)	118.2
C(7)-C(6)-H(6)	118.2
C(6)-C(7)-C(2)	121.3(2)
C(6)-C(7)-H(7)	119.3
C(2)-C(7)-H(7)	119.3
N(10)-C(9)-N(8)	124.6(2)
N(10)-C(9)-C(12)	116.8(2)
N(8)-C(9)-C(12)	118.6(2)
C(13)-C(12)-C(17)	119.9(2)
C(13)-C(12)-C(9)	119.7(2)
C(17)-C(12)-C(9)	120.4(2)
C(14)-C(13)-C(12)	119.7(2)
C(14)-C(13)-H(13)	120.1
C(12)-C(13)-H(13)	120.1
C(15)-C(14)-C(13)	120.0(2)
C(15)-C(14)-H(14)	120.0
C(13)-C(14)-H(14)	120.0
C(16)-C(15)-C(14)	120.5(2)
C(16)-C(15)-H(15)	119.7
C(14)-C(15)-H(15)	119.7
C(15)-C(16)-C(17)	120.1(2)
C(15)-C(16)-H(16)	120.0
C(17)-C(16)-H(16)	120.0
C(16)-C(17)-C(12)	119.7(2)
C(16)-C(17)-H(17)	120.1
C(12)-C(17)-H(17)	120.1
C(19)-C(18)-C(23)	122.8(2)
C(19)-C(18)-N(11)	118.3(2)
C(23)-C(18)-N(11)	118.9(2)

C(18)-C(19)-C(20)	118.2(2)
C(18)-C(19)-H(19)	120.9
C(20)-C(19)-H(19)	120.9
C(21)-C(20)-C(19)	120.0(2)
C(21)-C(20)-H(20)	120.0
C(19)-C(20)-H(20)	120.0
C(22)-C(21)-C(20)	120.8(2)
C(22)-C(21)-H(21)	119.6
C(20)-C(21)-H(21)	119.6
C(23)-C(22)-C(21)	119.8(2)
C(23)-C(22)-H(22)	120.1
C(21)-C(22)-H(22)	120.1
C(22)-C(23)-C(18)	118.4(2)
C(22)-C(23)-H(23)	120.8
C(18)-C(23)-H(23)	120.8
C(2)-N(1)-H(1A)	124(2)
C(2)-N(1)-H(1B)	117(2)
H(1A)-N(1)-H(1B)	117(3)
C(3)-N(8)-C(9)	117.6(2)
N(11)-N(10)-C(9)	117.06(19)
N(10)-N(11)-C(4)	124.56(19)
N(10)-N(11)-C(18)	114.49(18)
C(4)-N(11)-C(18)	120.92(18)
C(24)-O(1)-H(1O)	108(3)

Table B.3 Bond lengths (Å) and angles (deg) for **3.2**.

C(3)-N(4)	1.330(2)
C(3)-N(2)	1.341(2)
C(3)-C(11)	1.486(2)
C(5)-C(6)	1.378(2)
C(5)-C(10)	1.403(2)
C(5)-H(5)	0.9500
C(6)-C(7)	1.395(3)
C(6)-H(6)	0.9500
C(7)-C(8)	1.376(3)
C(7)-H(7)	0.9500
C(8)-C(9)	1.400(2)
C(8)-H(8)	0.9500
C(9)-N(1)	1.387(2)
C(9)-C(10)	1.409(2)
C(10)-N(4)	1.378(2)
C(11)-C(16)	1.389(2)
C(11)-C(12)	1.392(2)
C(12)-C(13)	1.388(2)
C(12)-H(12)	0.9500
C(13)-C(14)	1.380(2)
C(13)-H(13)	0.9500
C(14)-C(15)	1.395(2)
C(14)-H(14)	0.9500
C(15)-C(16)	1.393(2)

C(15)-C(25)	1.486(2)
C(16)-H(16)	0.9500
C(17)-C(22)	1.372(3)
C(17)-C(18)	1.383(3)
C(17)-N(1)	1.435(2)
C(18)-C(19)	1.386(3)
C(18)-H(18)	0.9500
C(19)-C(20)	1.367(4)
C(19)-H(19)	0.9500
C(20)-C(21)	1.375(4)
C(20)-H(20)	0.9500
C(21)-C(22)	1.396(3)
C(21)-H(21)	0.9500
C(22)-H(22)	0.9500
C(25)-N(24)	1.330(2)
C(25)-N(26)	1.334(2)
C(27)-C(28)	1.370(3)
C(27)-C(32)	1.401(2)
C(27)-H(27)	0.9500
C(28)-C(29)	1.389(3)
C(28)-H(28)	0.9500
C(29)-C(30)	1.378(2)
C(29)-H(29)	0.9500
C(30)-C(31)	1.395(2)
C(30)-H(30)	0.9500
C(31)-N(23)	1.389(2)
C(31)-C(32)	1.415(2)
C(32)-N(26)	1.372(2)
C(33)-C(38)	1.381(2)
C(33)-C(34)	1.390(2)
C(33)-N(23)	1.432(2)
C(34)-C(35)	1.381(2)
C(34)-H(34)	0.9500
C(35)-C(36)	1.382(3)
C(35)-H(35)	0.9500
C(36)-C(37)	1.386(2)
C(36)-H(36)	0.9500
C(37)-C(38)	1.388(2)
C(37)-H(37)	0.9500
C(38)-H(38)	0.9500
N(1)-N(2)	1.3665(18)
N(23)-N(24)	1.3685(18)

N(4)-C(3)-N(2)	128.15(15)
N(4)-C(3)-C(11)	117.76(14)
N(2)-C(3)-C(11)	114.09(14)
C(6)-C(5)-C(10)	120.36(17)
C(6)-C(5)-H(5)	119.8
C(10)-C(5)-H(5)	119.8
C(5)-C(6)-C(7)	120.16(17)
C(5)-C(6)-H(6)	119.9
C(7)-C(6)-H(6)	119.9
C(8)-C(7)-C(6)	121.05(17)
C(8)-C(7)-H(7)	119.5
C(6)-C(7)-H(7)	119.5
C(7)-C(8)-C(9)	119.09(17)
C(7)-C(8)-H(8)	120.5

C(9)-C(8)-H(8)	120.5
N(1)-C(9)-C(8)	122.91(15)
N(1)-C(9)-C(10)	116.39(14)
C(8)-C(9)-C(10)	120.62(15)
N(4)-C(10)-C(5)	119.37(15)
N(4)-C(10)-C(9)	121.90(15)
C(5)-C(10)-C(9)	118.72(15)
C(16)-C(11)-C(12)	119.40(15)
C(16)-C(11)-C(3)	120.42(14)
C(12)-C(11)-C(3)	120.17(15)
C(13)-C(12)-C(11)	119.84(15)
C(13)-C(12)-H(12)	120.1
C(11)-C(12)-H(12)	120.1
C(14)-C(13)-C(12)	120.48(15)
C(14)-C(13)-H(13)	119.8
C(12)-C(13)-H(13)	119.8
C(13)-C(14)-C(15)	120.44(15)
C(13)-C(14)-H(14)	119.8
C(15)-C(14)-H(14)	119.8
C(16)-C(15)-C(14)	118.75(15)
C(16)-C(15)-C(25)	119.42(14)
C(14)-C(15)-C(25)	121.84(14)
C(11)-C(16)-C(15)	121.07(15)
C(11)-C(16)-H(16)	119.5
C(15)-C(16)-H(16)	119.5
C(22)-C(17)-C(18)	121.31(18)
C(22)-C(17)-N(1)	120.14(17)
C(18)-C(17)-N(1)	118.55(16)
C(17)-C(18)-C(19)	119.2(2)
C(17)-C(18)-H(18)	120.4
C(19)-C(18)-H(18)	120.4
C(20)-C(19)-C(18)	120.1(2)
C(20)-C(19)-H(19)	119.9
C(18)-C(19)-H(19)	119.9
C(19)-C(20)-C(21)	120.5(2)
C(19)-C(20)-H(20)	119.7
C(21)-C(20)-H(20)	119.7
C(20)-C(21)-C(22)	120.2(2)
C(20)-C(21)-H(21)	119.9
C(22)-C(21)-H(21)	119.9
C(17)-C(22)-C(21)	118.7(2)
C(17)-C(22)-H(22)	120.7
C(21)-C(22)-H(22)	120.7
N(24)-C(25)-N(26)	127.69(15)
N(24)-C(25)-C(15)	114.93(14)
N(26)-C(25)-C(15)	117.38(14)
C(28)-C(27)-C(32)	120.84(17)
C(28)-C(27)-H(27)	119.6
C(32)-C(27)-H(27)	119.6
C(27)-C(28)-C(29)	120.29(17)
C(27)-C(28)-H(28)	119.9
C(29)-C(28)-H(28)	119.9
C(30)-C(29)-C(28)	120.73(17)
C(30)-C(29)-H(29)	119.6
C(28)-C(29)-H(29)	119.6
C(29)-C(30)-C(31)	119.49(16)
C(29)-C(30)-H(30)	120.3

C(31)-C(30)-H(30)	120.3
N(23)-C(31)-C(30)	123.72(15)
N(23)-C(31)-C(32)	115.91(15)
C(30)-C(31)-C(32)	120.35(15)
N(26)-C(32)-C(27)	119.48(16)
N(26)-C(32)-C(31)	122.21(15)
C(27)-C(32)-C(31)	118.28(16)
C(38)-C(33)-C(34)	120.55(15)
C(38)-C(33)-N(23)	118.35(14)
C(34)-C(33)-N(23)	121.04(15)
C(35)-C(34)-C(33)	119.46(17)
C(35)-C(34)-H(34)	120.3
C(33)-C(34)-H(34)	120.3
C(34)-C(35)-C(36)	120.50(17)
C(34)-C(35)-H(35)	119.8
C(36)-C(35)-H(35)	119.8
C(35)-C(36)-C(37)	119.73(16)
C(35)-C(36)-H(36)	120.1
C(37)-C(36)-H(36)	120.1
C(36)-C(37)-C(38)	120.24(16)
C(36)-C(37)-H(37)	119.9
C(38)-C(37)-H(37)	119.9
C(33)-C(38)-C(37)	119.50(16)
C(33)-C(38)-H(38)	120.2
C(37)-C(38)-H(38)	120.2
N(2)-N(1)-C(9)	122.76(13)
N(2)-N(1)-C(17)	113.80(13)
C(9)-N(1)-C(17)	123.07(14)
C(3)-N(2)-N(1)	115.38(13)
C(3)-N(4)-C(10)	115.35(14)
N(24)-N(23)-C(31)	122.25(13)
N(24)-N(23)-C(33)	112.97(12)
C(31)-N(23)-C(33)	124.52(13)
C(25)-N(24)-N(23)	116.18(13)
C(25)-N(26)-C(32)	115.38(14)

Appendix C DFT calculation output parameters

Table C.1 Output parameters for **1.9**.

1|1|UNPC-UNK|FOpt|UB3LYP|6-31G(d,p)|C19H14N3(2)|PCUSER|12-May-2010|0||
OPT UB3LYP/6-31G(D,P) GEOM=CONNECTIVITY||b3lyp/6-31g(d,p) full optim
ization on parent benzotriazinyl radical||0,2|C,-1.7617349896,0.000452
1029,-0.1932243325|C,-1.7650769744,-0.0065023103,1.2320785673|N,-0.604
8074865,-0.0107337139,1.9585016645|C,0.5310088508,0.0596315575,1.25523
52153|N,0.6523796259,0.0414117684,-0.0773993001|N,-0.502253081,-0.0649
267224,-0.7967543032|C,-0.2991520476,-0.1825656504,-2.2063410963|C,1.8
092867249,0.15328614,2.0117950623|C,-2.9676229693,0.1055689846,-0.9030
383427|C,-4.172991713,0.1457077023,-0.2094450851|C,-4.194769037,0.0909
471411,1.1919981198|C,-3.0054611499,0.0223099244,1.9010472351|C,-0.965
9479309,-1.1689507342,-2.9423835838|C,-0.7310798755,-1.2832987541,-4.3
119607205|C,0.1730193532,-0.4306063889,-4.9472595338|C,0.8492756971,0.
5385467869,-4.2027678416|C,0.6185196832,0.6662891486,-2.8351960513|C,1
.7818676464,0.2401366202,3.4114794582|C,2.9692438489,0.3316052087,4.13
45678122|C,4.1980343513,0.3378180477,3.4716968568|C,4.2321192149,0.250
2717781,2.0780779562|C,3.0476334962,0.1579560424,1.3511509955|H,5.1846
643323,0.2515326353,1.5559278277|H,5.1230773781,0.4091603189,4.0367537
416|H,1.5582911587,1.202006975,-4.6886645443|H,0.3549139298,-0.5252212
375,-6.0133075981|H,-5.1422698811,0.1156819639,1.7211740814|H,2.935164
3218,0.3989309377,5.2182166938|H,3.0684307167,0.0844574058,0.270100663
8|H,0.821042554,0.2339017127,3.9125848284|H,-1.246519277,-2.0527814148
,-4.8786411525|H,1.1416089155,1.407754007,-2.2430440827|H,-1.644795381
,-1.8508162062,-2.4423861729|H,-2.9851143678,0.0050754238,2.9854420612
|H,-2.9608910921,0.1634346441,-1.9840445627|H,-5.1018697961,0.22500342
41,-0.7656123621||Version=IA32W-G03RevC.02|State=2-A|HF=-896.6984255|S
2=0.766719|S2-1=0.|S2A=0.750168|RMSD=7.789e-009|RMSF=2.808e-005|Dipole
=-0.4836894,0.001476,-1.0694845|PG=C01 [X(C19H14N3)]||@

Table C.2 Output parameters for **2.1**

1|1|UNPC-UNK|FOpt|UB3LYP|6-31G(d,p)|C20H16N3(2)|PCUSER|03-Mar-2010|0||
B3LYP/6-31G(D,P) OPT||b3lyp/6-31g(d,p) full optimization on 7-methyl
 benzotriazinyl radical||0,2|C,1.1765543517,-0.8994056067,-0.020421379
6|C,0.2175979679,-1.9453093853,0.08907829|N,-1.1260995824,-1.695615652
8,0.1656271394|C,-1.4909030954,-0.4121405597,0.066196268|N,-0.68007606
82,0.6490109587,-0.0119441095|N,0.6626347999,0.3999103515,0.0199902815
|C,1.4691877087,1.5790009422,0.0301536013|C,-2.9474226944,-0.104978789
7,0.0545083418|C,2.5364940733,-1.1993180559,-0.1949412589|C,2.97756473
37,-2.5223999401,-0.2085875027|C,2.0327057719,-3.556825595,-0.05217472
84|C,0.6849567697,-3.2752172701,0.0863642167|C,2.5229569266,1.71545213
27,0.9416442524|C,3.2776841611,2.8877952566,0.9521156373|C,2.979768030
6,3.9280575123,0.0705897365|C,1.9146393749,3.7929207958,-0.8227885975|
C,1.1574598646,2.62425677,-0.8467348272|C,-3.8782920344,-1.1539908206,
0.0743354374|C,-5.2449572023,-0.8829974628,0.0617226867|C,-5.700418147
2,0.4363864905,0.0289406355|C,-4.7784563136,1.4854956384,0.0102296683|
C,-3.4113786936,1.219229125,0.023445975|C,4.4408376363,-2.846216298,-0
.3883738744|H,4.8465408032,-3.3540078528,0.4947783592|H,5.0348209748,-
1.9441463246,-0.5565558855|H,4.5977546458,-3.5157973288,-1.2415974492|

H,-5.1256415409,2.5145785853,-0.0122769863|H,-6.766246389,0.6462526145
,0.019285319|H,1.6725182284,4.5998416571,-1.5078379475|H,3.5682100954,
4.840244782,0.0846921514|H,2.3693520591,-4.590147617,-0.0547404699|H,-
5.9561834436,-1.7039577629,0.0769213645|H,-2.6914793733,2.0292253036,0
.0143918216|H,-3.5103262553,-2.1729755546,0.1002813389|H,4.0909553158,
2.991731576,1.6640243768|H,0.3226650175,2.508495313,-1.5276965349|H,2.
7346942319,0.9193718912,1.6467615559|H,-0.054991948,-4.0628440675,0.18
10115744|H,3.2526683924,-0.3977740933,-0.3289712382||Version=IA32W-G03
RevC.02|State=2-A|HF=-936.0193217|S2=0.766832|S2-1=0.|S2A=0.750168|RMS
D=6.491e-009|RMSF=3.338e-006|Dipole=1.2716928,0.3272389,-0.1078881|PG=
C01 [X(C20H16N3)]||@

Table C.3 Output parameters for **2.2**

1|1|UNPC-UNK|FOpt|UB3LYP|6-31G(d,p)|C20H16N3O1(2)|PCUSER|02-Mar-2010|0
||# B3LYP/6-31G(D,P) OPT||b3lyp/6-31g(d,p) full optimization on 7-meth
oxy benzotriazinyl radical||0,2|C,3.1498884579,-1.7245404534,-0.127529
403|C,2.452231914,-2.9373210692,0.0121543516|C,1.0683653409,-2.9164317
947,0.1257895774|C,0.3433517747,-1.7123114608,0.1177330803|C,1.0758983
726,-0.4902854586,0.0180869146|C,2.4638739795,-0.5051504728,-0.1295038
008|N,-1.0238422305,-1.7374589585,0.1743477554|C,-1.6392423947,-0.5541
220904,0.0748108152|N,-1.0570673835,0.6485593478,0.0040234769|N,0.3083
974963,0.6757669451,0.0452964676|C,0.8611241739,1.9939520361,0.0371745
334|C,-3.1276729846,-0.5461606703,0.0510966239|O,4.5020277523,-1.62657
94701,-0.2696681023|C,5.2684026891,-2.8222463766,-0.2973202129|C,1.852
5144628,2.3579608687,0.9556155508|C,2.3579044702,3.6574756098,0.945179
1614|C,1.8708627564,4.5977393909,0.0360421427|C,0.8671200422,4.2331501
015,-0.8640810463|C,0.3595221516,2.9361505874,-0.8676158208|C,-3.82889
16397,-1.7609401161,0.0564811121|C,-5.2219342652,-1.7705700012,0.03168
97843|C,-5.9336487029,-0.5697698518,0.0014564758|C,-5.2413698703,0.643
31226,-0.0026730089|C,-3.8487514511,0.6576247643,0.0224077596|H,6.3052
263238,-2.5096759405,-0.4272710233|H,4.9784445007,-3.4690908338,-1.134
6099339|H,5.1757761264,-3.3838452103,0.6405875344|H,-5.7882901815,1.58
17086363,-0.0232368317|H,-7.0197942945,-0.5785800026,-0.0175808781|H,0
.4787232219,4.9603701231,-1.5707529444|H,2.2653084577,5.6091715217,0.0
336322533|H,-5.7533380026,-2.7180601216,0.0354995146|H,-3.3068095556,1
.5961490314,0.0241494186|H,-3.2638531784,-2.6854086486,0.0808626545|H,
3.1244875349,3.9367544713,1.6616209915|H,-0.4247904257,2.6411736242,-1
.5546186279|H,2.2096442462,1.6357110068,1.6811321578|H,3.034891417,0.4
050105746,-0.2527149524|H,2.9767115997,-3.8845573213,0.0216562749|H,0.
5017293516,-3.8373613076,0.2113477676||Version=IA32W-G03RevC.02|State=
2-A|HF=-1011.2235575|S2=0.767709|S2-1=0.|S2A=0.750175|RMSD=4.106e-009|
RMSF=4.063e-006|Dipole=1.3786811,0.0589037,-0.0894919|PG=C01 [X(C20H16
N3O1)]||@

Table C.4 Output parameters for **2.3**.

1|1|UNPC-UNK|FOpt|UB3LYP|6-31G(d,p)|C19H15N4(2)|PCUSER|03-Aug-2009|0||
B3LYP/6-31G(D,P) OPT||b3lyp/6-31g(d,p) full optimization on Nick's T
RZ radical||0,2|C,2.449193989,3.1933167253,-0.3588614022|C,1.300859348
1,3.9681225939,-0.1849270107|C,0.059374478,3.3545785975,0.0105980355|C
,-0.0140467505,1.9283107703,0.0297580016|C,1.1804105694,1.1707906795,-
0.0936244016|C,2.4124804189,1.8014806375,-0.314347337|N,-1.2484820428,

1.3457511837,0.1245775079|C,-1.2778520884,0.0083261263,0.0489704043|N,
-0.2210101484,-0.80397277,-0.0213562908|N,1.0131029679,-0.2183251259,-
0.0179952045|C,2.0950842395,-1.1493658121,0.0022927389|C,-2.6041017998
,-0.6678179127,0.0569171112|N,-1.1036000836,4.0643516524,0.2151740446|
C,3.1715673414,-0.9739760004,0.8804844391|C,4.20225918,-1.9123969166,0
.904294211|C,4.1606109986,-3.0303592899,0.0696864069|C,3.0745483634,-3
.2094261907,-0.7900053747|C,2.0418971406,-2.2756892792,-0.8273903726|C
,-2.7018491654,-2.0683250936,0.0443394702|C,-3.9489950657,-2.688127615
8,0.0483279734|C,-5.1169613807,-1.9223526301,0.0662109914|C,-5.0275507
558,-0.5293993942,0.081151403|C,-3.7813846566,0.0939544313,0.076568593
9|H,3.3998779628,3.6886801952,-0.5321191171|H,1.3641760921,5.052248187
2,-0.2061858534|H,3.3144097596,1.2231377666,-0.4600941834|H,-1.9435545
134,3.5079429958,0.1245021706|H,-1.1505669821,4.9937489315,-0.17350660
88|H,3.190233523,-0.1208892991,1.5491937321|H,5.0324483689,-1.77418084
99,1.5904196553|H,4.9642077244,-3.7599038125,0.0938991555|H,3.03123666
77,-4.0788869856,-1.4391193492|H,1.1896318542,-2.4059148488,-1.4835480
087|H,-1.7930315352,-2.6583577999,0.0359943292|H,-4.0097986056,-3.7726
807299,0.0398306401|H,-6.0886949538,-2.4078353719,0.0699863473|H,-5.93
07623404,0.0739861288,0.0963251929|H,-3.7031542988,1.1744043536,0.0889
582059||Version=IA32W-G03RevC.02|State=2-A|HF=-952.0618167|S2=0.767664
|S2-1=0.|S2A=0.750189|RMSD=8.355e-009|RMSF=6.206e-006|Dipole=0.5835543
,0.3026094,-0.3702627|PG=C01 [X(C19H15N4)]||@

Table C.5 Output parameters for **2.20**.

1|1|UNPC-UNK|FOpt|UB3LYP|6-31G(d,p)|C19H16N4(1+,2)|PCUSER|05-Mar-2010|
0||# B3LYP/6-31G(D,P) OPT||b3lyp/6-31g(d,p) full optimization on ammon
iumtriazinyl radical cation||1,2|C,-2.4114735882,3.2430179522,-0.27230
14383|C,-1.2322702743,3.9940856146,-0.1679523202|C,-0.0437461939,3.295
7014873,-0.0419579394|C,0.0331920255,1.8942179935,-0.0067285101|C,-1.1
784935798,1.163422921,-0.0773190636|C,-2.3941818788,1.8486738416,-0.23
35395417|N,1.263194434,1.3183455019,0.0773639935|C,1.2843283419,-0.031
1697843,0.0404697891|N,0.1966471495,-0.8099723672,-0.0041168736|N,-1.0
250864622,-0.2160069826,-0.0099113116|N,1.2962825533,3.9126293049,0.05
16132693|H,1.5492917362,4.469731265,-0.7701898393|H,1.9180992852,3.055
2792299,0.1092441819|H,1.4238667846,4.4899405227,0.8884671801|C,-2.133
4702363,-1.1328495701,-0.0006921449|C,2.5829303381,-0.7336356366,0.063
7061215|C,-3.140473412,-1.0005613295,0.9601864269|C,-4.1946945457,-1.9
131514545,0.9677998826|C,-4.2351233135,-2.9484426333,0.0320799726|C,-3
.2143125199,-3.078354432,-0.9126686523|C,-2.1559565044,-2.1728412654,-
0.9335423523|C,3.7851615062,-0.0122512954,-0.0206772275|C,5.0079529278
,-0.6758449157,0.0010608102|C,5.0469848343,-2.0679027904,0.1092682705|
C,3.8563331962,-2.7935920971,0.1939450315|C,2.6311077979,-2.135226736,
0.1710238416|H,3.8834850872,-3.8749907217,0.2807666906|H,6.0014442752,
-2.5846209771,0.1275986737|H,-3.241586,-3.8855499454,-1.6372444626|H,-
5.056520144,-3.6573735363,0.0436804786|H,5.9311576325,-0.1093268,-0.06
79130871|H,1.7061255623,-2.6943122893,0.2417791673|H,3.7578651283,1.06
7259218,-0.1101163423|H,-4.9753648388,-1.8221566188,1.7158737513|H,-1.
352782786,-2.2633464508,-1.6557632433|H,-3.0867742916,-0.2157741306,1.
7074193324|H,-3.3586722802,3.7569067569,-0.3895027056|H,-3.3194875987,
1.2949923592,-0.3269037585|H,-1.2601808006,5.0785987,-0.1948052976||Ve
rsion=IA32W-G03RevC.02|State=2-A|HF=-952.4378456|S2=0.762409|S2-1=0.|S
2A=0.750109|RMSD=9.989e-009|RMSF=3.108e-006|Dipole=0.2221322,4.0500394
,-0.0467873|PG=C01 [X(C19H16N4)]||@

Table C.6 Output parameters for **3.2** (singlet state).

1|1|UNPC-UNK|FOpt|UB3LYP|6-31G(d,p)|C32H22N6|PCUSER|09-Aug-2009|0||#P
UB3LYP/6-31G(D,P) OPT SCF=TIGHT GUESS=MIX VSHIFT=200||ub3lyp/6-31g(d,p
) full optimization BSS singlet on triazinyl dimer||0,1|C,1.2168085005
,-2.4224259501,0.0017697006|C,1.2100368986,-3.8252949889,0.0003393483|
C,-0.000006975,-4.5161154061,-0.0000113114|C,-1.2100504025,-3.82529422
51,-0.0003570892|C,-1.2168210148,-2.4224251694,-0.001777064|C,-0.00000
60373,-1.7307971515,-0.0000011157|C,2.512192353,-1.6891220108,0.000632
6018|C,-2.5122042548,-1.6891202972,-0.0006349527|N,2.4152060752,-0.354
6528325,0.0113765454|N,3.5846102722,0.3473825533,0.0253867554|C,4.8257
055981,-0.2789032769,-0.1276252122|C,4.8064233464,-1.7040122711,-0.094
245744|N,3.6383454085,-2.4109926184,0.0060163574|N,-3.6383577028,-2.41
09897164,-0.0060265541|C,-4.8064350856,-1.7040092519,0.0942391227|C,-4
.8257172823,-0.2788998969,0.1276270955|N,-3.5846197105,0.3473855669,-0
.0253833622|N,-2.4152169481,-0.3546514268,-0.0113712202|C,6.0312694667
,0.4066660992,-0.3412918798|C,7.2189440162,-0.3084660683,-0.4584261816
|C,7.2223629255,-1.708595475,-0.3746623335|C,6.0303875266,-2.394964919
6,-0.2022208548|C,-6.0303982998,-2.3949640772,0.2022113886|C,-7.222374
0514,-1.7085978642,0.3746607968|C,-7.2189560177,-0.3084695257,0.458437
3308|C,-6.0312826459,0.4066650842,0.3413052243|C,3.4084756383,1.758935
6103,0.1548016636|C,-3.4084725792,1.7589374024,-0.15479704|C,4.1878487
72,2.4978298014,1.053367855|C,3.9742704926,3.8692591896,1.1853085565|C
,2.9804011043,4.5050908314,0.4396199476|C,2.1921259631,3.7580357232,-0
.4389639445|C,2.4002765321,2.3886934408,-0.5847166721|C,-2.4002751245,
2.3886831785,0.5847336311|C,-2.1921053468,3.7580228526,0.4389836638|C,
-2.9803578551,4.505087637,-0.4396120509|C,-3.9742225879,3.8692676072,-
1.1853166887|C,-4.187820357,2.4978409859,-1.0533783125|H,-4.5783617676
,4.4370309198,-1.8865128862|H,-2.8169394031,5.5729737923,-0.5474756708
|H,1.4108395662,4.2415960635,-1.0176208406|H,2.8169980568,5.5729791792
,0.5474852112|H,-8.1475543465,0.2296611193,0.6211375198|H,-8.156581623
7,-2.2549295501,0.4598515558|H,8.1565714374,-2.2549253171,-0.459854559
4|H,8.1475422903,0.2296673128,-0.6211175987|H,-1.4108212097,4.24157346
25,1.017651721|H,-4.9372923066,1.9992827083,-1.6576832416|H,-1.7887475
042,1.7959070991,1.2541511575|H,4.5784291448,4.4370156624,1.8864935063
|H,1.7887322673,1.7959248285,-1.2541255151|H,4.9373268094,1.9992621623
,1.657658099|H,-5.9935985226,-3.4783214936,0.1625120716|H,-6.038074225
1,1.4861731943,0.4228921133|H,5.9935888587,-3.4783226298,-0.1625289764
|H,6.038058308,1.4861757871,-0.4228661829|H,-0.0000073285,-5.602251611
4,-0.0000152728|H,-2.1574705401,-4.3513256649,0.0000443908|H,-0.000005
7093,-0.6494163603,0.0000029322|H,2.1574566882,-4.3513270527,-0.000066
0628||Version=IA32W-G03RevC.02|State=1-A|HF=-1561.1382552|S2=1.031495|
S2-1=0.|S2A=0.257994|RMSD=9.652e-009|RMSF=7.408e-007|Dipole=0.0000045,
1.9739801,0.000003|PG=C01 [X(C32H22N6)]||@

Table C.7 Output parameters for **3.2** (triplet state).

1|1|UNPC-UNK|FOpt|UB3LYP|6-31G(d,p)|C32H22N6(3)|PCUSER|07-Aug-2009|0||
#P UB3LYP/6-31G(D,P) OPT SCF=TIGHT||ub3lyp/6-31g(d,p) Triplet full opt
imization on triazinyl dimer||0,3|C,1.2168630775,-2.4226768512,0.00177
88375|C,1.2100909996,-3.8255982984,0.0003592113|C,-0.000000684,-4.5163
609143,-0.0000067431|C,-1.2100890942,-3.825592509,-0.0003789231|C,-1.2
168546072,-2.4226710258,-0.0018129334|C,0.0000058885,-1.731033289,-0.0
000199377|C,2.5118610312,-1.6891167574,0.0005378851|C,-2.5118492821,-1

.6891049065,-0.0005804789|N,2.4148390554,-0.3545621526,0.0122050792|N,
3.584441192,0.3474682175,0.0262149826|C,4.8253531736,-0.2787491714,-0.
1276377733|C,4.8061300294,-1.7038829299,-0.0952801237|N,3.6380697167,-
2.4109521736,0.0048700676|N,-3.6380616524,-2.4109359465,-0.0048852674|
C,-4.806117365,-1.7038612895,0.0952847422|C,-4.8253315721,-0.278728472
8,0.1276427433|N,-3.5844218879,0.347483724,-0.0262240929|N,-2.41482108
81,-0.3545502065,-0.0122425335|C,6.030956051,0.4068352844,-0.341211711
2|C,7.2185006107,-0.3083387702,-0.4592957923|C,7.2219403228,-1.7085396
678,-0.3766018527|C,6.0299663157,-2.3949015401,-0.2042409283|C,-6.0299
5808,-2.3948698052,0.204260437|C,-7.2219248766,-1.7084967542,0.3766311
031|C,-7.2184742434,-0.3082948106,0.4593165413|C,-6.0309248586,0.40686
89166,0.3412197112|C,3.4083443439,1.758942645,0.1564187129|C,-3.408340
4716,1.7589603626,-0.1564171084|C,4.1879309264,2.4974125903,1.05514770
75|C,3.9743903462,3.8687823619,1.187816863|C,2.9803143472,4.5049790796
,0.4427203961|C,2.191800625,3.7583404341,-0.4360044059|C,2.3999354168,
2.389074248,-0.5824975964|C,-2.3999108052,2.3890981567,0.5824655891|C,
-2.1918048343,3.7583695654,0.4359802727|C,-2.980372006,4.5050066526,-0
.4426983868|C,-3.974475664,3.8688046791,-1.1877536865|C,-4.1879866078,
2.4974294997,-1.0550936128|H,-4.5788696518,4.4362162889,-1.8890161819|
H,-2.8170054352,5.5728427092,-0.5511381395|H,1.4103299997,4.2421638293
,-1.0141960168|H,2.8169242015,5.5728107544,0.5511677426|H,-8.147042267
7,0.229918867,0.621946723|H,-8.156077353,-2.2547912777,0.4625960698|H,
8.1560889974,-2.2548421965,-0.4625572279|H,8.1470740272,0.2298663476,-
0.6219235593|H,-1.4103159388,4.2421985103,1.0141425896|H,-4.9376464364
,1.9985744519,-1.6589247725|H,-1.7881227254,1.7966591002,1.2519430382|
H,4.5787378698,4.4361934804,1.8891197992|H,1.7881866485,1.7966340214,-
1.252009977|H,4.9375626182,1.9985619152,1.6590163339|H,-5.9930364837,-
3.4782533257,0.1653653295|H,-6.0378051992,1.4864357258,0.4219929511|H,
5.9930354473,-3.4782847049,-0.1653448385|H,6.0378490332,1.4864000051,-
0.4219978325|H,-0.0000032766,-5.6024993237,-0.0000017447|H,-2.15748017
75,-4.3516601622,0.0000308184|H,0.000008457,-0.6496551021,-0.000025473
6|H,2.157479574,-4.3516704264,-0.0000458339||Version=IA32W-G03RevC.02|
State=3-A|HF=-1561.1383204|S2=2.034958|S2-1=0.|S2A=2.000718|RMSD=7.859
e-009|RMSF=8.497e-007|Dipole=-0.0000009,1.9710831,0.0000158|PG=C01 [X(
C32H22N6)]||@

Table C.8 Output parameters for **3.9**.

1|1|UNPC-UNK|FOpt|UB3LYP|6-31G(d,p)|C27H17N4O2(2)|PCUSER|29-Jan-2010|0
||# B3LYP/6-31G(D,P) OPT||b3lyp/6-31g(d,p) full optimization on benzen
e diimide monoradical||0,2|C,-0.9146590113,-3.655670967,-0.2642498446|
C,0.4191126793,-3.2522074836,-0.140392803|C,0.7280184844,-1.9042484424
,-0.0178751471|C,-0.2911336773,-0.9184611338,-0.0253078465|C,-1.643936
1311,-1.362719812,-0.0801911826|C,-1.9463564291,-2.7235291131,-0.22991
91996|N,0.0366798487,0.4047041361,-0.0213661942|C,-0.9827318064,1.2680
037139,-0.106729312|N,-2.2858417024,0.9674479224,-0.1078833874|N,-2.60
92360421,-0.3539504055,-0.025005836|C,-4.0142104141,-0.6056780957,0.06
03994238|C,-0.6596519884,2.7171746761,-0.193939245|N,2.0812305707,-1.4
844124559,0.0744106725|C,-4.5221772949,-1.4709238567,1.0361071392|C,-5
.8980182456,-1.6801533198,1.1202367663|C,-6.7667161029,-1.023131263,0.
2473042283|C,-6.2531751959,-0.1472192129,-0.711759355|C,-4.8801413948,
0.0658793819,-0.8091453292|C,0.6803483592,3.1294873631,-0.2338048147|C
,0.997913069,4.483375609,-0.3166853745|C,-0.0157860757,5.4423472129,-0
.3606413654|C,-1.3522544541,5.0383656594,-0.3201364529|C,-1.674462523,
3.6860838381,-0.2369803613|C,3.0180172479,-1.6016485481,-0.9781631496|

C,4.2575688293,-0.9360570464,-0.4820500693|C,4.0201080269,-0.4565284476,0.8061392185|C,2.6218474152,-0.8038975207,1.1940058762|C,5.4862611812,-0.7682879838,-1.1046136602|C,6.4840452825,-0.0946614407,-0.3893738091|C,6.2463590614,0.3853897832,0.9052322238|C,5.0034789707,0.2074146798,1.5254663263|O,2.8224873077,-2.1453059971,-2.0440182137|O,2.050530776,-0.5971422937,2.2405902374|H,7.0404541878,0.9034604302,1.4344433241|H,7.4585865558,0.0586585033,-0.8429816692|H,4.8073179316,0.5728195253,2.5281087224|H,5.6582061083,-1.1465604397,-2.1069547031|H,-2.1459095527,5.7793053629,-0.3510566941|H,0.2333418945,6.4977524734,-0.4247053075|H,-6.9234668276,0.3711367154,-1.3906307862|H,-7.8374938667,-1.1869966561,0.318447323|H,2.0393489169,4.7905616714,-0.3467788476|H,-2.70956398,3.3675132664,-0.1996017664|H,1.4576435282,2.375760865,-0.1971794941|H,-6.2902628886,-2.3476516217,1.881389909|H,-4.466851102,0.7481239684,-1.542526101|H,-3.8477037983,-1.9574088553,1.7321312166|H,-1.1503950038,-4.7078382588,-0.3840466269|H,-2.9749312817,-3.0458795413,-0.3283153616|H,1.2216986098,-3.9806848425,-0.1510033954||Version=IA32W-G03RevC.02|State=2-A|HF=-1408.5939485|S2=0.766144|S2-1=0.|S2A=0.75016|RMSD=6.566e-009|RMSF=4.459e-006|Dipole=-0.2344662,-0.2284342,0.0272004|PG=C01[X(C27H17N4O2)]||@

Table C.9 Output parameters for **3.10**.

1|1|UNPC-UNK|FOpt|UB3LYP|6-31G(d,p)|C31H19N4O2(2)|PCUSER|01-Feb-2010|0||# B3LYP/6-31G(D,P) OPT||b3lyp/6-31g(d,p) full optimization on naphthalene diimide monoradical||0,2|C,1.5755430606,-3.6089654649,-0.231679452|C,0.2288809825,-3.2378062758,-0.1391037551|C,-0.1142824346,-1.8993220331,-0.0563505504|C,0.8741585676,-0.8877864401,-0.0539687633|C,2.2390458196,-1.2929268804,-0.0966251365|C,2.5801561489,-2.6479777037,-0.2147772012|N,0.5072529,0.4256933149,-0.0379119837|C,1.5011622014,1.3174261216,-0.1298008651|N,2.8122096786,1.0549914326,-0.14158478|N,3.174758162,-0.255971718,-0.0490434965|C,4.5863120205,-0.4635778112,0.0419210432|C,1.1356580865,2.7571530018,-0.2111992421|N,-1.4955114395,-1.5031492683,0.0142043009|C,-2.1595663026,-1.2669137573,-1.2068256697|C,-3.5590940065,-0.7805188176,-1.1094894728|C,-4.1543888016,-0.5499136022,0.1569112047|C,-3.4262459115,-0.7771708573,1.3524055003|C,-2.0252011127,-1.2651521059,1.2991587664|C,-4.2785165897,-0.5528768362,-2.268846192|C,-5.6096511734,-0.0912230754,-2.2027720125|C,-6.2093627048,0.1391972514,-0.9817651065|C,-5.5021551735,-0.0814647355,0.2292492695|C,-6.0745167613,0.1433282128,1.5088439433|C,-5.3465342571,-0.0833891223,2.6586730576|C,-4.0161990793,-0.5457141867,2.5819062157|O,-1.6002460175,-1.4720626449,-2.2714109493|O,-1.3551123027,-1.4718660106,2.2974196614|C,5.4334687281,0.2300296315,-0.8290382304|C,6.8122539127,0.0614473064,-0.7263124989|C,7.3505629643,-0.7921931527,0.2392754753|C,6.500455575,-1.4710148892,1.1137453753|C,5.1188986179,-1.3058176325,1.0247365405|C,-0.2158015509,3.128729349,-0.2628916741|C,-0.5735940687,4.472825481,-0.3419962356|C,0.4108087864,5.4624313412,-0.3706344309|C,1.7584648261,5.0990135231,-0.3182638126|C,2.1207933251,3.7566494691,-0.2385062769|H,-5.7957787677,0.0938099147,3.6307683492|H,-3.4315998984,-0.7272782767,3.4772630149|H,-6.1614479017,0.0827788444,-3.1211756994|H,-7.0994584736,0.4994835984,1.568903451|H,-7.2350141916,0.4950198945,-0.9322224791|H,-3.7940028394,-0.7367993839,-3.2216538577|H,2.5295094722,5.8638918348,-0.3373744041|H,0.1303254449,6.5101231653,-0.4322911185|H,6.9113325327,-2.1209797837,1.8802650812|H,8.42580672,-0.9216616363,0.3143317499|H,-1.6235584073,4.7483253468,-0.3822171579|H,3.1646343333,3.4691670004,-0.1923873232|H,-0.9696649998,2.3509258015,-0.2399061234|H,7.4678057392,0.5

96909422,-1.4063493629|H,4.4584592214,-1.8082668149,1.7227906259|H,5.0
007856873,0.8944236941,-1.5675888127|H,1.841534549,-4.6569646802,-0.32
12132689|H,3.6177991344,-2.9440231717,-0.2993763564|H,-0.5546480708,-3
.9874337072,-0.1441631694||Version=IA32W-G03RevC.02|State=2-A|HF=-1562
.2482006|S2=0.766233|S2-1=0.|S2A=0.750161|RMSD=2.685e-009|RMSF=2.107e-
006|Dipole=-0.3870074,-0.1351319,0.0646312|PG=C01 [X(C31H19N4O2)]||@

Appendix D ^{1}H-NMR and ^{13}C-NMR spectra

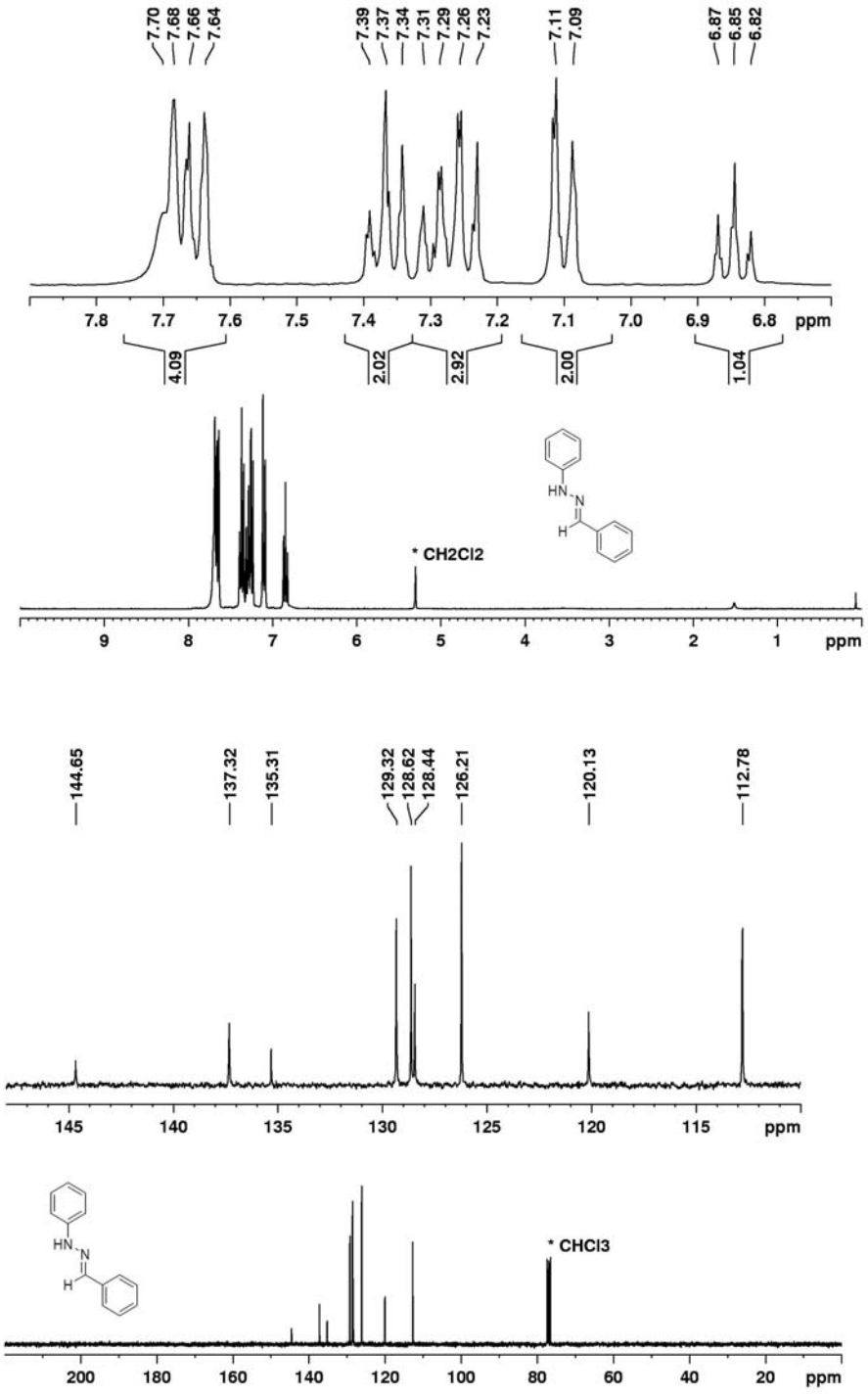

Figure D.1 ^{1}H-NMR spectrum in CD_2Cl_2 (top) and ^{13}C-NMR spectrum in $CDCl_3$ (bottom) of hydrazone **1.17**.

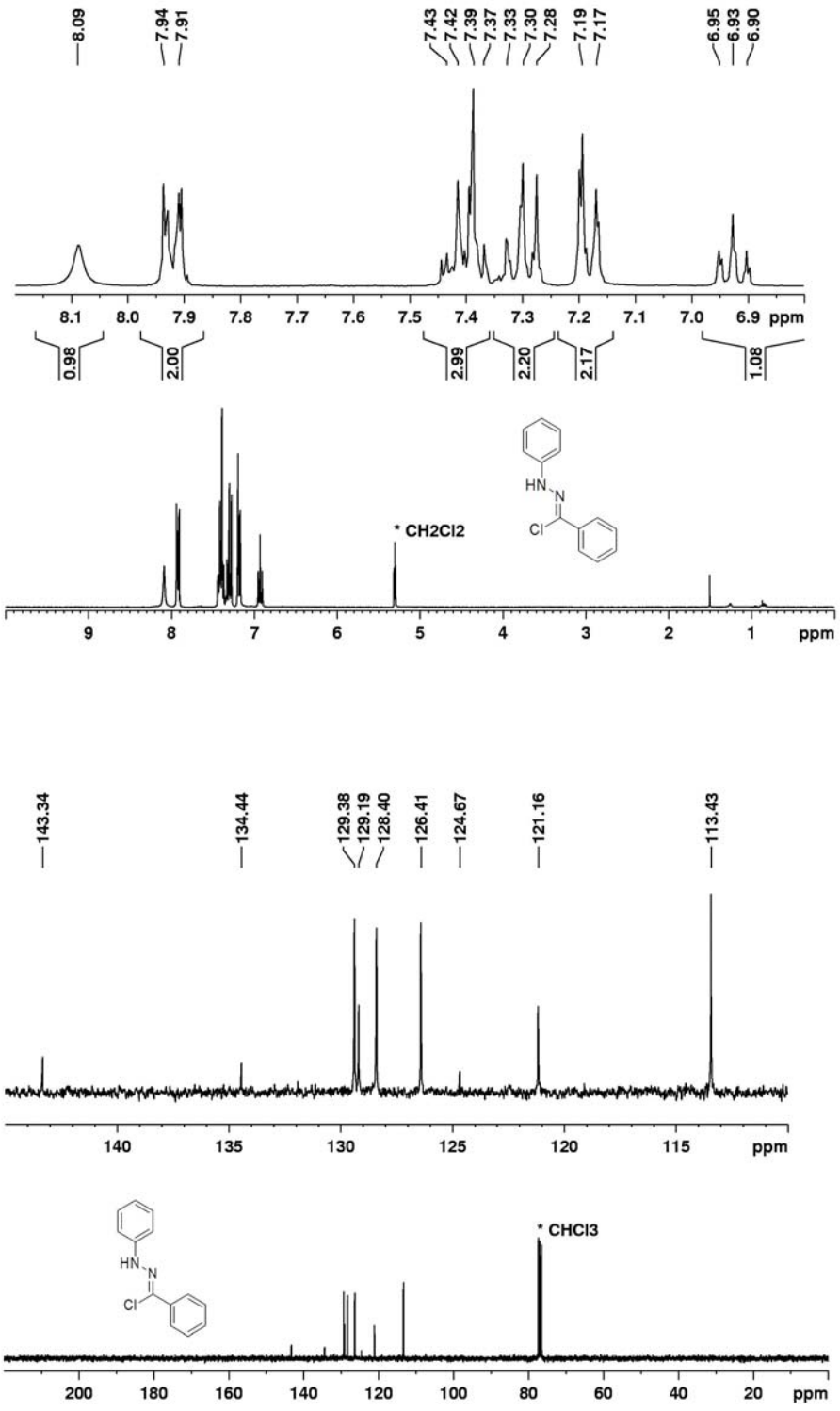

Figure D.2 ^{1}H-NMR spectrum in CD_2Cl_2 (top) and ^{13}C-NMR spectrum in $CDCl_3$ (bottom) of chlorohydrazone **1.18**.

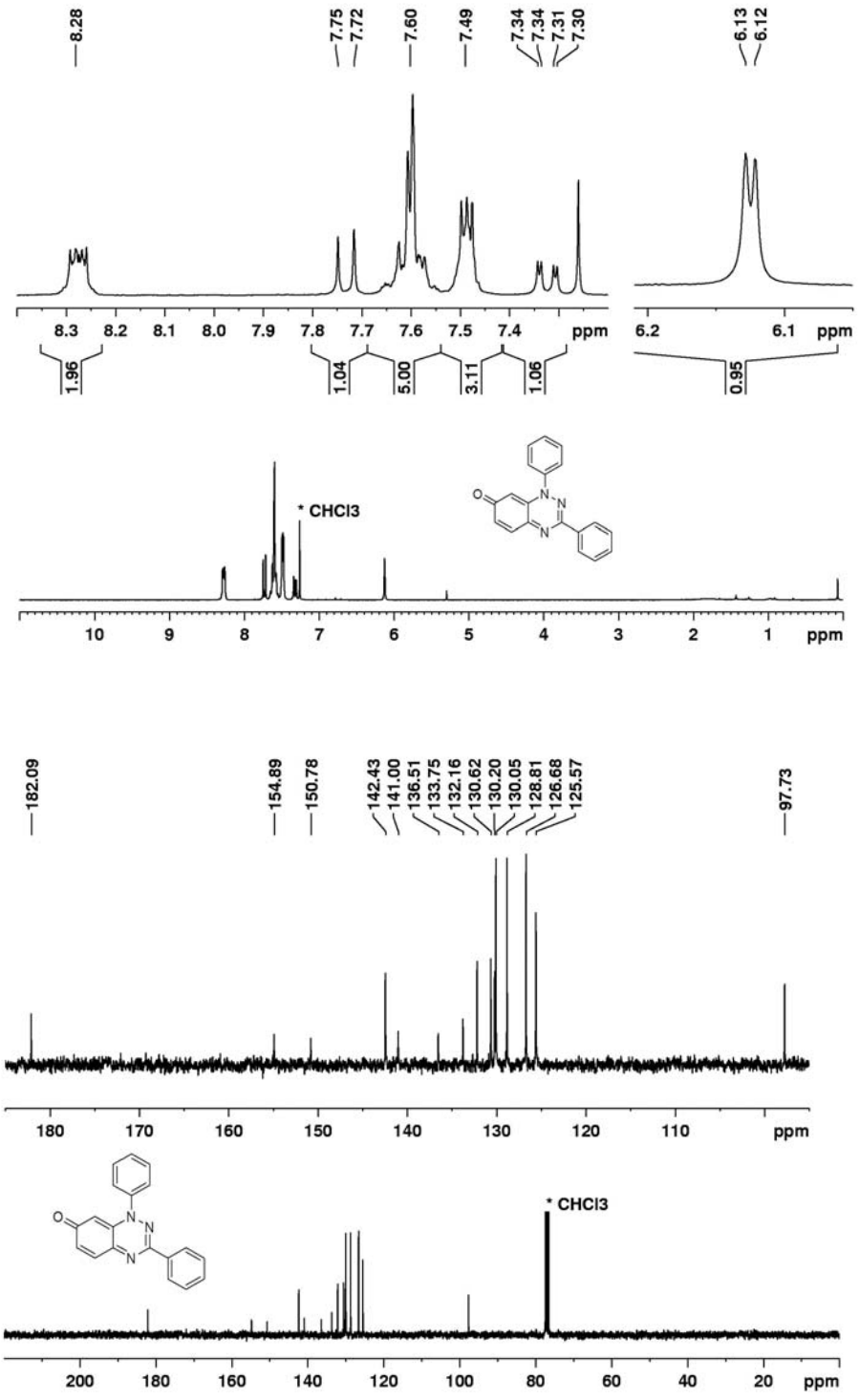

Figure D.3 ^{1}H-NMR (top) and ^{13}C-NMR (bottom) spectra of iminoquinone **2.15** in $CDCl_3$.

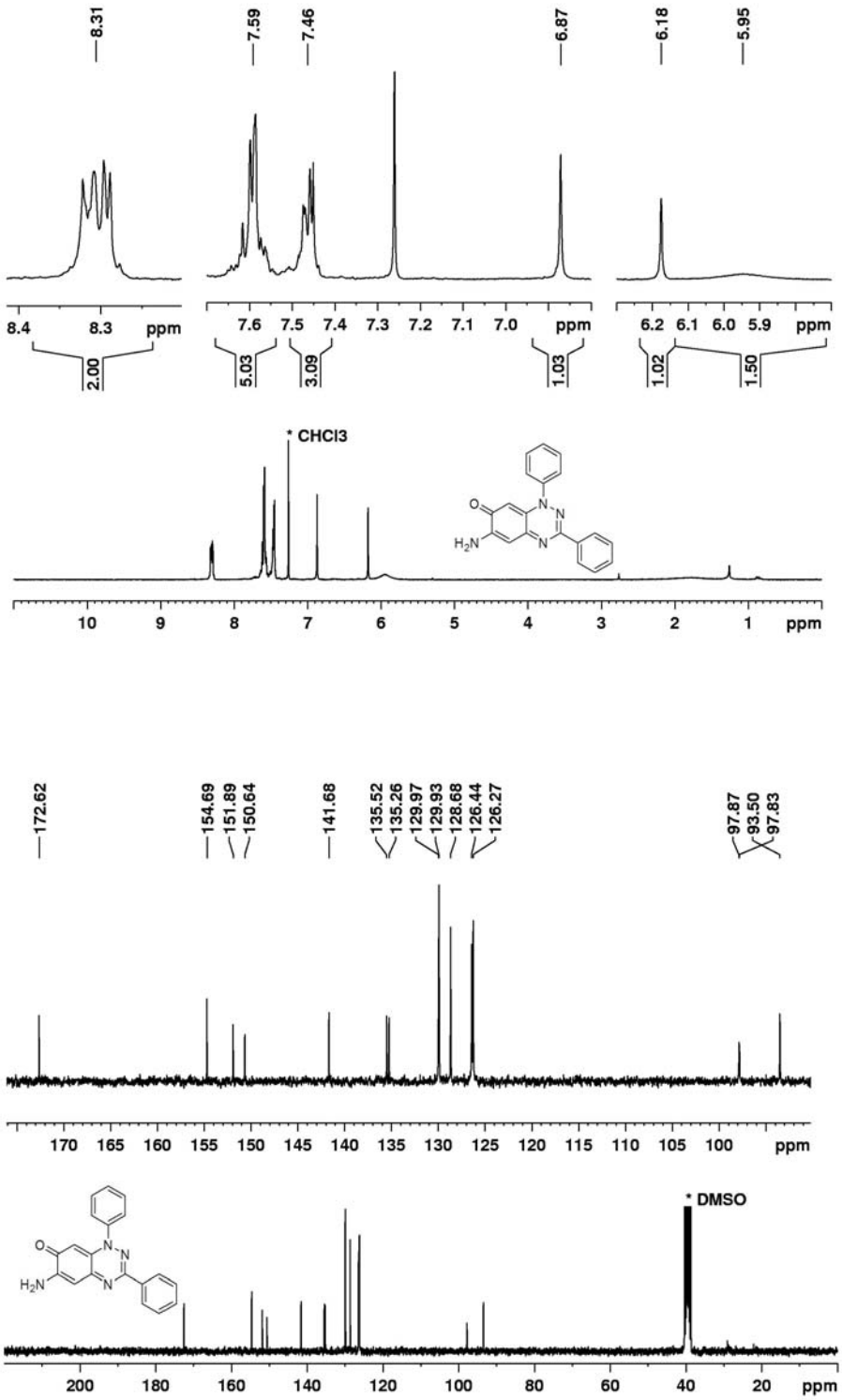

Figure D.4 ^{1}H-NMR spectrum in $CDCl_3$ (top) and ^{13}C-NMR spectrum in d6-DMSO (bottom) of iminoquinone **2.16**.

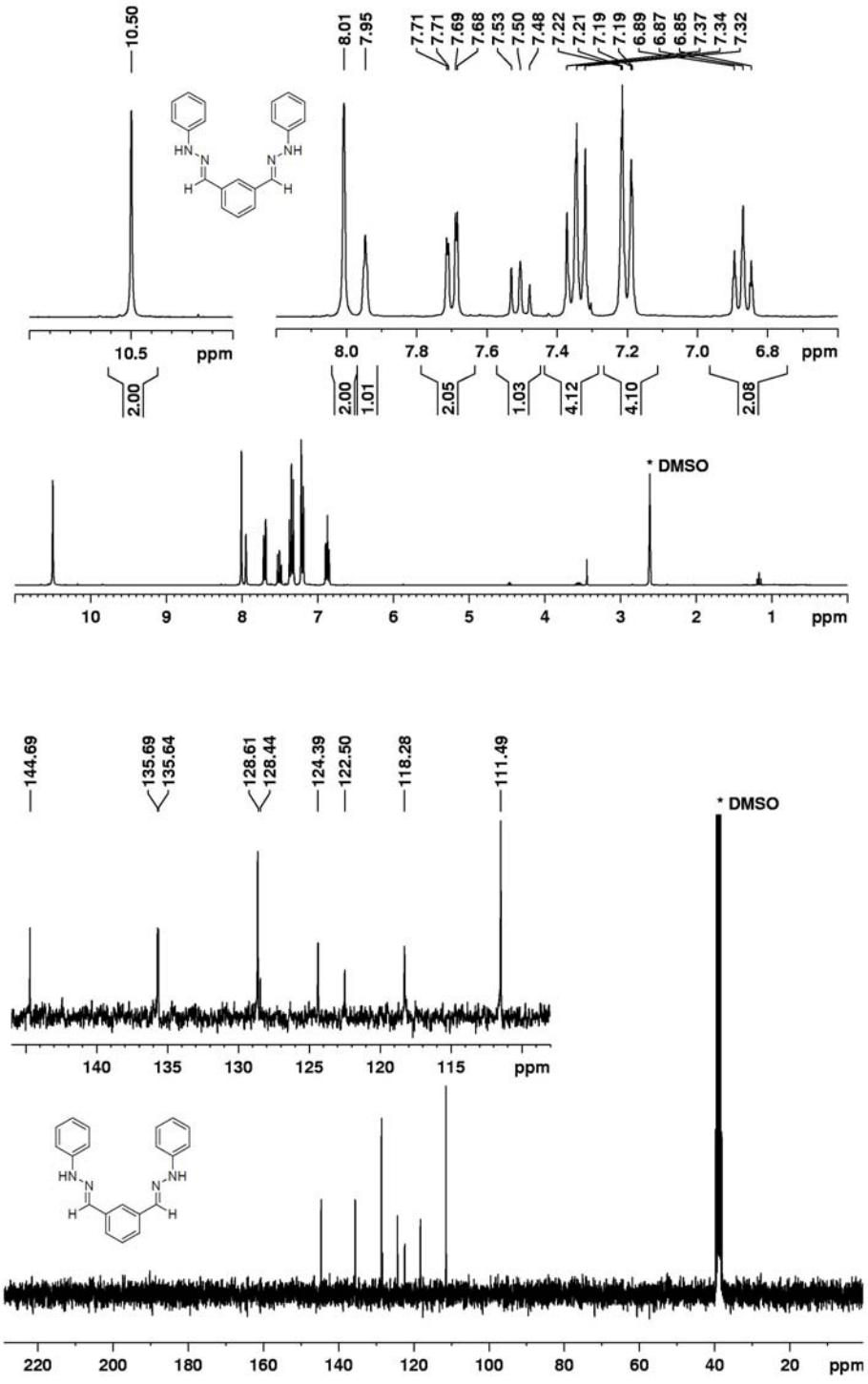

Figure D.5 ^{1}H-NMR (top) and ^{13}C-NMR (bottom) spectra of dihydrazone **3.8** in d6-DMSO.

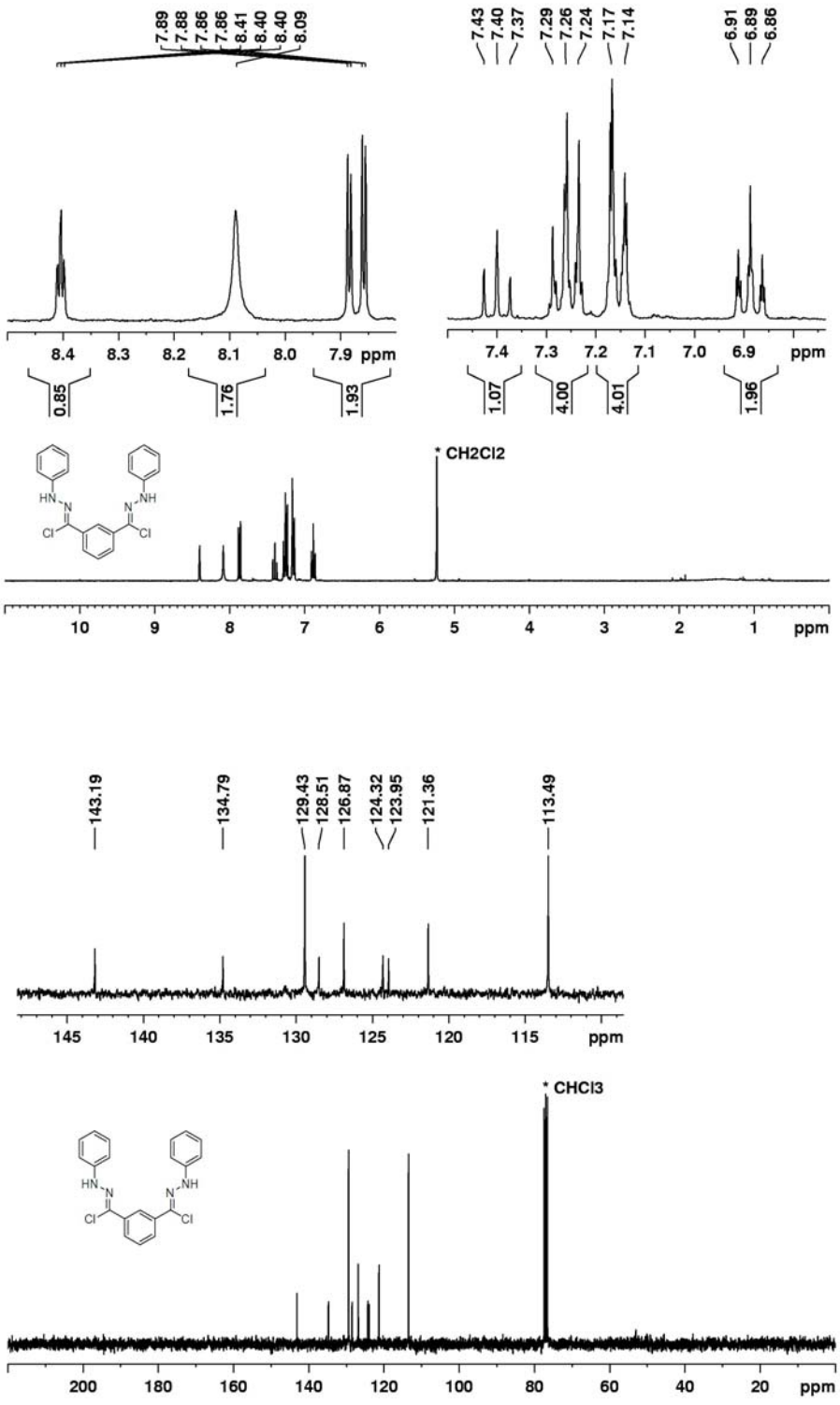

Figure D.6 ^{1}H-NMR spectrum in CD_2Cl_2 (top) and ^{13}C-NMR spectrum in $CDCl_3$ (bottom) of dichlorohydrazone **3.9**.

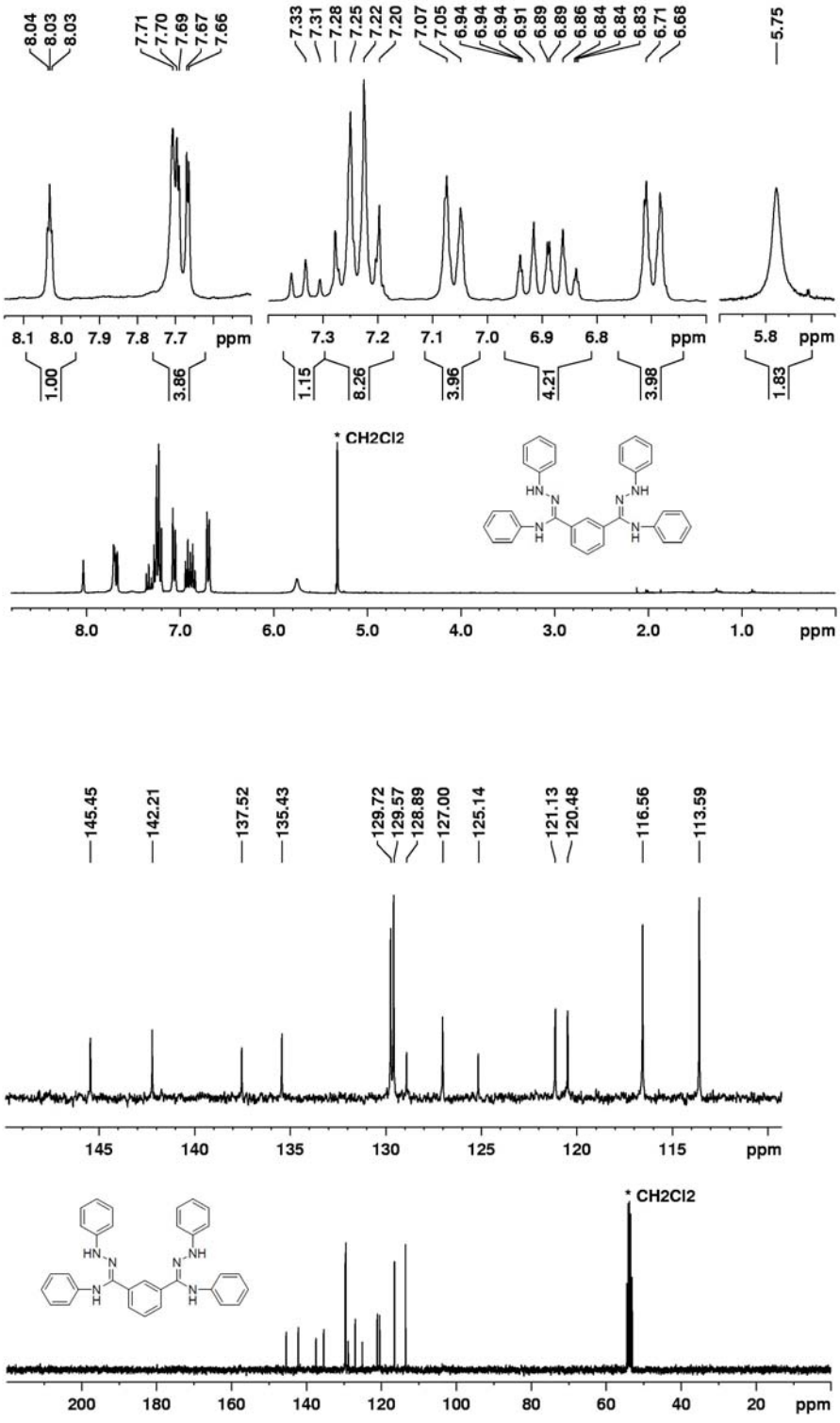

Figure D.7 ^{1}H-NMR (top) and ^{13}C-NMR (bottom) spectra of diamidrazone **3.10** in CD_2Cl_2.

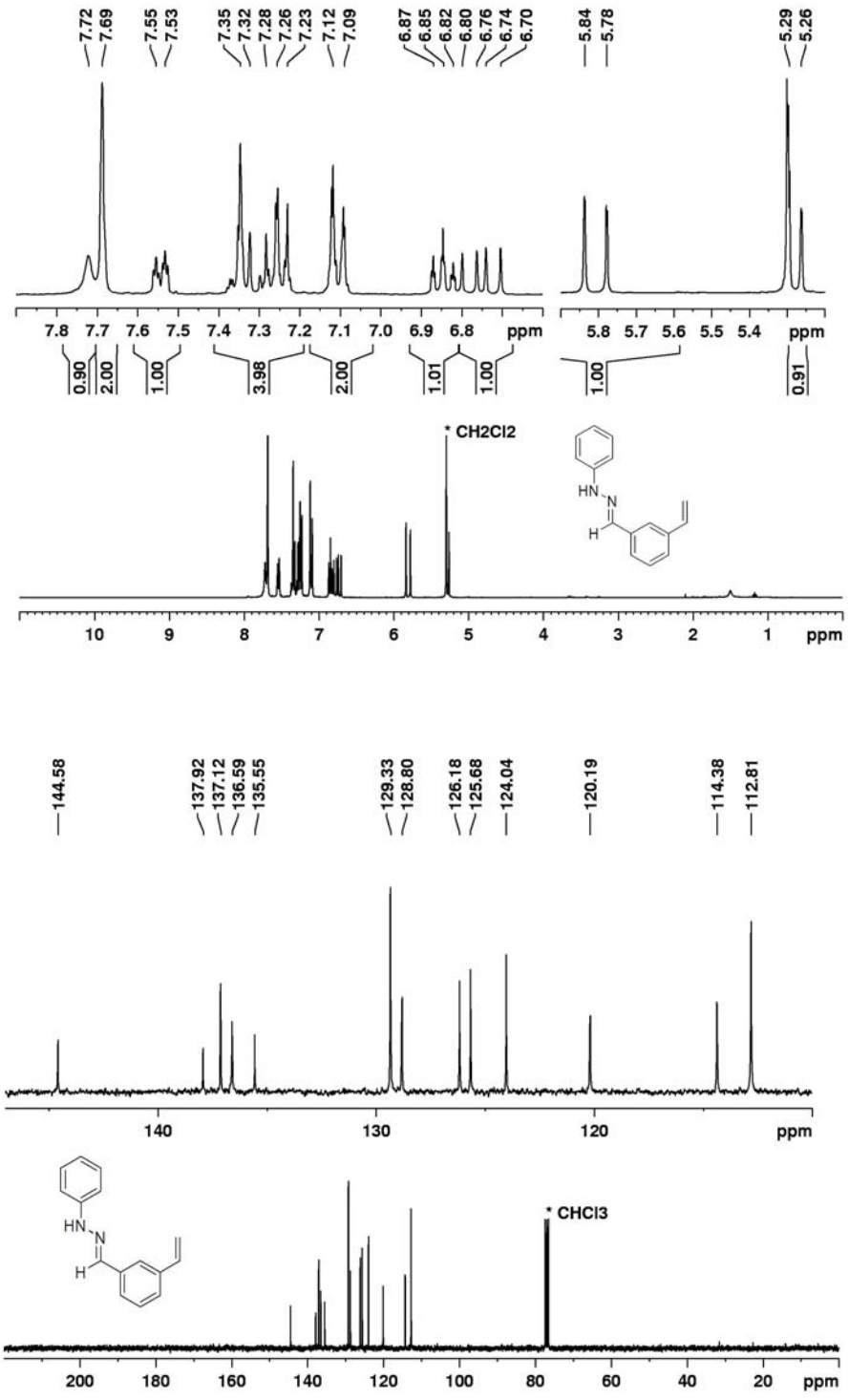

Figure D.8 ^{1}H-NMR spectrum in CD_2Cl_2 (top) and ^{13}C-NMR spectrum in $CDCl_3$ (bottom) of vinylhydrazone **5.6**.

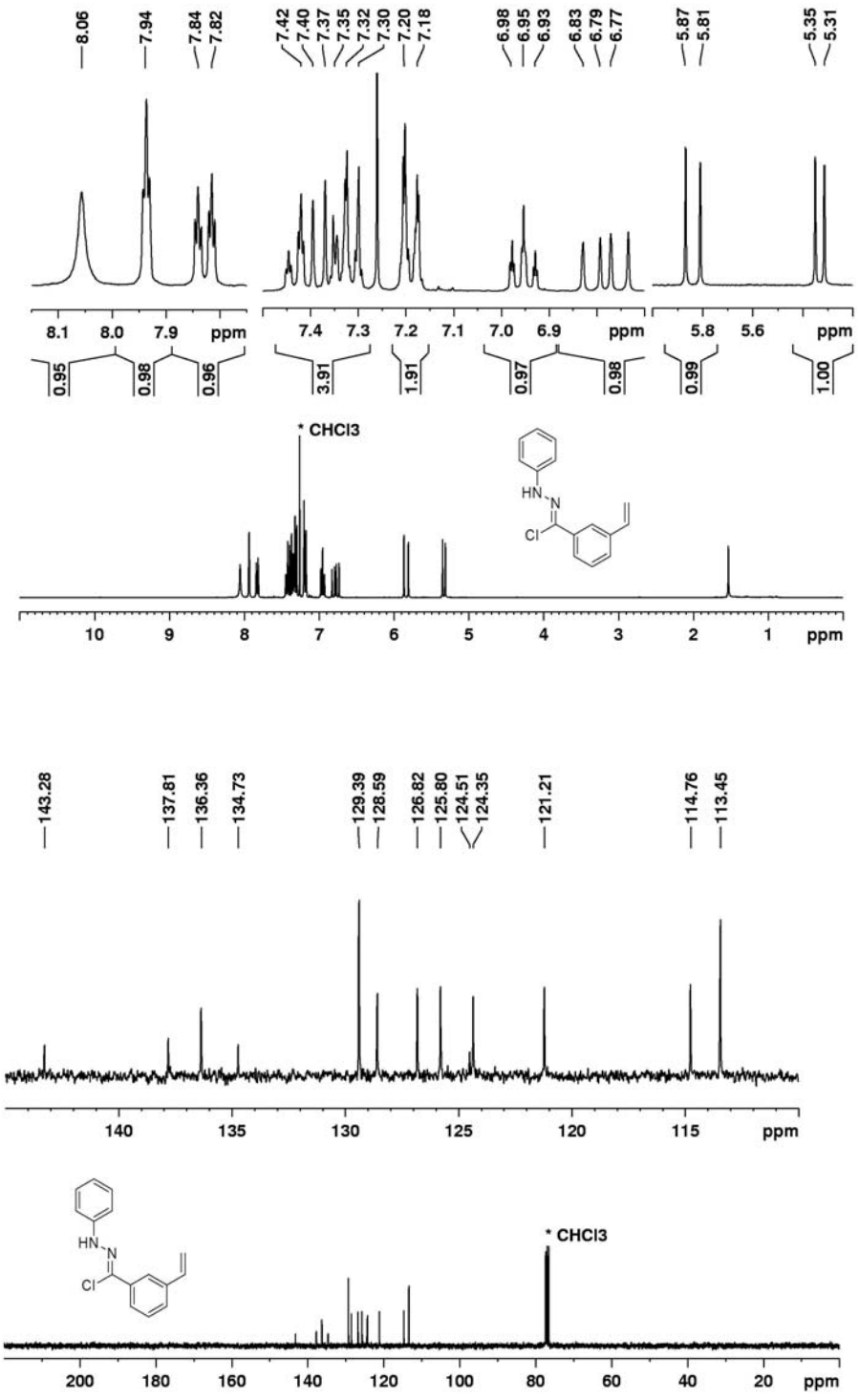

Figure D.9 ^{1}H-NMR (top) and ^{13}C-NMR (bottom) spectra of vinylchlorohydrazone **5.7** in $CDCl_3$.